The Development of a Field Emission Electron Source

for a Cathode Ray Tube.

MUSHTAQ AHMED SALIM   B.Sc. , M.Sc.

A Thesis submitted for the Degree of

Doctor of Philosophy.

The University of Aston in Birmingham.

October, 1984.

I dedicate this thesis

to my parents

and my nephew Tahir

The University of Aston in Birmingham

The Development of a Field Emission Electron

Source for a Cathode Ray Tube

Mushtaq Ahmed Salim   B.Sc. ,   M.Sc.

A Thesis submitted for the Degree of Doctor of Philosophy,   1984.

SUMMARY

Computer techniques have been used to design two-anode electro-static field emission guns, focal length   300 mm and 50 mm.   These were subsequently tested using a demountable proto-type cathode ray tube (C R T) with a carbon fibre field emission source.   It has been demonstrated that such guns have a satisfactory electron optical performance in this application. Subsequently, two commercial "thermionic" C R T's, one a standard type and the other a miniature high resolution type, were adapted to contain field emission guns. The successful operation of these tubes highlighted the great potential of carbon fibre as a field emission electron source.
    Initially, the final display of these C R T's exhibited a flick-ering which was found to be due to an inherent instability associated with the carbon fibre field emission source. This undesirable effect was satisfactorily eliminated firstly by using an external electronic feed-back system, and secondly by using a pulsed field technique which had the effect of reducing the instability by $\sim$ 90% . By using scanning electron microscopy, it was shown that this instability was the result of an explosive phenomenon which is normally encountered during the initial "switch-on" of "virgin" carbon fibre cathodes. This destructive process was eliminated using a pre-heat treatment of the emitter, which resulted in considerably longer life times and a significant reduction in the noise in the total emission current. The energy spectra of the field emitted electrons from heat-treated cathodes were measured using an U H V high resolution specrometer, and were shown to be both single and multi-peaked. For single peaked spectra, the half width is found to increase with field, whereas the spectral shift from the Fermi level decreases. These and other properties of carbon fibre emitters have been interpreted in terms of a hot-electron emission mechanism.

Key words: Field Electron Emission

                Cathode Ray Tube.

                Carbon Fibre.

CONTENTS

LIST OF FIGURES

...

CHAPTER 1

INTRODUCTION

The emission of electrons from a metal surface into vacuum under the influence of a strong electric field applied at the solid-vacuum interface is called field electron emission and was first reported by Wood [1] in 1897. Subsequently, following the development of ultra high vacuum techniques, the phenomenon was extensively studied under controlled conditions using the field emission microscope [2, 3, 4]. This uses etched micropoint specimen emitters having a tip radius typically of $\lesssim 0.1 \, \mu m$ in order to obtain at relatively low voltages ($\lesssim 1 \, kV$) a geometrically enhanced threshold field of $\gtrsim 3 \times 10^9 \, V \, m^{-1}$ which is required for a quantum mechanical tunnelling mechanism to occur [5]. More recently, studies have been extended to semiconductor emitters [6, 7] and the role of adsorbed atoms, particularly in relation to surface catalysis [8, 9].

From a practical point of view, the characteristic properties of a field emission source, such as its high emission current density ($\sim 10^{10} \, A \, m^{-2}$) and small optical source size ($\sim 3 \, nm$) (which together resulting in it having a very high source brightness of $\sim 6 \times 10^8 \, A \, m^{-2} \, Sterads^{-1}$), its instantaneous start, and the fact that it is a 'cold' source (thus eliminating heater power), give it many advantages over conventional thermionic cathodes. Therefore, the suitability of the field emission source for variety of technological applications, which include microwaves amplifiers, transducers, flash x-ray devices, switch tubes and electron microscopes, has been considered for example by Dyke [10] and Crewe et al [11]. The most widely used emitter material has been tungsten, since apart from

being readily available, it has a high melting point, a good electrical conductivity, is sufficiently strong mechanically to withstand the electrostatic stresses imposed on the emitter by the applied electric field and can be easily electro-chemically etched from the wire form of the material to give a well defined and highly stable micro-point profile with a typical tip radius of $\lesssim$ 500 n m. However, these emitters suffer from the serious practical limitation of requiring ultra high vacuum conditions ($\lesssim 10^{-10}$ mbar) for stable operation. This is mainly because (a) the stability of the emission current is very sensitive to the surface adsorption of gas atoms, and (b) the sharp profile of the emitter can easily be destroyed by ion sputtering processes. Furthermore, even when tips are operated under good vacuum conditions, they are prone to contamination by surface diffusion mechanisms, so that complicated procedures have to be incorporated for in situ "flash" cleaning them [12].

Carbon fibre field emitters on the other hand have been shown not to suffer from many of the above limitations [13]. In particular, their performance, including their life time, is largely independent of the vacuum pressure in the range of interest, (i.e. $\sim 10^{-5} - 10^{-7}$ mbar). Consequently it is in principle possible to use carbon fibre as a field emission electron source in commercial sealed-off devices where the ultra high vacuum (U H V) condition cannot be attained. One such device which has been extensively studied by Wilson [14] and Latham and Wilson [15] using such a source, is a demountable proto-type cathode ray tube. In this investigation a commercial tube was electron optically redesigned to incorporate an electrostatically focused field emission gun employing carbon fibre as field emitter instead of conventional thermionic source. Wilson demonstrated that such a system provided a well focused spot ($\sim$ 0.2 mm diameter)

suitable for producing $_a$ raster pattern of adequate brightness with

~ 10 μ A total emission current. Furthermore, he showed that the

tube could be operated with adequate life-time in a pressure range

compatable to that found in conventional thermionic sealed cathode

ray tubes (C R T) i.e. $\gtrsim 10^{-7}$ mbar. However, whilst the electron

optical performance of the tube was satisfactory, it suffered from

a residual instability in the screen image which represented a

serious obstacle to the commercial application of the source. The

origin of this instability is directly associated with the complex

nature of the field emission pattern of a carbon fibre source, which

consists of many discrete emission spots, when each is continuously switch-

ing 'on' and 'off', and thus giving rise to fluctuations of both the

emission pattern and the total current. It follows therefore that

this serious problem has to be overcome before the carbon fibre tips

can provide a satisfactory electron source for use in C R tubes.

The main emphasis of this present study has therefore been to

consider ways in which the instability at the screen can be overcome.

Two broad approaches have been considered. Firstly, feed-back tech-

niques have been developed for externally compensating for its presence.

These have included (a) the use of 100 MΩ series resistor and (b) a valve-

type feed-back system in series with the emitter to stabilise the total

emission current, and (c) the sampling of the screen current to con-

trol the current drawn from the tip. The approaches 'a' and 'c' have

involved redesigning the electrostatic lens used in the electron gun

to make its focusing properties less susceptible to fluctuations in

the beam energy. Also, these studies involved developing an optical

monitoring system for quantitatively measuring the instability in

the screen image. The second approach is based upon the recognition

that the instabilities are directly associated with the hot-electron

3.

emission mechanism [16] that is thought to be operating in the carbon fibre field emitters and occurs at several independent and discrete centres distributed over the emitter tip, the image instability is a consequence of an inherent instability in this mechanism that results in each sub-centre switching on and off randomly with time. As a result, two techniques have been developed, namely, pre-heat treatment of the cathodes and pulsed field emission, to directly control the emitter characteristics and thereby eliminate the instabilities "at source".

On the practical level, these stabilising techniques have been evaluated in terms of the performance of a microfocus cathode ray tube.

CHAPTER 2

2.0 FIELD ELECTRON EMISSION FROM METALS, SEMICONDUCTORS AND COMPOSITE REGIMES.

2.1 Introduction

The phenomenon of electron emission from the surface of a cold cathode under the influence of a high electric field ($\geqslant 10^9$ V m^{-1}) has been long established. Historically, cold emission or field electron emission (F E E) from metals has been extensively studied, and is well understood [2]. The phenomenon involves the tunnelling of electrons through a deformed surface potential barrier resulting from the applied field and the image force correction. At low temperatures ($\leqslant 300^\circ$ K), these field emitted electrons originate from or just below the Fermi level of the cathode material; a fact that can be readily confirmed by electron spectroscopy. Thus F E E differs fundamentally from both thermionic (or Schottky) emission and photo-emission, where the electrons have to acquire sufficient energy to go over the barrier. At a more detailed level, it should be noted that in the case of F E E, the atomic surface conditions are found to play a crucial role in the process. This is particularly true for semi-conductors where the density of surface states, which control the supply of electrons, is particularly vulnerable to these surface conditions.

Another type of F E M mechanism has been identified which can occur when a metal substrate is overlayed by an insulating film. The earliest interpretation of this effect is due to Malter [17] who assumed that the vacuum surface of the insulator becomes charged with

a layer of a positive charge that sets up an internal electric field, which if sufficiently large, will enable electrons to tunnel from the underlaying metal substrate into the insulator and subsequently field emitted. Such a mechanism (the "Malter effect") was originally proposed to explain his observation of a greatly enhanced secondary emission from oxide coated Al when bombarded with primary electrons. More recently, a fresh interest in this type of "non-metallic" F E E process has emerged from the studies of the physical origin of the pre-breakdown currents that flow between vacuum-insulated high voltage electrodes. These studies have indicated [18] that these currents arise from a field emission process that occurs at microscopically localised sites that have been associated with insulating surface inclusions. On the basis of electron spectroscopy evidence [19], a new type of emission process has been proposed that is based on the concept of a field-induced electron heating [20].

It should also be noted at this point that recent spectroscopy studies of carbon fibre field emitters [14, 21], have strongly suggested that a similar non-metallic process is responsible for the electron emission. This topic will however be considered in greater detail in chapter 3.

2.2 FIELD ELECTRON EMISSION FROM METALS.

The earliest explanation of the field electron emission from metals was due to Schottky [22] who, taking a classical approach, proposed a connection between the thermionic and 'cold' electron emission (field electron emission) mechanism. That is, field emission is due to the complete reduction of the surface potential barrier. However, this interpretation was subsequently rejected on

theoretical grounds and superseded by the Sommerfield Free Electron Model for

metals see [Fig. 2.1 (a)]. In this, electrons are confined to a minimum

energy at 0° K corresponding to the Fermi level within the metal, by a

potential barrier of height $\emptyset$, where $\emptyset$ is the work function of the

metal. On microscopic scale this step potential barrier is in fact

curved as shown in Fig. 2.1 (b), since it arises from including the

image force potential. In the presence of an applied electric field,

this curved potential barrier is further modified to Fig. 2.1 (c),

thereby lowering the height of the surface potential barrier, i.e.

equivalent to a reduction of the work function by an amount $\triangle \emptyset$. At

relatively low applied fields, this decrease in thermionic work

function has been experimentally established to be in full agreement

with Schottky's prediction. For a complete reduction in the barrier

height however, fields in the excess of 1×10^{10} V m^{-1} for

tungsten are necessary, where as F E E occurs at much lower fields

of $\sim 5 \times 10^{8}$ V m^{-1}. Furthermore the effect is independent of

temperature. Clearly the classical approach was unable to explain

the field emission phenomenon and so it was concluded that some other

mechanism must be responsible.

An alternative explanation was supplied by quantum mechanics,

whereby in the presence of a high external electric field acting on

an atomically clean metal surface, the potential barrier becomes so

thin that electrons near the Fermi level are able to tunnel accross

the small distance, $\triangle$ x in Fig. 2.2 . For this to occur, the wave

function ψ of an electron in the surface of the metal must still be

finite beyond the barrier; i.e. the barrier width $\triangle$ x must be com-

parable to the de Broglie wavelength of the electron. In practical

terms, this requires a surface field of $\gtrsim 3 \times 10^{9}$ V m^{-1} (5).

Alternatively, this can be understood by considering the Heisenberg
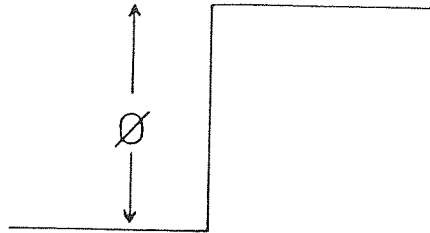
(a) Basic surface potential barrier.
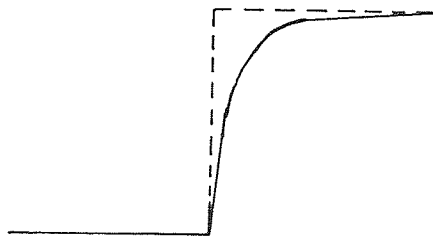
(b) With image force correction.
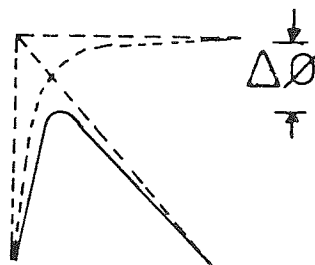
(c) On application of an electric field.

Fig. 2.1 Schematic representation of Free Electron Model of a
          metal and the effect of an applied high electric field.
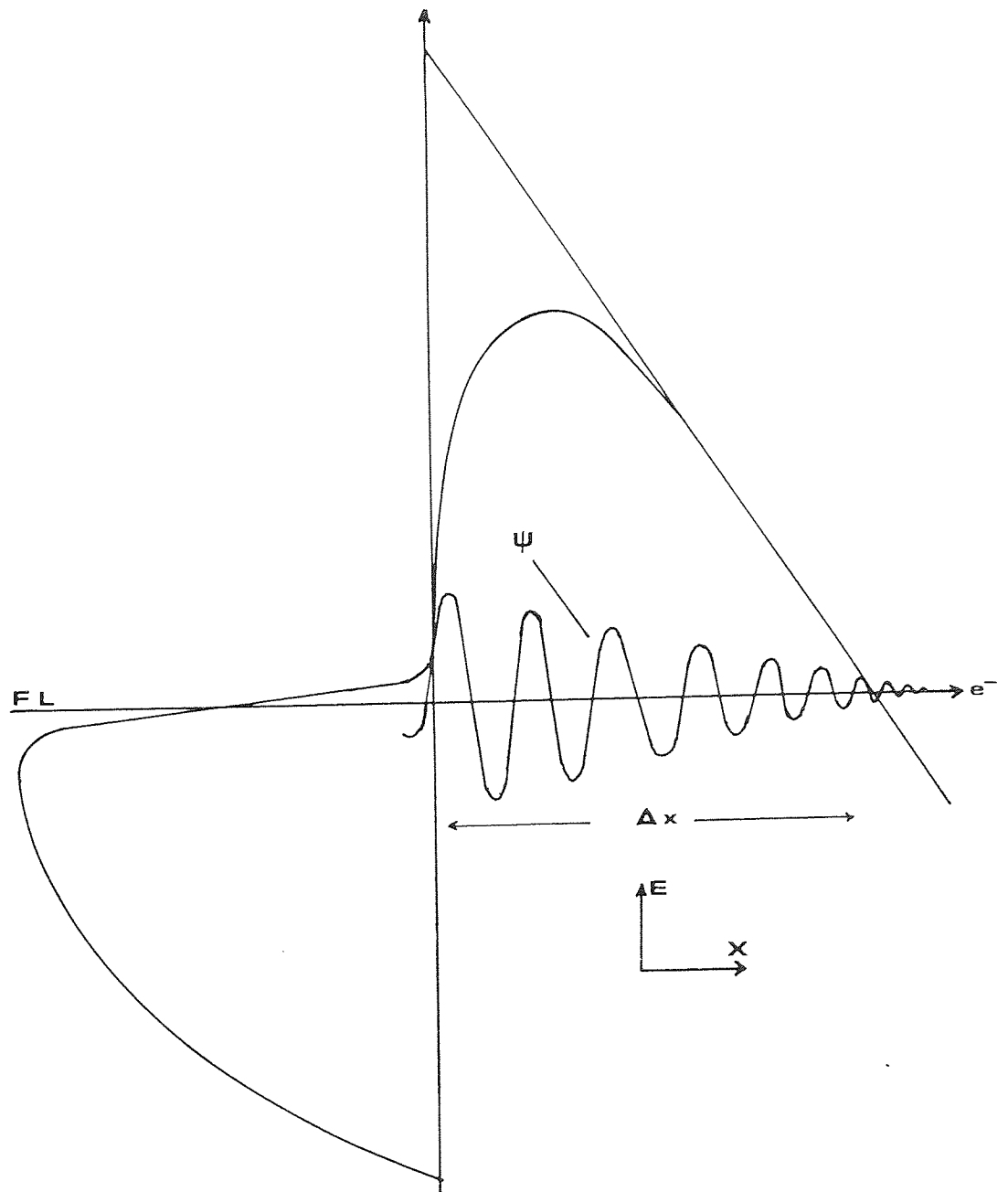
Fig. 2.2   A schematic representation of the quantum mechanical

tunnelling mechanism by which a field emitted electron

escapes from the surface of a metal.

Uncertainty Principle, where, if Δp is the uncertainty in momentum, then corresponding uncertainty in position, Δx , is given by

$$\Delta p \cdot \Delta x \approx \hbar/2 \qquad\qquad (2.1)$$

where $\hbar = h/2\pi$ and h is Planck's constant. Thus, if an electron is near the Fermi level, the uncertainty in momentum is that corresponding to barrier height $(2 m \phi)^{\frac{1}{2}}$, so that the corresponding uncertainty in position will be

$$\Delta x \cong \frac{h}{2} (2 m \phi)^{\frac{1}{2}} \qquad\qquad (2.2)$$

If this is of the order of the barrier _width_ $\lesssim 10^{-9}$ m , there is a finite probability of finding an electron on either side of the barrier. An important feature of the tunnelling mechanism is that no exchange in energy of the electron occurs. Therefore the energy of an electron outside the barrier is equal to the energy of the electron within the metal, i.e. at the Fermi level. A complete theoretical analysis of the above model was formulated by Fowler and Nordheim in 1928 [5] for the case of the metal obeying Sommerfield Free Electron theory. They considered a quantum mechanical electron tunnelling mechanism [23] through a thinned potential barrier resulting from a high applied electric field acting on an atomically clean metal surface. Their model is illustrated in Fig. 2.3 and shows the one dimentional variation of the potential energy, $V(x)$, of an electron with its position x from the surface. For $x > 0$

$$V(x) = -(e^2/4 x) - e E x \qquad\qquad (2.3)$$

where e is the electronic charge and E is the applied electric field.
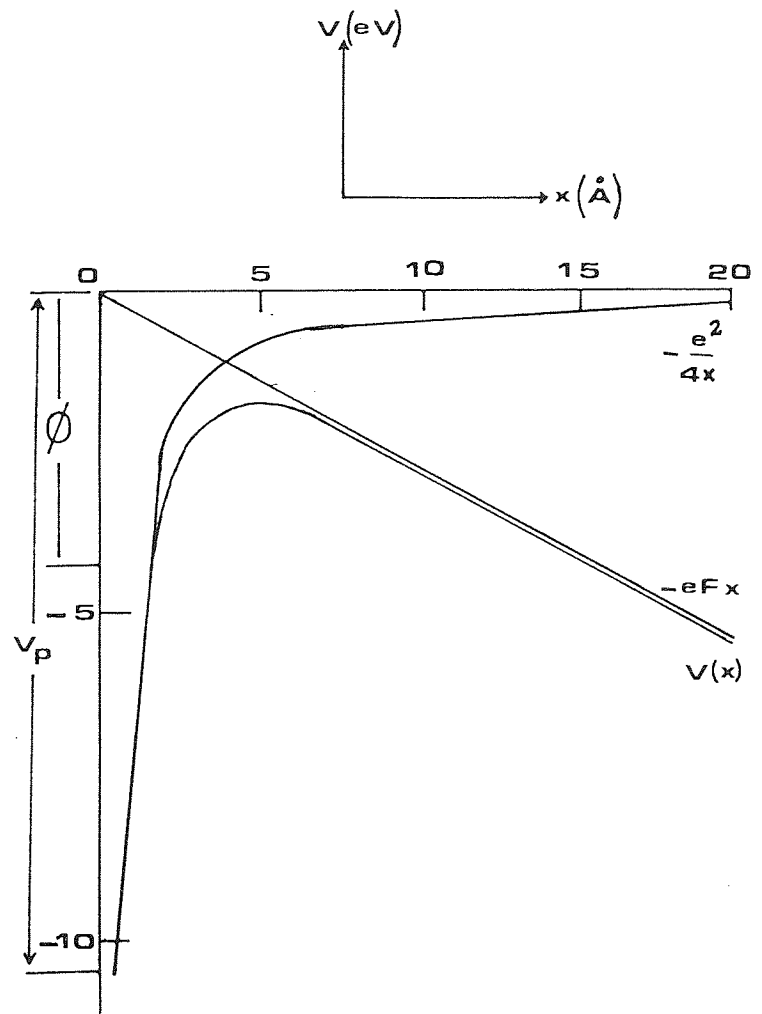
Fig. 2.3 The potential energy $V(x)$ of an electron as a function
of its distance x to the metal surface.

If the total energy of the electron inside the metal is denoted by W , then the x part, which determines the probability of an electron penetrating the potential barrier, will be

$$W_x = \frac{P_x^2}{2m} + V(x) \qquad (2.4)$$

where m is the mass of the electron and P_x the momentum in x direction. The derivation of the Fowler-Nordheim equation, which gives the dependance of the field emitted current density J on the field strength E and the work function $\emptyset$, conveniently falls into three parts. Firstly, a supply function, $N(W_x) \, d \, W_x$ is defined, which gives the number of electrons with the x component of their energies in the range of W_x and $W_x + d \, W_x$ that arrive at the metal surface per unit area and time. Next a transmission coefficient $D(W_x)$ is defined, which gives the probability that an electron with an energy between W_x and $W_x + d \, W_x$ will tunnel through the barrier and be emitted. Then finally the number of electrons within the above energy range that will be transmitted, $P(W_x)$, into the vacuum is obtained by multiplying together the supply function and the transmission coefficient, i.e.

$$P(W_x) \, d \, W_x = N(W_x) \cdot D(W_x) \, d \, W_x \qquad (2.5)$$

which is also known as normal energy distribution. The total field emission current density J is then found by integrating over all the energies and multiplying by electronic charge e ,

$$J = e \int P(W_x) \, d \, W_x \qquad (2.6)$$
over all
energies

12.

The electron supply function is derived by using the Fermi-Dirac statistics (24) and is given by

$$N(W_x) = \frac{4\pi\, m\, k\, T}{h^3} \cdot Ln\left(1 + \exp\left(-\frac{W_x - \phi}{k\,T}\right)\right) d\,W_x$$

$$(2.7)$$

where k is Boltzmann constant and T the absolute temperature. The transmission coefficient $D(W_x)$ is obtained by solving the Schrodinger equation,

$$\frac{d^2\psi}{d\,x^2} + \frac{2\,m}{\hbar^2}\left(W_x - V(X)\right)\psi = 0 \qquad (2.8)$$

with the potential energy function V(x) given by equation (2.3). The solving of this Schrodinger equasion and the evaluation of $P(W_x)\,d\,W_x$ and the integration are fully treated in modern comprehensive review articles by Nordheim (25), Good and Muller (24) and Van Oostrom (26). Thus one finds that for low temperatures $(\leqslant 300^\circ$ K) the current density is given by

$$J = \frac{e^3\,F^2}{8\,\pi\,h\,\phi\,t^2(y)}\ \exp\left(-\frac{4}{3}\cdot\frac{(2\,m)^{\frac{1}{2}}}{\hbar\ e}\cdot\frac{\phi^{3/2}}{F}\cdot f(y)\right) \quad (2.9)$$

or after evaluating the fundamental constants, as

$$J = \frac{1.54 \times 10^{-6}\,F^2}{\phi\,t^2(y)}\cdot\exp\left(-\frac{6.83 \times 10^9\,\phi^{3/2}\,f(y)}{F}\right) \qquad (2.10)$$

where few electron states above Fermi level are occupied as shown by the low temperature Fermi-Dirac electron energy distributions. In equations (2.9) and (2.10) , F is the surface electric field in ($V\,m^{-1}$) and ϕ is the work function of the emitting surface

in e V , t(y) and f(y) are slowly varying tabulated dimention-less eliptic functions (24, 26) of the parameter y given by

$$y = 3.79 \times 10^{-5} \times \frac{F^{\frac{1}{2}}}{\phi}$$ (2.11)

such that for the field range of stable emission $2 \times 10^9 < E < 6 \times 10^9$ V m^{-1} these functions can be taken as

$$t(y) \simeq 1$$ (2.12)

$$f(y) \simeq 0.956 - 1.062 \ y^2$$ (2.13)

The substitution of equations (2.12) and (2.13) in (2.10) and taking logarithms yields the Fowler-Nordheim (F-N) equation in the convenient form of

$$\text{Ln } (\frac{J}{F^2}) = \text{Ln } (\frac{1.54 \times 10^{-6} \times 10^{4.54 \ \phi^{-\frac{1}{2}}}}{\phi}) - \frac{2.84 \times 10^9}{F} \cdot \phi^{3/2}$$

(2.14)

This equation can be further developed in terms of experimentally measured quantities by noting firstly that the total emission current I will be given by

$$I = \int_0^A J \ d \ A$$ (2.15)

where A is the total emitting area, and for point to plane geometry the field acting on the tip of the radius r is given by

$$F = V/K \ r$$ (2.16)

where V is potential difference between cathode and anode and K

is a constant usually taken to have value of ~ 5 [4]. Substituting the equations (2.15) and (2.16) into (2.14) we have

$$Ln \left(\frac{I}{V^2}\right) = Ln \left(\frac{1.54 \times 10^{-6}\, A \cdot (1/K^2) \cdot 10^{4.54\, \phi^{-\frac{1}{2}}}}{\phi\, r^2} \right) - \left(\frac{2.84 \times 10^9 \cdot \phi^{3/2} \cdot r}{V\,(1/K)} \right) \qquad (\,2.17\,)$$

From this equation it is seen that a plot of $Ln\,(\,I/V^2\,)$ versus $(\,1/V\,)$, known as a Fowler-Nordheim (or F-N) plot should give a straight line of slope

$$m = \frac{2.84 \times 10^9 \times \phi^{3/2} \times r}{(\,1/K\,)} \qquad (\,2.18\,)$$

and the intercept

$$c = Ln \left(\frac{1.54 \times 10^{-6} \cdot A \cdot (\,1/K\,)^2 \cdot 10^{4.54\, \phi^{-\frac{1}{2}}}}{\phi \cdot r^2} \right) \qquad (\,2.19\,)$$

Thus from F-N plot we are able to find K indirectly provided that the radius r and ϕ , the work function of the emitter, which is assumed to be the same as for the bulk, are known.

Haefer [27] was the first to test the Fowler-Nordheim theory for a point cathode to plane anode geometry and later Dyke et al (28, 29) tested the theory much more extensively. By using micro-point emitters whose geometry was well known they were able to determine the field on the point cathode. They found a good agreement with the theory over a large range of magnitude of current density. At higher current densities, the departure from the theory was satisfactorily explained in terms of space charge effects.

2.3 FIELD EMISSION FROM SEMICONDUCTORS.

The mechanism responsible for field emission from semiconducting emitters is generally more complex than for metals since the following additional factors have to be taken into account;

(i) A more complex energy band structure,

(ii) possibility of field penetration

(iii) the existence of electronic surface states and

(iv) bulk resistivity effects.

Thus, in contrast to the case of a metal, when a strong electric field is applied to a surface of a semiconducting material, there will generally be some degree of field penetration, due mainly the the sparse population of electrons in the conduction band that are unable to effectively screen the bulk of the emitter from the external field. As a result, the electrostatic potential will change within the penetration region and this gives rise to a downward bending of the bands. This situation is illustrated in Fig. 2.4 (a) and is a non-degenerate case; however, if the band bending becomes severe enough for the bottom of the conduction band to dip below the Fermi level, and we would then have the degenerate situation of Fig. 2.4 (b) (i.e. electrons inside it obey Fermi-Dirac statistics rather then Boltzmann statistics). The severity of band bending is controlled by the number of free charges and the strength of applied field.

Deformation of the band structure at the semiconductor-vacuum interface may be further influenced by the existance of surface states which may lie within or overlap with the bulk energy bands. Although these states exist in metals, they are of greater significant in semiconducting materials because of their limited electrical conduct-

Conduction Band

Fermi
Level

Valence
Band

(a) NON-DEGENERATE

Conduction Band

Fermi
Level

Valence
Band
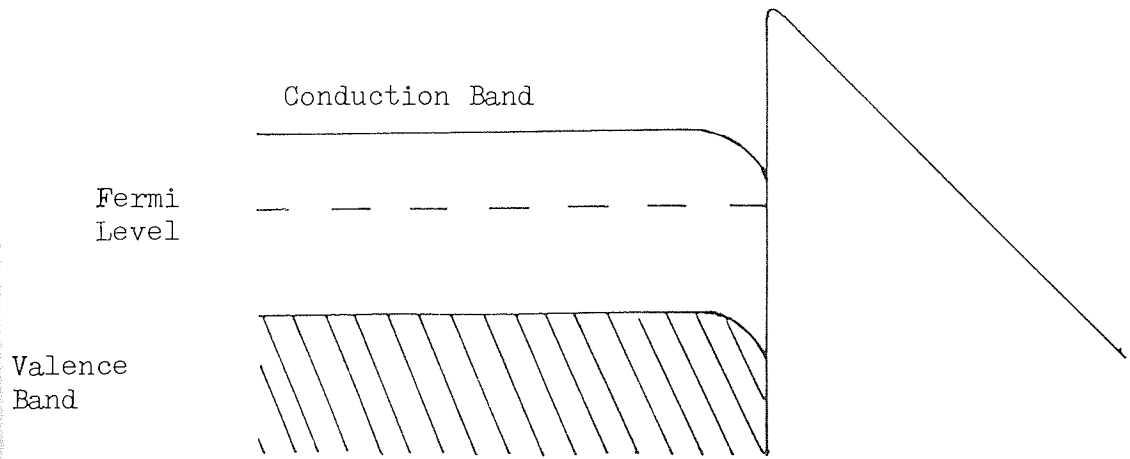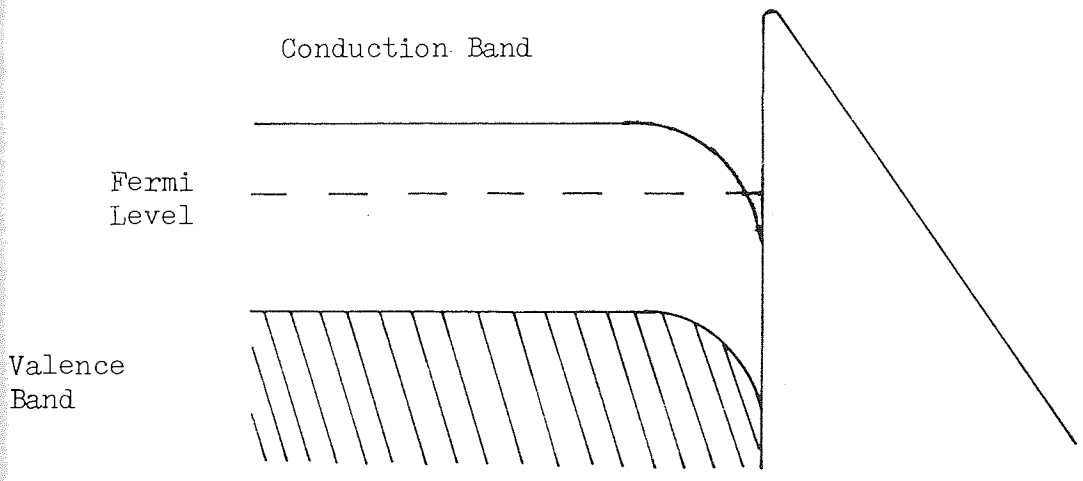
(b) DEGENERATE - HIGHER FIELD

Fig. 2.4   Electron potential diagram showing internal potential

drop due to field penetration.

ivity. The physical origin of these states has been discussed by various authers (e.g. Tam (30), Shockley (31) and Bardeen (32) but are generally assumed to be a consequence of the fact that the periodic lattace conditions, which give rise to well defined energy bands in the bulk will no longer be satisfied at the surface where there is, on the one hand, a rearrangement of the lattace atoms associated with the abrupt termination of the lattace, and on the other hand, almost inevitable existance of the imperfections and impurity atoms at the surface.

In practice, the semiconductor has both Donor and Acceptor type states, where the Donor states are positively charged when they lie above the Fermi level and therefore neutral when occupied by electrons; the Acceptor state on the other hand are negatively charged when occupied by electrons and lie below Fermi level. In the case of the n-type semiconductor illustrated in Fig. 2.5 (a), it therefore has a substantial number of Acceptor states which at absolute zero fill up to the Fermi level with electrons from the conduction band or the Donor levels. Thus creates a layer of negative charges at the surface, and consequently there is an electrostatic repulsion between these surface state electrons and the conduction band electrons within the semiconductors. This leaves a positive space charge which is entirely due to uncompensated Donor ions. The resulting strong electrostatic field directed towards the surface opposes any further flow of electrons into the surface states, or alternatively expressed, the energy of the surface is raised with respect to the bulk material represented by upward bending of the energy bands as illustrated in Fig. 2.5 (b). For a p-type semiconductor this negative charge on the surface can become zero or even positive. Thus, as the Fermi level is moved towards the valence band, the surface charge can become

18.

Conduction Band

Fermi Level
Donor Level

Empty Surface
State

Filled
States
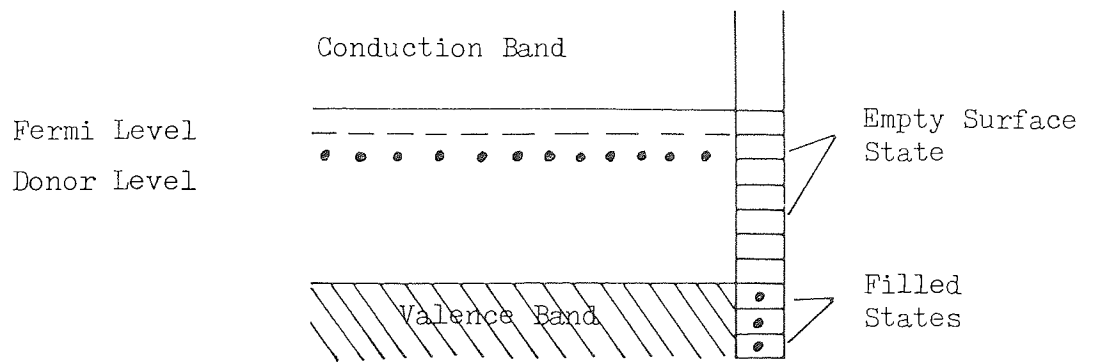
(a)   n-type before equilibrium

Conduction Band

Fermi Level
Donor Level

Ionised
Donors

Valence Band

(b)   n-type after equilibrium

Conduction Band

Acceptor Levels

Fermi Level
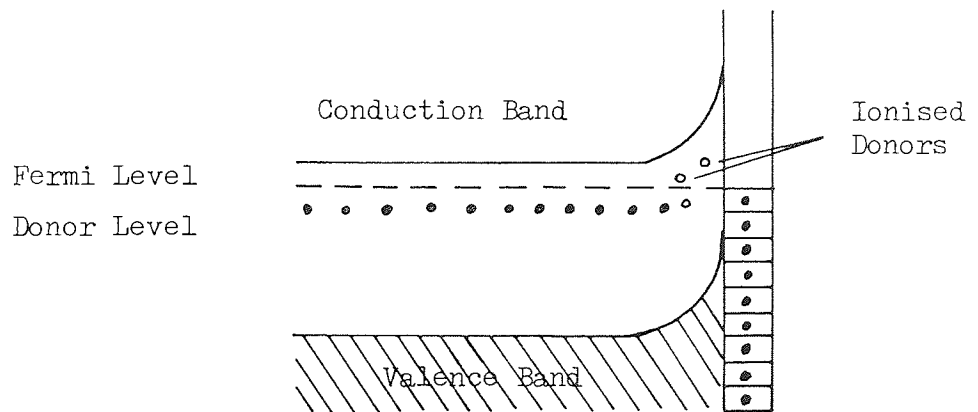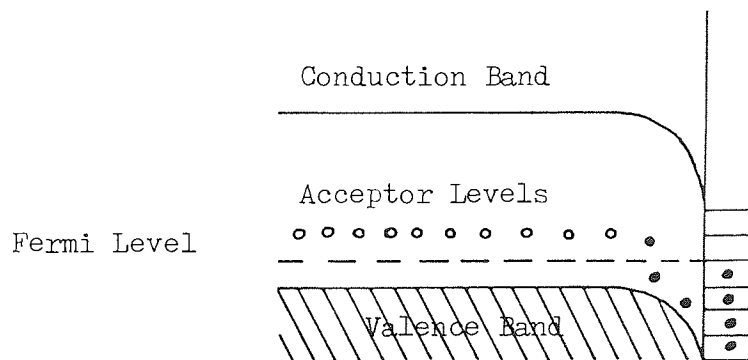
Valence Band

(c)   p-type after equilibrium

Fig. 2.5   To show the effect of surface states on the band

structure of n- and p-type semiconductor.

19.

positive. This indicates donor surface states to be close to the valence band but acceptor states nearer the middle of the band gap. Again a space charge region, in this case negative, is set up and therefore causes the potential with respect to the bulk to be reduced and this will be represented by downward bending of the band as shown in Fig. 2.5 (c).

Finally, the flow of large field emission currents through the body of the emitter can result in a voltage drop with a consequent variation of Fermi level (4, 33). Therefore, in order to determine the Fermi level, as is required in most experimental measurements due to the particular arrangement used, it is necessary to refer back to the contact. This is purely an ohmic effect and is particularly relevant in semiconductors which have a high value of resistivity compared to metals. The voltage drop is mainly concentrated at the apex of the emitter where the current densities are highest where there is also an associated Joule heating effect. The variations in the electron potential energy diagram for semiconductor, Fig. 2.6 , shows an internal potential drop due to three independant effects, (a) due to difference in work function at the metal-semiconductor interface in region (iii), (b) bulk resistivity in region (ii), and (c) due to field penetration in region (i).

2.4.1 ENERGY DISTRIBUTION OF ELECTRONS FIELD EMITTED FROM METALS.

In 1931 Henderson and Badgley (34) first employed a retarding potential analyser to measure the Field Emission Energy Distribution (F E E D) of electrons emitted from a platinum wire cathode. Even though the resolution of their instrument was very poor, they were able to show that the field emitted electrons originated from energy levels at or below the Fermi level as predicted by Fowler-Nordheim

Fermi Level

iii ii i

Conduction
Band

Valence
Band

Metal   Cathode
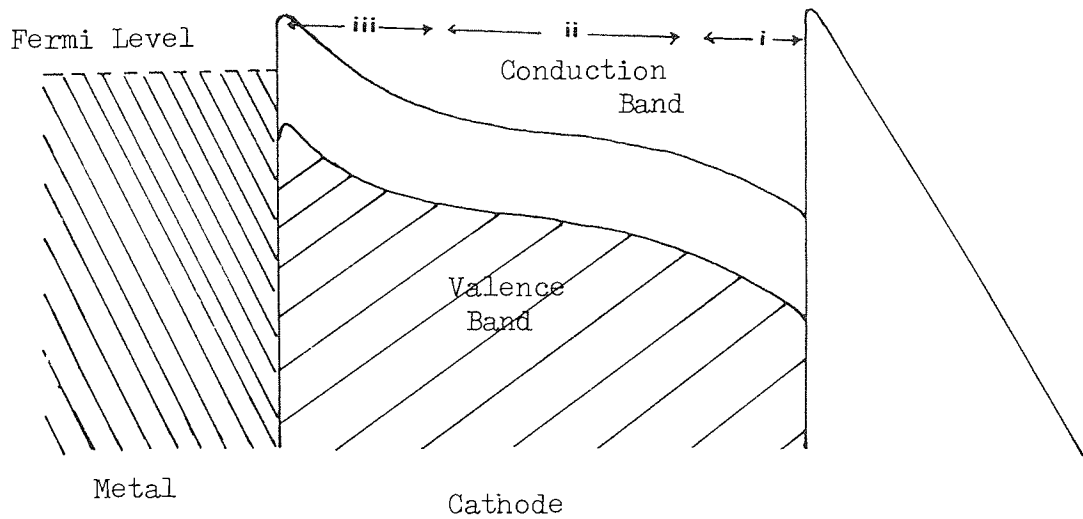
Fig. 2.6   Energy diagram for semiconductor having internal potential

drop due to   (i) field penetration   (ii) bulk resistivity

and   (iii) difference in work function [6].

theory. Subsequently, Dalstron, Mackenzie and Henderson (35), using a concentric sphere retarding potential analyser in conjunction with a micropoint tungsten emitter, measured the energy distribution and showed it to be in good agreement with that predicted by the theory, as shown in section 2.2 .

However a real break through came when Young and Muller (36) obtained the energy distributions with their new improved retarding potential analyser and found it to be a thirdof those previously recorded and that predicted by the theory. These authors therefore pointed out that the good agreement previously obtained with the theory was due to poor resolution of the instruments used. The energy distribution used in the derivation of the Fowler-Nordheim theory is the Normal Energy Distribution (N E D). This is defined as the distribution of kinetic energy associated with the component of momentum perpendicular to the emitting surface. This however is not reliable in practice, since, as soon as the electrons leave the emitter, they are acted upon by the applied field and their tangential components of velocity are converted to normal components as the electrons approach the anode; this is particularly true for the case of a spherical analysing geometry. Therefore, in these energy distribution measurements, it is the total energy distribution which is measured and not the normal energy distribution. Hence, the Total Energy Distribution (T E D) is defined as the distribution in total energy of field emitted electrons brought to a single potential outside the emitter. Therefore the total energy distribution should provide details concerning the origin of field emitted electrons, and also permit a clear mental picture of energy distribution as a product of Fermi-Dirac distribution function and exponentially decreasing penetration probability. Figure 2.7 shows the calculated plots of

TOTAL ENERGY THEORY
NORMAL ENERGY THEORY
$F = 45 \times 10^6$ V/CM
$\phi = 4.40$ ev

CURRENT PER UNIT ENERGY

ELECTRON ENERGY IN
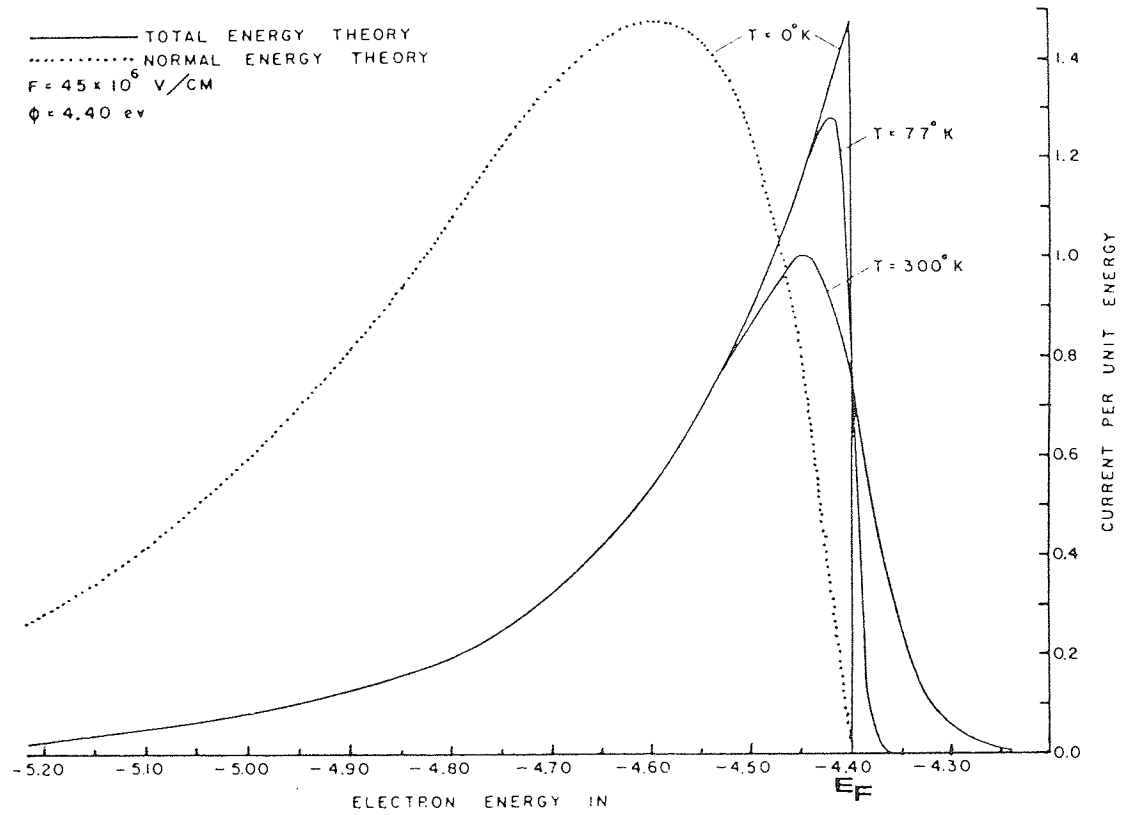
Fig. 2.7 Calculated total and Normal energy distributions at various temperatures.[37]

total and normal energy distributions at various temperatures.[37]
Young and Muller [36] also measured the total energy distribution
as a function of temperature, Fig. 2.8 (a and b), and obtained a
reasonably good agreement with the theoretical curves. This
indicates that the use of free electron model in the theory of field
electron emission is quite justified.

These measurement of total energy distributions by Young and
Muller subsequently led Young [37] to calculate total energy
distribution by re-formulating the F-N equasion. This he did by
defining some new parameters to include the concept of total energy
distribution. The new parameters are defined as follows:-

N (W, E) d W d E $\equiv$ number of electrons with total energy in the

range of E to E $+$ d E, and whose x-part of the

energy lies between W and W $+$ d W, incident on

the surface x $=$ 0 per unit area and time.

(2.19)

D (W) $\equiv$ probability that an electron with energy W will

penetrate the barrier. (2.20)

P (W, E) d W d E $=$ N (W, E) D (W) d W d E (2.21)

$=$ Number of electrons in the given energy range

penetrating the barrier.

P (E) d E $= \int_{W} P$ (W, E) d W d E (2.22)

$=$ total energy distribution
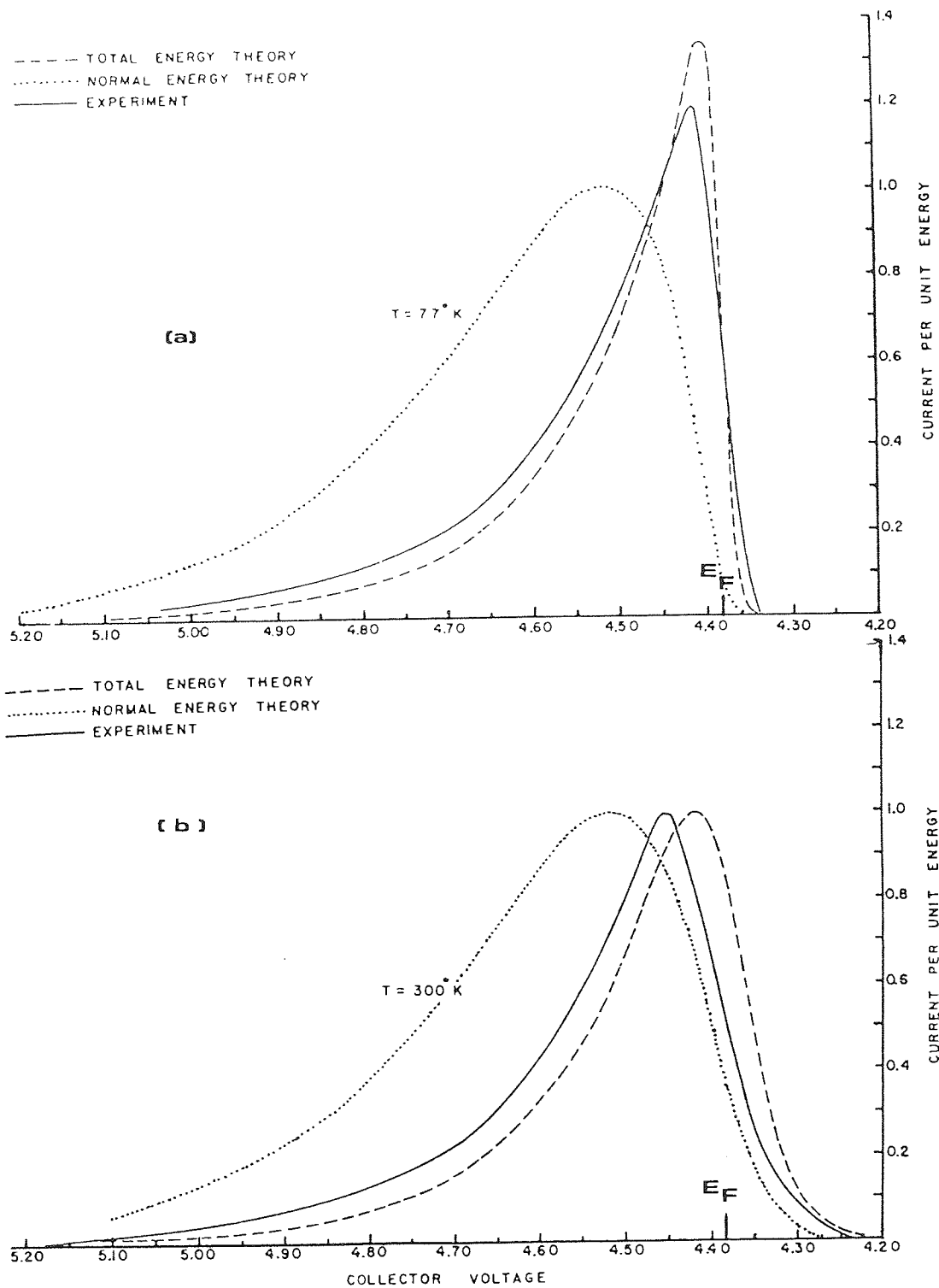
Fig. 2.8 Theoretical and experimental total-energy distribution
at (a) 77°K and (b) 300°K.[37]

$$J = e \int P(E) \, dE \qquad (2.23)$$

$= $ Electric current per unit area

$= $ Fowler-Nordheim equation

Then Young showed that the integration leads to

$$P(E) \, dE = \frac{4 \, \Pi \, m \, d}{h^3} \exp\left(-c - \frac{E_F}{d}\right) \cdot \frac{\exp\left(\frac{E}{d}\right)}{\exp\left(\frac{E - E_F}{KT}\right) + 1} \cdot dE$$

$$(2.24)$$

which is the total energy distribution of field emitted electrons, where

$$c = \frac{4 \, (2 \, m \, \phi^3)^{\frac{1}{2}}}{3 \, h \, e \, F} \times f(y) \qquad (2.25)$$

$$d = \frac{h \, e \, F}{2 \, (2 \, m \, \phi)^{\frac{1}{2}} \cdot t(y)} \qquad (2.26)$$

and $\phi = - E_F = $ work function, with rest of the parameters already having been defined earlier in the chapter. At $0 \, ^{\circ}K$ the total energy distribution is seen to have a half width of 0.14 e V as opposed to 0.48 e V for normal energy distribution. The magnitude of the maxima of the T E D decreases rapidly with temperature, whereas the magnitude of the N E D remains uneffected over a wide range of temperature as illustrated in Fig. 2.7 . It is easily shown that the energy at which the maximum in the T E D occurs is

$$E_{max} = E_F - K T \cdot Ln\left(\frac{d}{KT} - 1\right) \qquad (2.27)$$

which reduces to $E_{max} = E_F$ at $0 \, ^{\circ}K$. The half width of the T E D

at $0^{\circ}K$ is

$$\sigma(0) = 0.693 \, d \qquad\qquad (2.28)$$

The measured T E D spectra can therefore be characterised, following
the accepted convention of Young, in terms of (i) its full width at
half maximum (F W H M), normally referred to simply as "half width", and
(ii) the shift of 78% point up the high energy slope from the Fermi
level of the substrate cathode. For metallic emitters at room
temperatures, the characteristic spectrum is similar to that measured
for tungsten which is normally used as a reference, and has a half
width of 0.24 e V, a very steep energy slope width of 0.11 e V,
and the spectral shift is zero for these type of metallic emitters.
At lower energies the exponential drop found for all types of field
emitters is due to the decrease in barrier penetration.

When the measured T E D is divided by the theoretically calculated
free electron energy distribution the enhancement factor $R(\mathcal{E})$ is
obtained i.e. $R(\mathcal{E}) = J'(\mathcal{E}) / J_o'(\mathcal{E})$, where $\mathcal{E}$ is energy
E relative to Fermi energy E_F i.e. $\mathcal{E} = E - E_F$. This enhancement
factor is plotted as a function of energy and is discussed by Gadzuk
and Plummer [38]. When the results of energy distribution are
presented in this way, they reveal the fine structure contribution
which is due to non-free electrons. Such structure was first observed
from a (100) plane of tungsten by Swanson and Crouser [39, 40],
where they observed a sharp peak in T E D curve at ~ 0.35 e V below
the Fermi level. This was interpreted as being due to d-band surface
states and is clearly shown when the enhancement $R(\mathcal{E})$ is plotted
against $\mathcal{E}/d$ as in Fig. 2.9 to reveal a sharp peak at ~ 0.35 e V
below Fermi level for the particular case of the (001) direction.

Similar effects were observed from tungsten by Plummer and Bell (41).

In another study the T E D from the (110) plane of a copper crystal

grown on a tungsten micro-point emitter was measured by Jones and

Roberts (42) and found it to feature an additional peak about

0.7 e V below Fermi level as shown in Fig. 2.10 . However since

this additional peak disappears when an overlayer of copper ad-atoms

is deposited, on it ,it is therefore assumed to be due to virtual surface

states, the existence of which is said to be due to band structure

effects. These surface states exist along certain crystallographic

directions of copper and their influence on the energy distribution

from the (111) plane has been calculated by Kar and Soven (43)

who showed that the field emission spectroscopy is highly sensitive

to such states.

More recently, the F E E D of certain other metals such as

molybdenum (44), and platinum, iridium, rhodium, palladium (45)

and nickel (46) have been obtained and these exhibit deviations

from free electron theory which can be explained in terms of band

structure effects and the local density of states. In another type

of investigation Bell and Swanson (47) have studied the effects of

such parameters as emitter size, current density and work function

on the half width of F E E D measurements at extremely high current

densities (10^{10} to 10^{12} A $\underline{m}^{-2}$). They found that whilst there

was no shift in the position of the F E E D spectrum relative to

the Fermi level, there was anomalous broadening of the half width

which they explain in terms of a coulomb (space charge) interaction

in the vacuum region in front of the emitter. It was also noted

that both internal energy broadening mechanisms i.e. such as the

relaxation processes involving electron scattering in the bulk,

(48, 49) (the mechanism for replacement of emitted electrons)
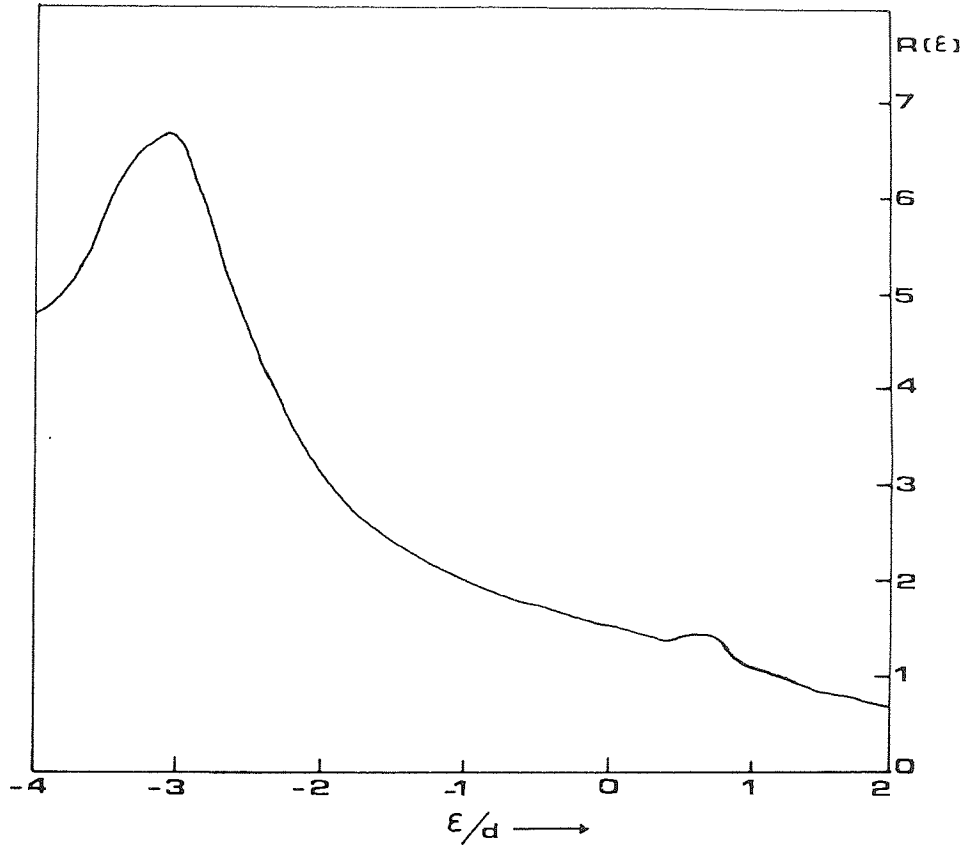
Fig. 2.9   The enhancement factor curve R( ) for the $\left[001\right]$

direction of the tungsten emitter.
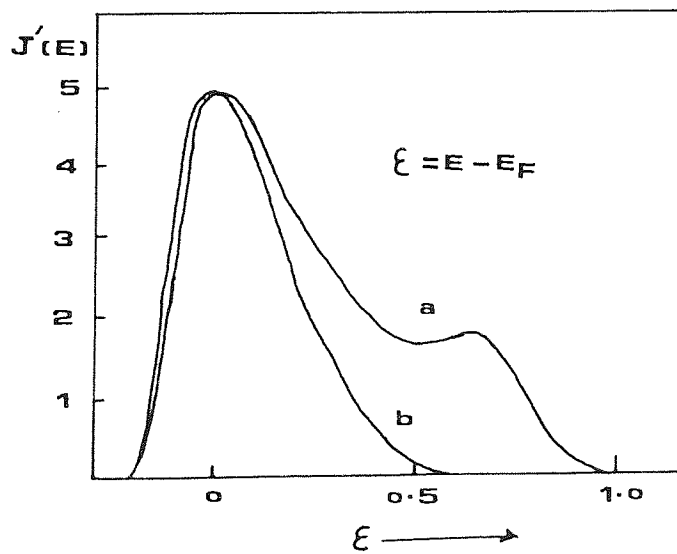
Fig. 2.10   Total energy distribution from crystal plane centres

for (a) annealed crystal (b) after addition of

5×10^{18} atoms $/ m^2$ at $28^\circ K$.

and energy broadening due to life time tunnelling (50) could not
be ruled out.

2.4.2   THE ENERGY SPECTRA OF ELECTRONS FIELD EMITTED FROM

  SEMICONDUCTORS.

Although the energy distribution of field emitted electrons
should provide an insight into the physical basis of the emission
mechanism, the interpretation can be very complicated in the case
of semiconductors where the band structure effects have to be taken
into account. The earliest comprehensive study was due to Stratton
$(6, 51, 52)$ who, through a series of papers, proposed an extensive
theoretical analysis of field emission energy spectra and the I-V
characteristic of semiconductor emitters. However, whilst he
considered the effect of surface states on the field penetration,
he did not allow for the possibility of emission from these states.
His theory therefore predicted that at low fields, emission would be
predominantly from the valence band, whilst at high fields, emission
from conduction band would become the dominant feature. In his
analysis, Stratton assumed a Fowler-Nordheim type of barrier at the
surface but modified the image force correction to allow for the
dielectric constant of the material. This barrier was then used in
conjunction with two models of a semiconductor, one with no surface
states and the other where surface states were present. In the case
of no surface states, Stratton showed that the applied field penetrates
the surface and caused the conduction band to become degenerate at the
surface, and derived an expression for the field at which this occurs.
He then extended this model in order to obtain equations for field
emitted current density as a function of applied field for the cases
of with and without field penetration.

In the second model, Stratton assumed surface states and considered the effect as the applied field is slowly increased. The main predictions of this model are shown diagrammatically in Fig. 2.11 . Initially, the applied field induces charges into unoccupied surface states, which then effectively shield the bulk from the applied field. As a result very low current densities are predicted, with valence band emission dominating the process as shown in Fig. 2.11 (a); There may however also be some contribution from the Boltzman tail of electrons in the conduction band. As the field is further increased, it is eventually able to overcome the screening effect by charges in the surface states and as a result, the field penetrates the surface of the semiconductor, and lowers the conduction band near the surface. The severity of band bending is controlled by the amount of field penetration, and when this is low, the energy distribution of Fig. 2.11 (b) is practically the same as shown in Fig. 2.11 (a), although both peaks may shift towards lower energies with respect to the Fermi level. Also at this stage, the increasing field gives rise to an increased electron population in the conduction band and hence a greatly enhanced electron emission: in consequence, the I-V characteristic displays a more rapid field dependence. At even higher fields, there is sufficient penetration to pull the conduction band edge below the Fermi level and so cause it to be degenerate near the surface. As a result, the dominant peak of the F E E D will be located at the Fermi level and is due to electrons emitted from the conduction band. The peak will have metallic like properties, i.e. exhibiting no shift with increasing field, Fig. 2.11 (c).

These theoretical total-energy plots were later modified and re-plotted by Arther (53) who considered the two cases when the conduction is non-degenerate and degenerate. For the non-degenerate case, i.e. when
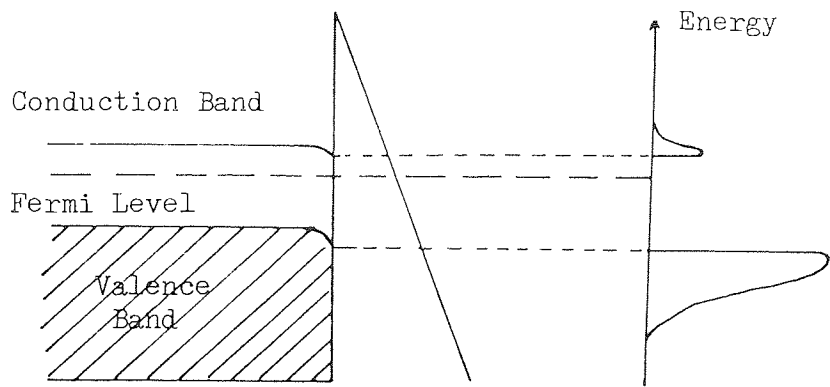
(a)
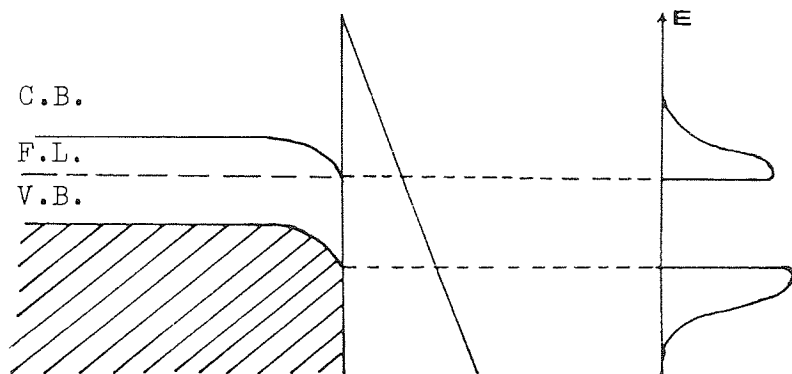
(b)
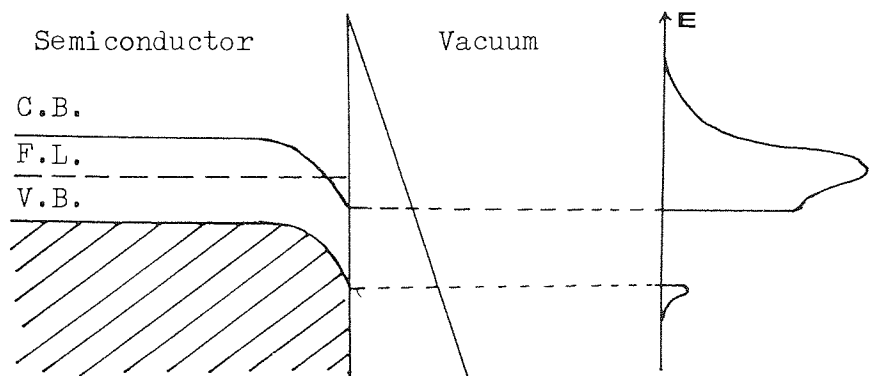
(c)

Fig. 2.11   Predicted F E E D from a semiconductor as field is

increased slowly until the conduction band becomes

degenerate.

the charge is residing in the surface states, the T E D has contrib-
utions from both conduction band and valence band. This results in
the two-peak type of distribution shown in Fig. 2.12 (a), where the
peak-separation is determined by the appropriate cut-off energies,
which will be equal to forbidden energy gap, (0.7 e V for Ge).
For the degenerate case, which Arthur calculated could approach
~ 0.3 e V for Ge at field of 4.5×10^9 V m^{-1} , the theoretical
energy distribution, shown in Fig. 2.12 (b), is seen to approach the
distribution predicted for metals (47). However the experimental
energy distributions firstly measured by Arthur (53) for Ge and
later by Hughes and White (54) and Lewis and Fischer (55) from
gallium arsenide and silicon respectively, were found to be wider
(approximately twice that found for tungsten) and different in
shape (approximately Gaussian) to that predicted theoretically for
either conduction band or valence band emission.

Modinos (7) therefore proposed that the observed energy
distribution should alternatively be explained in terms of emission
from surface states, and proposed a model to include the emission
from these states. Although his theory was specifically concerned
with the particular case of Ge , Modinos suggested that it could
also be used qualitatively to understand emission from semiconductors
in general. The model that he adopted for a Ge surface was origin-
ally proposed by Handler (56) and assumed the existance of surface
states of a uniform density and starting from well within the valence
band and extending to the lower part of the conduction band. Modinos
then used his theoretical expression to numerically calculate the
total energy distributions for p-type, intrinsic and n-type Ge for
three different fields at 300° K. As shown in Fig. 2.13 , the energy
distributions of intrinsic Ge are qualitatively very similar to that
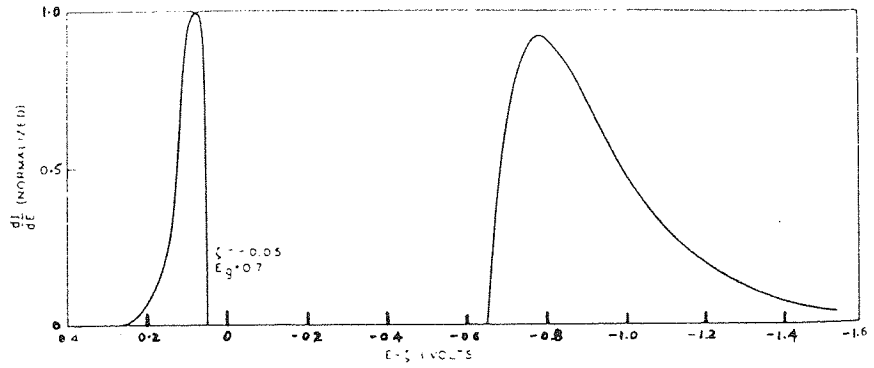
Theoretical energy distribution for emission from non-degenerate conduction
band and valence band. $F = 4.5 \times 10^7$ V/cm.

(a)
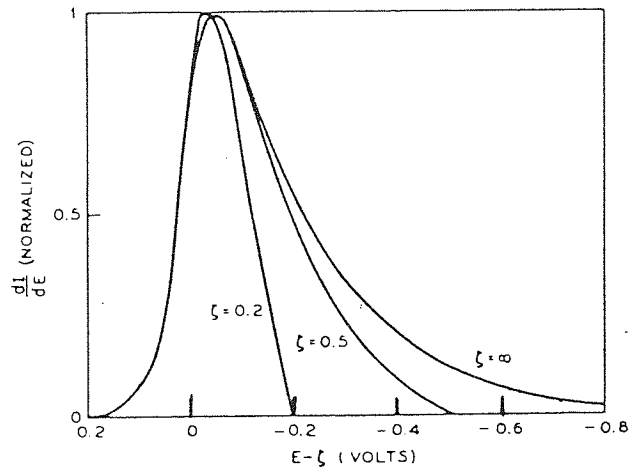
Theoretical energy distribution for emission from degenerate conduction
band. $F = 4.5 \times 10^7$ V/cm.

(b)

Fig. 2.12   Theoretical total energy distribution for Ge. (53)

34.
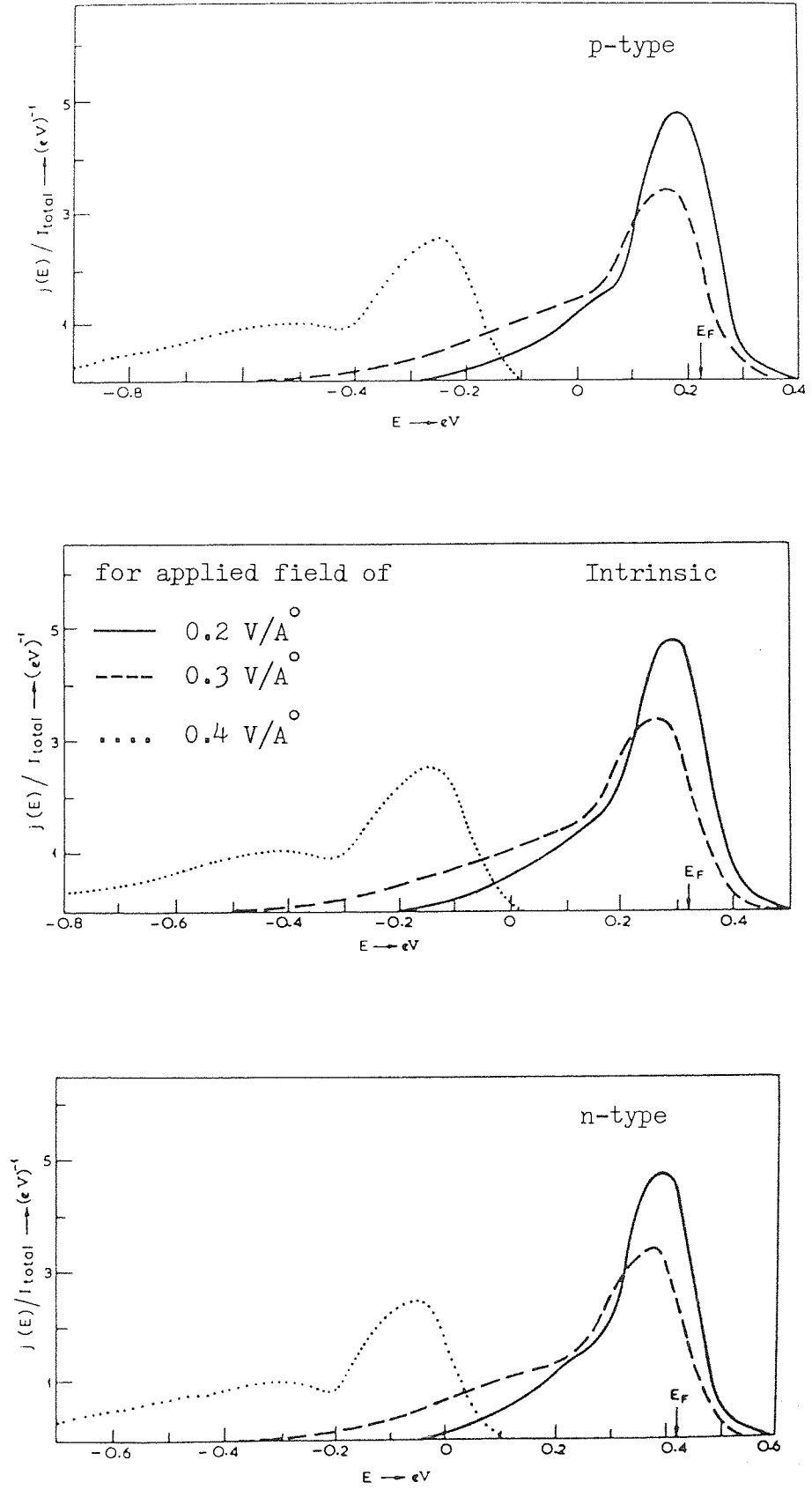
Fig. 2.13 Theoretical total energy distributions for Ge according
to Modinos (7).

of the p and n-type materials, both in terms of its shape and its position relative to their respective Fermi levels, the position of which being determined by the amount of p or n-type impurity in the semiconductor. Furthermore, the T E D shifts with respect to the Fermi level towards lower energies as the applied field is increased. This theory was primarily concerned with low emission current levels, and in general predicts that at current densities below 10^6 A m^{-2}, the majority of electrons originate from energy regions immediately below the Fermi level, with lesser contributions coming from both surface states and valence band. A particularly attractive feature of this model is that it provides an explanation of the low energy tail of the experimentally measured distributions, viz that it arises from electrons tunnelling from the valence band. The model further predicts a shift in T E D with increase in applied field, and thus current density; also that at low current densities $< 10^6$ A m^{-2} the emitted electrons mostly originate from the surface states and to a lesser extent from valence band. At higher current densities, the emission from the conduction band increases along side the emission from valence band: however the contribution due to conduction band is small relative to the total emission current. At higher fields the conduction band becomes increasingly degenerate and it can be observed intuitively that this will be accompanied by an increased current. However, the theory in its present form is not applicable to these conditions of high emission current densities.

The total energy distributions obtained experimentally for Ge emitters by both Shephard and Peria (57) and Arthur (53) confirmed the main theoretical predictions of the Modinos's model; namely, that most of the emitted electrons come from surface states and to a lesser extent from the valence band. It was also confirmed that the

T E D was generally characterised by a high energy peak correspond-
ing to emission from surface states and low energy peak arising from
valence band emission. However, the predicted position of the high
energy peak, which according to the model should be immediately
below the Fermi level, was less well confirmed: Thus, whilst the
work of Arthur [53] was in agreement with the theory, that of
Shephard and Peria [57] showed the high energy peak to lie between
0.6 to 0.7 e V below Fermi level. Such inconsistencies high-light
the theoretical difficulty in interpreting the many complicated
effects that can arise from the many ways in which the band structure
of a semiconductor can be affected. Clearly therefore, the theory of
field emission from semiconductors must be regarded as in its infancy.

2.5   FIELD ELECTRON EMISSION FROM COMPOSITE REGIMES.

The realisation that copious electron emission can occur from
composite structures consisting of a metallic substrate overlayed by
a dielectric material arose out of studies into the origin of pre-
breakdown electron emission between broad-area high voltage electrodes
[20]. Typically this type of emission occurs at fields of 5 to
10 M V m^{-1} and, in common with the metallic Fowler-Nordheim emission
mechanism discussed earlier, has I-V characteristic that give a
linear plot of Ln (I/V^2) versus (1/V).

The pre-breakdown currents were originally thought to stem from
micron-sized metallic protrusions or whiskers on the electrode surface, where
the microscopic gap field was enhanced by a factor β; typically
$\sim$ 100 - 1000 [58, 59, 60], as determined in-directly from the
F-N plots. However several recent experimental studies [20, 61]
have shown that this interpretation has several weaknesses. Firstly
it has not been possible to observe such protrusions on virgin or

un-arced electrodes (62, 63). Secondly, Farrall et al (64, 65)

have obtained indirect evidence that emission occurs from insulating

inclusions (e.g. Si).

Thirdly Cox and co-workers (66, 67) developed an -anode- hole

probe technique for locating emission sites (with greater accuracy)

in situ in a S E M, but failed to observe any direct evidence of any

projections which could justify high β-factors $\gtrsim 250$ and widely

varying emitting areas. Fourthly, there is an associated optical

emission phenomenon with this type of emission process with wavelength

spread of 500 to 750 n m. This was investigated by Hurley and Dooley

(68) and Hurley (69) for various types of cathodes and shown to

be electroluminescent in origin, i.e. obeying the Alfry-Taylor

relation, and hence was inconsistent with the metallic field emitting

protrusion model. Therefore Hurley suggested that the observed

electron emission and associated electroluminescence originated from

semiconducting type of inclusions. Lastly, inconsistencies of the

"metallic" emission model were pointed out by results from F E E D

measurements, where it is well established that the electrons

emitted from a particular field emission process have a characteristic

energy spectra. Thus Allen and Latham (19) measured the energy

spectra of electrons field emitted from individual cathode sites and

on comparing the typical energy spectra obtained with that from a

reference tungsten micro-point emitter Fig. 2.14 , three important

differences were identified, i.e.

(i) the spectrum is shifted towards the lower energies by $\gtrsim 0.4$ e V.

(ii) the spectrum is broader by at least 0.1 e V.

(iii) the shape of the spectrum is more symmetrical, lacking the

characteristic sharp . . high energy slope present in the spectrum

from a metallic emitter. In a later investigation (67, 70) a 10 μ m

(a)

(b)

FL   O 2eV   ENERGY decreasing
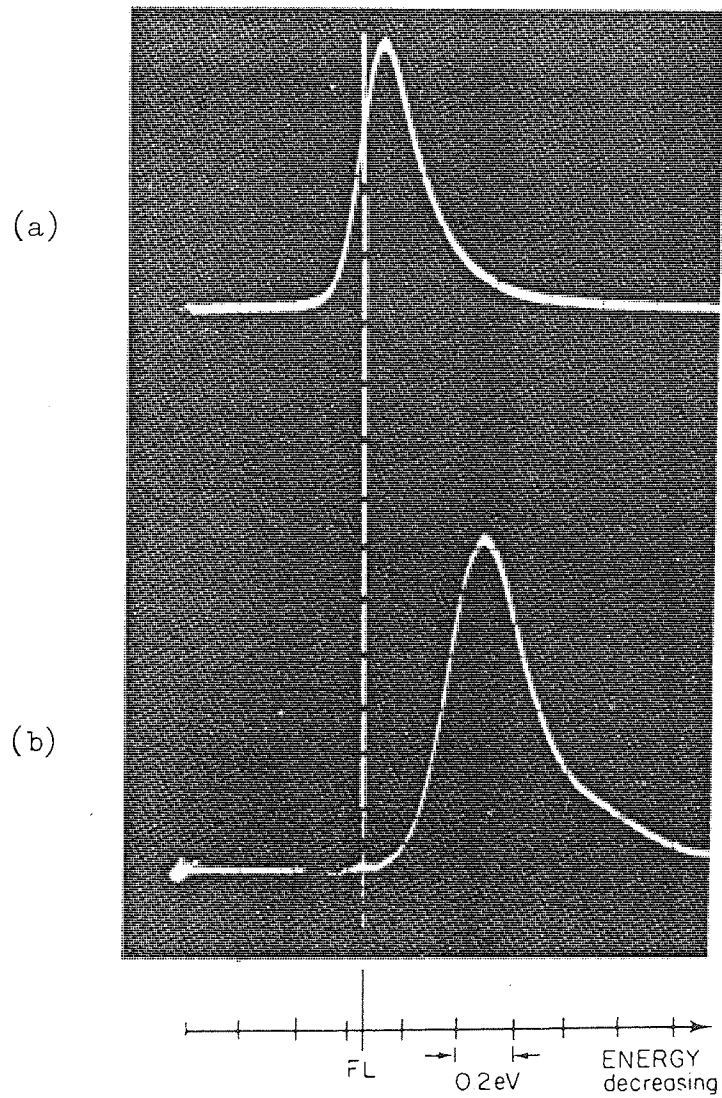
Fig. 2.14   Electron energy spectra obtained from   (a) a reference
tungsten micropoint emitter, and   (b) an emission site
on broad-area copper electrode (19).

site location technique showed that emission sites are frequently associated with insulating type of inclusions.

Summarising therefore, such localised emission sites are characterised by having: (i) linear high-β ($\gtrsim 200$) Fowler-Nordheim I-V characteristics, (ii) no significant field enhancing surface structure, (iii) associated electroluminescence effects, and (iv) electron emission spectra that are typically shifted by 0.4 e V towards lower energies.

On the basis of such findings, the electron emission from broad-area electrodes is now thought to originate from composite regimes consisting of a metallic substrate overlayed by insulating or semi-conducting impurities, rather than from metallic micro-protrusions. As will be described later in this thesis, the carbon fibre micro-point emitters have remarkably similar characteristics. Because of the importance of this emission mechanism to the present investigation, a brief review will now be given of the physical models that have been proposed to explain this phenomenon.

2.5.1 ELECTROFORMED FILAMENTARY MODEL.

This interpretation of the electron emission process observed on high voltage electrodes was due to Hurley (69, 71) and is based on the model proposed by Dearnaley (72) for "electroformed" insulating/semiconducting layers sandwiched between two metal electrodes. On the application of a high electric field to these films, particularly oxides, nitrides, flourides and amorphous semiconducting glasses of thickness between 10 n M to a few microns, they exhibit a well known Ovshinsky-type switching (73, 74) phenomenon of typical switching time < 1 μ sec. The device switches from a non-conducting, "OFF" to a highly conducting, "ON" state, where the conductivity of

the film may increase by as much as 10^8. If however the field is

applied for a sufficient length of time, typically between a millisecond

to a second, the *filament* becomes "electroformed" through the permanent

or semi-permanent rearrangement of the atoms or molecules. In this

state, it exhibits a range of interesting phenomena such as a negative

resistance region in the I-V characteristics, electron emission and

electroluminescence; the latter two of which are also common to the

hot-electron model [75] described later.

Dearnaley [72] explains the observed phenomenon in terms of

the growth of the conducting channels or filaments during the switch-

ing and subsequent electroforming process, where the cross-sectional

diameters of these channels are thought to be dependant on the film

thickness. The negative resistance region is interpreted in terms of

the rupturing of a filament, then almost all the applied voltage will

be dropped accross it and as a result, the electrons are accellerated

as hot carriers and are subsequently emitted through the top of the

electrode. However, some electrons will be scattered at this high

resistance spot into the surrounding semiconductor giving rise to the

electroluminescence. In his model, Hurley [69, 71] suggests that

similar channels are formed in the oxide layers on the electrodes as

illustrated in Fig. 2.15 . In such a configuration, the electro-

formed filament behaves rather like a metallic-like whisker, and hence

provides the necessary local field enhancement for "metallic" field

emission, whilst high resistance spot gives rise to the observed

electroluminescence effects. From other experimental evidence,

Hurley [76] points out that the random fluctuations in the current

emitted from the site also corresponds to the fluctuations in the

associated emitted light intensity. It is also relevant to note that

the current flow in the filament also leads to Joule heating and at a

Emitted Electrons

Local intensification of field produces field emission of electrons

Photons emitted by the decay of excited states

VACUUM

High energy electrons scattered into dielectric from high resistance spots

OXIDE

Variation in stoichiometry of interface may produce junction effects at electron source

METAL
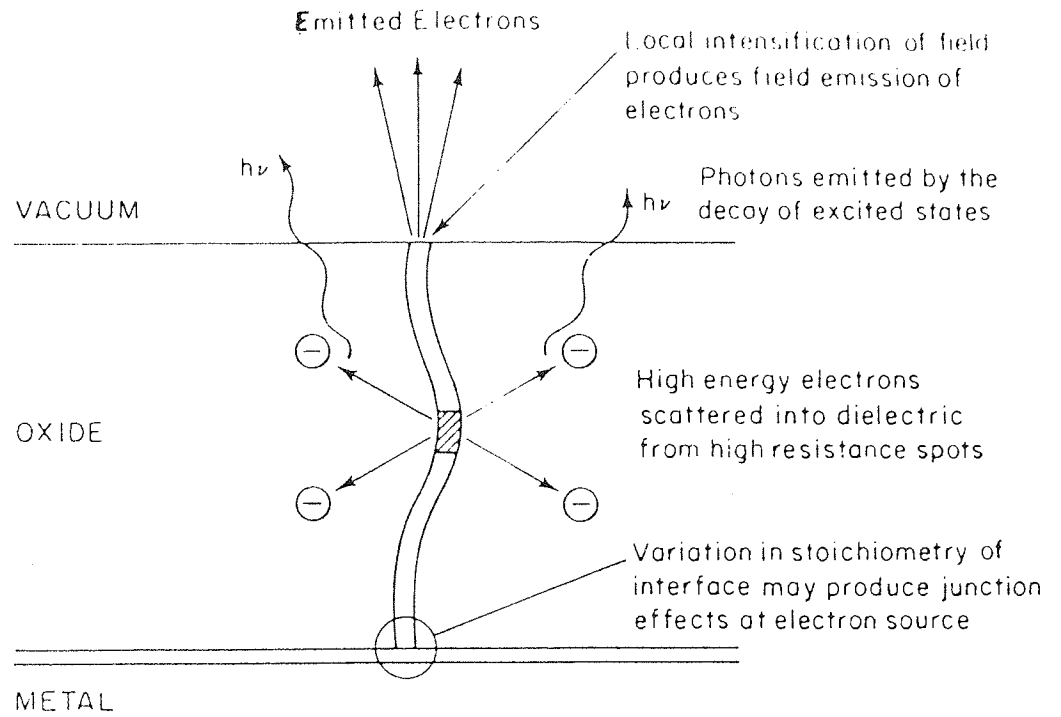
Fig. 2.15 Electron emission from an electroformed conducting filament in an oxide micro-impurity.[18]
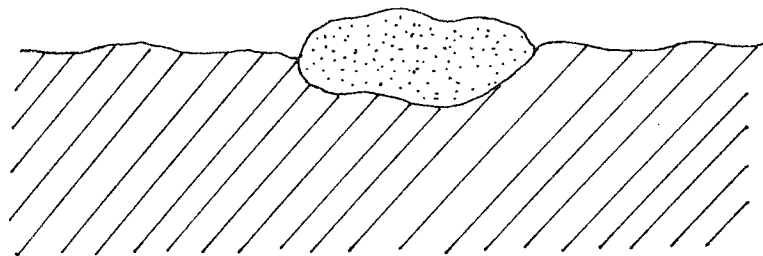
Fig. 2.16 The insulating microregime responsible for electron emission processes on broad-area electrodes.[18]

certain current level, the channels would become thermally unstable and eventually 'explode' to eject the molten impurity and thus lead to voltage breakdown between the broad-area electrodes.

With this model, some of the irregularities observed in the I-V characteristics can now be plausibly explained in terms of thermal rupturing, or possible reforming of the filaments or "switching on" of a new filament. This model also provides an explanation for the suppression of the emission current and the electroluminescence by "active" gases such as O_2 , CO and N_2 , experimentally observed by several authors; (77, 78, 69) i.e. it is assumed that the filament becomes poisoned as discussed by Dearnaley (79).

2.5.2   THE HOT-ELECTRON INSULATOR SWITCHING MODEL.

The original model proposed by Latham and his co-workers (70, 80) emerged from detailed electron spectroscopy measurements of the microscopically localised field emission processes on broad-area high voltage electrodes. It is based on the physical emitting regime of an insulating micro-impurity in intimate contact with, or partially embedded in, the metallic electrode material as shown in Fig. 2.16 . The existance of such processes involving insulating material rather than semiconducting material is strongly supported by electrolumines-cence effects. In fact their spectra, which typically lies in the range of 500 - 750 n m (69), also confirm that the band gap of the emitting regime must be $\gtrsim$ 2.5 e V; i.e. indicating it to be insulat-ing material. From the point of view of promoting a continuous emission, such a material, by having favourably low dielectric constant with $\mathcal{E}_r \longrightarrow 1$, satisfies the requirement for the complete initial field penetration. In the absence of the applied field, the band structure of such a composite regime is illustrated in Fig. 2.17(a)

43.
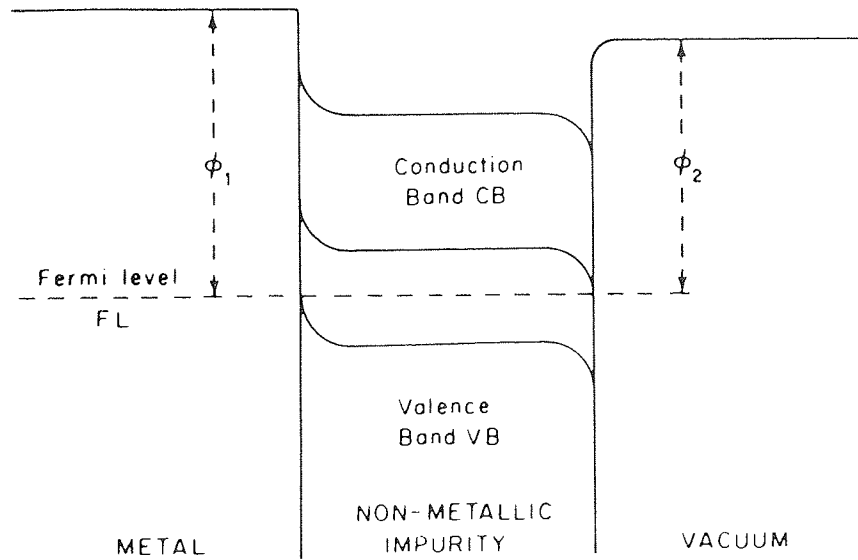
(a)
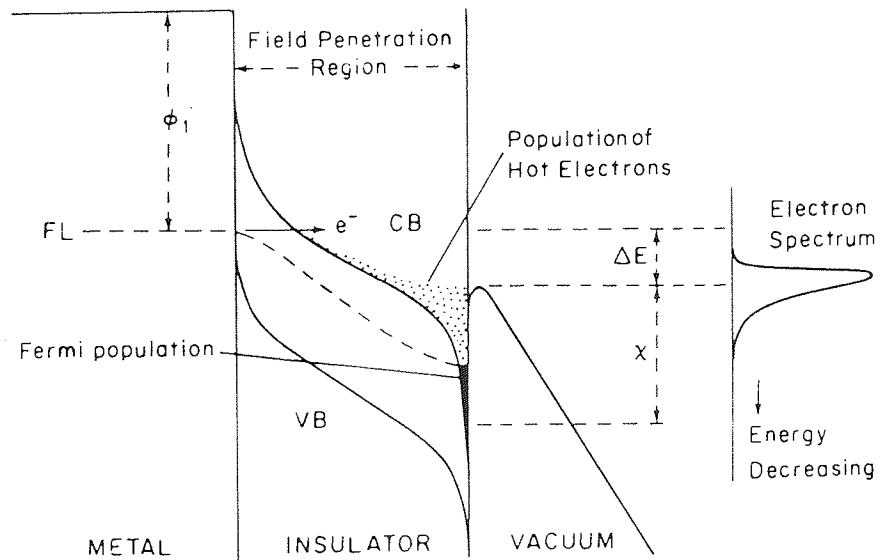
(b)

Fig. 2.17 Energy band configuration of the composite microregime at (a) zero field, and, (b) a high field.[18]

where the distortion in the band structure at the two interfaces is due to the difference in the work functions $\emptyset_1$ and $\emptyset_2$ of the substrate metal and the micro impurity. When a high external electric field is applied to the insulating impurity, the dielectric properties of the impurity allows the field to penetrate right up to the electrode material to give the very highly distorted band structure Fig. 2.17 (b). This high distortion, particularly at the metal-insulator interface, provides the necessary conditions for electrons from the Fermi level of the metal substrate to tunnel into the bottom of the conduction band of the impurity. Where these electrons come under the influence of the penetrating field, they are consequently accelerated or "heated" by several electron volts so that they are able to acquire sufficient energy to escape over the depressed surface potential barrier. As a result, the spectrum of these emitted electrons is shifted with respect to the metal substrate Fermi level, (i.e. Fig. 2.17 (b). However this model did not readily explain how a significant number of the hot electrons are able to cross the micron-dimension layer of insulating material without losing some or most of their energy through phonon scattering processes, whilst the filament model does not correctly account for the shift in electron spectra from the Fermi level.

To overcome these limitations, Athwal and Latham [75] revised their original model to include the Ovshinsky type of "switching" processes [73, 74] that is precipitated by an avalanche in the insulating material. According this model, the process is initiated by one or more electrons tunnelling from the Fermi level of the metal substrate into the conduction band of the insulating impurity. Here they experience an accelerating field that penetrates through the insulator and hence causing these electrons to be heated. These

initial population of hot electrons then undergo electron-phonon

scattering processes and thereby create further charge carriers by

the production of electron-hole pairs by impact ionization which

rapidly gives rise to a current avalanche. Following the ideas of

Adler, Henisch and Matt (81), it is then assumed that these elec-

trons and holes migrate respectively to the localised states at the

insulator-vacuum interface and the metal-insulator interface, and

gives rise to the necessary high field conditions to cause the insulating

material to undergo a transition in the form of an Ovshinsky type of

threshold switching (73) to the more stable high conductivity "ON"

state depicted by Fig. 2.18 . On switching, there is a rapid

rearrangement of energy band configuration of the model illustrated

in Fig. 2.17 (b) to that illustrated in Fig. 2.18 , where the emission

regime is now characterised by two high field regions located at the

two interfaces. Under these circumstances, electrons will tunnel

from the metal accross the first high field region, are then rapidly

thermalised and thus are able to cross the extended low field region

in the bottom of the conduction band of the insulating material where

their life time can be 10^{-8} s (82). The electrons then enter the

second high field region in front of the insulator-vacuum interface,

where they are again heated through the necessary 2 - 3 e V, required

firstly for electrons to escape over the depressed surface potential

barrier into vacuum, and secondly for exciting the electron transi-

tions responsible for generating the electroluminescent photons known

to be associated with the emission process (76). Two mechanisms

may be considered for the production of these photons. In the first,

a hot electron creates an electron-hole pair by impact ionization,

following which the hole starts to migrate towards the metal but soon

gives up its energy to excite a luminescent centre. The optical
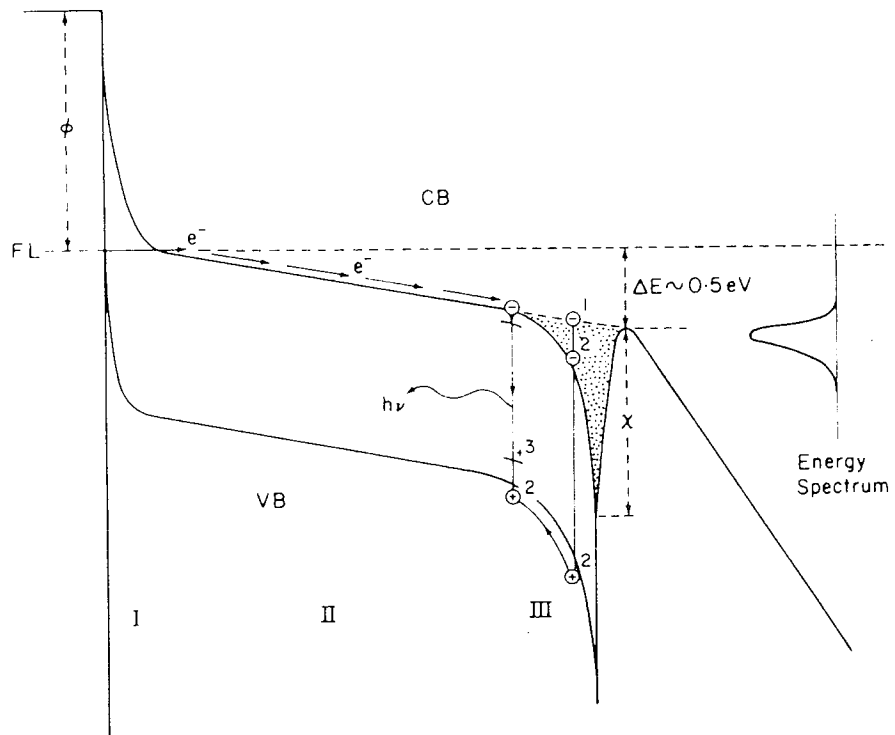
Fig. 2.18 Energy band configuration of composite microregime after "switching" to a high conductivity state.[18]

emission then occurs as a result of the recombination event with a conduction band via an excited state. In the second mechanism an electron-hole pair would be produced by the field ionization of a luminescent centre in the high field region. The typical optical spectra expected then would lie between 500 - 750 n m which is close to that found experimentally.

With this model, Athwal and Latham [75] were able to explain the experimentally observed electron spectral shift of 0.2 e V to 0.5 e V with respect to substrate Fermi level for emission sites on broad-area electrodes as being due to three main contributions. Referring to Fig. 2.18 , these are (i) the energy lost when electrons are thermalised into the bottom of the conduction band in region I, (ii) ohmic energy loss in region II, and finally (iii) the energy lost in region III due to electron-phenon scattering. Since all of these processes are dependant on the tunnelling current, it could be anticipated that the spectral shift would increase with increasing applied field. In fact this was very clearly demonstrated experimentally by Athwal and Latham [75] and their findings are illustrated in Fig. 2.19 .

This theoretical model has been quantified by Latham [20], by making the initial assumption that the population of hot electrons in insulator conduction band in the high field region III obey Maxwell-Boltzman statistics, so that the emission mechanism could be treated as a quasi-thermionic process. Then, by analogy with the Richard-Dushman relation, the emitted current density would be given by

$$ J = A T_e^2 \exp \left(\frac{- e \phi_x}{K T_e} \right) \qquad (2.29) $$

where, here T_e is the field-enhanced temperature of the hot electrons

(i)

(ii)

FL 0·2eV/division ENERGY (decreasing)
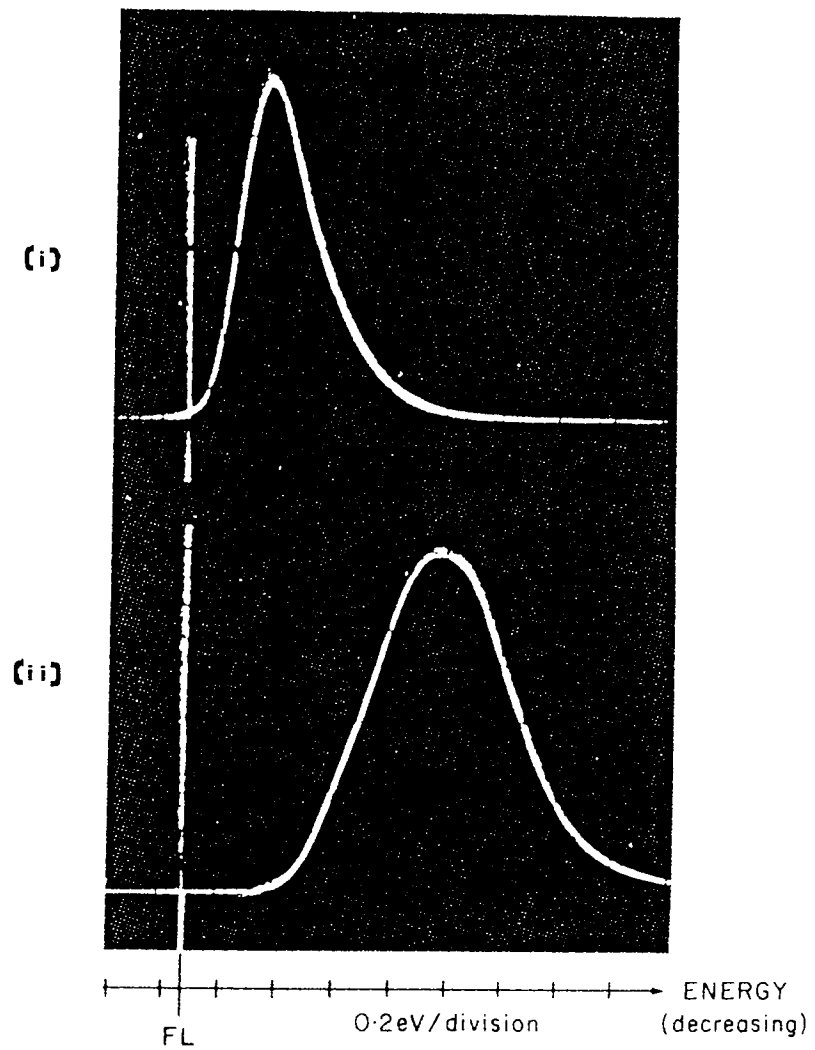
Fig. 2.19 Energy spectra of electrons field emitted from the microregime under (i) low-field and (ii) high-field conditions.[18]

in region III and ϕ_x is the surface potential barrier height at the insulator-vacuum interface; i.e. the electron affinity. Then if V is the potential drop accross the high field region due to the field penetration, we have

$$e \, \Delta V = \frac{3}{2} \, K \, T_e \qquad (2.30)$$

Then assuming that ΔV can be approximated by the potential drop that would exist accross the insulating inclusion due to field penetration on the application of an external field (due to dielectric properties of the insulator) as illustrated in Fig. 2.17 (b) one has

$$\Delta V \simeq \frac{1}{\mathcal{E}} \cdot \frac{\Delta d}{d} \cdot V \qquad (2.31)$$

where d is the electrode separation, Δd the thickness of the insulating micro-regime (where $\Delta d << d$), and $\mathcal{E}$ is relative dielectric constant of the insulator. Substituting now (2.30) and (2.31) in (2.29) gives

$$J = A \left(\frac{2 \, e}{3 \, K} \, \frac{\Delta d}{d} \cdot \frac{1}{\mathcal{E}} \right)^2 V^2 \cdot \exp \left(- \frac{e \, \phi_x}{K} \cdot \frac{2 \, e}{3 \, K} \cdot \frac{\Delta d}{d} \cdot \frac{1}{\mathcal{E}} \cdot V \right) \qquad (2.32)$$

Finally if a is the effective emitting area, the total emitted current from the site will be given by

$$I = Ja = Aa \left(\frac{2 \, e \cdot \Delta d}{3 \, K \, d \, \mathcal{E}} \right)^2 \cdot V^2 \cdot \exp \left(- \phi_x / \left(\frac{2 \, \Delta d}{3 \, d \, \mathcal{E}} \right) \cdot V \right) \qquad (2.33)$$

Thus when this is plotted in the form of Log (I/V^2) against ($1/V$), (i.e. equivalent to a normal F-N plot) it should give a

straight line of a slope

$$m = -3 \phi_x \, d\mathcal{E} / 2 \triangle d \qquad\qquad (2.34)$$

It should be noted that in terms of the traditional F-N interpretation of pre-breakdown currents, where the slope is given by

$$m_{F-N} = \frac{-2.84 \times 10^9 \, d \, \phi^{3/2}}{\beta} \qquad\qquad (2.35)$$

it will be seen from a comparison with equasion (2.35) that the field enhancement factor β in this case has the physical significance

$$\beta = \frac{1.89 \times 10^9 \times \phi^{3/2} \cdot \triangle d}{\phi_x \cdot \mathcal{E}} \qquad\qquad (2.36)$$

Finally the observation that the field dependance of the spectral half-width (75) is in good quantitative agreement with the theoretical dependance for thermionic emission (37), viz

$$(\triangle E)_{\frac{1}{2}} = 2.45 \, K \, T \qquad\qquad (2.37)$$

which from equasions (2.30) and (2.31) becomes

$$(\triangle E)_{\frac{1}{2}} = \frac{1.62 \triangle d}{\mathcal{E}} \cdot E \qquad\qquad (2.38)$$

where E is the applied field.

The composite emission regime model discussed here is based on very complex physical phenomena that are far from fully understood, mainly due to the difficulties in knowing the exact nature and composition of these micron-sized emission regimes. However, even in its present relatively simple form, it offers a very plausible

explanation for experimental observations from not only emission

sites on broad-area electrodes, but as will be discussed in chapter 3

also the emission from carbon fibres micropoint emitters.

CHAPTER 3

CARBON FIBRE AS FIELD EMISSION SOURCE.

3.1 THE NATURE OF HIGH-MODULUS CARBON FIBRES.

3.1.1 Introduction.

It has long been recognised (3) that the properties of a
field emission source, viz its small size, small energy spread, high
current density and non requirement of   heater power, has important
practical advantages over the conventional thermionic cathode. In
the majority of   field emission studies, the most commonly used
material for the field emitter has been tungsten. However if these
emitters are operated in systems with pressures greater than 10^{-7} m bar,
the emission becomes highly unstable and the life time of the source
is reduced to a few seconds. Therefore to satisfactorily operate
such an emitter, it is not only necessary to have an ultra high
vacuum of $\lesssim 10^{-10}$ m bar, but also provisions for the in situ cleaning
of the tip (12). The tungsten emitter also suffers from the
disadvantage of being readily destroyed by discharge events such as
would arise from the excessive localised emission associated with an
electrical breakdown.

For the present application, which requires an emitter to
operate in the pressure range of 10^{-5} to 10^{-7} m bar an alternative
material to tungsten is necessary. In this context, the work of
Baker et al (13) is particularly important since it showed that
carbon fibre offered considerable promise as being such an emitter
material. Interest in carbon fibre in fact extends back to 1880

when Edison (83) developed the electric light filament by carbon-
ising various fibrous organic precursors. Commercial carbon fibres
have been in existance since the late 1950's, initially they were
made from rayon precursors, but later from polyacrylonitrile, lignin
and pitch fibres. However the exceptionally high theoretical strength
and elastic moduli of long fibres were not achieved until the 1960's,
when a method of manufacturing highly orientated crystalline fibres
was discovered. This was done by subjecting the precursor fibre to a
continuous tensile stress during a high temperature treatment (84,
85, 86). The modern industrial production techniques used to
produce high strength high Modulus commercial carbon fibres will now
be discussed.

3.1.2 <u>PRODUCTION TECHNIQUES OF COMMERCIAL CARBON FIBRE</u>.

The starting material for manufacturing a high performance
carbon fibre is a precursor of organic fibres, of which polyacrylo-
nitrile (P A N) is the most commonly used. The ultimate properties
of a P A N-based carbon fibre are mainly determined by the processing
temperature during manufacture. Initially, tows of P A N fibres
containing approximately ten thousand individual fibres are produced,
then the conversion of this precursor to the final carbon fibre is
completed in two main stages, viz oxidation and carbonisation as
shown in Fig. 3.1 . During the oxidation process, the tows of P A N
fibres are wound onto frames to restrain them from shrinking (which
would otherwise be of $\sim$ 75%). Accordingly, the fibres are put
under a high strain during their heating to 220°C in an air oven.
During this process, the molecular structure of the fibre is changed
from linear polymer to an oxidised ladder polymer, by the conversion
of the thermo-plastic P A N into a cyclic or ladder compound, this prevents

Special
Acrylic Fibre

Oxidation

Carbonization

Surface
Treatment

inert
gas

Grafitization

Oxidised
Acrylic Tow
Grafil 'O'

1

2

3
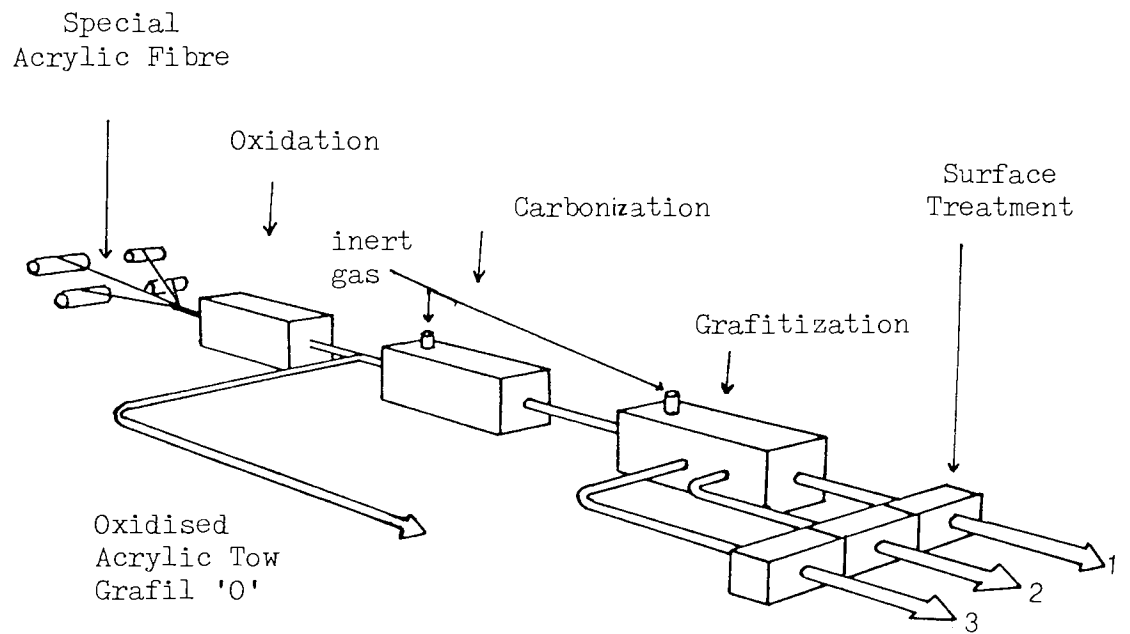
(1) Grafil H M-S

(2) Grafil X A-S

(3) Grafil A-S

Fig. 3.1 Grafil Manufacturing Process of Carbon Fibres.

the fibre from melting during carbonization. The ladder polymer

structure is approximately parallel to the fibre axis and may be

regarded as the template for the formation of the orientated carbon

fibre. After the oxidation process, the fibres are removed from the

frames and then successively carbonized in an inert gas atmosphere

at temperatures of 1000° C and then between 1500 and 3000° C. During

this treatment, H_2 , N_2 and O_2 atoms are driven off together

with some products of thermal decomposition. The already cross-linked

molecular chains then rearrange themselves to form a familiar plate

like crystalline structure of graphite. The extent to which the

graphatization proceeds depends on the processing temperature. By

altering the temperature, a range of fibres of varying strength and

modulii can be produced as illustrated in Fig. 3.2 . Therefore it

is possible to produce a family of carbon fibres with various com-

binations of properties that can be suited to particular requirements.

Finally, after carbonization, the fibres are surface treated where

the final products are carbon fibre type A - high strain, X A - high

performance and H M - high modulus.

3.1.3 THE STRUCTURE OF CARBON FIBRE.

Before considering the structure of the high modulus carbon

fibres, it is useful to briefly consider the atomic structure of the

graphite crystal. The hexagonal crystal structure shown in Fig. 3.3

has two important features. Firstly, there are the planar layers, in

which an extensive array of carbon atoms are joined by shorter

(1.415 $\overset{\circ}{A}$) covalent bonds, and secondly, there is relatively large

separation (3.354 $\overset{\circ}{A}$) between these layers. Each carbon atom is

covalently bonded with the neighbouring atom in the same layer but the

layers themselves are held together by weak Van der Waals forces, and
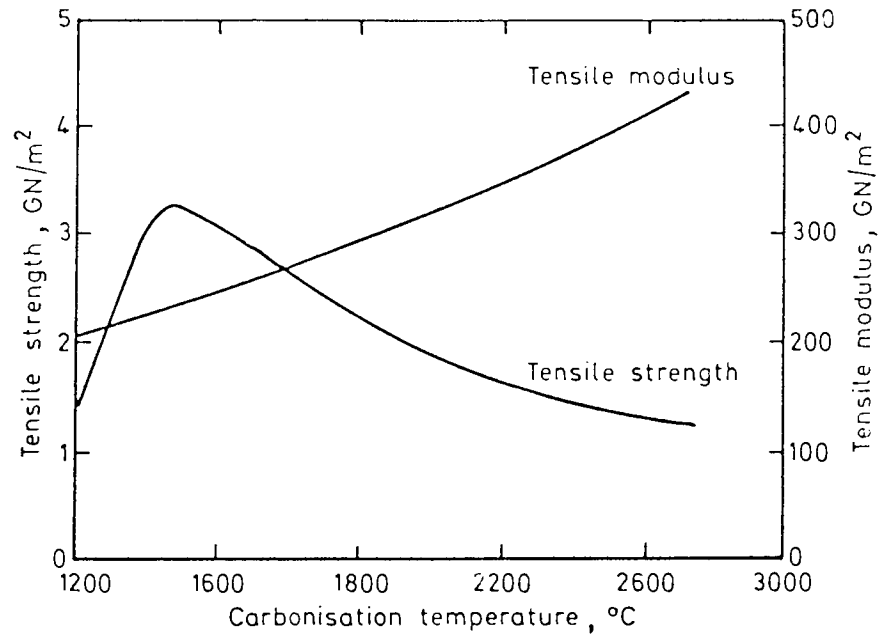
Fig. 3.2 The effect of carbonization temperature on the properties of the carbon fibre.
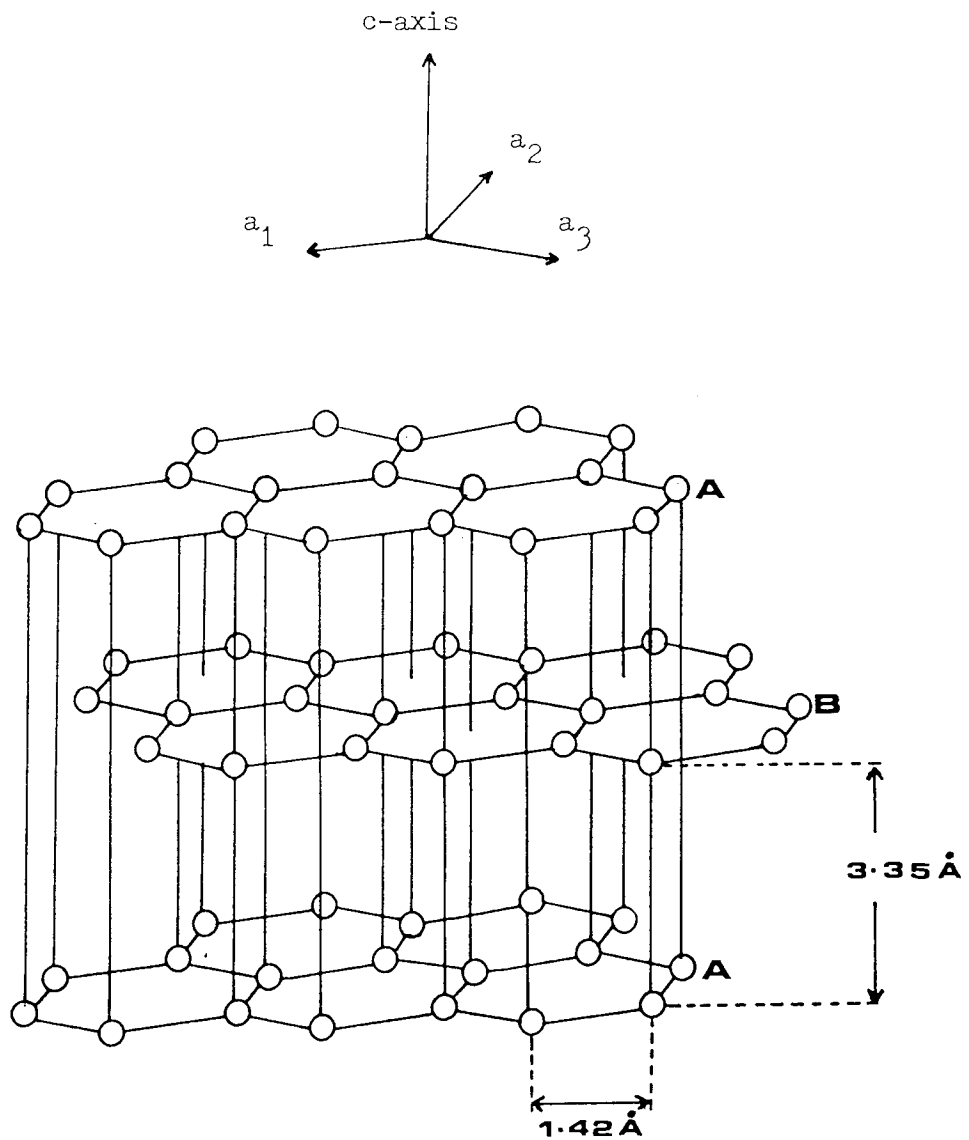
Fig. 3.3 Atomic arrangement in the graphite form of carbon.

stacked together in a hexagonal A B A sequence as shown in Fig. 3.3 .
The layer structure of graphite explains many of the peculiar features
of the material; in particular, the importance of the orientation in

polycrystalline graphite. In graphite, with its highly aniso-
tropic crystalline structure, a high modulus of elasticity is there-
fore found when stress is applied in the direction parallel to layer
plane (a-direction), where the measured Young's modulus is
1020 G N m^{-2}, but a low modulus of only 36.36 G N m^{-2} is found
when the stress is applied in direction perpendicular to layer planes
(87) (c-direction). The orientation of the layer planes relative
to the carbon fibre axis can therefore be expected to have a con-
trolling effect on the fibre modulus because of the exceptional
anisotropy of the graphite structure. It is found that the orient-
ation of the layer planes relative to the fibre axis, as measured by
x-ray diffraction, is closely related to the Young's modulus of the
fibre. In fibres with a Young's modulus of 41 G N m^{-2}, the planes
are within $\pm$ 10 % of the fibre axis. Lower modulus fibres have
wider spread of layer plane orientations.

In recent years, the micro-structure and texture of carbon
fibres have been studied extensively using the various analytical
techniques of x-ray diffraction, electron microscopy, electron
diffraction and optical microscopy. As a result, various models for
the structure have been proposed, where the two most notable were
due to Johnson and Tyson (88) and Ruland (89). Thus Johnson
and Tyson measured the x-ray diffraction parameters and found
La = 7 n m and Lc = 6 n m, which suggested that the length of the
crystallites and their width normal to the layer planes are nearly
equivalent; accordingly, the model of these workers was based on a
system of discrete building blocks having these dimensions. However

a high-resolution transmission electron microscopy studies of the slivers of high modulus carbon fibres (as used in majority of the present work) has shown them to consist of a continuous ribbon-like structure, i.e. very similar to the description of the structural features of carbon fibre originally proposed by Ruland (89).

More recent microscopy studies of carbon fibres (90) show that the crystallites are grouped together in units termed micro fibrils, which are sub-units of the fibre. The carbon atoms form two-dimensional hexagonal layers in the form of long winding ribbons having a width of about 6 n m and a length which is greater than 200 n m (90), the ribbons are stacked above each other forming the structural unit, the fibril; which are preferentially orientated parallel to the fibre axis so that parallel stacking of layers is preferentially perpendicular to the fibre axis. The increase of the heat treatment temperature and the streaching of the fibres improves the orientation of the carbon layers, with the result that the layers tend to be relatively straight in the longitudinal direction, as is found in the case of high modulus carbon fibres. Although there is a two dimentional hexagonal structure within the layers in carbon fibres, the stacking of the atoms is not regular and the separation of the layers is 3.44 $\overset{\circ}{A}$, i.e. indicating that the material is turbostatic. Fourdeaux et al (90) have also resolved a graphatic lattice in cellulose-based carbon fibres; they stress however the undulating nature of the layer planes and relate the low La values obtained by x-ray diffraction to the length of the straight regions of the layers. No lattice imperfections are included in their model, which is two-dimensional representation of both curved and straight layer planes with pores between them. The bending and twisting of the fibrils result in voids which are determined by the shape and

orientations of the fibrils. The voids constitute a system of pores which are long (> 300 n m) and narrow ($1 - 2$ n m) [91], and have the same preferred orientations as the fibrils since they are bound by the larger planes of the fibrils.

The carbon fibre cross-sectional structure following the oxidation of the precursor fibre, i.e. before the high temperature treatment [91], can be divided into the three main concentric areas of the outer layer termed "skin", the middle layer or the "sheath" and the inner layer or "core" structure [92, 93]. With a high modulus carbon fibre, the skin, sheath and core have approximate radial thicknesses of 1.5μ m, 1μ m and 3μ m respectively, as shown in Fig. 3.4 . In this case the micro-fibrils in the skin are more highly aligned than in remainder of the fibre and the graphatic layers in the skin have preferred orientations that are concentric about the fibre axis, i.e. in contrast to their respective radial and random orientations in the sheath and core [94]. The skin has a continuously undulating crystalline structure with graphatic layers running parallel to both the fibre axis and circumference. There is also an interweaving of microfibrils in the skin, with pores and surface flaws also being present. In the case of the sheath, the crystalline structure form a web with the graphatic layer running generally parallel to both fibre axis and fibre radii. This type of structure extends throughout, so that there will be numerous randomly distributed pockets of amorphous carbon, voids and cavities. The size and shape of the individual amorphous carbon pockets also varies randomly, but they tend to be aligned along the fibre axis and surrounded by the crystalline webs. The sectional area of the amorphous pockets (excluding large flaws) ,compared to the total cross-sectional area of the fibre, varies from 9 to 17% [92]. It therefore

Skin Sheath   Core

Amorphous
Carbon
Pockets
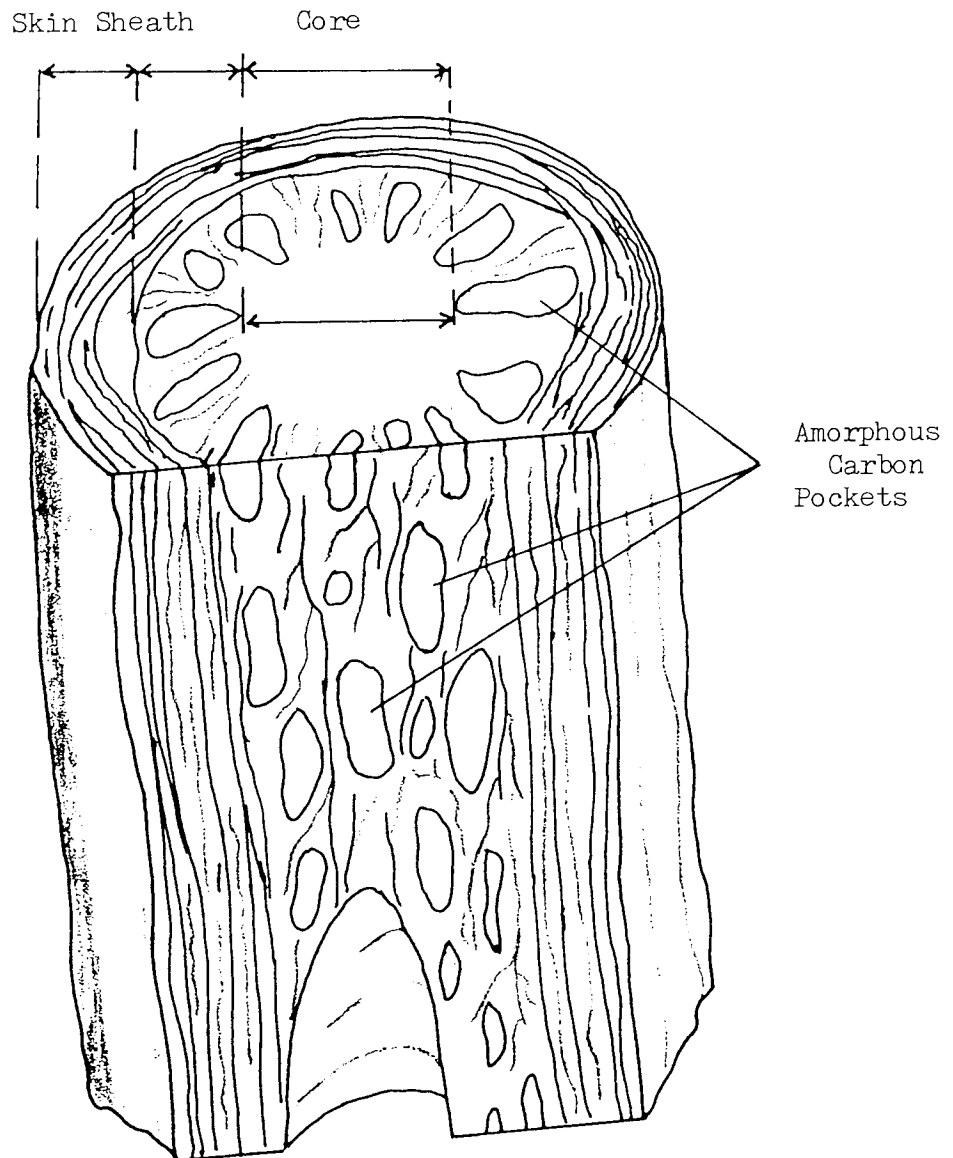
Fig. 3.4   Cross-sectional structural model for high modulus

carbon fibre.

follows from this description that when a fibre is electrolytically etched, the surface of the conical end form will contain a structure that is representive of these three regions.

Various workers have studied the surface of carbon fibre using high energy photo electron spectroscopy [95, 96] and Esca and Auger electron spectroscopy [97]. These investigations have revealed the presence of oxygen, sulphur and chlorine, although in the case of oxygen it is mostly concentrated at the surface with none being found at a depth greater than 50 n m. Silicon has also been found in the outer most layer of the carbon fibre, although it is thought to stem from the surface treatment process.

3.2 FIELD EMISSION FROM CARBON FIBRES.

The possibility of using an electrolytically etched carbon fibre as a field emission electron source for electron beam devices was first reported by Baker et al [13] in 1972. The fibres they used were approximately 7 μ m in diameter (i.e. similar to those used for present work) and were etched to a fine point using a controlled corona discharge in readiness for testing their behaviour under a variety of vacuum condition. Thus it was found that whilst the tips readily emitted at a pressure of 10^{-3} m bar the emission was very noisy and the emitter life times unacceptably small for currents greater than 10 μ A. However they found that the life time parameter could be improved to better than 2400 hours at an emission current of 10 μ A and pressures in the range of 10^{-7} m bar to 10^{-8} m bar, at which most sealed-off vacuum devices are operated. They also measured the emitter life-time in the similar pressure range for emission currents of 100 μ A and 200 μ A and found it was reduced to 500

hours and 24 hours respectively. The emitted electrons were usually confined to within a conic angle of 60° although this could be reduced to 10° by modifying the electrode geometry. An investigation of the emission noise characteristics revealed it to be predominantly low frequency (i.e. < 200 Hz) and diminished rapidly with increasing frequency becoming difficult to measure above 1 kHz . They further reported on the successful adaption of a simple scanning electron microscope to use a carbon fibre field emitter operating at a pressure of 10^{-7} m bar to 10^{-8} m bar when the resolution of this instrument was better than 0.2 μ m.

Lea (98) and later English, Lea and Lilburne (99) also investigated the stability of carbon fibre as a field emission electron source. They used Courtaulds high strength type (HT-U) fibre which had been coated with tungsten to allow them to be spot welded onto a tungsten filament for in situ heating. The electron emission pattern was found to contain many small emission centres, which they interpreted as being due to surface asperities. The spread of emission pattern was reduced to a single spot after a combination of heat treatment firstly in oxygen at 10^{-5} m bar and then in vacuum at 10^{-9} m bar. Such a treatment however results in the emitter becoming fragile, so that the maximum emission current that could be drawn was limited to about 5 μ A. An investigation of the F-N current-voltage characteristics of these emitters showed that both the work function and the emitting area were insensitive to the vacuum pressure. A consequence of this property is that whereas a tungsten emitter requires an operating pressure of $\sim 10^{-10}$ m bar for an acceptably low level of emission current noise, the same requirement can be realised with a carbon fibre emitter at a pressure of $\sim 10^{-8}$ m bar.

In a follow-up investigation of the emission characteristics of

carbon fibres, Baker et al [100] reported that the conic half-angle of the emission from their tips was typically between 30° to 45°, being rather large compared to the 20° obtained for pre treated tips [98]. They further reported that freshly prepared virgin emitters exhibited a switch-on phenomenon. Thus, instead of observing the expected smoothly increasing emission current with slowly increasing applied voltage, they in fact obtained no current until a certain critical voltage was reached, when the emission current suddenly exhibited a step-like switch-on effect where in most cases the current rose uncontrollably and led to the destruction of the tip. However, by using a 100 mΩ feed-back resistor and subsequently pre conditioning the tip by increasing the voltage until the emission current is significantly greater than the working current, this difficulty was largely overcome. At the same time, a large reduction was obtained in the noise fluctuation in the total emission current, particularly at higher pressures of $> 5 \times 10^{-7}$ m bar. Baker et al [100] also reported on the use of a carbon fibre field emitter in a thermionic electron gun of a conventional cathode ray tube. They found that whilst the electron optical properties were satisfactory, with a focused spot of diameter $\sim$ 200 μm compared to 500 μm for the conventional thermionic cathode ray tube, the final image suffered from an unacceptable level of flickering. In 1975, Braun et al reported on a field emission microscopy study of carbon fibre field emitters. They found that emission may be obtained from both polished conical tips and fibres with blunt end forms, although the latter required higher voltages to obtain emission.

The apparent potential of carbon fibres as an electron source led Rohrbech et al [102] to construct a simple scanning electron microscope with a tip mounting technique that enabled the in situ

heating of the emitter. In this application a total emission of 40 μ A was drawn from their carbon fibre tip, which gave a beam current of $\sim$ 5 n A that was satisfactorily focused into a spot of 1 μ m in diameter. The use of carbon fibre field emitters in field emission microwave amplifiers has been briefly considered by Sangster [103]. This application however requires a beam current of $\gtrsim$ 2 m A, which is clearly not obtainable from a single 7 μ m diameter carbon fibres such as used by Baker et al [100]. Accordingly, a multi-array of fibres having larger diameters of 11 μ m and 22 μ m were investigated [104], where it was found possible to draw emission currents of $\sim$ 1 m A and 4 m A respectively. Fibre bundles having an approximate diameter of 1 m m, and containing several thousand single fibres, have been used by Faubel et al [105] as a field emission electron bombardment source, where an emission current of 1 - 5 m A was obtained with an extraction voltage of 2 - 5 k V. In their case, the working pressure was below 10^{-6} m bar, at which the emission was stable within 1 - 3%, and was entirely intensitive to ion bombardment or spark discharges.

Finally, Latham and Wilson [15] and Wilson [14] have investigated in detail several other important properties of the carbon fibre emitter which are of crucial practical importance to their application as commercial electron source. Firstly, they identified the characteristic emission pattern of a carbon fibre as consisting of a random distribution of emission sub-centres, which switch "on" and "off" randomly with time. Using a cine photography technique Wilson [14] showed that the on and off times are typically of the order of a second, whilst the switch-on and switch-off times are less than 4 m sec. This type of switching phenomenon ultimately leads to flickering of the final image. Secondly, it was confirmed

that a carbon fibre emitter invariably "explodes" during the initial switch-on event, with the end-form vertually disintigrating. From the electron-optical point of view, such a propensity is clearly an undesirable feature in this type of emitter. The other important property considered by these workers was the poor angular confinement of the emitted electron beam which, using a simple diode arrangement, was shown to be $\sim 30^{o}$ and almost independent of the emission current. Therefore when considering the practical application of such a source to a C R T, where several micro amps are required in the focused electron beam, it is necessary to use a gun that accepts wide angles of emission so that the total current can be limited to a reasonable level for ensuring a long life of the emitter. Wilson [14] also investigated the influence of pressure in the range $10^{-6} - \sim 10^{-10}$ m bar, and also the influence of various residual gases, including nitrogen, oxygen and helium, on the variations in the total emission current. It was found that nitrogen and oxygen had no significant effect on either the magnitude of the current or its stability. The introduction of helium however had the effect of reducing the total emission current from about 13μ A to about 4μ A. Also, the absolute amplitude of the noise level of the emission current in this environment is reduced although this was probably due to the lowering of the total emission current. Finally, the electron optical properties of a purpose-built carbon fibre field emission gun were evaluated in a proto type cathode ray tube, where it performed satisfactorily [14, 15], with a focused spot of ~ 0.2 m m in diameter which was suitable for generating a display raster. The system did however suffer from serious defocusing effects and intensity fluctuations in the screen image.

3.3 ENERGY DISTRIBUTIONS OF ELECTRONS FIELD EMITTED FROM CARBON

FIBRE TIPS.

Several groups have previously reported on electron energy

distribution measurements of electrons field emitted from carbon

fibre tips. The first of these were due to Braun et al $^{(106)}$ who

used a Van Oostrom type of retarding potential analyser, where the

emitter was prepared by first electroplating one end of a short length

of carbon fibre with copper and electrolytically etching the other

end in a 1 N sodium hydroxide solution. They reported that the energy

distribution had a narrow half width of 0.21 ± 0.01 e V, from which

it was assumed   that the electrons were emitted by a metallic type

of emission mechanism similar to that operating with tungsten tips.

Heinrich et al $^{(106)}$ in 1977 also measured the energy distribution

of an electrolytically etched carbon fibre emitter using a high resolu-

tion Wien filter analyser (resolution better than 0.01 e V) as

an electron spectrometer. The half width of the energy distribution

of electrons that had been accelerated to 30 k V in poorish vacuum

of about 10^{-6} m bar was $\sim$ 0.215 e V with a small emission current

of $\lesssim 10^{-9}$ A: They found however that the half width of the

distribution increased with emission current. This effect was

attributed both to instabilities in the surface structure due to ion

bombardment and to the presence of more than one emission centre

contributing to the total emission current.

In contrast, the energy distribution of the electrons field

emitted from carbon fibres reported by Latham and Wilson $^{(21)}$

were made under ultra high vacuum conditions ($\lesssim 10^{-10}$ m bar) and

using an advanced 180° deflection field emission spectrometer that

had resolution of $\lesssim$ 30 m e V. Furthermore, this instrument had a

built-in capability of relating the emission spectra to the Fermi level of the metallic substrate material, thus providing valuable information about the origin of the emitted electrons. The energy spectra they obtained were basically of two types; viz single -peaked or double-peaked although the former were found to be the most common. In the case of a single-peaked spectra recorded for an emission current of $\sim 1 \times 10^{-8}$ A, they found the half-width to be ~ 0.40 e V, compared to ~ 0.24 e V for a tungsten emitter measured under similar conditions. They also found that the emission spectra of carbon fibres were shifted towards low energies with respect the metal substrate Fermi level. Furthermore, they found that the slopes of the leading edge of the energy spectra were much less steep than those found for a metallic tungsten emitter. Both of these quantities, viz the half width and the spectral shift, were found to increase with increasing emission current. The double-peaked spectra were found to be sensitive to the total emission current in a similar way, where the respective heights of the two peaks, and their displacement from the Fermi level increased with increasing emission current. The multi-peaked spectra were interpreted as arising from electrons that had crossed the insulator in more than one conduction band minima; i.e. the explanation originally used by Athwal [107] to explain the multi-peaked spectra obtained from broad area specimens.

Finally, Latham and Wilson [21] reported on another interesting phenomenon, where the magnitude of the electron energy spectral peak recorded at a constant field is found to increase in height when the emitter was irradiated by light of a wavelength < 470 n m. After removing the light source, the spectral peak height relaxes to its original level after about 30 seconds, which was attributed to a slow-non-metallic type of relaxation processes.

3.4 FIELD ELECTRON EMISSION MODEL FOR CARBON FIBRES.

From a comprehensive study of the I-V characteristics of emitters (98, 99), which invariably gave linear F-N plots, Lea (98) concluded that the emission originated from "metallic" asperities on the surface of the tip that emit according to the F-N theory. This interpretation   also seemed to be supported by the narrow spectral half-width measurements (101) of typical value ∼ 0.21 e V. However, several observations of Wilson (14) and Latham and Wilson (21) described above, indicated that the emission mechanism was "non-metallic" in nature of particular significance where (a) the shift of energy distribution with respect to Fermi level, (b) the photosensivity of the emission spectra, and (c) the observation of an associated electroluminescence phenomenon (16), all of which are uncharacteristic of a metallic type emission mechanism.

To accommodate these findings, Latham and Wilson (16, 21) proposed an alternative emission mechanism based on the composite micro-regime described in chapter 2. This consisted of a metallic substrate provided by carbon fibrils, with an overlayed insulating medium of perhaps 0.1 to 1 μm thick provided by the pockets of amorphous carbon in the fibre. Therefore on the initial application of an external field to such an emitting regime it penetrates the insulating material up to the metallic substrate and under favourable conditions gives rise to suffiecient band bending at the metal-insulator interface, as shown in Fig. 2.17 (a), to allow electrons to tunnel from the Fermi level of the metal into the conduction band of the insulator. As a result of the penetrating field such electrons will be heated and thus acquire sufficient energy for some of them to be emitted over the surface barrier. The remainder of this population of 'hot' electrons will undergo phenon scattering processes to create

an avalanche of further charge carriers (i.e. electron-hole pairs)

by impact ionization. It is then assumed that these holes and

electrons will then migrate respectively to the metal-insulator and

insulator-vacuum interfaces and create the necessary high field

conditions for the insulator to undergo an Ovshinsky type switching

processes [74] to a more stable high conductivity state. The band

structure of this switched-on state is illustrated in Fig. 2.18,

and is seen to be characterised by two high field regions, one at the

metal-insulator and the other at the insulator-vacuum interface, with

an extended intermediate low-field region. The emission process

starts with the electrons tunnelling from the metal Fermi level

through the first high field region and then being rapidly thermalised

to the bottom of the conduction band so that they hence are able to

cross the extended low-field region in the bottom of the insulator

conduction band before entering the second high field region of about

10 n m thickness. Here, some of the electrons are heated through the

2 - 3 e V necessary to escape over the depressed surface potential

barrier, whilst the remainder are scattered by the insulator lattice

and excite the electron transitions required for producing the

electroluminescence spectrum [16], i.e. arising from the recombina-

tion of electrons and holes via trapped states. The switching

concept employed in this model also provides a plausible explanation

as will be discussed in chapter 6 for the well known temporal

instability of the individual and randomly orientated emission

centres that contribute to the field emission image of a carbon fibre

emitter and in particular it explains why this is uneffected by

vacuum conditions in the range of $10^{-7} - 10^{-10}$ m bar and temperature

in the range of $90^{\circ} - 300^{\circ}$ K [14].

CHAPTER 4

4. <u>THE DESIGN AND TESTING OF A CATHODE RAY TUBE USING A CARBON FIBRE</u>

   <u>FIELD EMITTING SOURCE</u>.

4.1 <u>INTRODUCTION</u>.

The use of a field emission cathode as a practical electron source has been considered by numerous workers over the past two or three decades for a wide range of technological applications. These include microwave amplifiers, switch tubes, transducers, flash x-ray devices, electron microscopes (10, 11) and, more recently, a field emission cathode ray tube as considered by Wilson (14). In the latter case, a field emission electrostatic gun, suitable for a field emission electron source, and based on the design of Crewe et al (108), was designed and incorporated in a purpose-built proto-type C R T as part of electron optical bench. Using this facility Wilson (14) then investigated the suitability of a carbon fibre tip as a field emission electron source and the electron optical properties of the field emission gun and found the overall performance to be satisfactory. However, there remained two serious unsolved residual problems. Firstly the flickering of the final image which was brought about by instabilities in the field emission current and the characteristic field emission pattern. Although Wilson (14) tried various techniques to stabilise these, he found the use of a 100 MΩ resistor in series with the emitter to be most effective. This resulted in a reduction of the fluctuations in the total current of 10 μ A from about 10% to less than 1% . This however introduces a second undesirable effect, viz unacceptable levels of focus fluctuation in the final image.

The work presented in this chapter is an extention of these earlier studies, where computer techniques have been used to examine various gun designs, firstly to produce a 300 mm focal length gun to minimise focusing effects, and secondly to produce a minature gun with a focal length of 50 mm. These guns were first tested in the previously designed proto-type C R T and subsequently incorporated in sealed-off standard and minature thermionic tubes with a carbon fibre as a field emitter. Finally, various feed-back techniques have been successfully used to firstly stabilise the total emission current without effecting the tip voltage and secondly to stabilise the intensity of the final image.

4.2 U.H.V. SYSTEM FOR DEMOUNTABLE EXPERIMENTAL TEST FACILITIES.

The ultra high vacuum system used for the demountable electron optical test chamber was a standard type, and capable of achieving a vacuum better than 10^{-9} m bar. Fig. 4.1 is a diagram of the test chamber and the vacuum system, which consists of an Edwards water-cooled, oil diffusion pump type E O 2 , using santo-Vac 5 fluid, which has a critical backing pressure of 0.3 m bar. The backing pressure was provided by an Edwards double-stage, E D 50 type rotary pump, where the backing pressure of 0.001 torr was easily achieved with the molecular sieve in the backing line immediately above the rotary pump. This prevents the diffusion pump fluid from being contaminated by the oil and water vapour from the rotary pump. Back-streaming of oil vapours from the diffusion pump into the experimental chamber was minimised by the cold water baffle and the liquid nitrogen trap situated immediately above the diffusion pump and below experimental chamber. Furthermore the liquid nitrogen trap is able to cryogenically pump condensible gases thus giving a

Fig. 4.1   Diagram to show the Test Chamber and the vacuum system.

(1)   Ionization gauge.

(2)   Test chamber.

(3)   Specimen manipulator.

(4)   Liquid Nitrogen trap.

(5)   Thermal switch.

(6)   Water cooled baffle.

(7)   Oil diffusion Pump.

(8)   Vacuum switch.

(9)   Air admittance valve.

(10)   Valve.

(11)   Pirani gauge.

(12)   Flexible bellows to reduce vibrations.

(13)   Molecular sieve trap.

(14)   Isolation / air admittance valve.

(15)   Rotary pump.
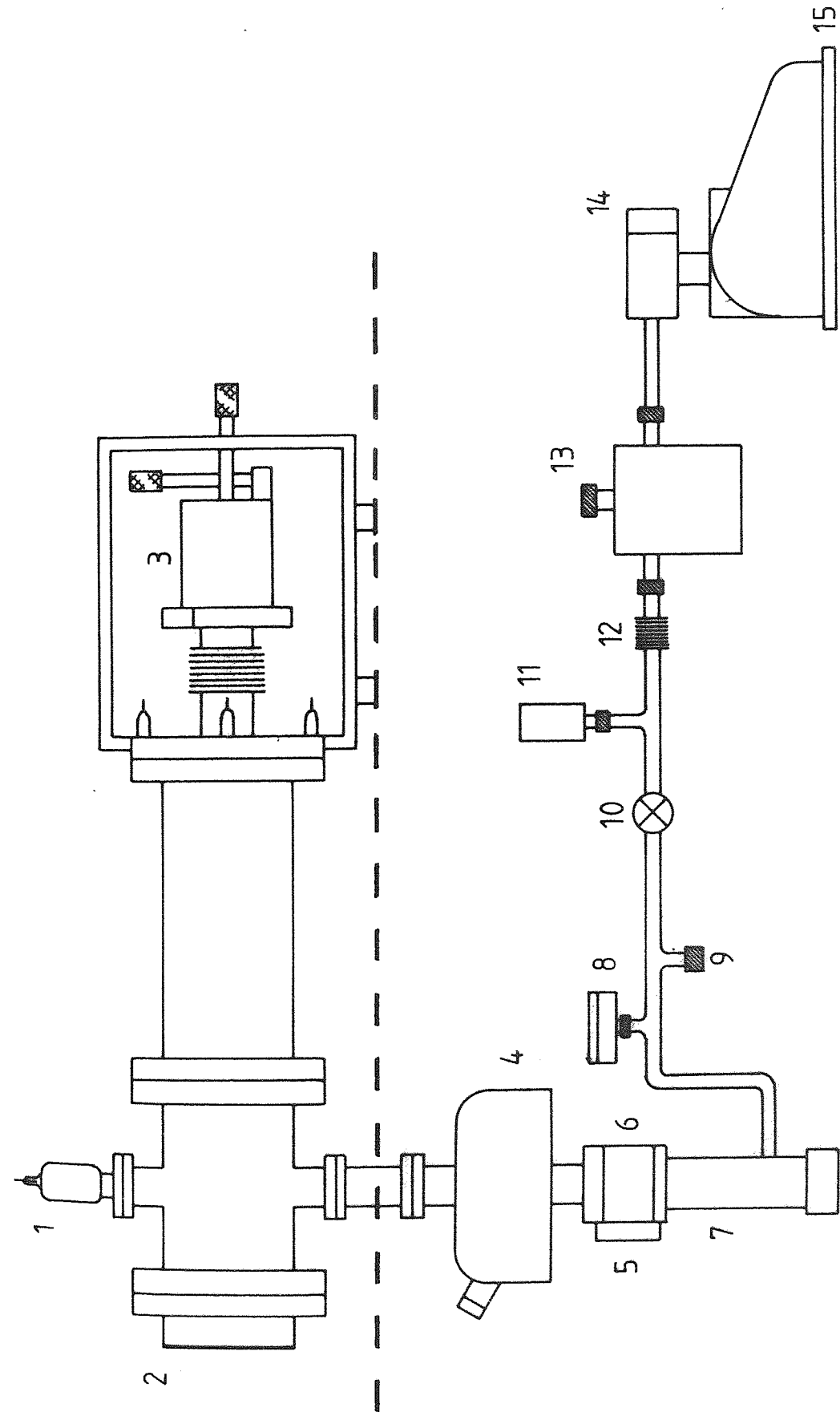
better vacuum. The experimental chamber is bakable when required and was normally baked to about $200°C$ by strapping heating tapes around the chamber. With a baked system and a full nitrogen trap, a pressure of $\lesssim 10^{-10}$ m bar was obtained. The other main feature of the vacuum system is that it is fully protected against power and water failure with an electrical trip circuit, vacuum switch, thermal switch and an isolation valve used in conjunction with the rotary pump. In the case of a power failure, the isolation valve closes just before the air is let into the rotary pump, thus maintaining the backing pressure for a time long enough to allow the diffusion pump to cool down. When the power is restored, the trip circuit will prevent the diffusion pump from coming on unless deliberately started, once the backing pressure is maintained and the vacuum switch is overcome. The thermal switch mounted on the diffusion pump protects it against water failure, which is set at about $4°C$ above the normal working temperature of the diffusion pump, so that if this is exceeded the diffusion pump automatically switches off and thus the system remains intact.

A similar vacuum system is employed for the field emission electron microscope, the experimental facility used for studying the electron emission behaviour of carbon fibre cathodes. The diagram of Fig. 4.2 shows the general view of the chamber and the vacuum system, which is protected against power and the water failure.

Fig. 4.2   Diagram to show   (a) Field Emission Microscope and
            pumping system   (b) The typical electrode arrangement
            used.

(1)   Field Emission Microscope.

(2)   U. H. V. Valve.

(3)   Liquid Nitrogen trap.

(4)   Thermal switch.

(5)   Water cooled Baffle.

(6)   Oil diffusion pump.

(7)   Air admittance valve

(8)   Valve.

(9)   Pirani gauge.

(10)   Flexible bellows to reduce vibrations.

(11)   Molecular sieve trap

(12)   Isolation / air admittance valve.

(13)   Rotary pump.

(14)   Electrical Feed - throughs.

(15)   Cathode assembly.

(16)   Extracting Electrode.

(17)   Phosphor screen.

(18)   Electrical contact to the screen.

To Ionization gauge
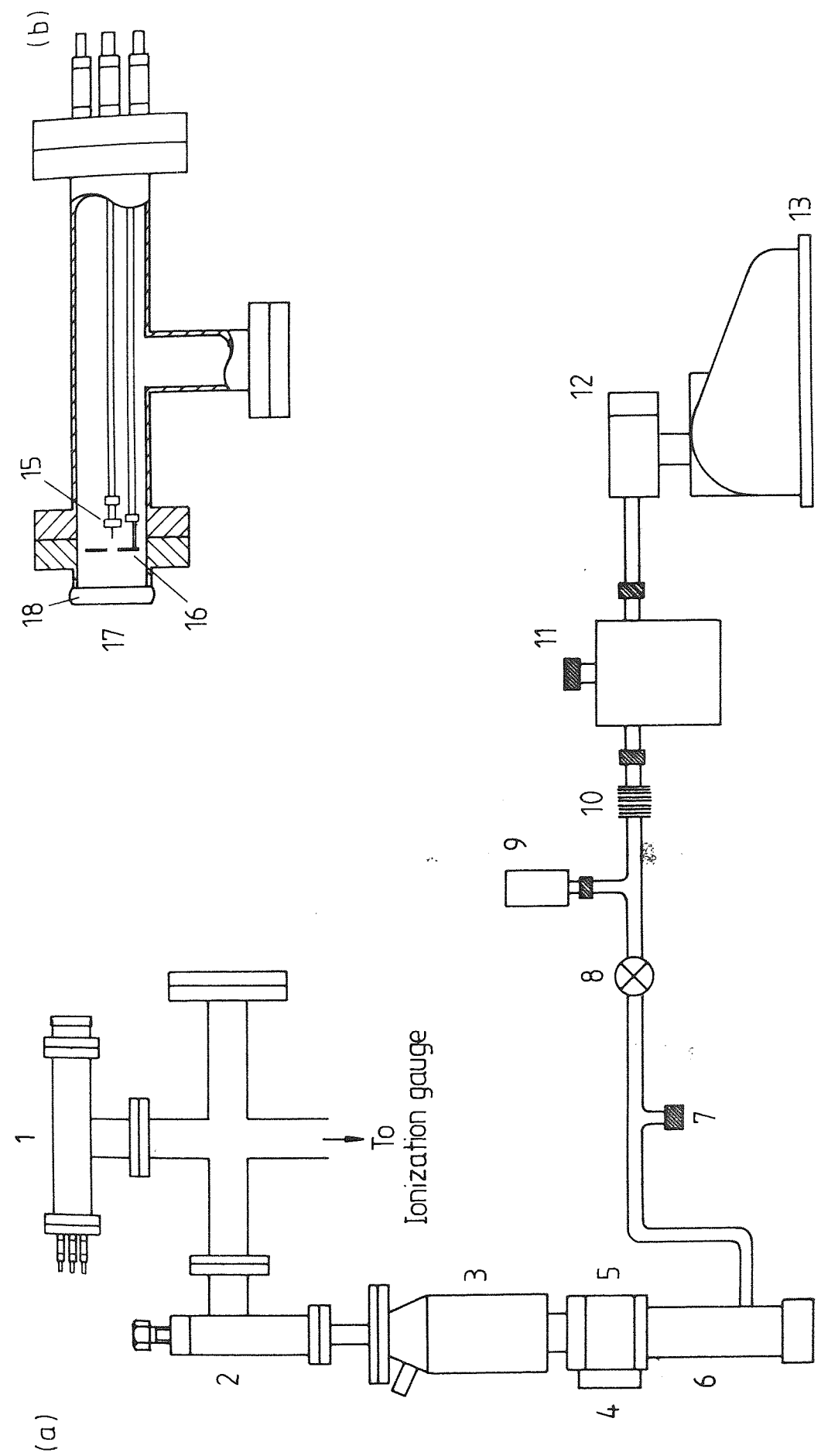
4.3 DEMOUNTABLE TEST CHAMBERS.

The demountable vacuum test chambers used for the experimental developement of a field emission cathode ray tube were basically of two types. The first of these was a proto-type cathode ray tube used for studying the electron optical properties of field emission electron guns. A photograph of this is shown in Fig. 4.3 which is the "long" version, corresponding to the use of an electrostatic gun having a focal length of 300 mm; i.e. the typical focal length used in standard thermionic commercial tubes. For studying the properties of miniature tubes having electrostatic electron guns of 50 mm focal length, it was possible to shorten the previous "long" version by removing an extention tube. This "short" version is shown in Fig. 4.4 . The other type of test chamber was a small field electron microscope as shown in Fig. 4.5 and basically consists of a 190 mm long stainless steel tube mounted on a stainless steel four-way manifold and connected to the vacuum system through a high vacuum valve. The chamber is sealed off at one end by a flange containing the screen deposited with P31 type phosphor, and at the other end with a flange containing electrical feed-throughs which extend about three quarters of the way into the chamber. This is shown in Fig. 4.2 together with the diode arrangement of the field emitter and extracting electrode, which is the typical arrangement used for carbon fibre cathodes.

Referring to Fig. 4.6 the main features of the "short" proto-type C R T are screen, electron gun and field emitting source with its external manipulator. The experimental chamber itself consists of the horizontal limb of a four-way stainless steel manifold. A view port closes one end, whilst the other is sealed off by a flange carrying the emitter manipulator assembly. For the "long" 300 mm
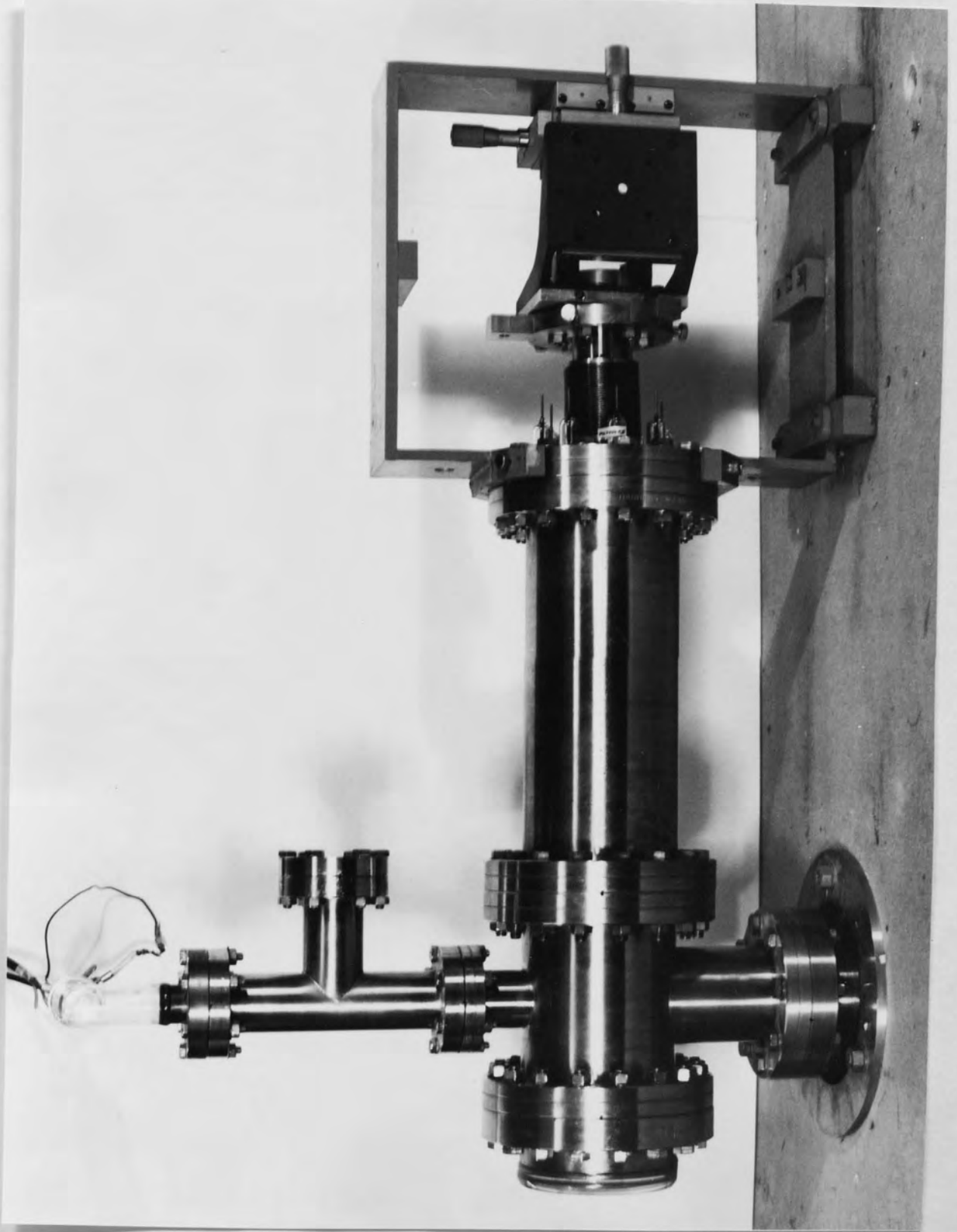
Fig. 4.3   "Long" version of the test chamber.
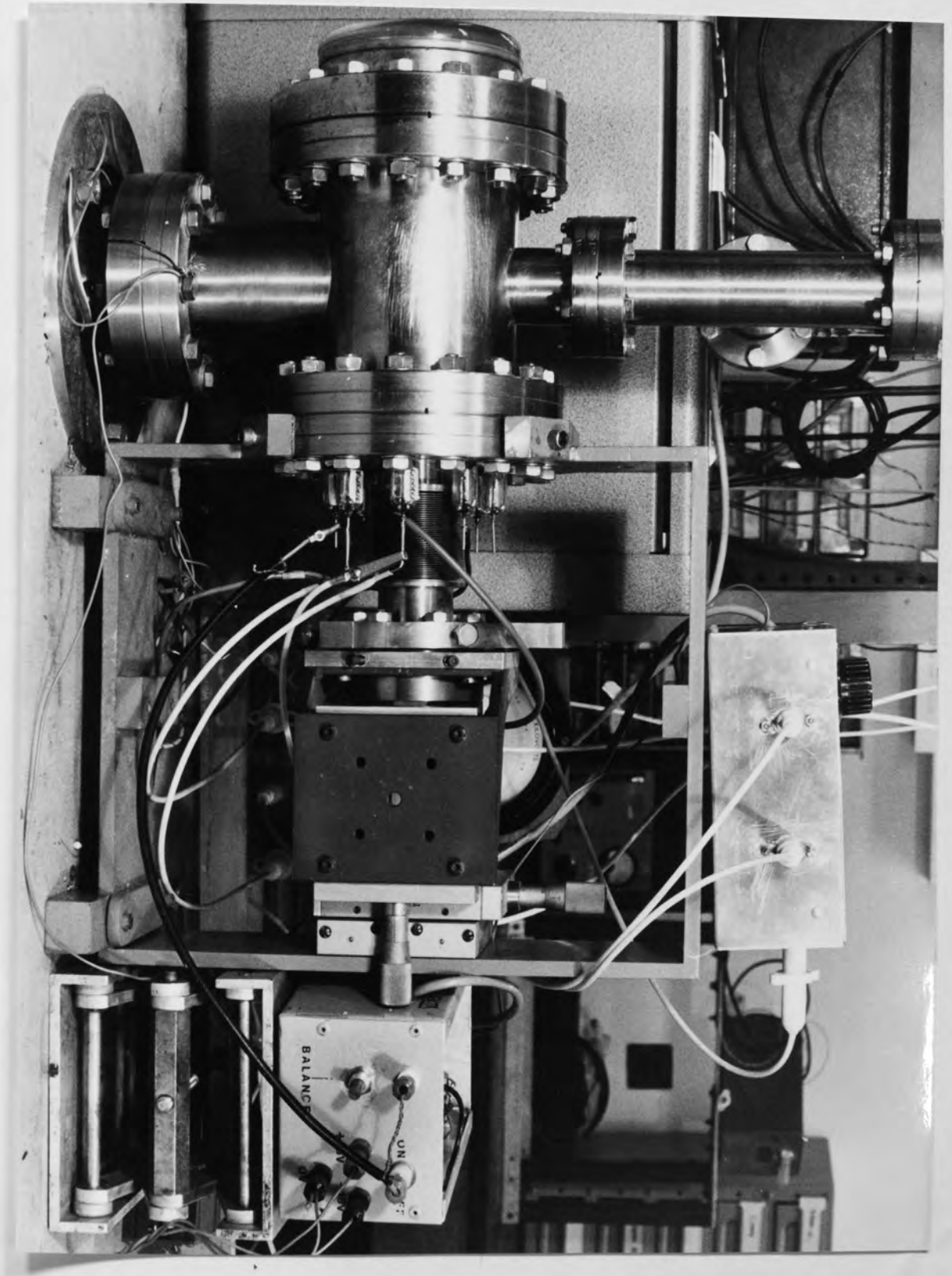
Fig. 4.4   "Short" version of the test chamber.
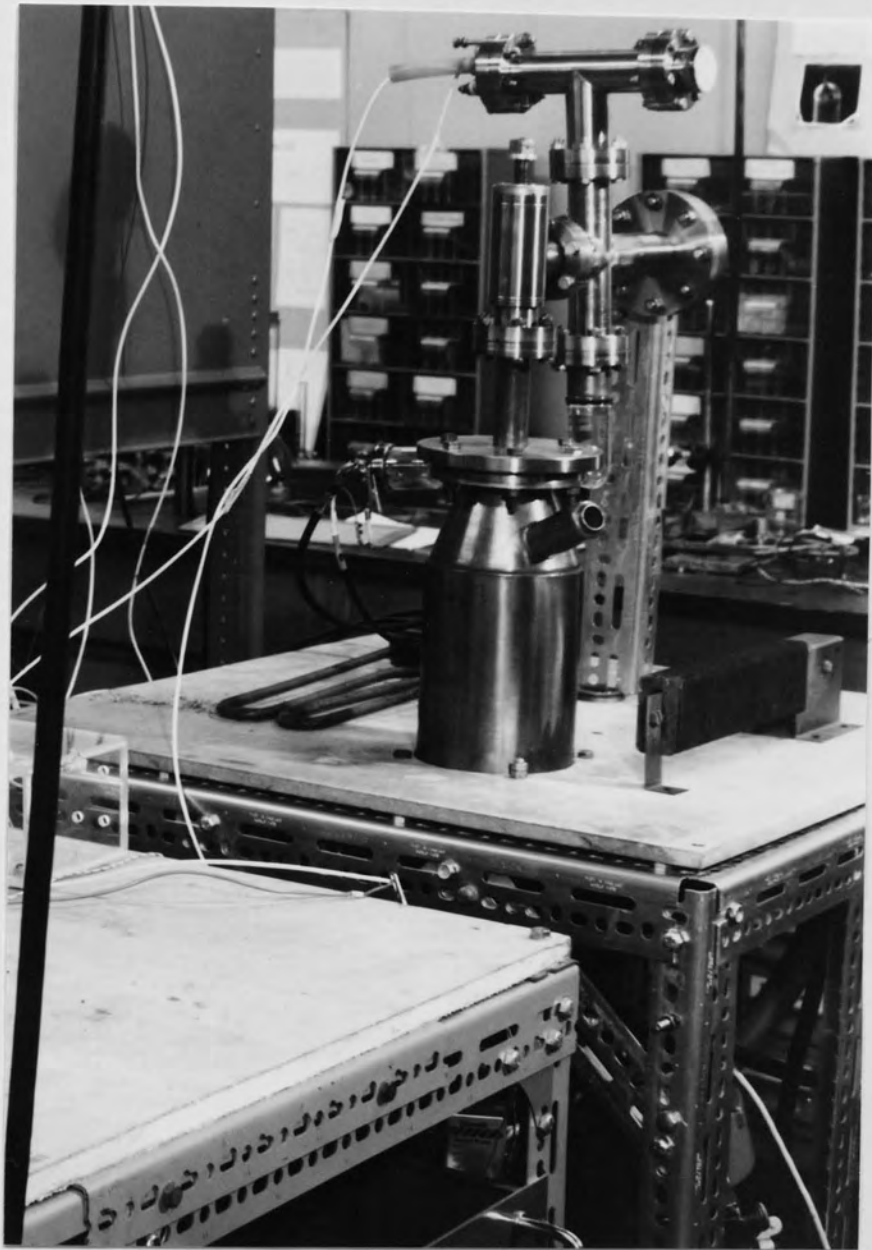
Fig. 4.5   Field Emission Microscope

Fig. 4.6   "Short proto - type CRT and the main features,

1. Phosphor screen.

2. Electrostatic gun module.

3. Cathode.

4. Telescopic cathode holder.

5. Telescopic gun holder.

6. Electrical feed - through.

7. Flexible bellows.

8. Specimen manipulator.

Fig. 4.6

83.

84
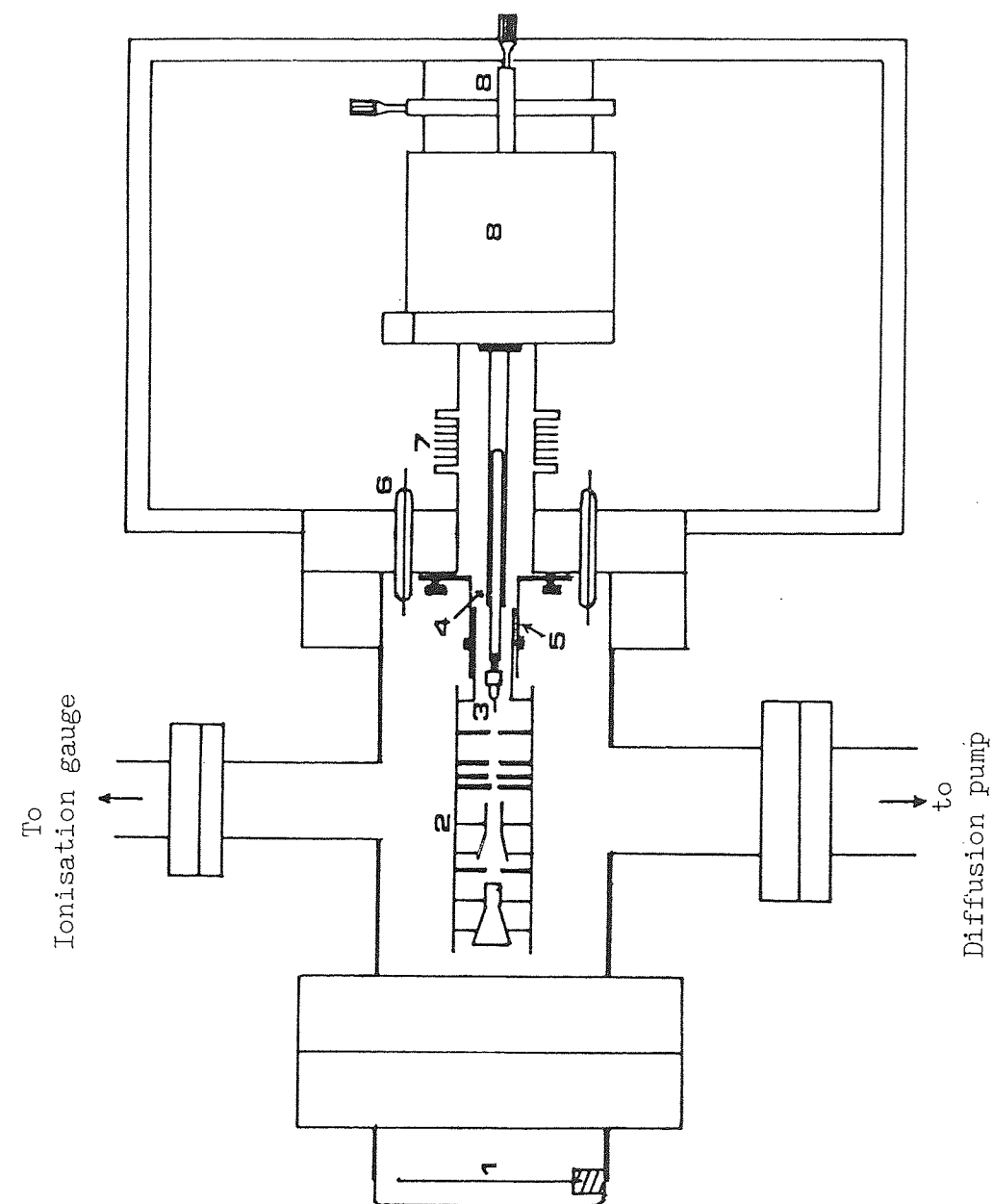
focal length tube, a 260 mm extention tube is inserted to give the required separation between the source plane and the image plane. The phosphor screen Fig. 4.7 is electrically insulated from the chamber, being mounted on a small ceramic base held in place just inside the view port by circular steel strips pressing against the wall of the tube. The screen is prepared from a 3 mm thick pyrex glass disc, which is first coated with a transparent film of tin oxide to ensure good electrical conductivity, and then by a relatively thin layer of phosphor. A good electrical contact is made to the screen via stainless steel contacts embedded inside the ceramic base, and this made it possible to measure the screen current and also apply small biasing voltage. The carbon fibre tips could be precisely aligned in-situ with respect to the extracting aperture by the bellows-linked x-y-z micro meter controlled manipulating assembly as illustrated in Fig. 4.2 and described in details else where (14). The tip holder consists of long tube extending well into the chamber, and on the end of this there is a small clamp to grip a small copper block on which the tip is mounted.The clamp assembly is insulated from the rest of the tube by a 10 mm diameter ceramic tube so that a voltage could be applied to the tip. The copper block has a fine slit along the centre of the block for locating the fibre tip. External connections to the tip, screen, and the various electrodes of the gun are provided by eight glass feed throughs evenly spread around 150 mm flange, (Fig. 4.2). The holder for the electron gun assembly consists of two concentric cylinders which can slide tele-scopically over each other for adjusting the distance between the image plane and the object plane: this same facility provides a simple means of interchanging different electron gun assemblies for experimental evaluation.
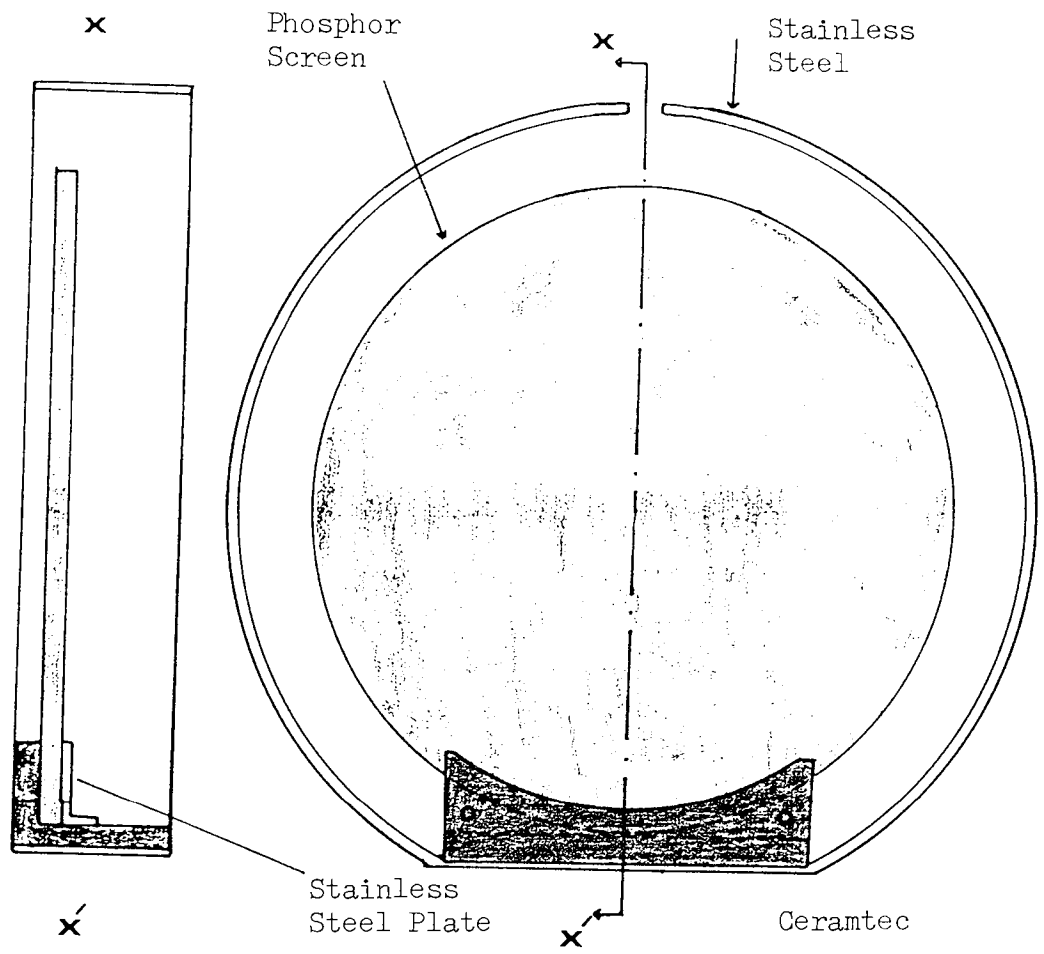
Fig 4.7   Phosphor screen assembly.

4.4 CARBON FIBRE MOUNTING AND ETCHING TECHNIQUES.

There are two basic requirements for a reliable emitter
mounting: firstly, there should be a good electrical contact between
the fibre and its holder, and secondly the mounting should have a
strong mechanical strength to withstand the electro-mechanical
stresses imposed by the high electrical fields ($\geqslant 10^7$ V m^{-1}). In
the case of carbon fibres, it is not possible to use the standard
mounting techniques used for metallic emitters where the tip is
spot-welded to a cathode bridge. Attempts have been made to artific-
ially strengthen carbon fibre by electroplating them [101] but it
was found that this made them brittle and difficult to spot weld.
An alternative method which to some extent was successfully used by
Wilson [14], involved mounting the carbon fibre in a fine slit
along the centre of a copper block at the end of the tip holder
Fig. 4.8 (a) and then to secure the fibre in position by a drop of
high conductivity silver paint. This technique however had one
serious drawback; viz that the carbon fibre so mounted tended to be
"pulled off" during operation due to the stresses imposed by the
applied field. To overcome this difficulty, the new two-part tip
holder shown in Fig. 4.8 (b) was developed. The first part was made
out of copper in the shape of an anvil, when the sharper end con-
tained a fine slit in which the carbon fibre was placed and then
secured in this position with a drop of high conductivity silver
electro-dag for it provided a good electrical contact; the fine slit
further insured that the fibre was square to the extractor anode
face. The carbon fibre was further secured in this slit by the
second part in the shape of a spoon which, ensured a constant pressure
on the fibre. In this way the fibre cathode was sandwiched between
the stainless steel spoon and copper anvil and this procedure prevented

Fine slit

Small threaded hole.

(a)

2mm

Spoon shaped spring

4mm

15mm

Cathode

(b)
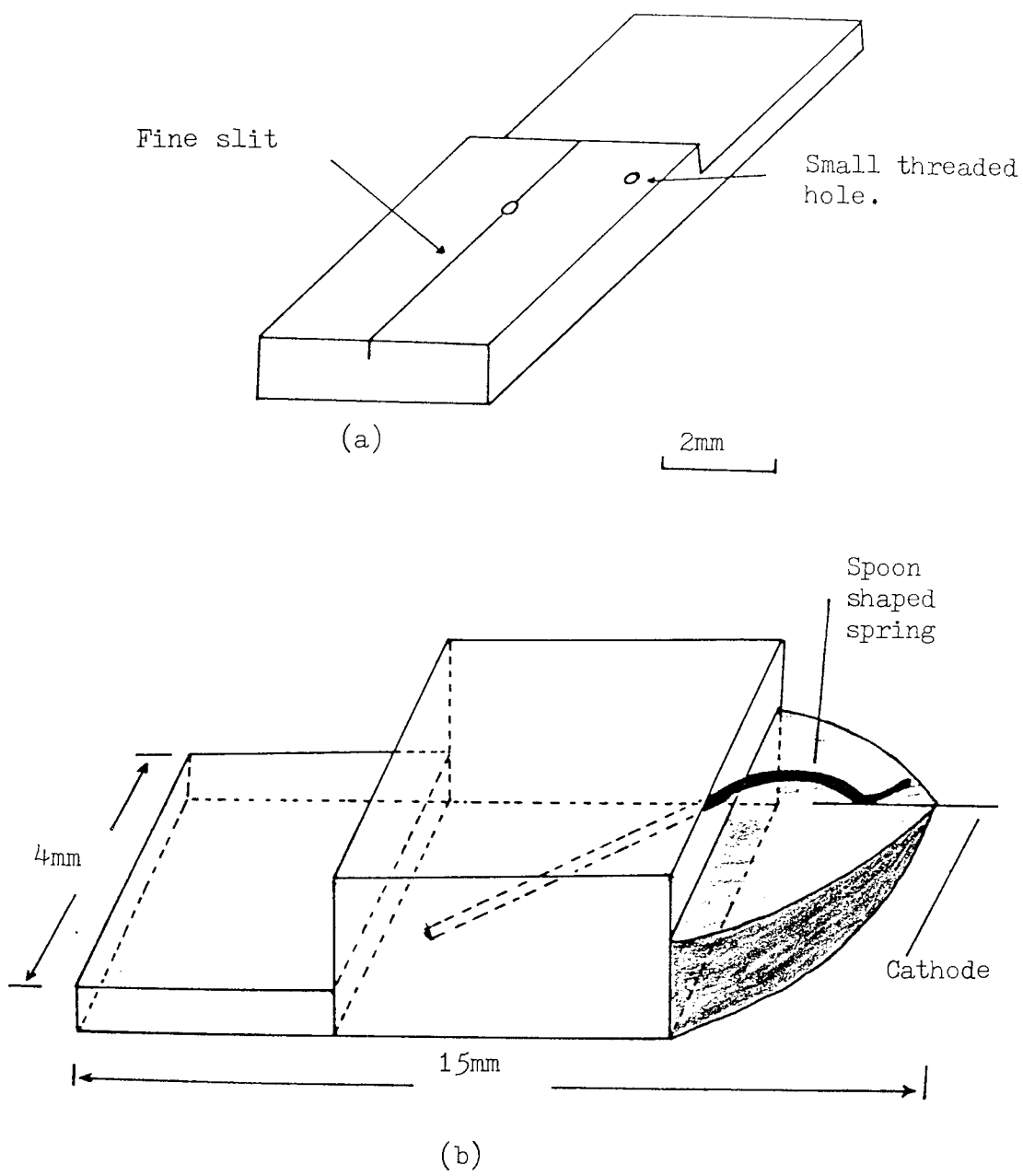
Fig. 4.8 Tip holders (a) Copper - block and (b) Anvil type.

it from being pulled off even under the highest fields.

Once the fibre is securely mounted, its end-form can then be sharpened to reduce the curvature, and hence minimise the magnitude of the applied voltages required to produce the high electric fields necessary to induce electron emission. Furthermore, the use of lower voltages means lower sputtering energies of electron-impact produced positive ions, and hence less likelyhood of voltage breakdown. The carbon fibre end form is sharpened by the standard electrically etching procedure illustrated in Fig. 4.9 . To etch the tip, the mounted fibre is lowered into the solution so that the end of the fibre is about 2 mm below the surface of the 0.1 N sodium hydroxide solution. The voltage is then increased until the required initial etching current of 20 - 45 μA is obtained. The etching of the tip occurs preferentially at the liquid / air interface and resulting in the gradual "necking" of the fibre, during which the etching current falls slowly to ~ 15 μA when the "necking" becomes very profound. Subsequently, the etching current then falls off quite rapidly until it reaches about 5 μA, where it abruptly falls to zero indicating that the lower part of the carbon fibre immersed in the liquid has completely necked-off to leave a conically-shaped tip above the liquid. Some control of the etched tip profile is available by a suitable choice of the initial etching current. Thus the currents in the range ~ 20 - 30 μA usually produce a tip with a long profile, whilst for a initial etching current in the range of ~ 35 - 45 μA the tips generally have a short profile. For this investigation, the optimum initial etching current was found to be 30 - 35 μA, which gave a medium profile. It was also found that tips having smoothly tapered profiles were more reliably obtained if the newly-prepared sodium hydroxide solution is left to stand in an air-tight container overnight before etching.

Magnified view of
necking of the fibre
at the liquid surface

Micro ammeter

Volt meter

Electrolyte
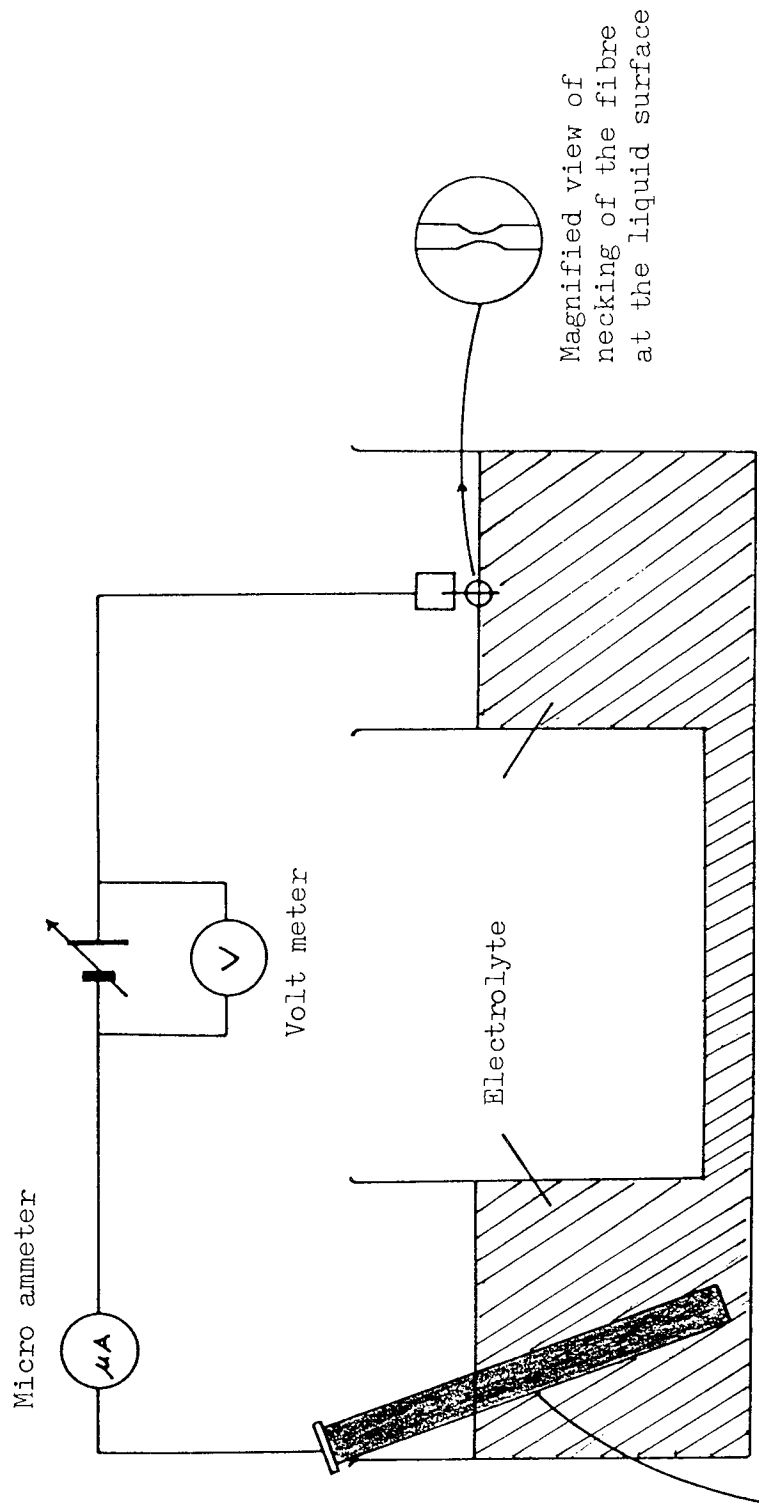
Carbon rod cathode.

Fig. 4.9 Carbon fibre tip etching procedure.

90.

4.5 THE TESTING OF A STANDARD 300 mm FOCAL LENGTH LENS MODULE.

With the aid of the demountable cathode ray tube assembly described in section 4.2, the performance of the 300 mm focal length electrostatic field emission gun previously designed by Wilson [14], was further evaluated. The aim of this was to improve its performance characteristics by gaining a better insight into the physical origin of the intensity fluctuations and the defocusing effects in the final visual display on the phosphor screen. The electrostatic gun chosen for this investigation was based on a two-element electrostatic lens that used flat electrodes with central circular apertures, and whose electron optical properties had previously been analysed by Wilson [14] using two programmes originally written by Munro [109]. The main features of the gun are outlined in Fig. 4.10, whilst the properties of the particular lens system are given in Fig. 4.11 . This latter figure shows the relation between source distance (S_o) and the ratio V_I / V_o of the image side voltage (V_I) to object side voltage (V_o), for a constant 300 mm focal length, which Wilson [14] had chosen to be 5 from Fig. 4.11 to avoid using excessively high voltages although the ratio was not optimum. To test this gun, a freshly prepared tip was mounted and pre-aligned with the extracting electrode aperture; this sub-assembly was then remounted in the main chamber and evacuated to about 5×10^{-9} m bar. By applying appropriate voltages to the various electrodes, Fig. 4.12 , such that condition $V_I / V_o = 5$ was satisfied, a finely focussed spot was obtained on the screen at 300 mm from the second lens element. The total emission current from the tip was about 7.8 μ A, of which about 6.1 μ A reached the screen indicating a high efficiency gun. However the focussed spot suffered from unacceptable levels of variations in both intensity and spot size due to defocussing.
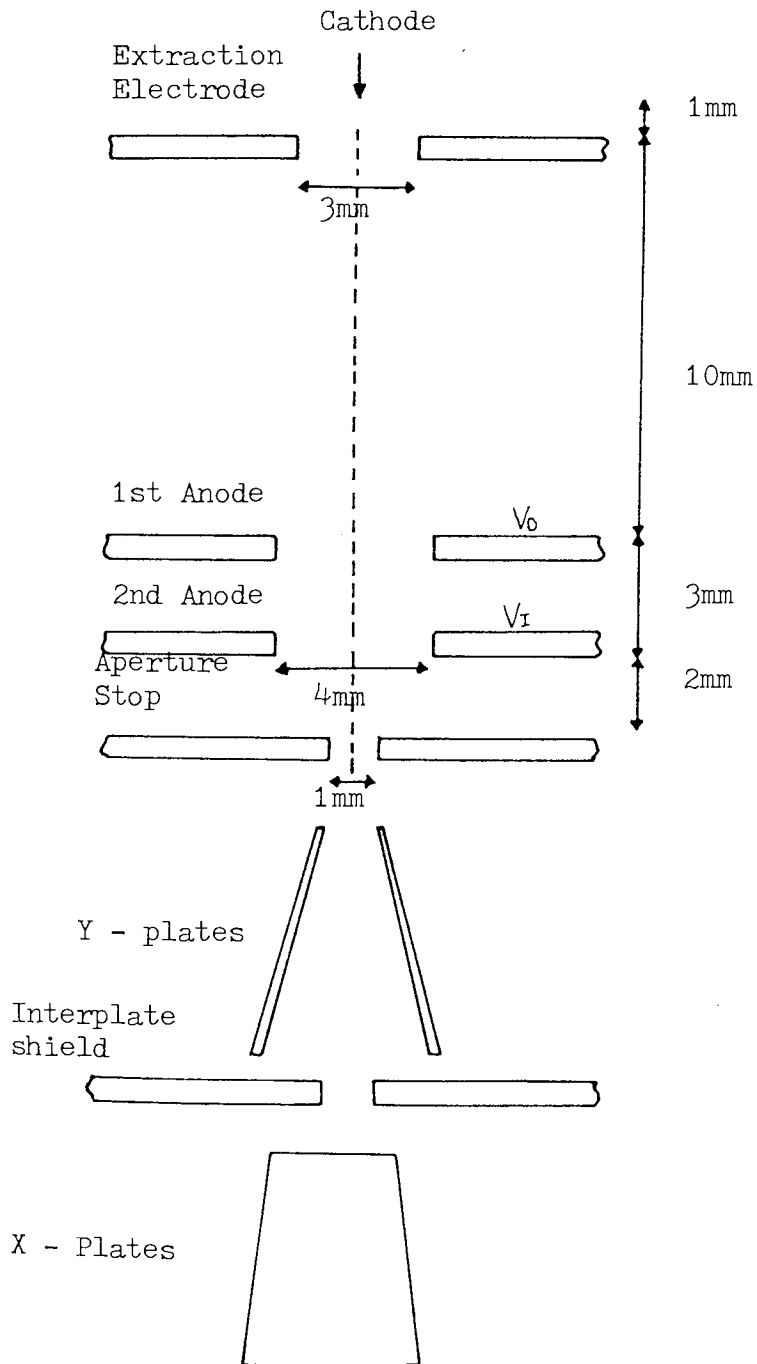
Fig. 4.10 Main features of Wilson's 300mm focal length gun.

(14)
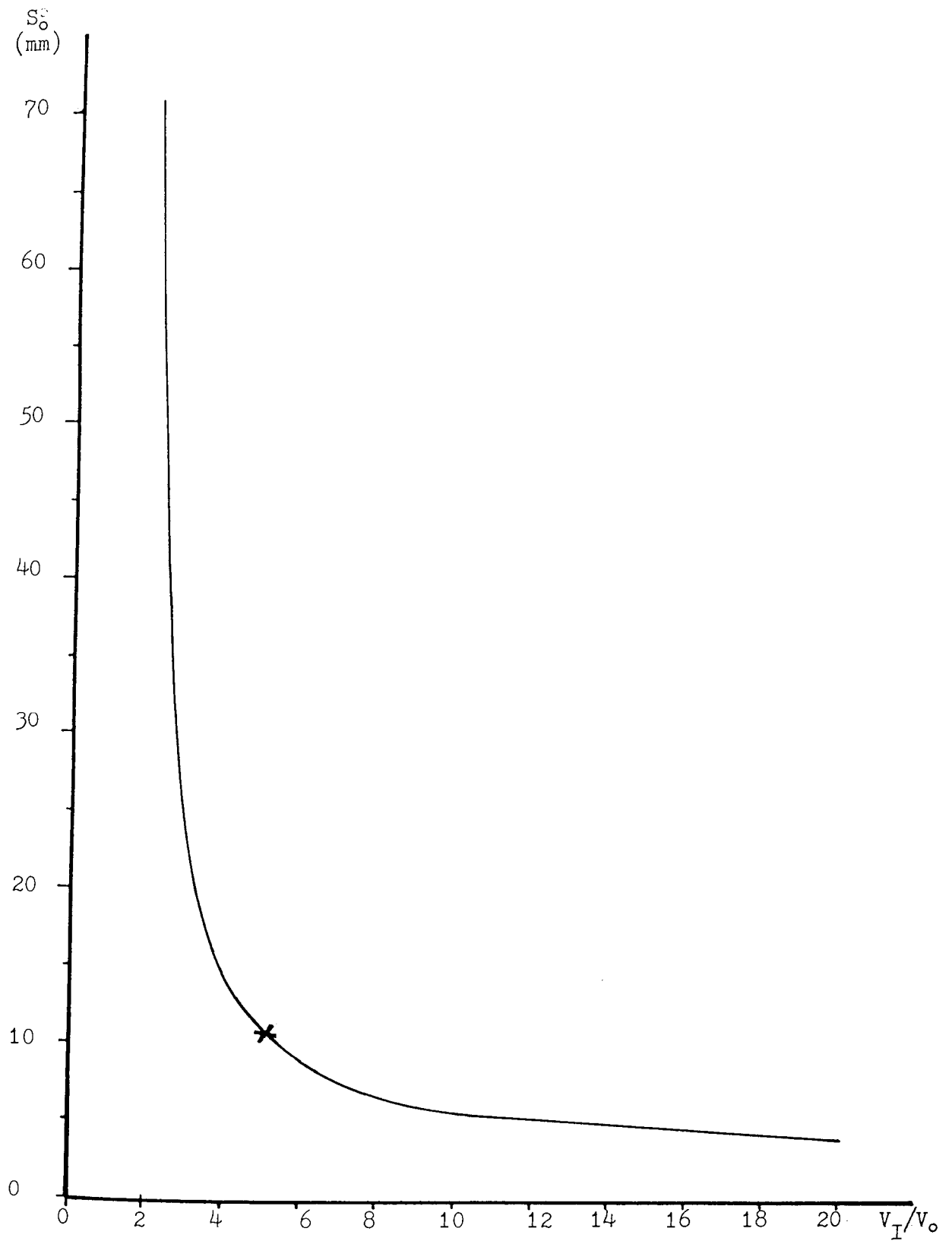
Fig. 4.11   Graph of object position as a function of the   voltage
ratio (V_I/V_o) for 1.8 mm electrode separation and
aperture 4mm.

Cathode

Extractor

1st Anode

2nd Anode

-2.5 KV

-2.0 KV

-2.0 KV

100 MΩ
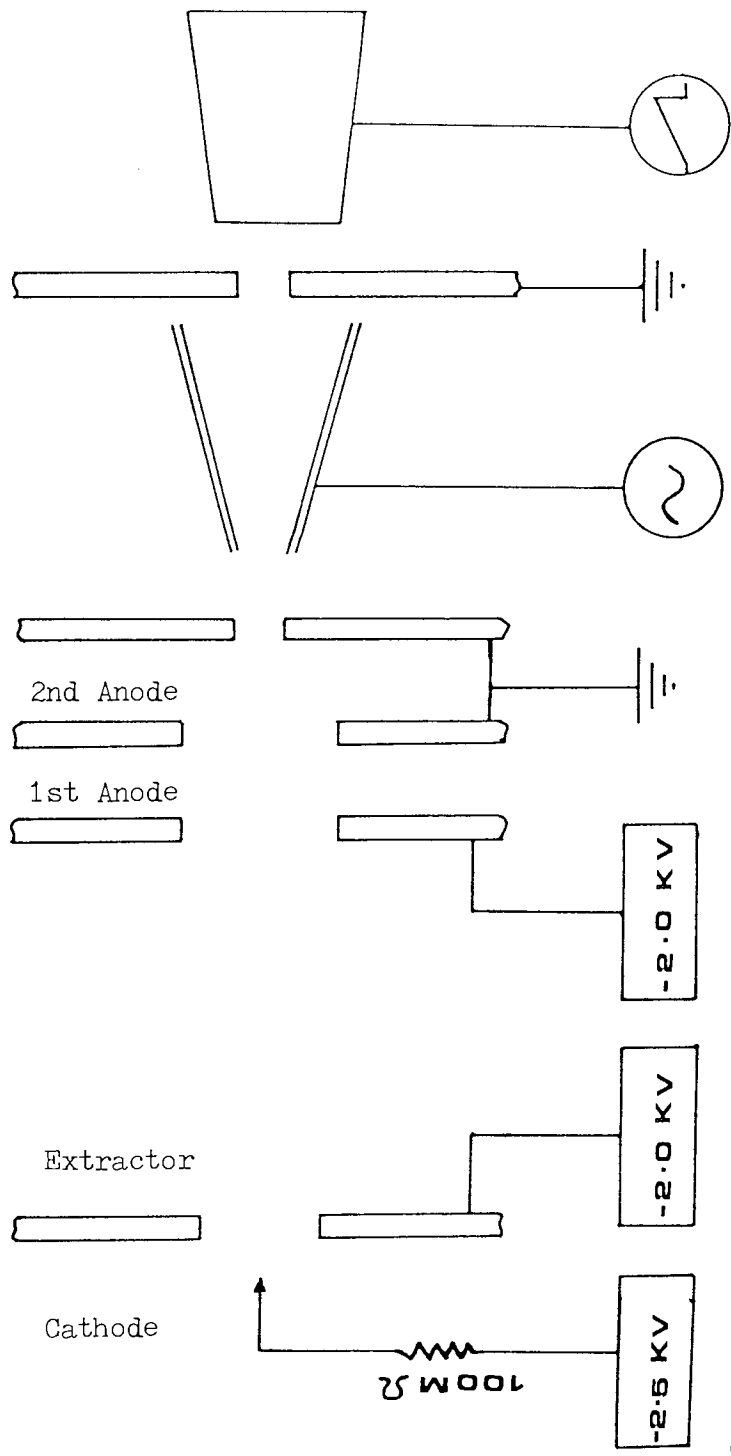
Fig. 4.12   300mm focal length gun with appropriate voltages.

94.

This effect was further investigated by slowly scanning the focussed spot across the screen by applying a slowly varying ramp voltage to the x-deflector plates, and photographing the spot scan with an open shutter camera. The total scan time could be varied from a few microseconds to 100 seconds, and a series of scan photographs were taken covering this range of sweep speeds for subsequent analysis. Traces of 10 μ s to 0.5 s scan time showed no significant fluctuations in intensity or focussing; however traces obtained from scans of one second duration of more, such as the example of Fig. 4.13 (a), showed high levels of fluctuations indicating that the typical frequency of these variations are below 1 Hz.

To investigate the possible causes of the fluctuations in focussing, the total cathode emission current, and the current collected by the extractor electrode and first lens element were simultaneously recorded on chart recorder for subsequent analysis. A typical example of such traces is shown in Fig. 4.14 , from which it can be seen that whilst the emission current, after stabilisation via 100 MΩ resistor, is quite stable, there are large fluctuations in both the extractor and first lens element currents, and were particularly marked in the case of the extractor current. While these various currents were being monitored, an electrostatic voltmeter was connected across the 100 MΩ resistor used to stabilise the emission current, and this showed large variations of 200 - 300 Volts across it. This therefore suggested that a strong correlation existed between the variations in the intensity of the final display at the screen and the characteristic field emission pattern falling on the extracting electrode, since the monitored current fluctuated dramatically although the stabilised total current is quite stable.

The variations in the voltage drop across the 100 MΩ resistor and
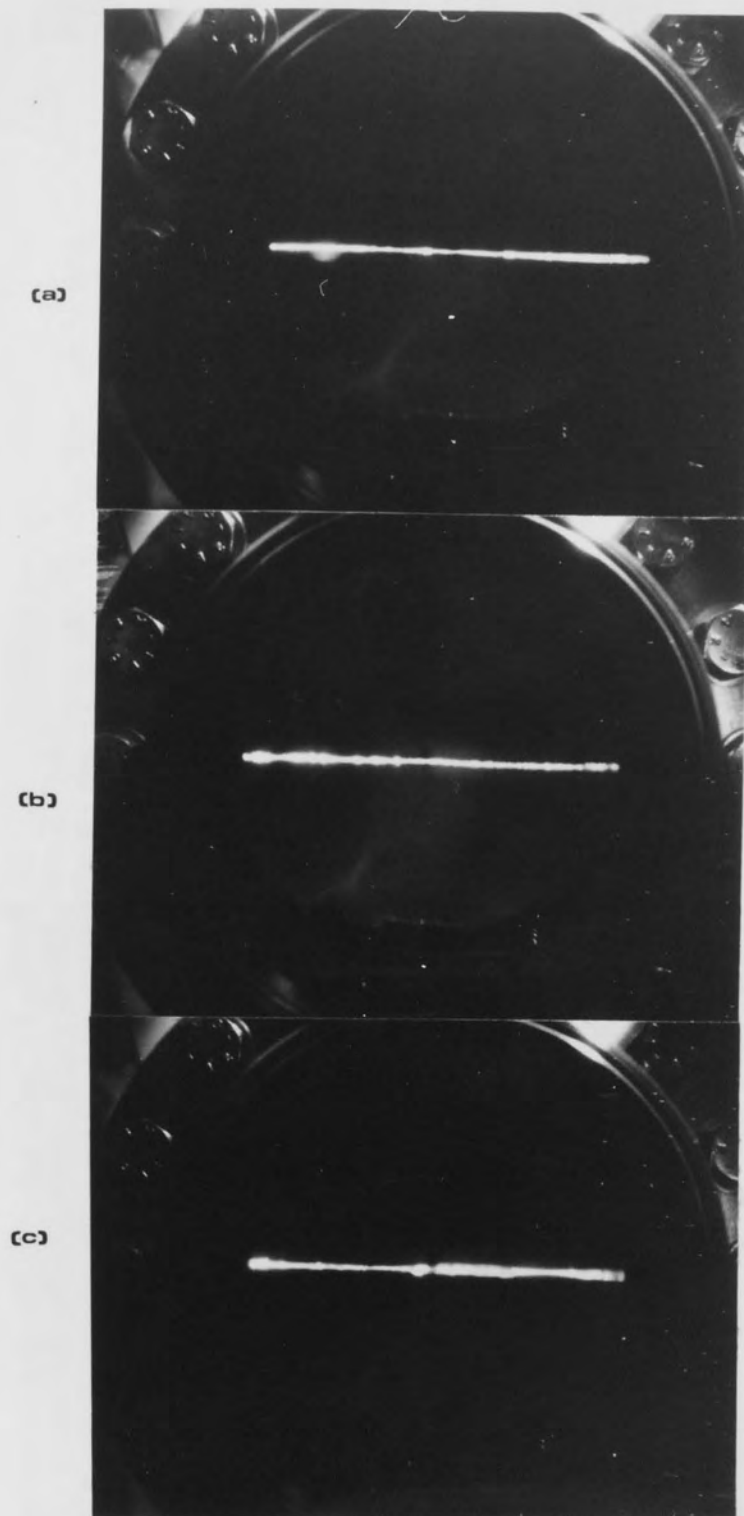
Fig. 4.13 Slow scan traces for (a) Wilson's gun ($V_I / V_o = 5$),

(b) $V_I / V_o = 10$ and (c) $V_I / V_o = 3.8$.
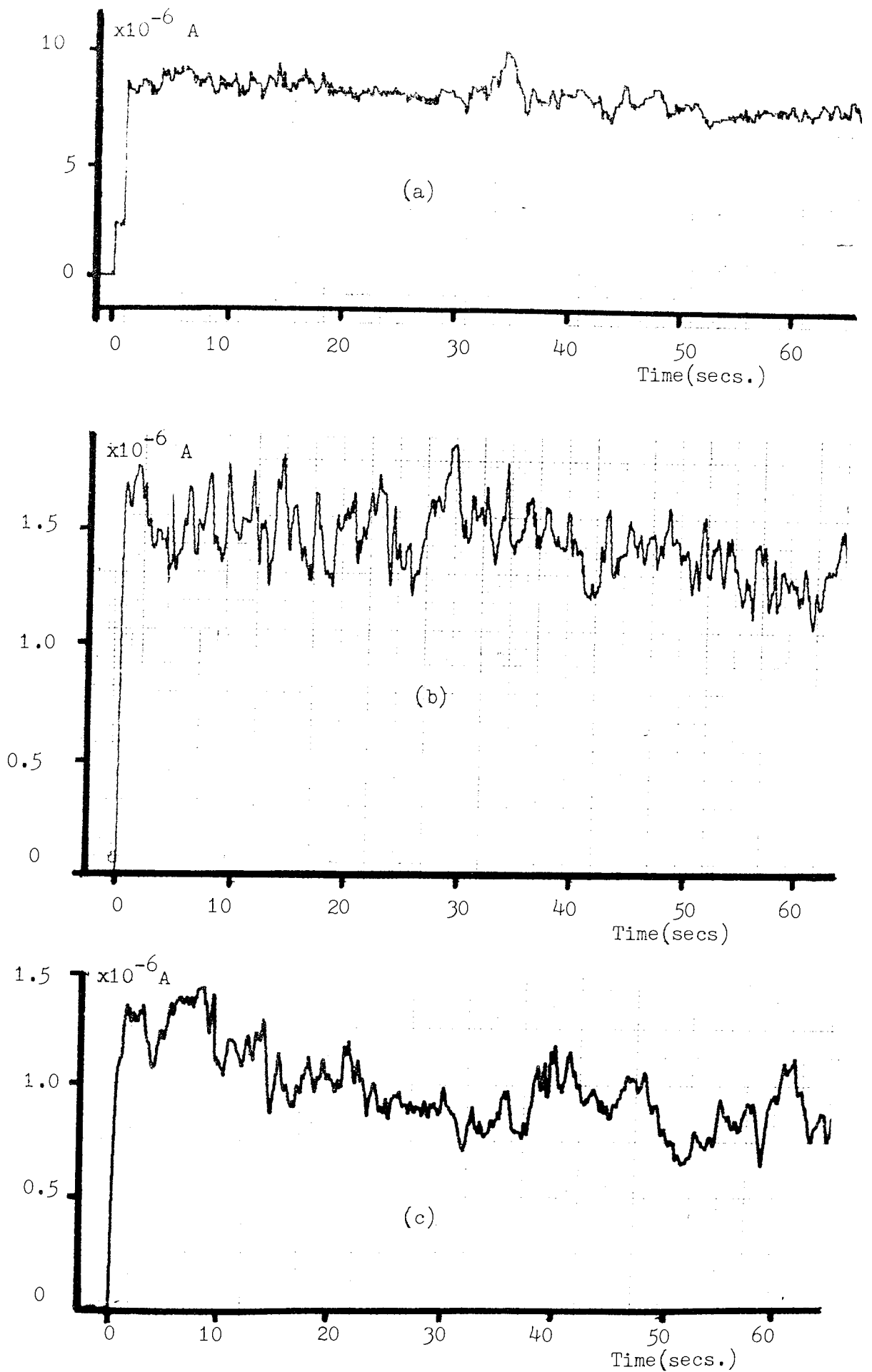
Fig. 4.14 Chart recorder traces of simultaneously monitored
(a) total emission current, (b) current collected
by extractor and (c) first lens element current.

therefore, the variation in the cathode voltage, would lead to defocussing effects.

The variation in the screen intensity will be discussed in more detail in the next section, whilst here, attention will be concentrated on first understanding, and then minimising the defocussing effects. Thus from an analysis of the above data, the defocussing effect could be understood in terms of the sensitivity of the gun to small changes in the voltage ratio (V_I / V_o), such as would result from variation in the tip voltage due to 100 MΩ feed-back resistor. This can be seen from graph in Fig. 4.11 outlining the focussing properties of the gun. Where the working point of the gun (marked with an x) is seen to lie on a quite a steep part of the curve; i.e. implying that a small change in V_I / V_o would require large changes in the object distance (S_o) to keep the beam focussed on the screen placed at 300 mm focal point of the gun. Since the object distance is fixed, the focal point of the gun therefore fluctuates to compensate. Therefore to reduce the defocussing effects of the gun to a satisfactory level, it is necessary to choose a better working point such that it lies on a flat part of the curve. Therefore to investigate the choice of a better working point for the gun that would improve its performance, two more gun modules having source distances of 6 mm and 16 mm, with working points at V_I / V_o = 10 and 3.8 respectively, were subsequently tested. The typical defocussing effects which were encountered in these are displayed respectively in Fig. 4.13 (b) and (c), and as expected, in the gun with working point at V_I / V_o = 3.8, the defocussing effects were found to be comparatively high; however, the gun with V_I / V_o = 10 showed little improvement in practice, even though a high degree of improvement had been expected. This was mainly due to the *effect of the* high voltage ratios used which

highlighted the aberrations in the focussing; i.e. resulting from
secondary emission at the apertures and fluctuations in the electron
energies due to variations in the voltage drop

across 100 MΩ resistor. The high voltages used to satisfy the
high voltage ratios (V_I / V_o) requirements, cause the electrons
to diverge from the main beam with sufficient energy to cause
secondary emission when they hit various electrodes. The image
formed on the screen by secondary electrons tends to fluctuate in
intensity due to variation of energy of diverging primary electrons
caused by fluctuating voltage drop across 100 MΩ feed-back
resistor. Furthermore the diverging of the electrons in this case
is made serious by small source distance, 6 mm, and therefore small
field free region between extractor and first lens element which is
in this case 5 mm as compared to 10 mm. To overcome these diff-
iculties, it was therefore decided to redesign the gun with the aim
of improving the defocussing instabilities.

4.6 AN EVALUATION OF THE RESIDUAL TEMPORAL AND SPATIAL INSTABILITY.

Although it was pointed out in section (4.5) that the
fluctuations in the intensity of the final image at the phosphor
screen are strongly correlated with the variations in both the total
emitted current and that intercepted by the extracting electrode,
the magnitude of their contribution,and how strongly the initial
variations are correlated to the final variations,is not known. It
is therefore necessary to gain further insight into the origin of
these variations before any steps could be taken to minimise these
effects. One way to do this would be to simultaneously measure
variations in the tip current, the extractor current variations and
the variations in the optical intensity of the final image.

Accordingly, a light detector was developed to monitor the intensity variation of the focused spot at the screen. The circuit diagram of this facility is shown in Fig. 4.15 , where the light intensity fluctuations on the screen are detected by the high-speed photo diode. The signal from this is then amplified in two stages using J-F E T amplifiers having large open loop gains,where the gain of the first amplifier was fixed and that of the second was made variable so that the sensitivity could be varied to obtain an output signal that is easily recordable on a chart recorder for subsequent analysis. In particular, it had to operate when the amplitude of the light signals from the screen were low; this was because it was found necessary to keep the intensity of the stationary focused spot as low as possible in order to prevent the screen phosphor from burning. Finally, as a third stage,a buffer amplifier was incorporated to firstly isolate the circuitry from electrical noise when connected to the chart-recorder, and secondly to match the two impedances. The output from the buffer amplifier was recorded using a J. J. Lloyd C552 type chart recorder, whose response time was limited by its writing speed to about one tenth of a second. However this was more than adequate to handle the low-frequency fluctuations displayed in the scan traces of Fig. 4.13 . To minimise the electrical noise picked up,the amplifier was housed in a dicast box which was securely bolted to the large aluminium cylinder containing the photo-diode as shown in Fig. 4.16 . The photo-diode assembly was further enclosed in another smaller aluminium cylinder, one end of which was covered with a very fine mesh which was found to be sufficient to screen the photo-diode from electrical noise picked from the tube itself whilst being sufficiently transparent to allow an adequate light intensity to reach the photo-diode. Before using the device,the focused spot was
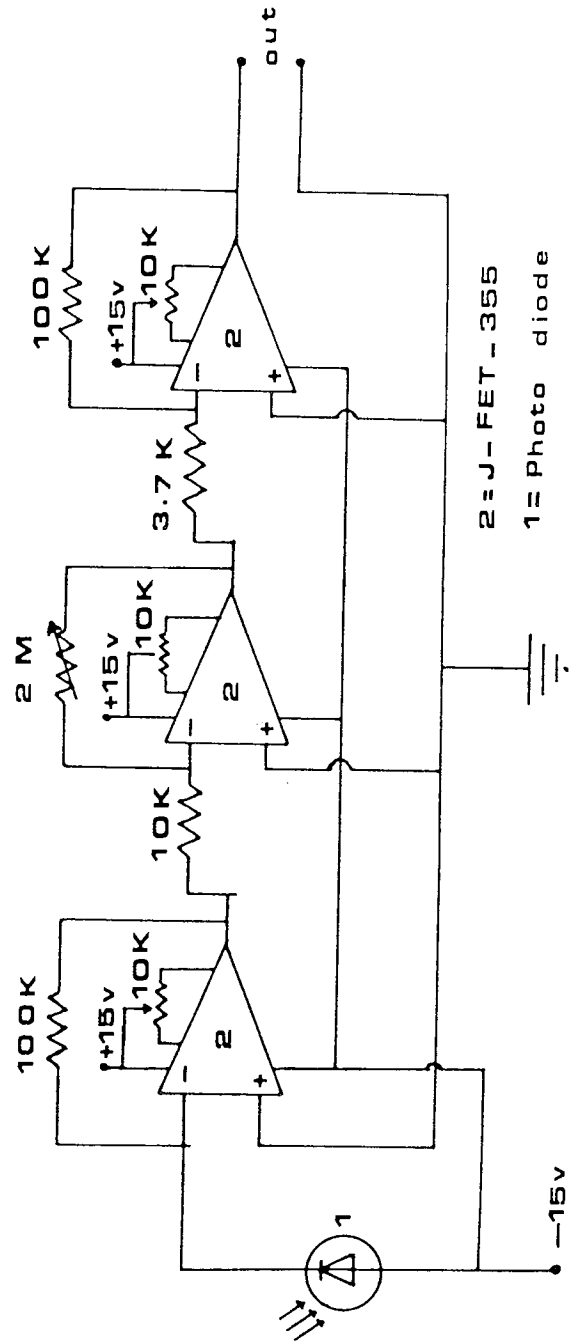
Fig. 4.15   Circuit diagram of optical monitor.

2=J-FET-355

1= Photo diode

To chart recorder

Amplifier

Fine mesh

Screen

Viewing hole

Photo diode

Outer cylinder

Inner cylinder
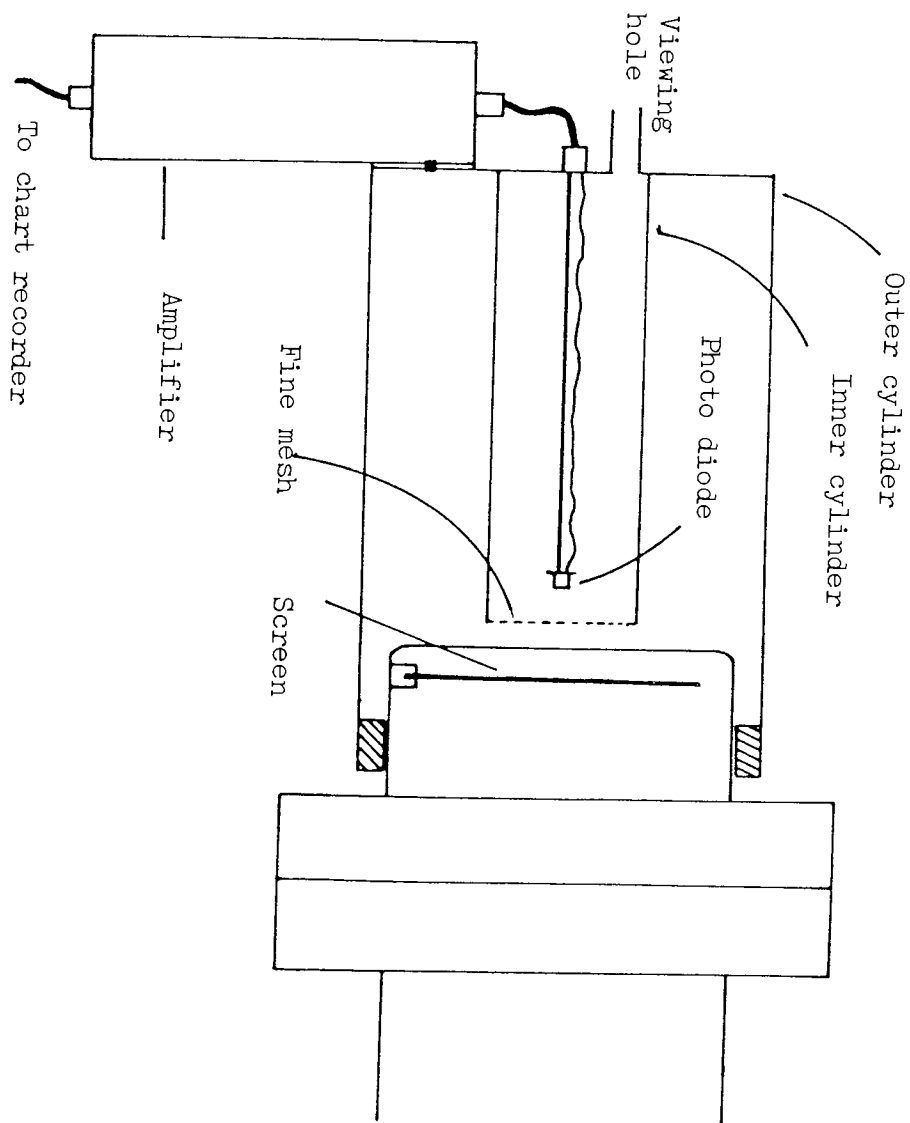
FIG. 4.16   Optical monitor lay-out.

first centralised by applying appropriate d.c. voltages to the x and y deflector plates until a maximum response was obtained on the chart recorder.

The first application of the light detector was to establish if there was any temporal correlation between the fluctuations in spot intensity and the simultaneously recorded total emission current. Thus referring to the typical result of Fig. 4.17 , it will be seen that the respective noise levels of the screen intensity and total emission current are $\sim$ 71% and 28% . A closer inspection also shows that there is a temporal correlation between the fluctuations in the two variations for lower frequencies; however, this is difficult to see at first, since the variations at the screen has other contributory factors introduced in the intermediate stages between cathode and the screen which will be described later. It can however be seen that when the tip current increases the intensity at the screen also increases. A similar comparison was made between extractor and the light intensity signals from the screen, see Fig. 4.18 , and again the two variations are just as vigorous. In addition, it is possible to identify an "inverse" temporal relationship between the fluctuations of the two signals, whereby when the extractor current increases, the intensity of the light emitted from the flourescent screen decreases. This therefore suggests that the extractor electrode also plays some role in bringing about the intensity   fluctuations occuring at the screen.

The exact nature of this role can be understood when the current emitted from the carbon fibre is imaged directly on the screen in a field emission microscope. Thus referring to Fig. 4.19 , it is seen to be composed of large number of emission spots of varying sizes, where the intensity of the light emitted from each of these regions
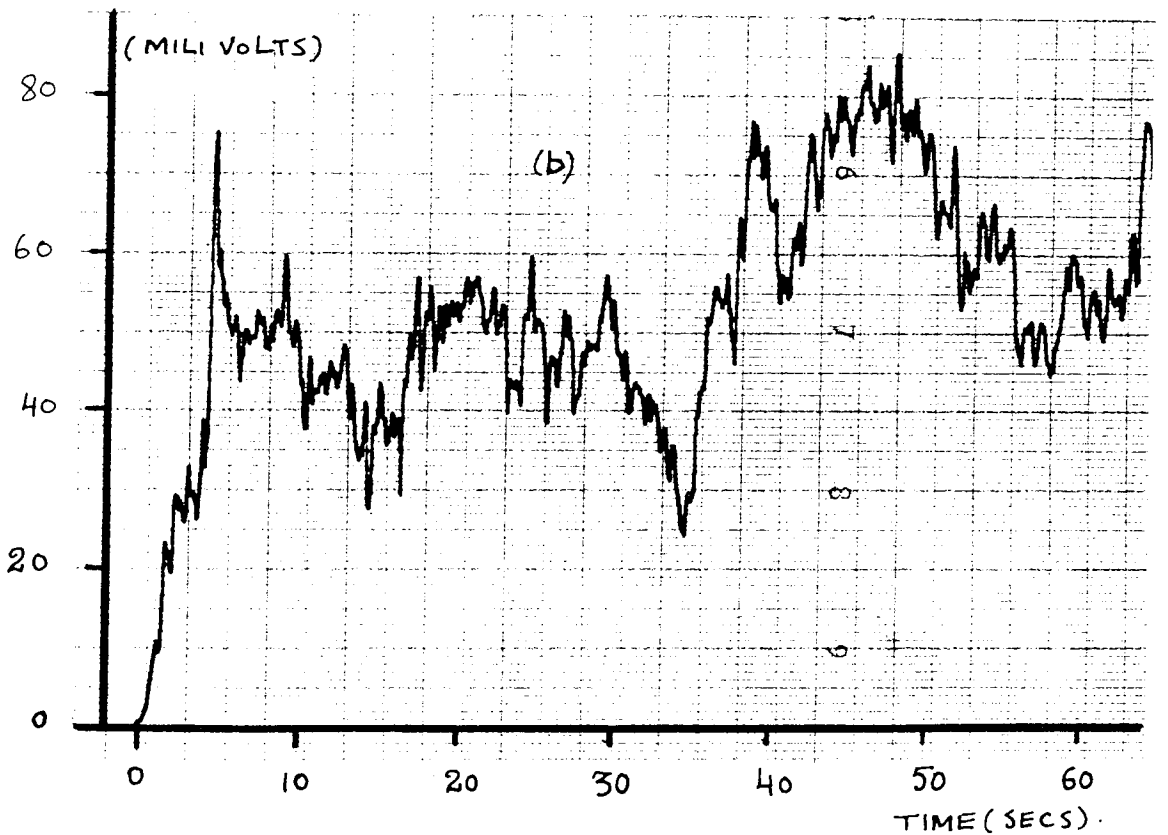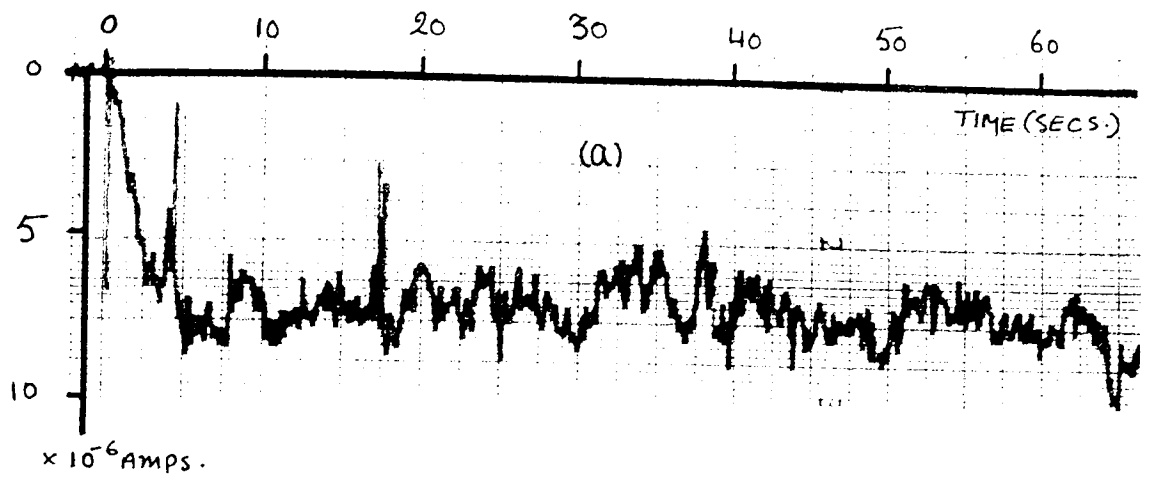
Fig. 4.17

Simultaneously monitored chart recorder traces of
(a) total current after stabilisation using 100 MΩ
resistor and (b) optically monitored light intensity
from the screen.
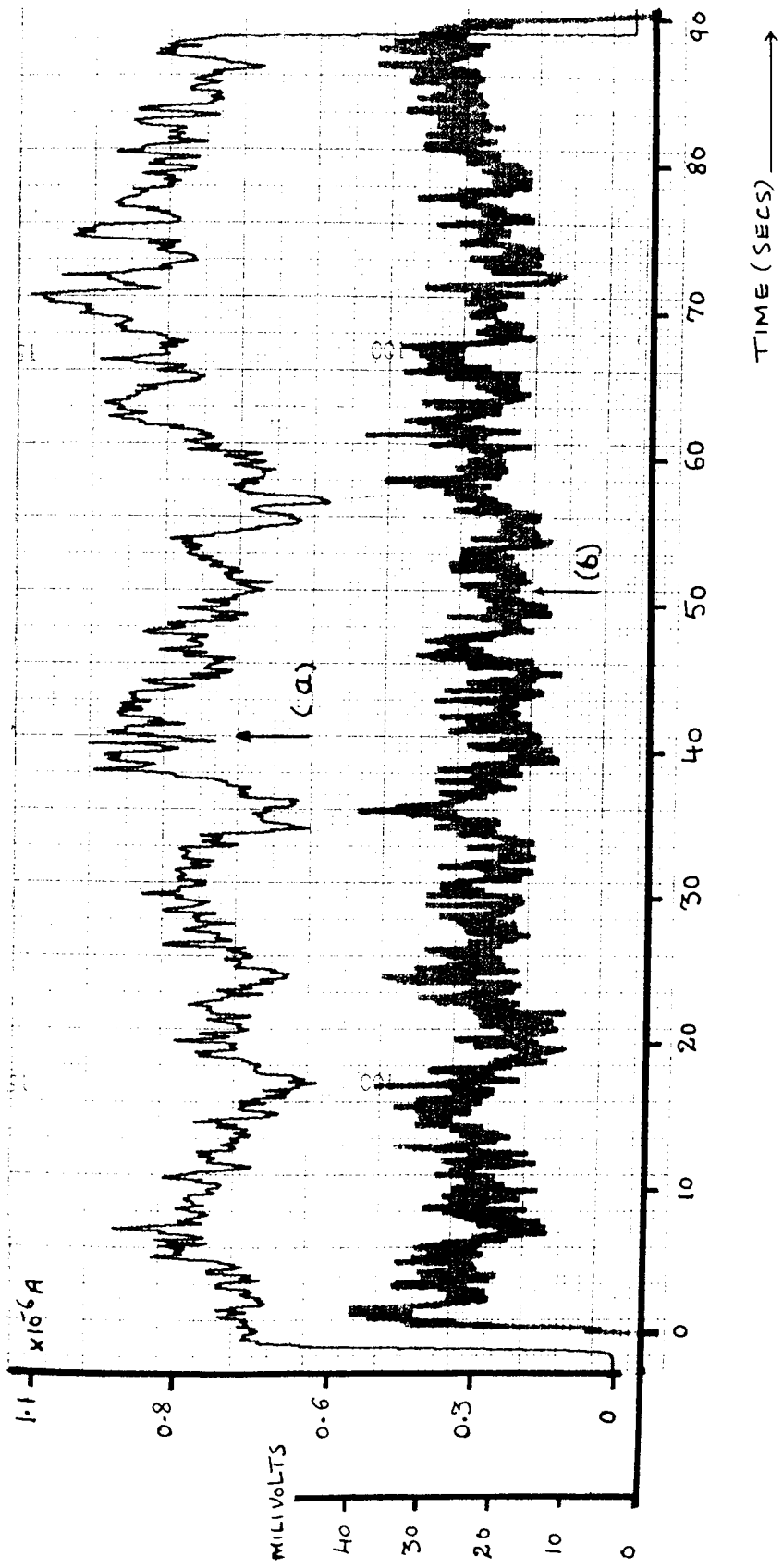
Fig. 4.18 Simultaneously monitored chart recorder traces of (a) current collected by extractor

(b) optical signal from the screen.
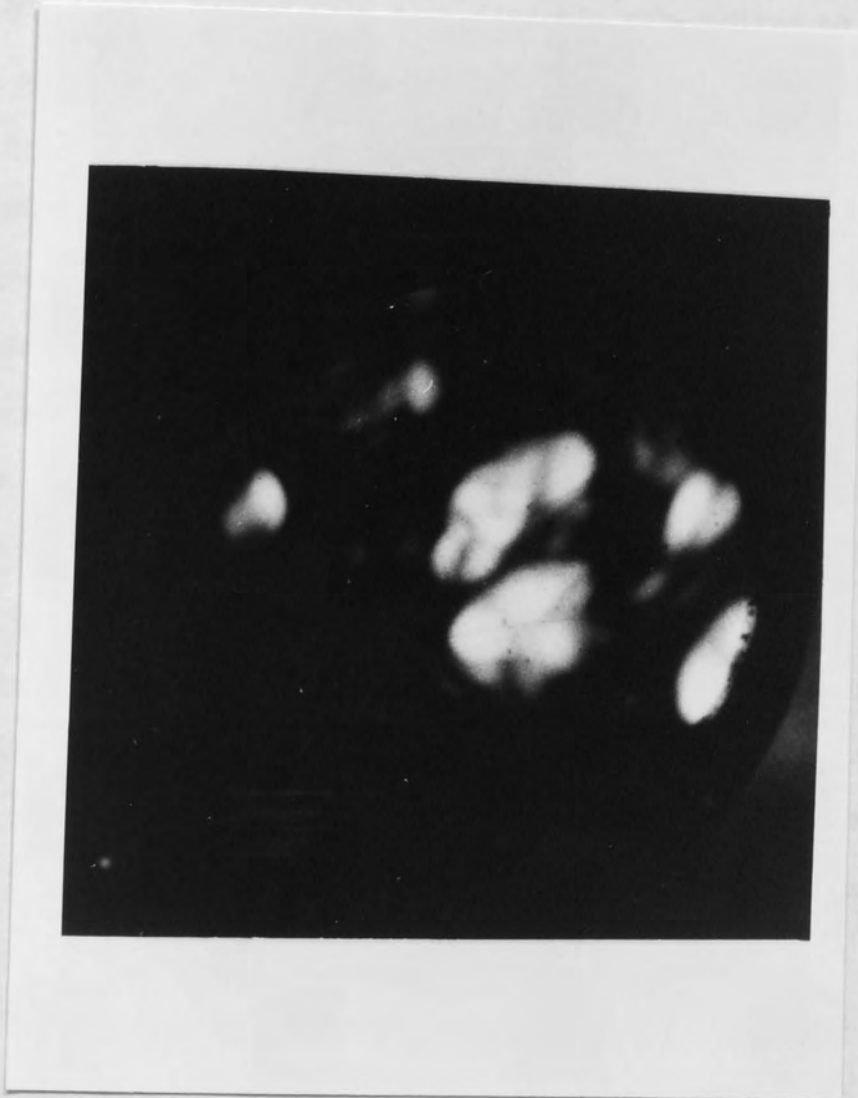
Fig. 4.19   Field emission image   from a carbon fibre.

is continuously and independently varying with time; infact, sometimes a spot will completely disappear and then randomly switch back on at some future time. From these observations, it is clear that the electron emission occurs from many discrete sub-centres on the cathode surface and that because the magnitude of the current emitted from each site is continuously changing, there are large resultant fluctuations in both the total current and visual display. It follows therefore that when such complex emission pattern falls on the extractor electrode, the magnitude of the current transmitted to the screen will be determined by both the number of spots, and their relative intensities that happen to be falling on the extractor aperture at any instant. This is clearly demonstrated in Fig. 4.20 (a) and (b) which shows the emission pattern falling on the extractor at two different instants for the same total emission current. At an instant 'a', the majority of the emission spots are falling over the extractor aperture and therefore the current reaching the screen will be large, whilst at a later instant 'b' the relative number of spots falling on the aperture is small and thus the current at the screen will drop and cause the visual display at the screen to correspondingly fluctuate. Thus although the total current can be stabilised to a satisfactory level by using a high valued resistor in series with the emitter, (the method initially used by Baker et al (13) to protect the tip against destruction due to these large surges in the total current), the characteristic variations in the individual spots of the emitted current falling on the extractor remains unchanged. In this context, the use of a high-valued resistor as a negative feed-back loop has one serious draw-back, in that it causes the voltage at the cathode tip to fluctuate by some 100 - 200 Volts which leads to the defocusing effects already

(a)

Extractor

Aperture Emission spots

(b)
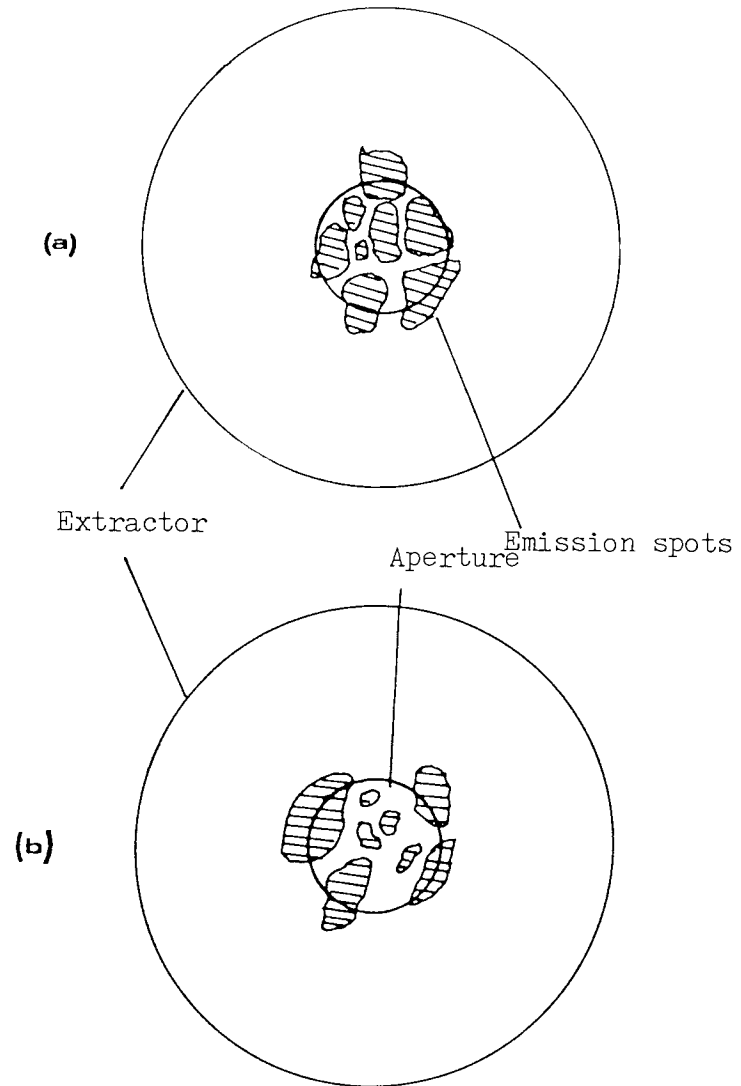
Fig. 4.20 To show variation in the current transmitted through
the extractor aperture.

described. To gain a perspective of the magnitude of this defocusing effect it should be noted that   if the tip voltage is deliberately increased by 100 Volts, a focused spot, originally of 0.2 mm in diameter, is defocused to about 1.15 mm, when monitored by a travelling microscope.

Summarising therefore, it should be possible to take practical precautions to minimise the two types of variations encountered at the screen. Firstly the defocusing effects could be treated by employing a suitably designed electrostatic lens system in which the variation of the tip voltage has only a small affect on its focusing properties; this can be achieved by arranging for the working point of the gun to be on the flat part of the curve in Fig. 4.11 at say a voltage ratio of around 5. Secondly, a feed-back system could be employed to stabilise the current reaching the screen: one possibility would be to sample the screen current and use this to control the total emission current. These two approaches will now be discussed in greater detail.

4.7 DESIGNING AND TESTING OF POSSIBLE ELECTROSTATIC LENS CONFIGURATIONS.

4.7.1 ELECTROSTATIC LENS DESIGNS.

The purpose of this study was twofold. Firstly to design a 300 mm focal length lens that would minimise the de-focusing effects described in the section 4.6 . Secondly, to design a field emission gun with a 50 mm focal length electrostatic lens suitable for use in a miniature high resolution cathode ray tube, M-O valve type LD 937, where it is necessary for the electrodes to be as close as possible so that the overall length of the tube could be kept to the required

length of 130 mm. Referring to Fig. 4.21 (a), the lens system that was investigated consisted of a two-element lens in the form of flat circular discs with central apertures, where the two elements, with aperture diameters of d_1 and d_2 and at potentials of V_0 and V_I with respect to cathode, are separated by a distance S so as to produce a focused image at S_I . The thickness of the lens element plates was chosen to be 0.6 mm as these were readily available from the G.E.C. M-O valve company. The distance S_0 from the tip of the cathode, where the emission is assumed to occur, to element A, is the object distance, and the distance S_I from the element A_2 to the focused spot is the image distance.

The electron optical properties of such asymmetrical lens system were then determined using two computer programmes previously used by Wilson [14] to design a 300 mm focal length gun. These modified programmes however needed further minor corrections so that the extended data used for this study could be fed in. The corrected programmes were first tested with data originally used by Munro for computing the properties of one of his lens systems, and then further tested by repeating computation made by Wilson [14] for one of his lenses. Once the programmes were running satisfactorily, the properties of the lens types described above were then computed in two stages using these programmes. The first programme calculates the axial potential distributions in the lens using the finite element method with boundary conditions determined by the lens geometry, as shown in Fig. 4.22 . For the case of this asymmetrical lens configuration, first a boundary surrounding the lens elements is chosen and here defined as ABCD. This boundary is fixed by a radial distance at which the inter-electrode field can be assumed to be uniform and axial distance at which the potential can be assumed to be constant.
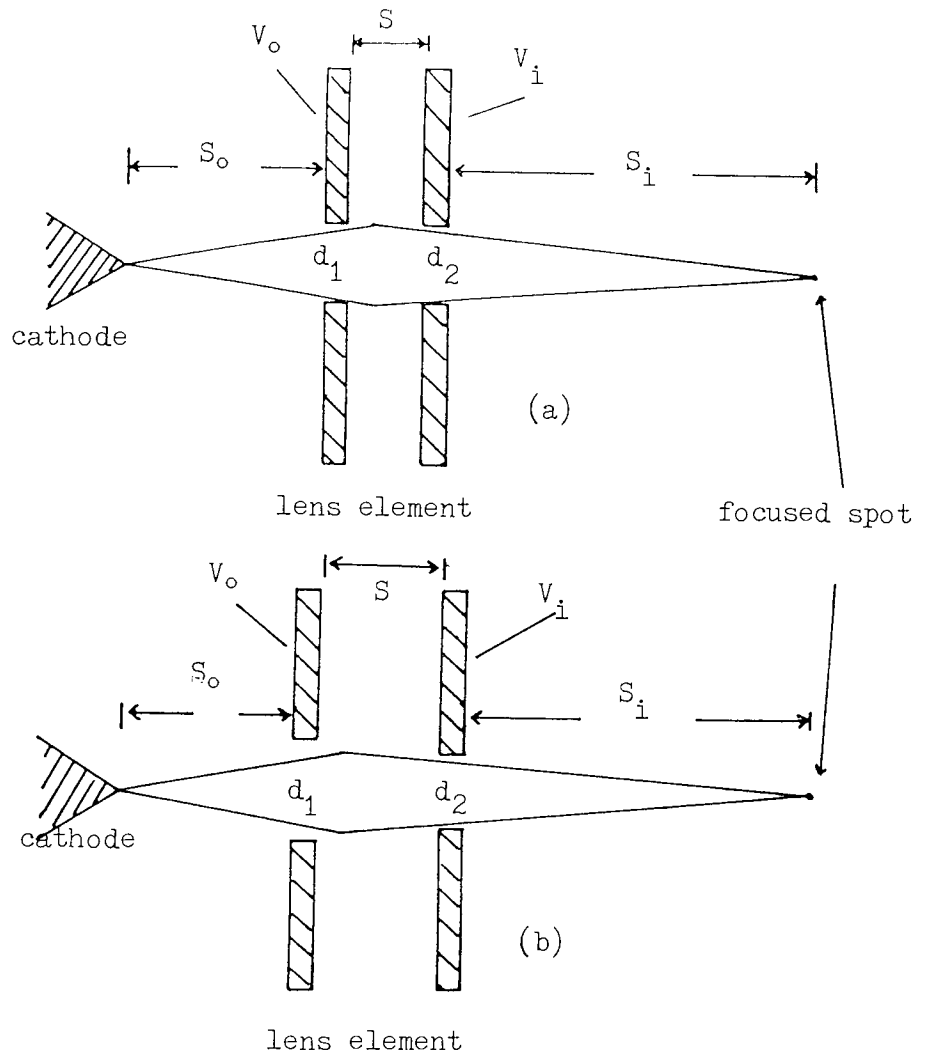
Fig. 4.21   Two types of lens systems investigated
(a) $d_1 = d_2$ and (b) $d_1 > d_2$.
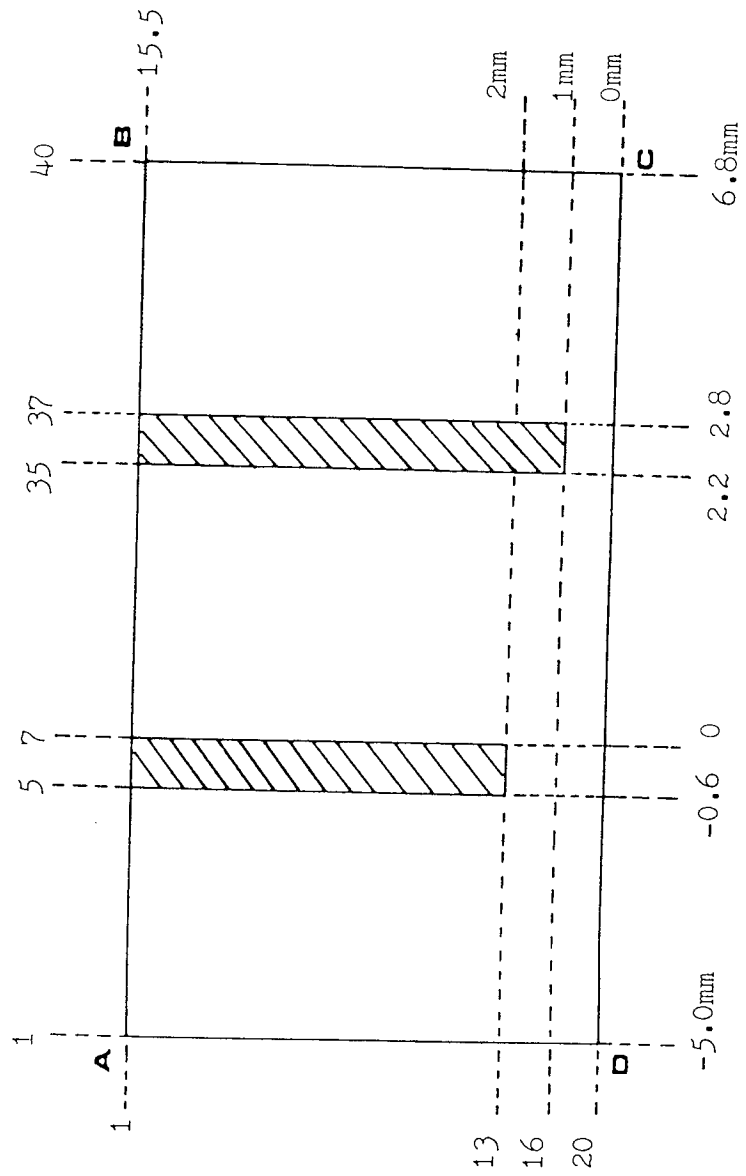
Fig. 4.22   To show lens boundary chosen for computer analysis.

The computer then divides this region into 40 mesh lines along AD and 20 in the AB direction to give a fine mesh for the finite element analysis where the programme then computes potentials at each mesh point and the axial potential distribution along BC. These two quantities were then computed for various apertures d, and d_2 for the two situations $d_1 = d_2$ and $d_1 > d_2$ over a range of separations 'S' between the lens elements as in Fig. 4.21 (b). These axial potentials are then used in the second programme to compute electron trajectories and optical properties for each lens configuration by solving the ray equation. The programme can handle Zero, Low, High and Infinite magnifications, depending on the boundary conditions decided by the working distance and the size of the image required. Then, for the specified range of the object side voltage, V_o and image side voltage, V_I , the programme computes the object plane or image plane (depending on the magnification mode chosen), the magnification, and the coefficients of spherical and chromatic abberation. The programme was used in its high magnification mode, in which case apart from V_o and V_I , the distance of image plane also has to be specified, where image distance 300 mm and 50 mm were considered, and voltages V_o and V_I were chosen such as to give voltages ratios (V_I / V_o) in the range of 2 and 20. When the programme is used in this high magnification mode, the optical properties, the object plane, magnification, and the coefficients of spherical and chromatic aberration obtained are then referred to the object side. These optical properties were then computed for various lens element aperture sets, for the both cases $d_1 = d_2$ and $d_1 > d_2$, while varying the inter element separation for each set in the range of 1.4 cm to 2.6 cm. These properties versus the voltage ratio (V_I / V_o), presented in two forms, where the optimum

Voltage ratio (V_I / V_0)	Object distance S_0 (mm)	Magnification M	Spherical aberration C_S (mm)	Chromatic aberration C_C (mm)
2	66·4	3·7	44404	114·7
4	18·0	12·2	2751	22·2
6	9·34	19·9	83·79	7·7
8	7·27	24·0	35·26	4·92
10	6·21	27·0	19·82	3·58
12	5·6	29·1	13·0	2·8
14	5·2	30·8	9·4	2·3
16	4·9	32·0	7·2	1·9
18	4·6	33·1	5·7	1·6
20	4·47	33·9	4·7	1·4

Fig 4·23 Table of lens properties for element apertures of $d_1 = d_2 = 4$ mm, seperation of 1·4 mm and image distance of 300 mm
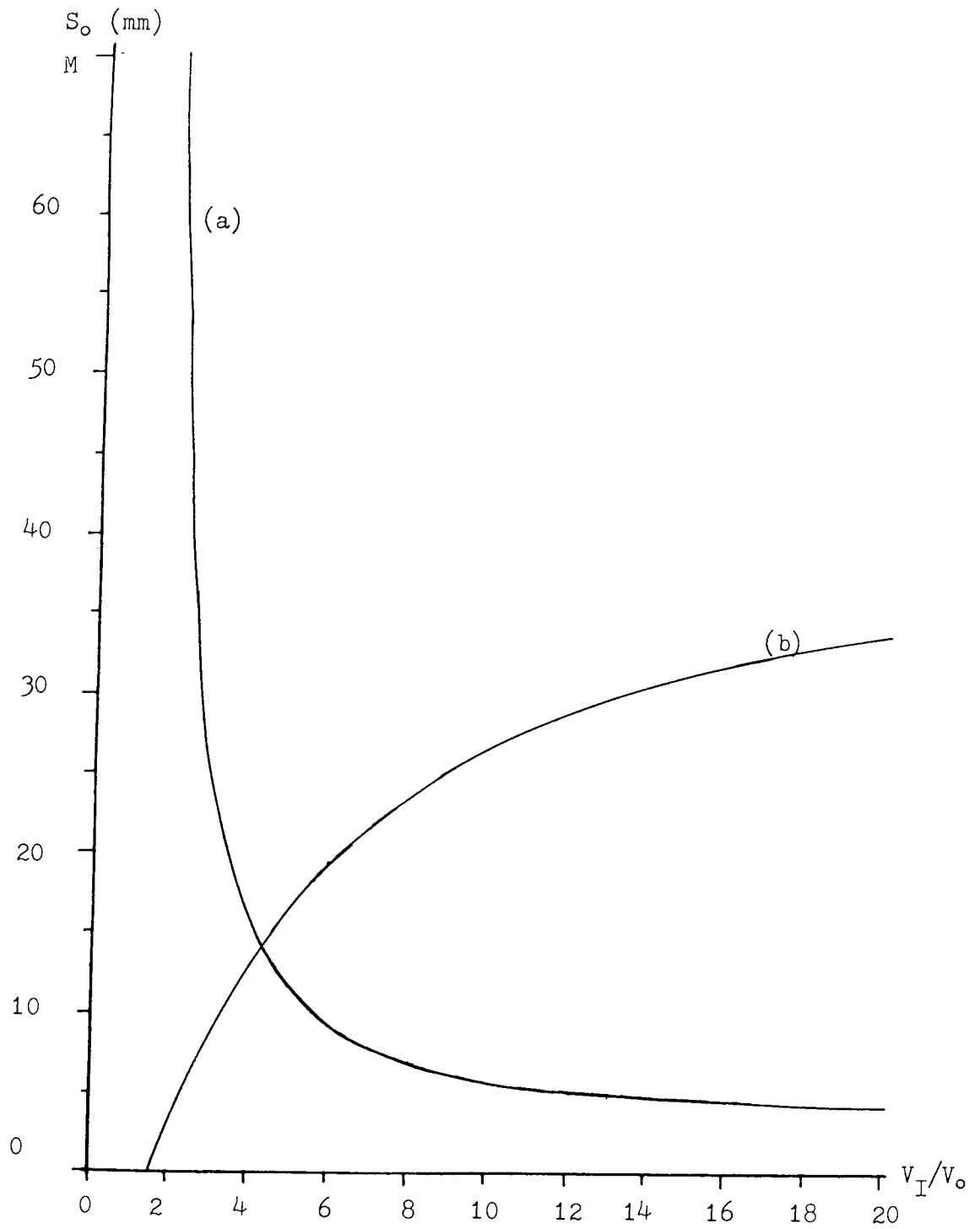
Fig. 4.24 Graphs of (a) source distance S_o and (b)

magnification as a function of voltage ratio V_I/V_o

for element apertures of $d_1 = d_2 = 4$ mm, separation

of 1.8 mm and image distance of 300 mm.

Fig. 4.25 Graph of spherical aberration (C_S) as a function of
voltage ratio (V_I/V_o) for element apertures of
$d_1 = d_2 = 4$ mm, separation of 1.8 mm and image distance
of 300 mm.

Fig. 4.26 Graph of chromatic aberration (C_c) as a function
of voltage ratio (V_I/V_o) for element apertures
of $d_1 = d_2 = 4$ mm, separation of 1.8 mm and image
distance of 300 mm.

Voltage ratio (V_I / V_0)	Object distance S_0 (mm)	Magnification M	Spherical aberration C_S (mm)	Chromatic aberration C_C (mm)
2	70·2	3·5	43257	123
4	15·5	11·5	252	80·1
6	9·4	19·2	80·3	8·1
8	7·2	23·4	33·9	5·2
10	6·1	26·3	19·1	3·8
12	5·45	28·5	12·5	3·0
14	5·0	30·2	9·0	2·4
16	4·7	31·5	6·9	2·0
18	4·5	32·6	5·6	1·7
20	4·3	33·5	4·6	1·51

Fig 4·27   Table of lens properties for element apertures of $d_1 = d_2 = 4$ mm and seperation of 2·2 mm and image distance of 300 mm.
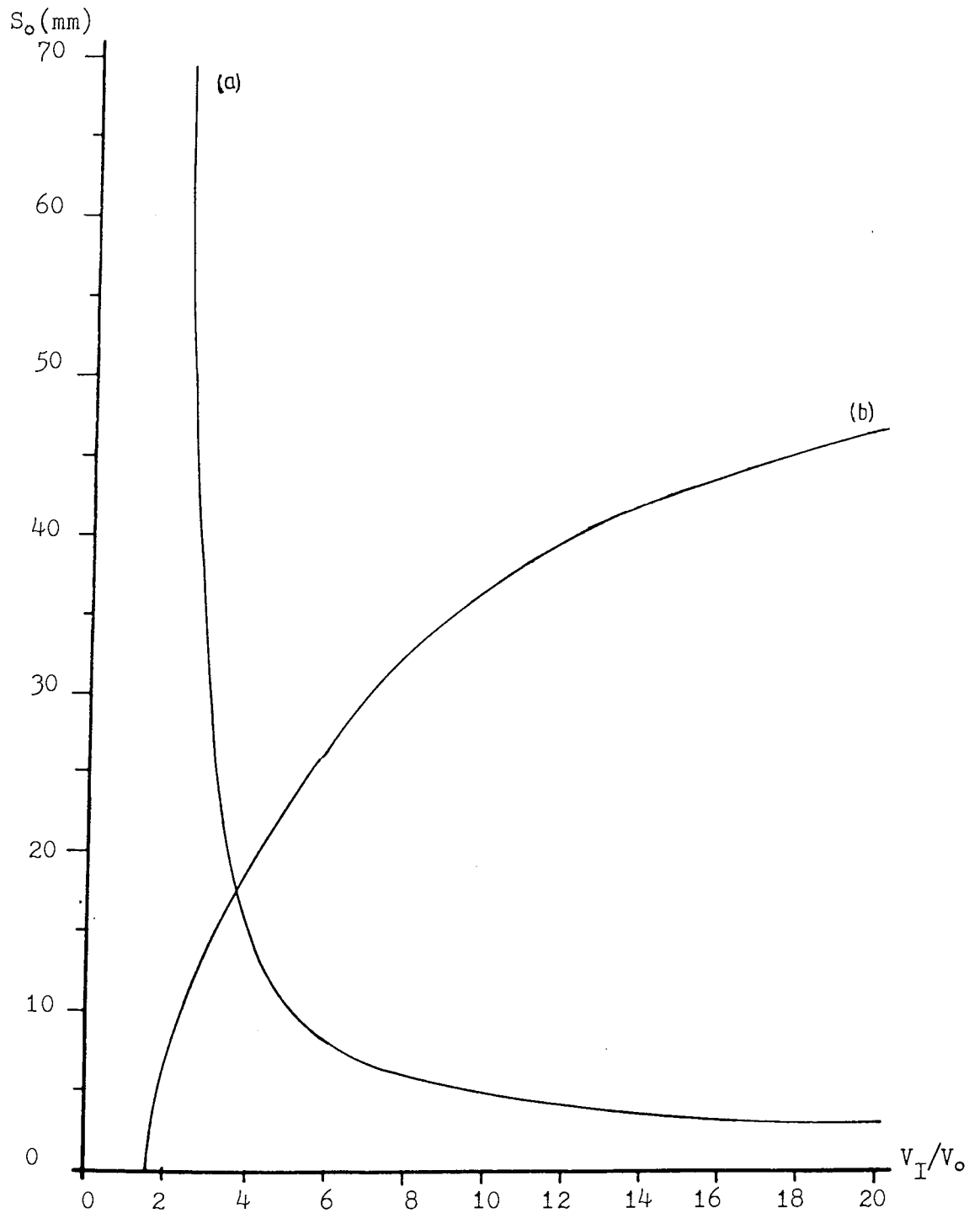
Fig. 4.28 Graphs of (a) source distance (S_o) and (b) magnification

(M) as afunction of voltage ratio (V_I/V_o) for element

apertures of $d_1 = d_2 = 3$ mm, separation of 1.8 mm and

image distance of 300 mm.
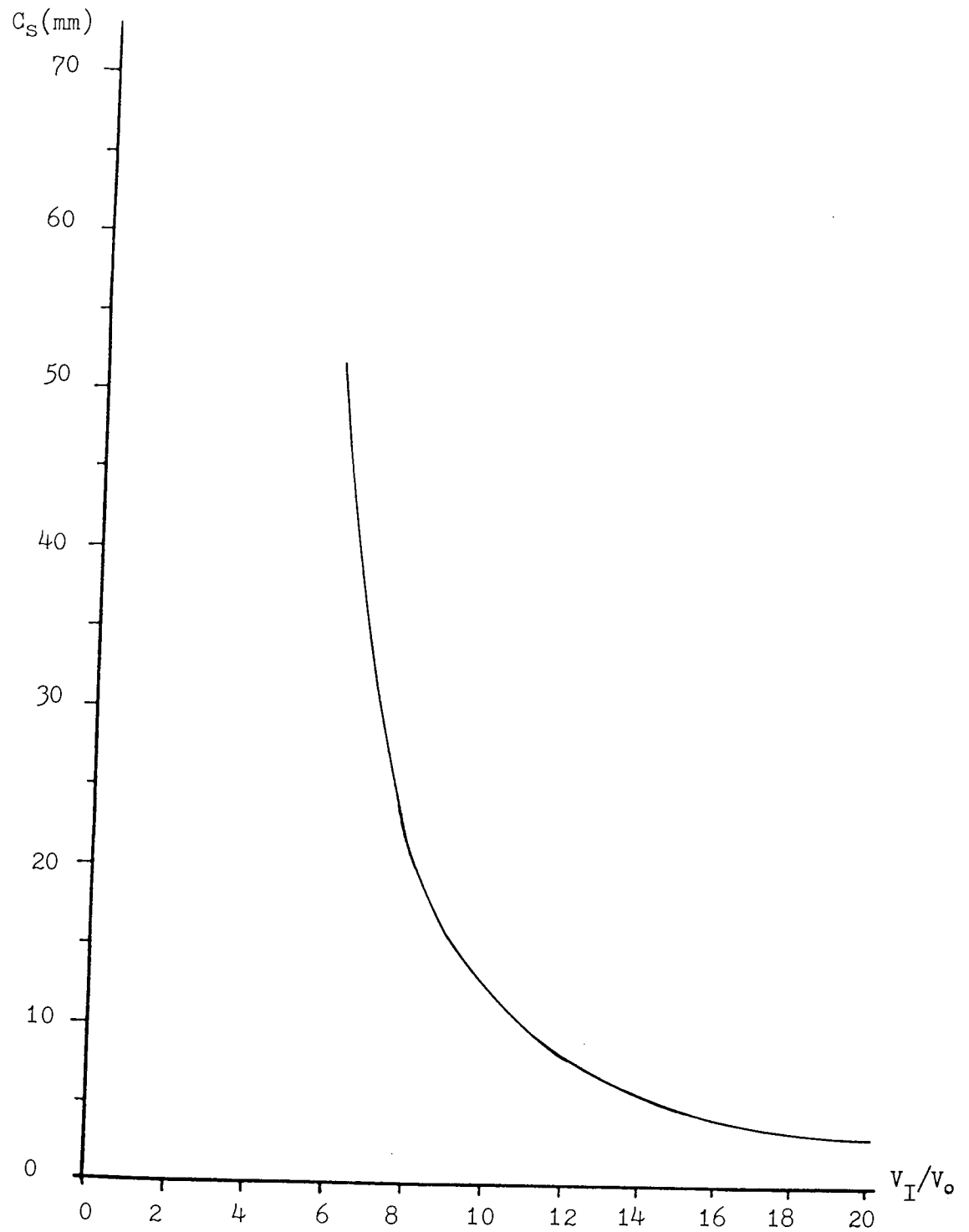
Fig. 4.29   Graph of spherical aberration (C_S) as a function of

voltage ratio (V_I/V_o) for element apertures of

$d_1 = d_2 = 3$ mm, separation of 1.8 mm and image distance
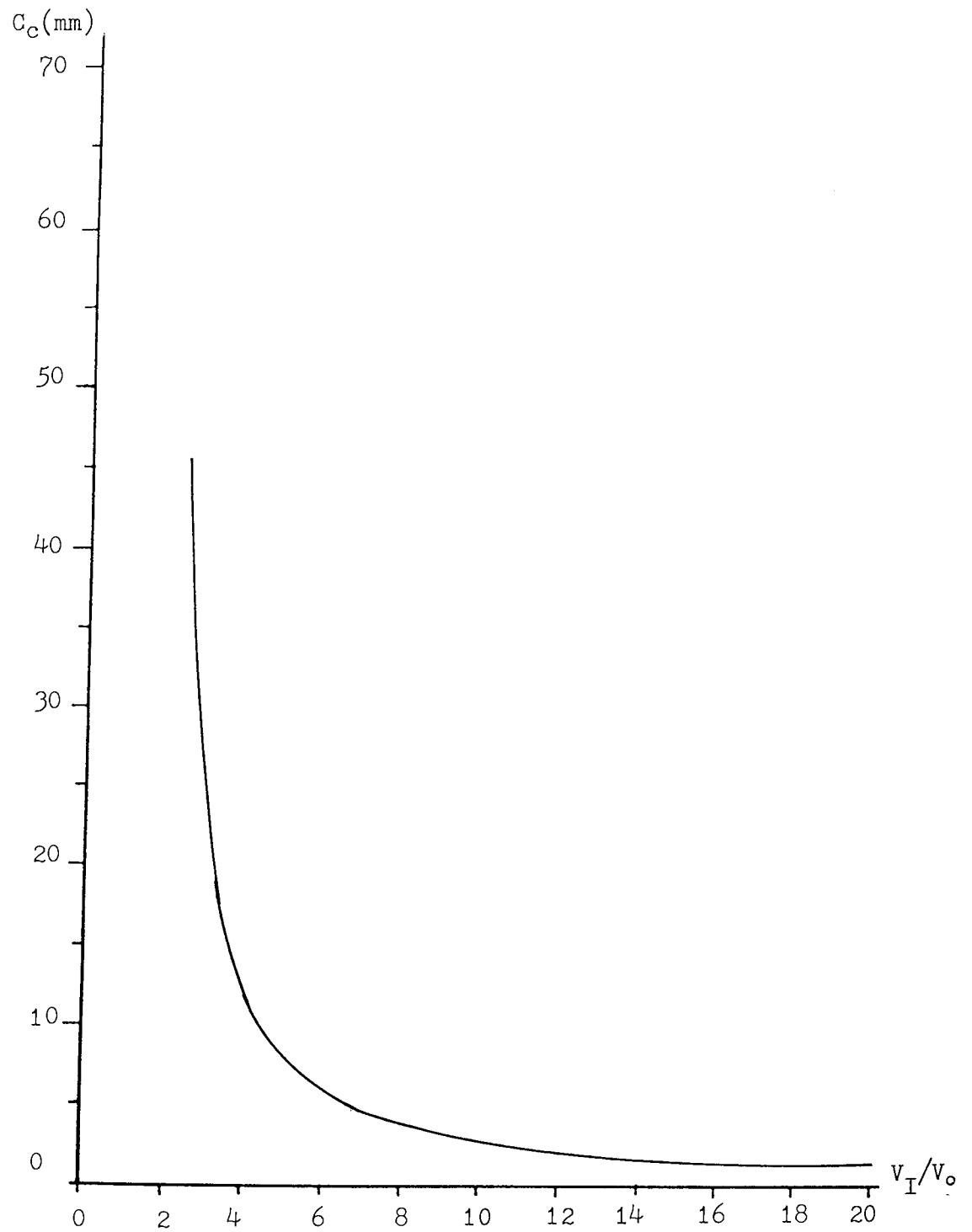
of 300 mm.

Fig. 4.30 Graph of chromatic aberration C_C as a function of

voltage ratio V_I/V_o for element aperture of $d_1 = d_2 =$

3 mm, separation of 1.8 mm and image distance of

300 mm.

Voltage ratio (V_I/V_0)	Object distance S_0 (mm)	Magnification M	Spherical aberration C_S (mm)	Chromatic aberration C_C (mm)
2	60·5	4·1	2×10^6	99·8
4	18·7	11·5	48120	21·4
6	8·9	20·9	3428	7·1
8	7·0	25·1	1288	4·6
10	6·0	28·1	662	3·4
12	5·4	30·3	404	2·6
14	5·0	31·9	274	2·13
16	4·7	33·2	200	1·8
18	4·5	34·2	154	1·5
20	4·3	35·0	123	1·3

Fig 4·31   Table of lens properties for element apertures of $d_1 = 4$ mm and $d_2 = 3$ mm and seperation of 1·4mm and image distance of 300mm.

Voltage ratio (V_I / V_0)	Object distance S_0 (mm)	Magnification M	Spherical aberration C_S (mm)	Chromatic aberration C_C (mm)
2	63·3	3·9	40735	110
4	18·9	11·4	849	22·2
6	8·9	21·0	73·4	7·2
8	6·9	25·4	31·1	4·7
10	5·9	28·4	17·5	3·4
12	5·3	30·7	11·6	2·7
14	4·9	32·4	8·4	2·2
16	4·6	33·7	6·4	1·8
18	4·4	34·8	5·2	1·6
20	4·3	35·6	4·3	1·3

Fig 4·32 Table of lens properties for element apertures of $d_1 = 4$ mm and $d_2 = 3$ mm, seperation of 1·8mm and image distance of 300 mm.
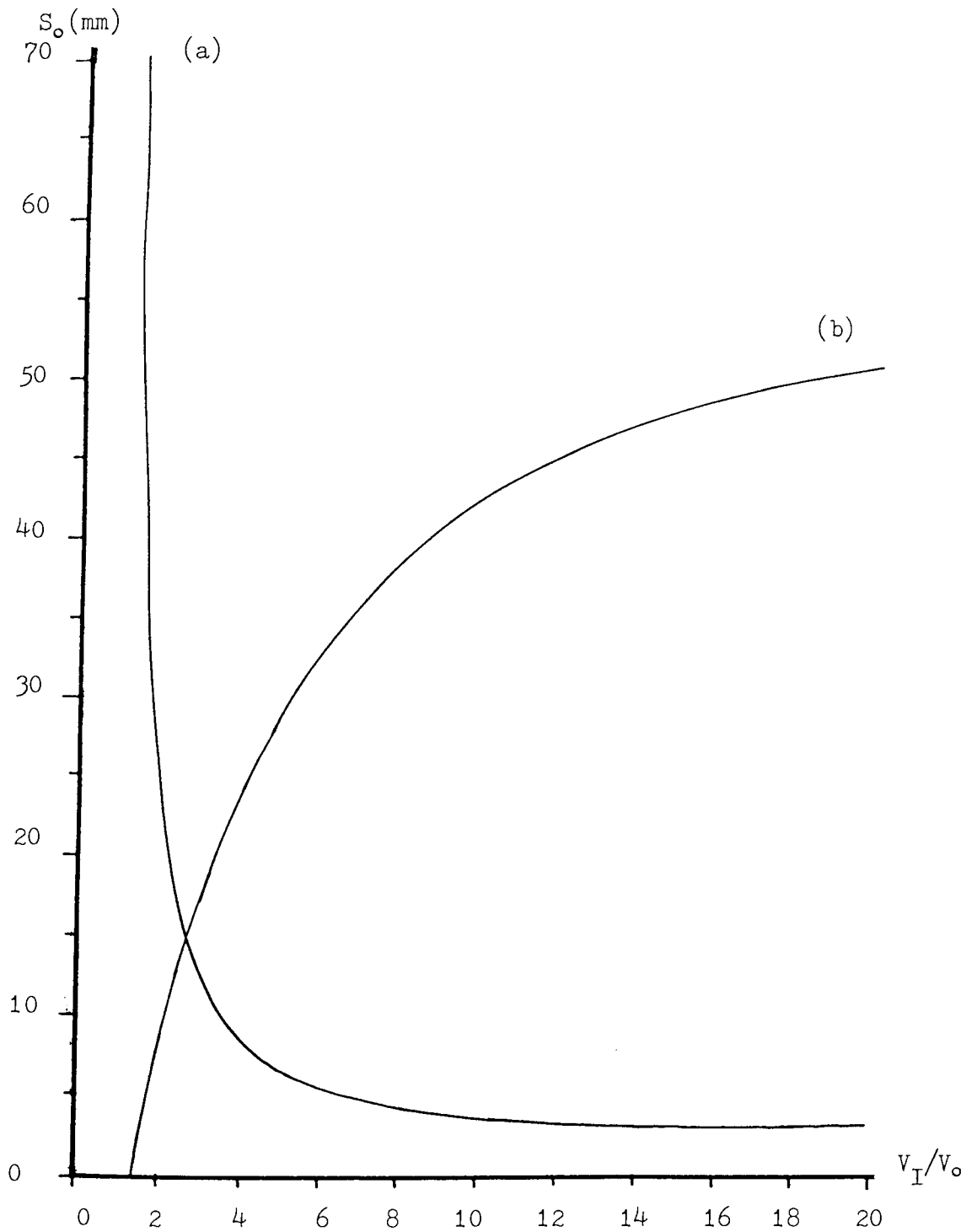
Fig. 4.33 Graph og (a) source distance (S_o) and (b) magnification

(M) as a function of voltage ratio (V_I / V_o) for

element apertures of d_1 = 4 mm and d_2 = 3 mm, separation

of 2.2 mm and image distance of 300 mm.
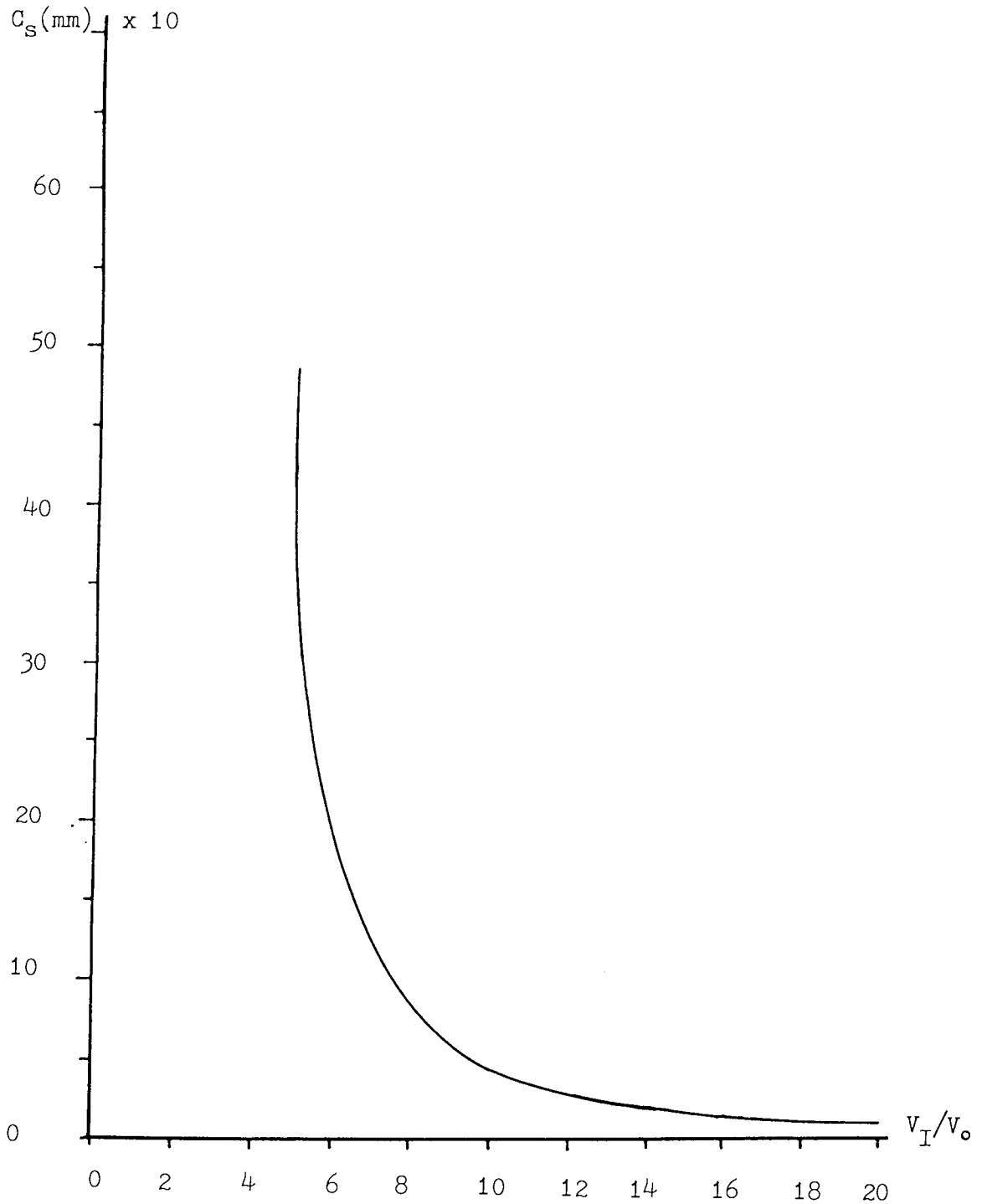
Fig. 4.34   Graph of spherical aberration (C_s) as a function of

voltage ratio (V_I / V_o) for element aperture of

d_1 = 4 mm and d_2 = 3 mm, separation of 2.2 mm grid image

distance of 300 mm.
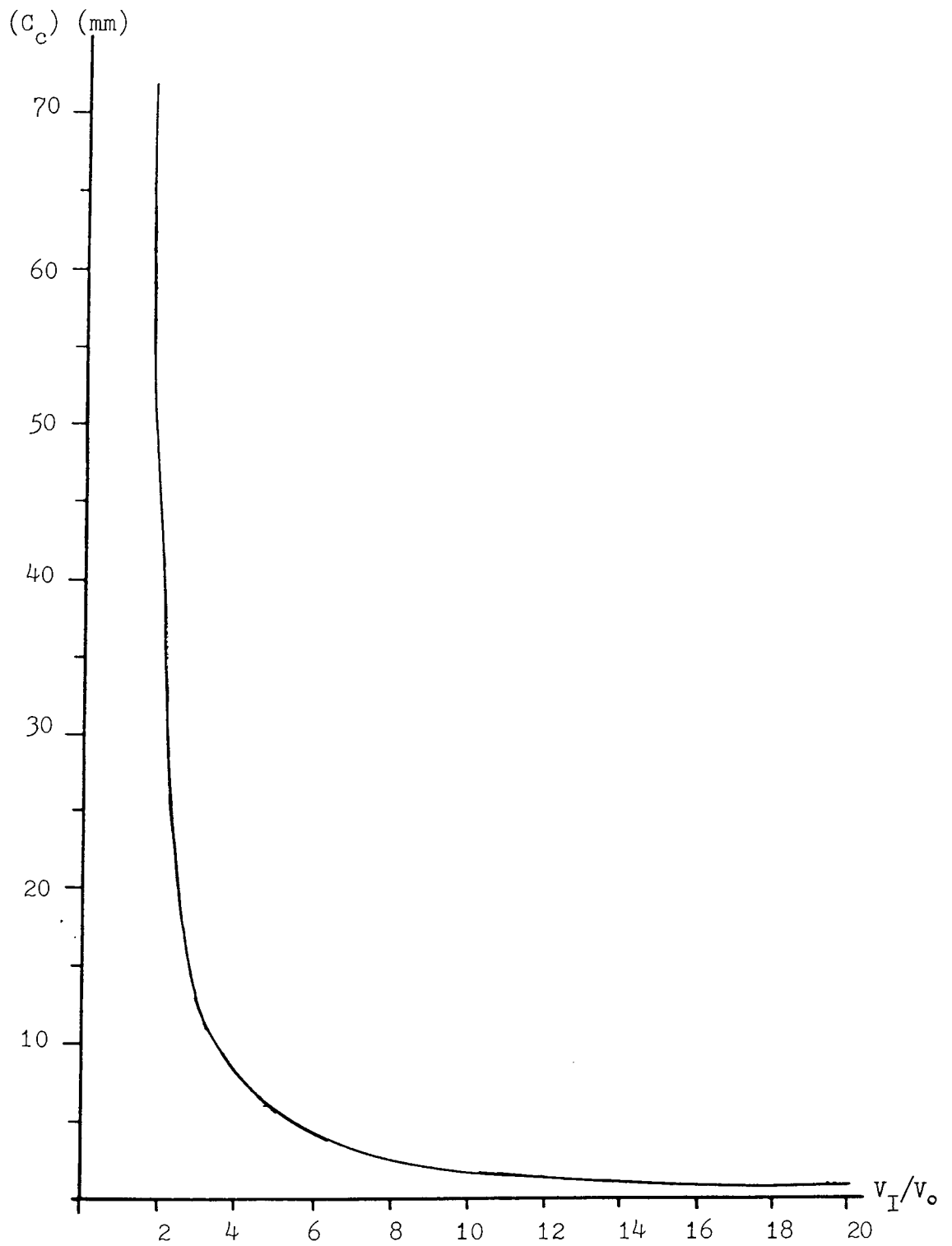
Fig. 4.35   Graph of chromatic aberration (C_c) as a function of

voltage ratio (V_I / V_o) for d_1 = 4 mm, d_2 = 3 mm,

separation of 2.2 mm and image distance of 300 mm.
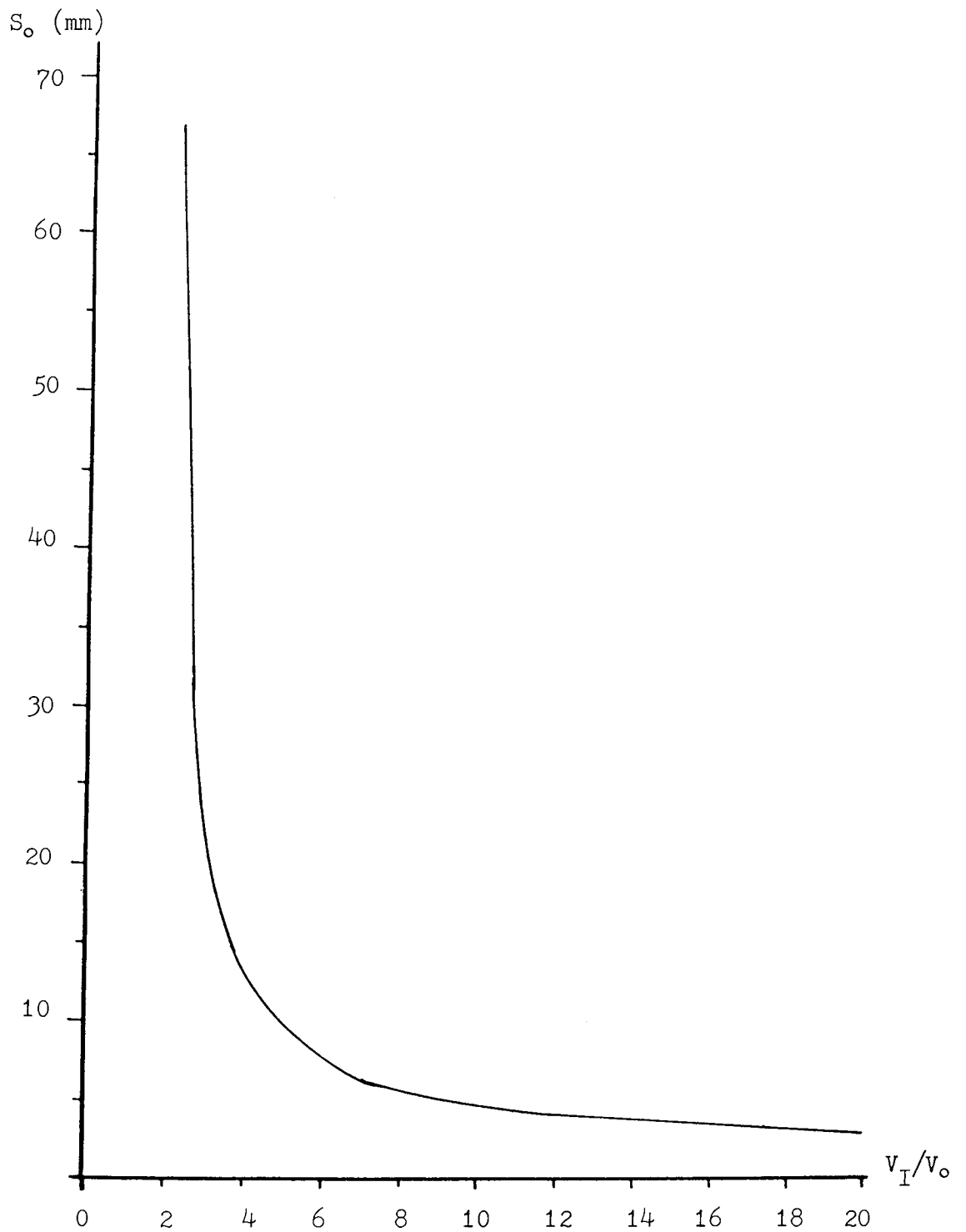
Fig. 4.36   Graph of source distance (S_o) as a function of

voltage ratio (V_I / V_o) for element apertures of

d_1 = 3 mm and d_2 = 2 mm, separation of 1.8 mm and image
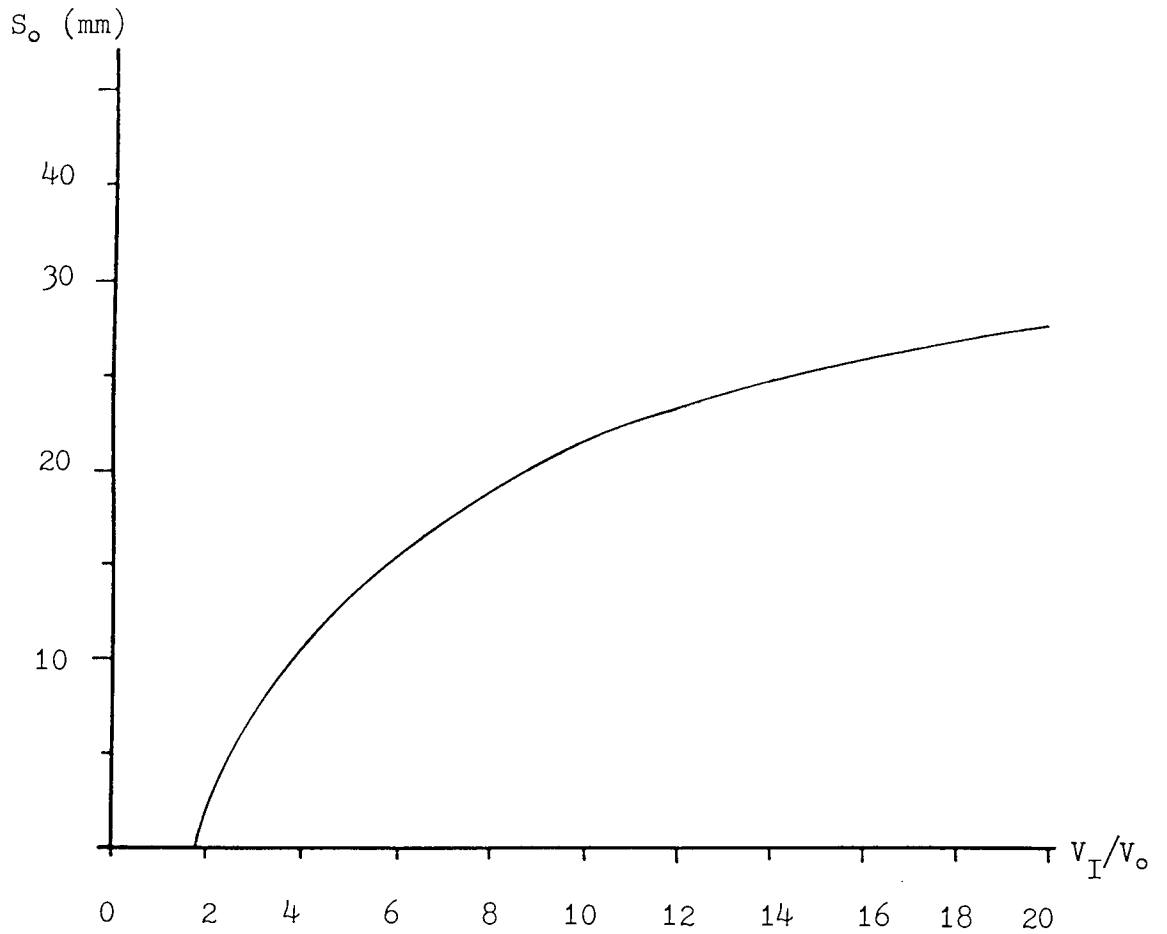
distance of 50 mm.

Fig. 4.37 Graph of magnification (M) as a function of voltage

ratio (V_I / V_o) for element apertures of d_1= 3 mm

and d_2 = 2 mm, separation of 1.8 mm and image distance
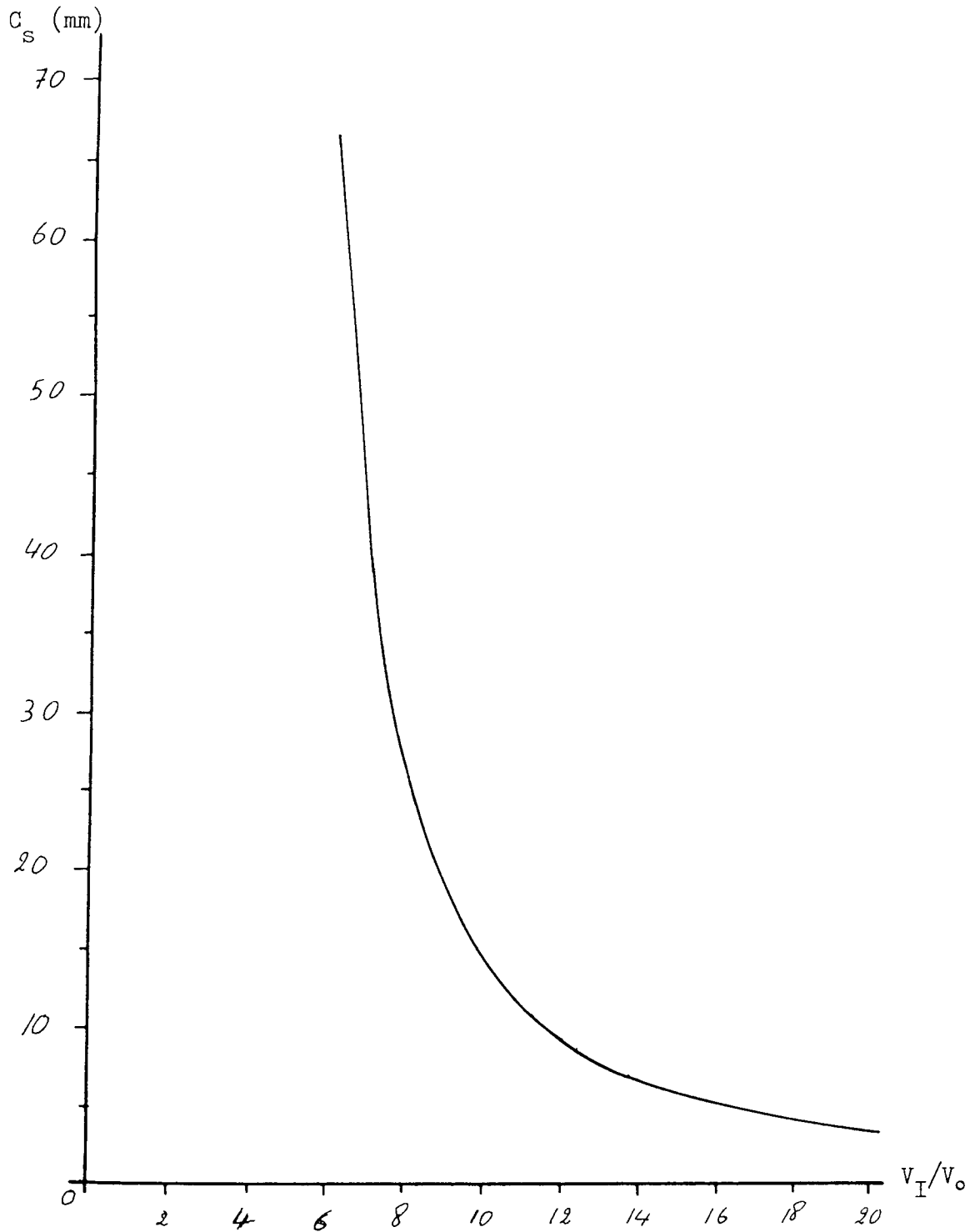
of 50 mm.

Fig. 4.38 Graph of spherical aberration (C_s) as a function of

voltage ratio (V_I / V_o) for element apertures of

d_1 = 3 mm and d_2 = 2 mm, separation of 1.8 mm and image
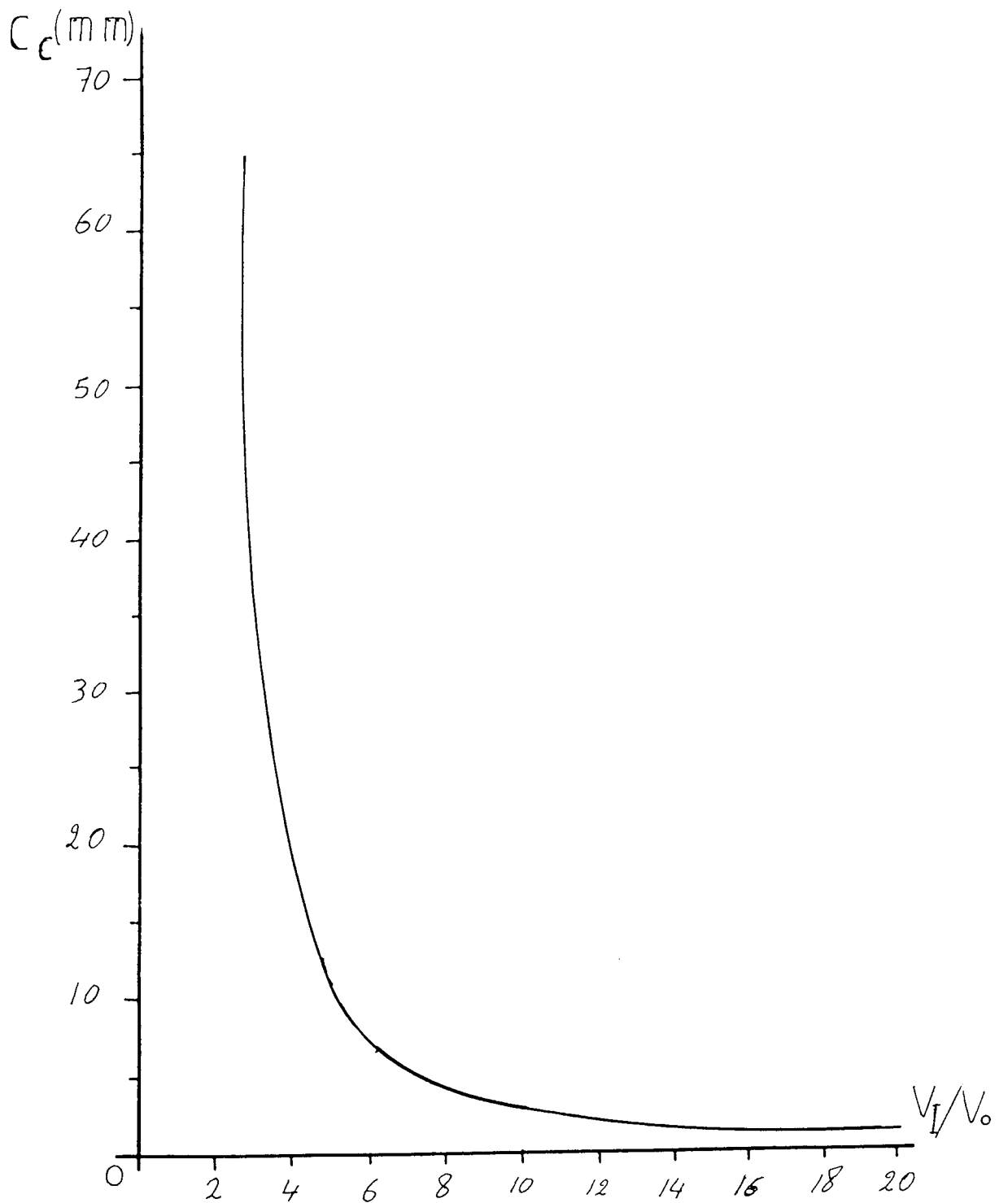
distance of 50 mm.

Fig. 4.39 Graph of chromatic aberration (C_c) as a function of

voltage ratio (V_I / V_o) for element apertures of

d_1 = 3 mm and d_2 = 2 mm, separation of 1.8 mm image

distance of 50 mm.

Voltage ratio (V_I / V_0)	Object distance S_0 (mm)	Magnification M	Spherical aberration C_S (mm)	Chromatic aberration C_C (mm)
2	-1·6	-21·7	26·8	-1·1
4	-1·3	-31·3	50·5	0·7
6	-3·7	-24·1	1031·6	9·7
8	-14·2	-9·5	91423	107·2
10	23·9	7·5	376428	231·3
12	8·9	24·6	4618·8	26·2
14	6·2	40·6	801·0	11·0
16	5·1	55·0	289·1	6·6
18	4·4	67·4	148·0	4·8
20	3·9	77·9	93·1	3·9

Fig 4·40   Table of lens properties for element apertures of $d_1 = 4$ mm and $d_2 = 2$ mm, seperation of 1·4mm and image distance of 50mm.

Voltage ratio (V_I/V_0)	Object distance S_0 (mm)	Magnification M	Spherical aberration C_S (mm)	Chromatic aberration C_C (mm)
2	1307·5	0·03	9×10^9	50569
4	24·7	1·5	2929·7	40·3
6	9·7	3·2	116·7	9·0
8	7·3	4·0	43·1	4·5
10	6·2	4·6	22·8	3·8
12	5·5	5·0	14·4	2·9
14	5·1	5·3	10·1	2·4
16	4·7	5·5	7·6	2·0
18	4·5	5·7	6·1	1·7
20	4·3	5·8	5·0	1·4

Fig 4·41   Table of lens properties for element apertures of $d_1 = 4$ mm and $d_2 = 2$ mm with seperation of 1·8 mm and image distance of 50mm
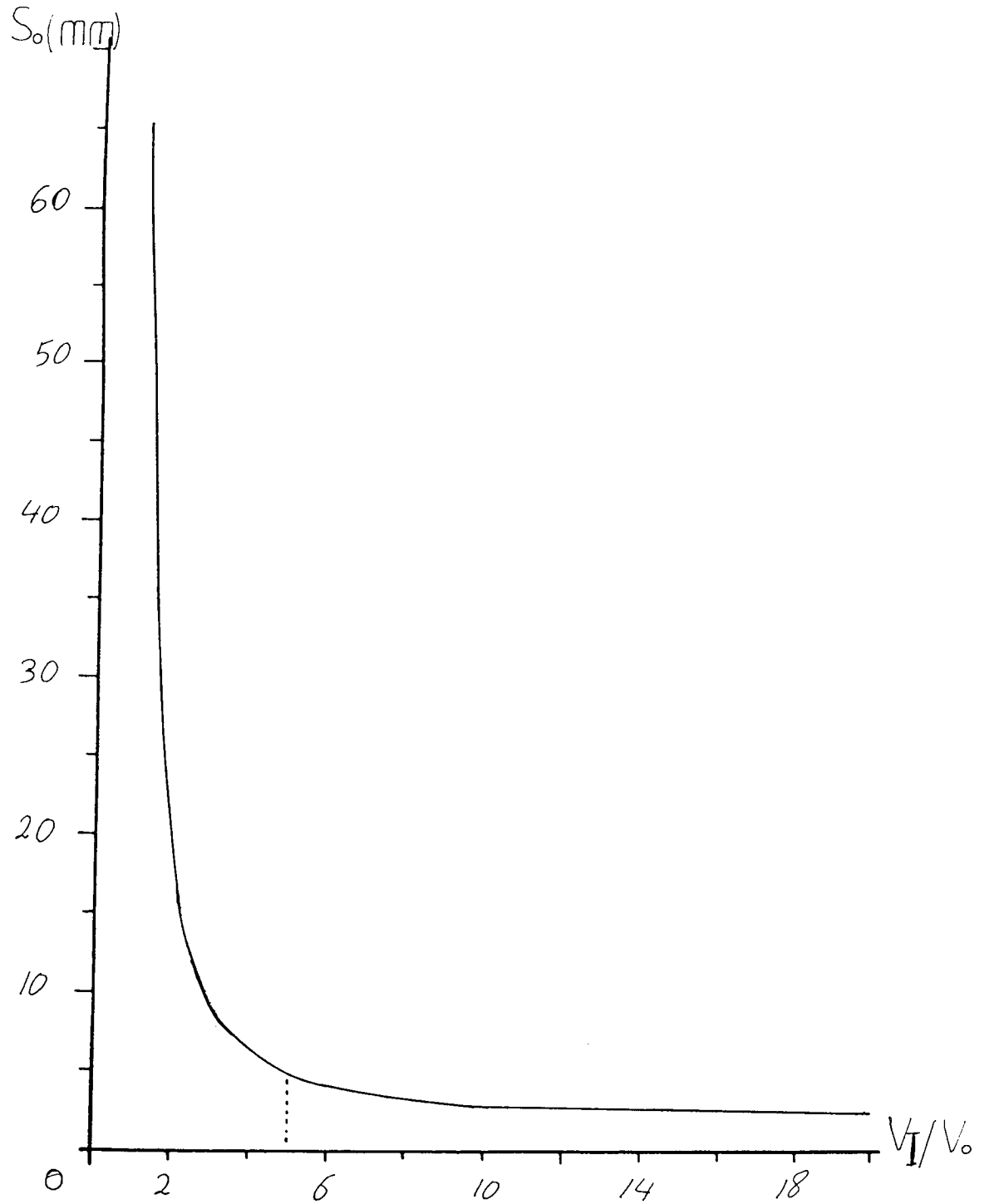
Fig. 4.42 Graph of source distance (S_o) as a function of

voltage ratio (V_I / V_o) for element apertures of

d_1 = 4 mm and d_2 = 2 mm, separation of 2.2 mm and image
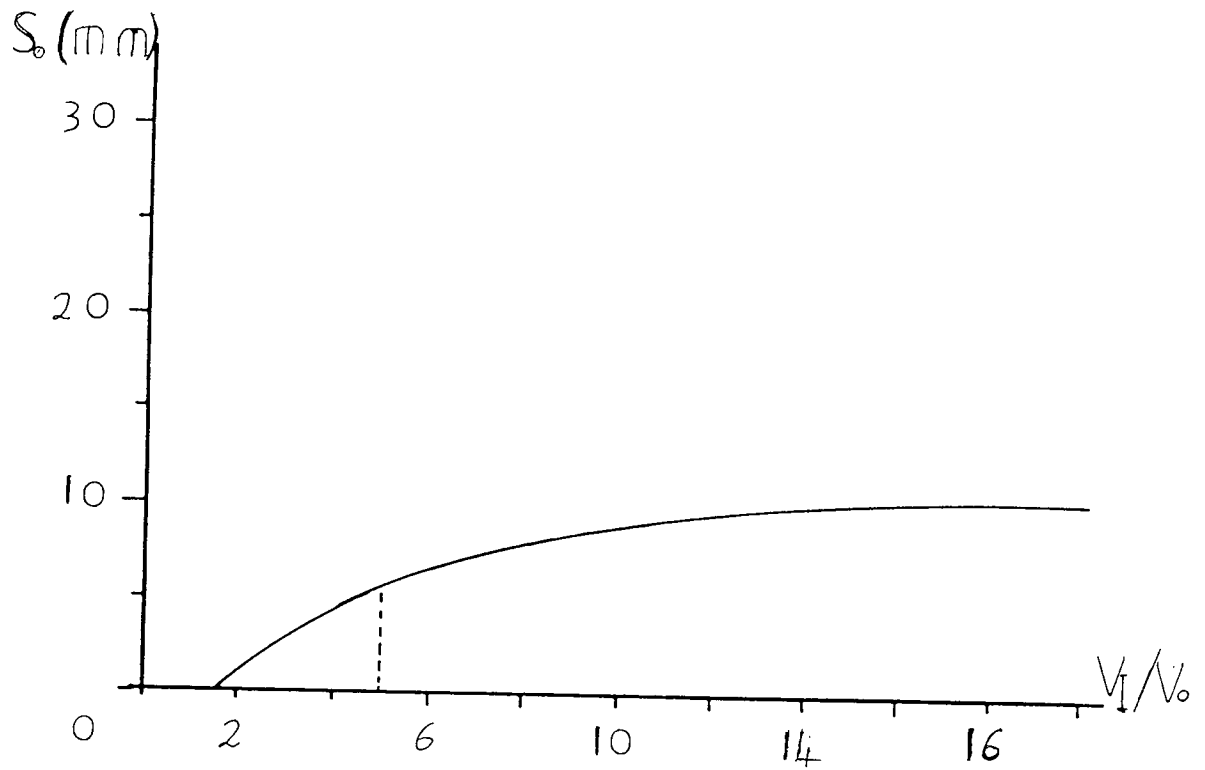
distance of 50 mm.

Fig. 4.43 Graph of Magnification (M) as a function of voltage

ratio (V_I /V_o) for element apertures of d_1 = 4 mm and

d_2 = 2 mm, separate of 2.2 mm and image distance of 50 mm.
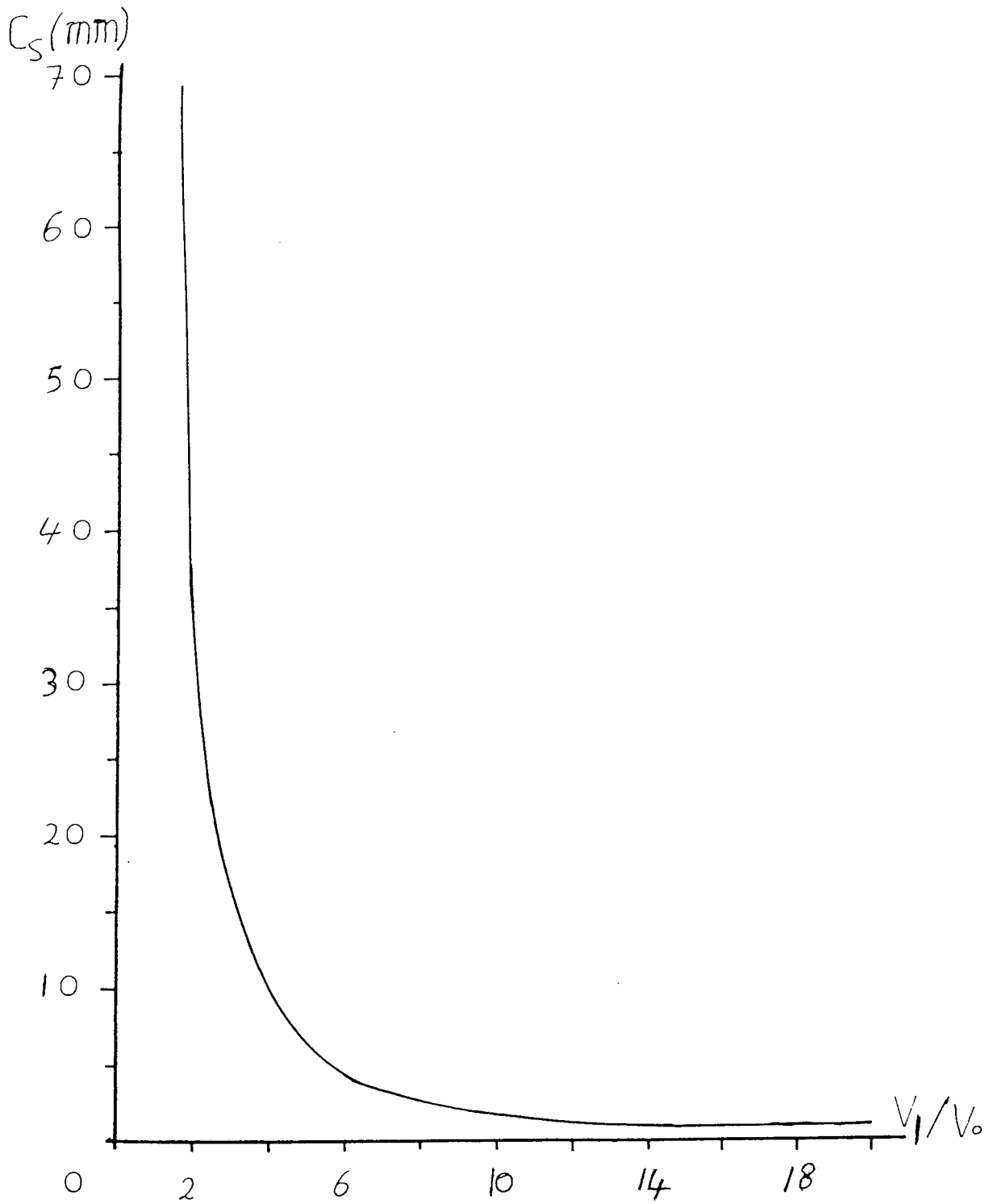
Fig. 4.44 Graph of spherical aberration (C_s) as a function of

voltage ratio (V_I / V_o) for element apertures of

d_1 = 4 mm and d_2 = 2 mm, separation of 2.2 mm and image
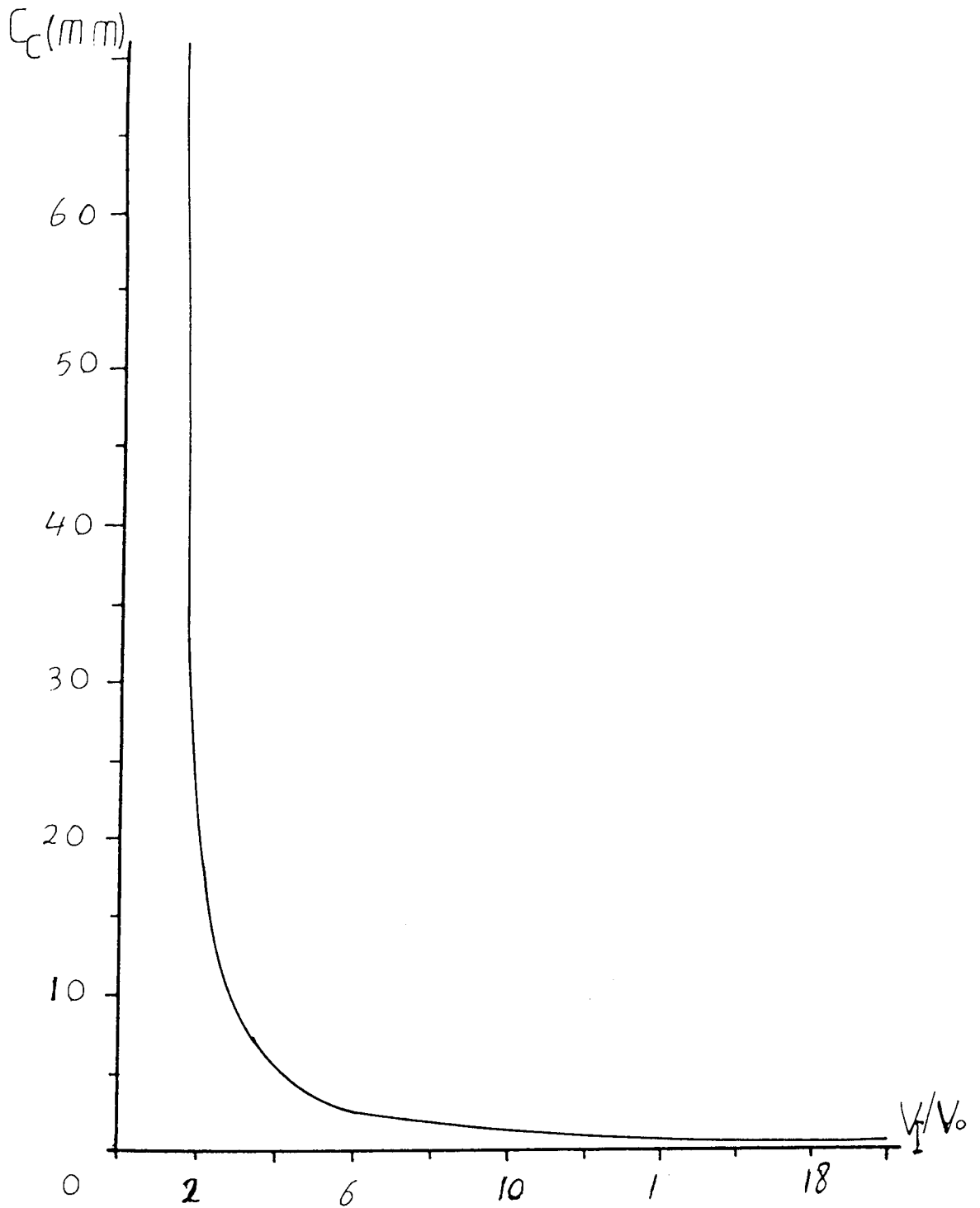
distance of 50 mm.

Fig. 4.45 Graph of chromatic aberration (C_c) as a function of

voltage ratio (V_I / V_o) for element aperture of

d_1 = 4 mm, d_2 = 2 mm, separation of 2.2 mm and image
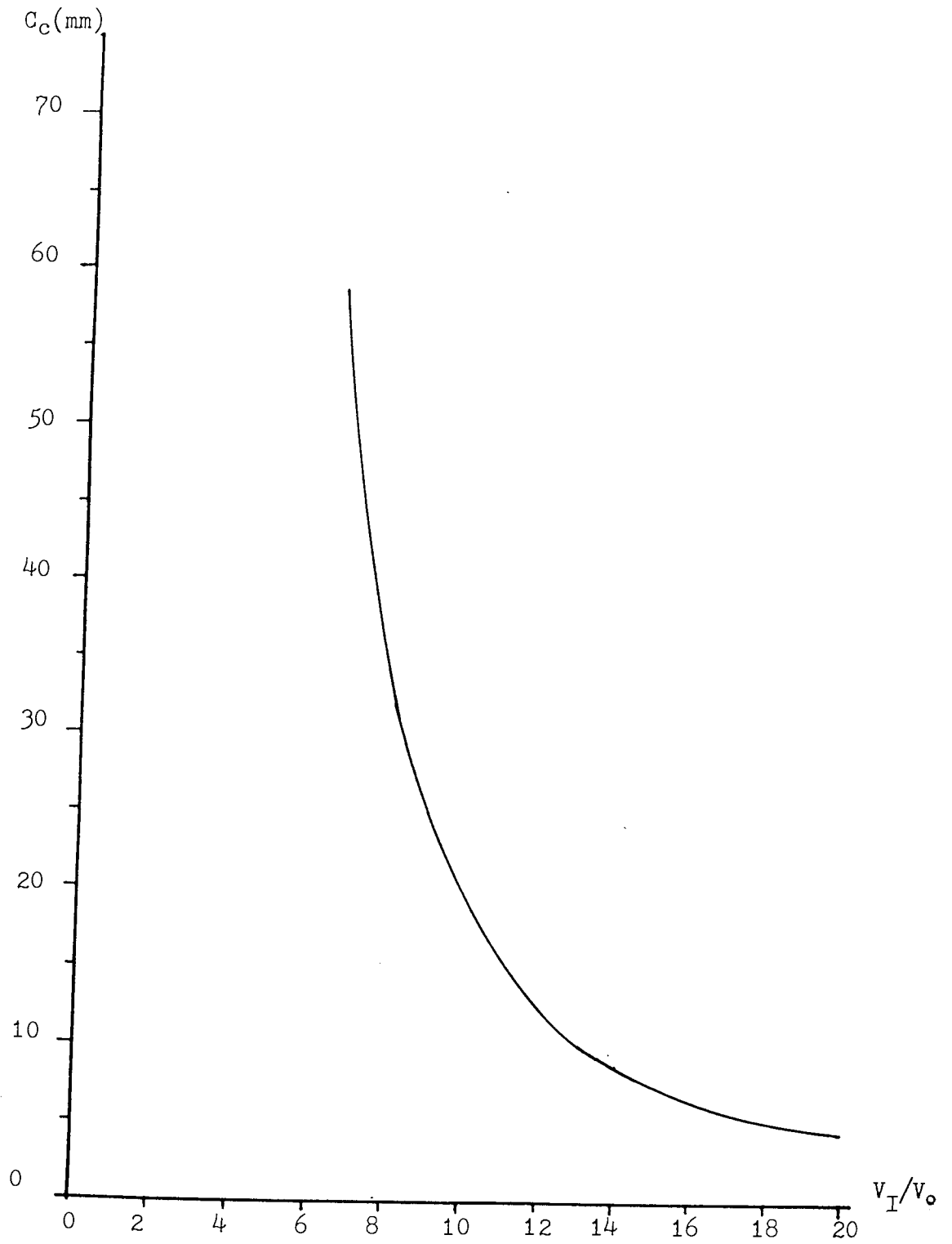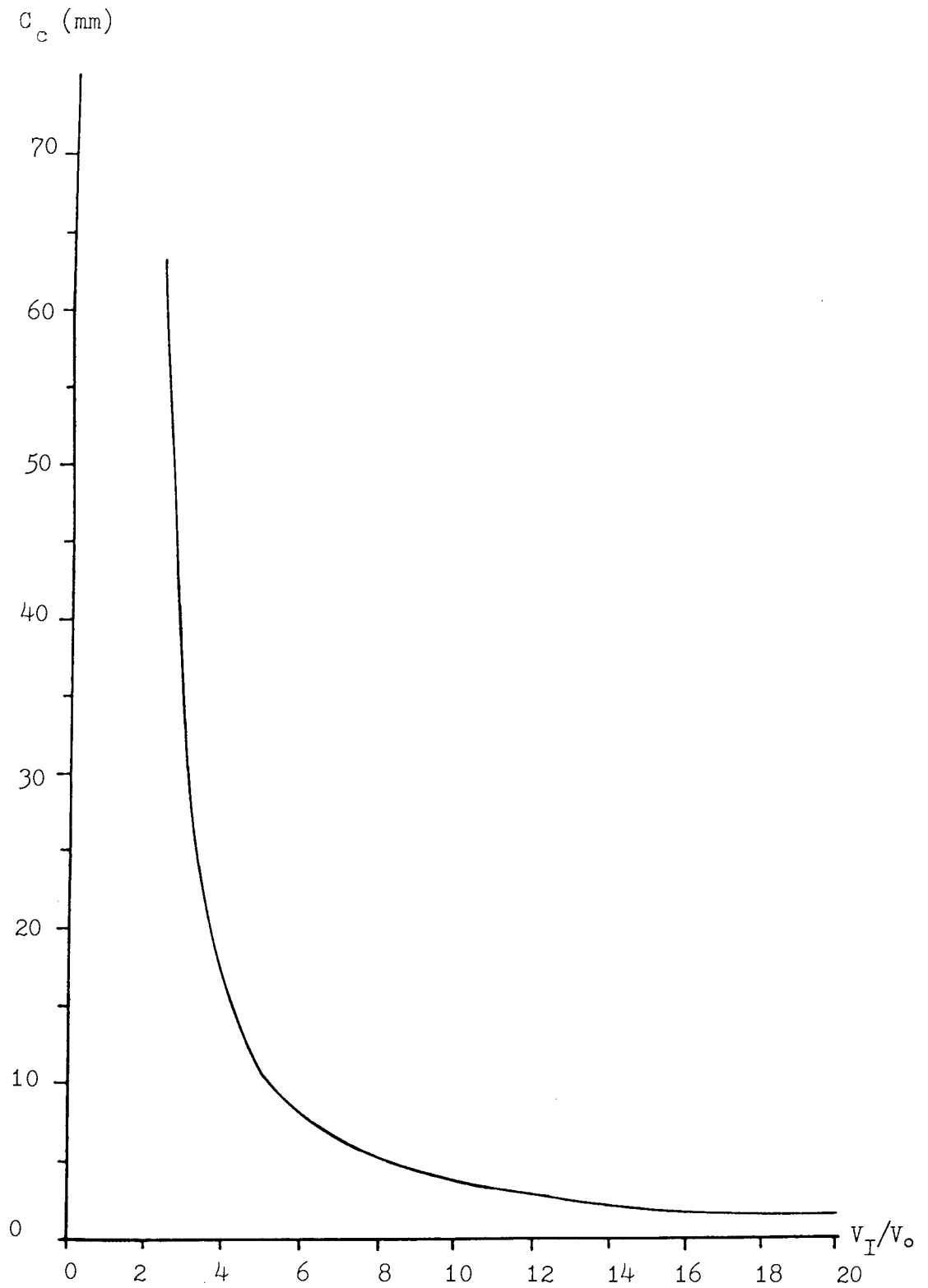
distance of 50 mm.

Voltage ratio (V_I / V_0)	Object distance S_0 (mm)	Magnification M	Spherical aberration C_S (mm)	Chromatic aberration C_C (mm)
2	-1005·5	-0·04	2×10^9	27518
4	27·7	1·3	3548	48·1
6	10·3	3·0	126·1	10·2
8	8·7	3·4	71·1	7·6
10	6·3	4·2	23·9	4·3
12	5·6	4·6	15·0	3·3
14	5·1	5·0	10·5	2·6
16	4·8	5·2	7·9	2·2
18	4·5	5·4	6·3	1·8
20	4·3	5·5	5·1	1·6

Fig 4·46   Table of lens properties for element apertures
of $d_1 = 4$ mm and $d_2 = 2$ mm, seperation of 2·4 mm
and image distance of 50mm.

Voltage ratio (V_I / V_0)	Object distance S_0 (mm)	Magnification M	Spherical aberration C_S (mm)	Chromatic aberration C_C (mm)
2	412·8	0·1	$8·3 \times 10^7$	4871·8
4	24·7	1·4	2647	38·9
6	9·8	3·0	115·3	9·3
8	7·3	3·7	42·9	5·7
10	6·1	4·2	22·7	4·0
12	5·4	4·6	14·4	3·1
14	5·0	4·8	10·1	2·5
16	4·6	5·1	7·6	2·1
18	4·4	5·2	6·1	1·8
20	4·2	5·4	5·0	1·6

Fig 4·47   Table of lens properties for element apertures of $d_1 = 4$mm and $d_2 = 2$mm, seperation of 2·6mm and image distance of 50mm.

that a gradual improvement in focusing properties was obtained as the apertures were progressively reduced, with the best configuration being when $d_1 = d_2 = 1$ mm. However, these small apertures result in an unacceptably low gun current efficiency. This approach was therefore abandoned and subsequently lens systems with elements of unequal apertures, i.e. $d_1 > d_2$, were then investigated. This procedure led to improved lens properties without any serious effect on the current efficiency, even when the aperture of lens element L_2 is 2 mm: The reason for this is that the lens geometry is such that it provides a converging field so that the converging electron beam is quickly brought to a focus with very little trimming.

The lens system with anode apertures of $d_1 = 4$ mm and $d_2 = 3$ mm separated by 2.2 mm for an image distance of 300 mm was therefore selected as being most consistent with the above requirements. Similarly, for the 50 mm image distance lens system to be used in the miniature C R tube, an electrostatic lens system with anode apertures of $d_1 = 4$ mm and $d_2 = 2$ mm, and separated by 2.2 mm was again chosen as the optimum design. The electron optical properties of these two lens systems are given respectively in Fig. 4.33 - 4.35 and Fig. 4.42 - 4.45 . From these, it can be seen that the coefficients of spherical and chromatic aberrations at the chosen working point are minimal, and in the case of the 50 mm image point lens system, it has a very low magnification coefficient as was required to give the necessary high resolution, i.e. small spot size.

4.7.2 TESTING OF THE TWO LENS SYSTEMS.

On the basis of these results, two guns were produced, where
a complete gun consisted of an extracting electrode, two lens
elements, a limiting stop aperture, and standard x and y deflecting
plates with an inter plate shield between them. The aperture of the
extracting electrode is determined by the conic angle of the emitted
electron beam and the emitter-extractor separation, where, for sake
of maximum current efficiency, the tip-extractor separation must be
less than the extractor aperture radius. However, there is no
advantage in using excessively large apertures since the beam would
have to be restricted at the subsequent electrodes to reduce the
resulting aberrations: on the other hand, it cannot be too small,
since this would present difficulties in the alignment of the
emitter which has to be about 1 mm from the extractor. Accordingly,
an extractor aperture of 3 mm diameter was found to be most satis-
factory. The extractor and the first lens element separation was
determined by the working point chosen in each case. Therefore,
for the lens system having a 300 mm image distance, the working point was
chosen at $V_I / V_o = 5$, and it can be seen from Fig. 4.30 that for
this condition to be satisfied, the object distance has to be about
7 mm. However since the cathode-extractor separation has to be 1 mm,
the extractor is therefore fixed at a position 6 mm from the first
lens element. The limiting aperture stop was then mounted at 2 mm
after the second element L_2 ; i.e. at the principal plane of the lens
system. To deflect the beam in the x, y planes the gun was fitted
with standard deflecting plates (used in conventional thermionic
cathode ray tubes), so that a standard sweep output voltage could
be used.

The complete assembly of this field emission electrostatic gun

is illustrated in Fig. 4.48 , which was then mounted in the "long" demountable chamber with a freshly prepared carbon fibre cathode so that its performance and characteristics could be evaluated. The cathode was pre-aligned with the extractor electrode aperture before sealing and evacuating the chamber to a pressure of about 10^{-8} m bar. To test the gun, the necessary voltages were applied to the appropriate electrodes in the manner already described (see Fig. 4.12), to maintain the condition $V_I / V_o = 5$, care being taken when the voltages are independently applied to the cathode and the extractor electrodes so that at no time an over-voltage be applied between the tip and extractor that could damage the cathode. Therefore usually, both the cathode and extractor voltages were both increased simultaneously until the value required for the extractor was reached, then the cathode voltage was further increased until the necessary emission current was obtained. To focus the beam at the phosphor screen, the first element voltage is slowly increased until the minimum spot size condition is reached whilst keeping the second lens element and limiting aperture stop at ground potential, this occuring when the extractor voltage and the first element voltage are approximately equal in magnitude, and the condition $V_I / V_o = 5$ is satisfied. For this gun, a properly focused image was obtained with the cathode, extractor and first element voltages of - 2.5 k V, - 2.0 kV and - 2.0 k V respectively. Having the cathode at - 2.5 k V rather than at ground potential, no accelerating voltage is necessary which usually will have to be applied to the screen and the concentric cylinder placed just inside the main chamber, with adequate insulation. There is therefore likelyhood of electrical breakdown even with this insulation due to current leakage. Furthermore with the screen at a raised potential there is a risk of electric shock. Therefore to

Fig. 4.48   Photograph of 300 mm focal length redesigned gun for

proto type C R T.

avoid this the voltages in the manner described above are applied. Where the potential difference between the cathode and extractor necessary to maintain an emission current of 10 μ A varies with the particular cathode, but usually between 500 to 1000 Volts are necessary. For the above operating conditions, this source gave 9.3 μ A of emission current, of which about 6.9 μ A reached the screen; i.e. making the gun to be about 75% efficient.

Having obtained a finely focused spot at the screen, the beam deflecting properties of the gun were next investigated by applying two sinusoidal signals to the x and y plates. As a result, the electron beam is subjected to two mutually perpendicular simple harmonic forces and hence the spot will execute Lissajous figures such that when the frequencies of the two signals are equal, the spot describes an ellipse as shown in Fig. 4.49 (a). It can be seen that the figure is well defined with adequate brightness, is evenly focused, and does not suffer from defocusing effects due to beam deflection. To evaluate the performance of the tube in a more conventional mode, a variable sweep voltage, obtained from the external x-output of a conventional oscilloscope was applied to the x-plate, whilst the y-plates were connected to a signal generator capable of generating either sinusoidal or square wave signals. The response of the gun was then investigated for frequencies in the range of 10 Hz to 10 mHz , for both sine and square wave signals, where the typical traces obtained on the phosphor screen are shown in Fig. 4.49 (b) and (c) respectively. Here again, the displays have constant and adequate brightness, with negligible defocusing effects due to beam deflection in the sinusoidal display: however, some distortion is detectable in the case of square wave signals, but this was later found to be due to a fault in the output of the

300 Hz (a)

100 kHz (b)

(c)
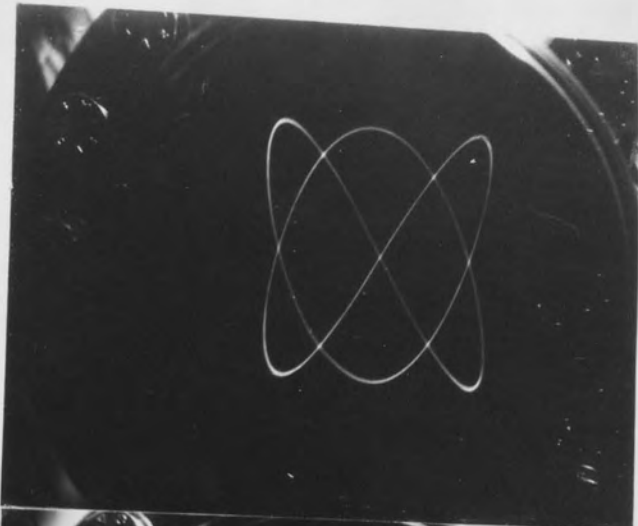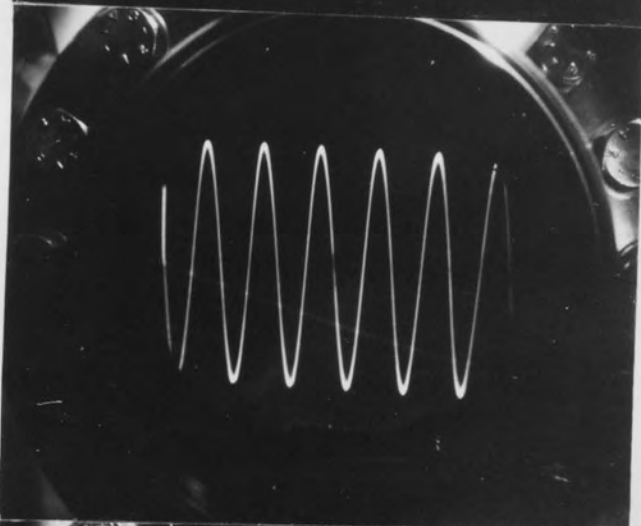
30 kHz
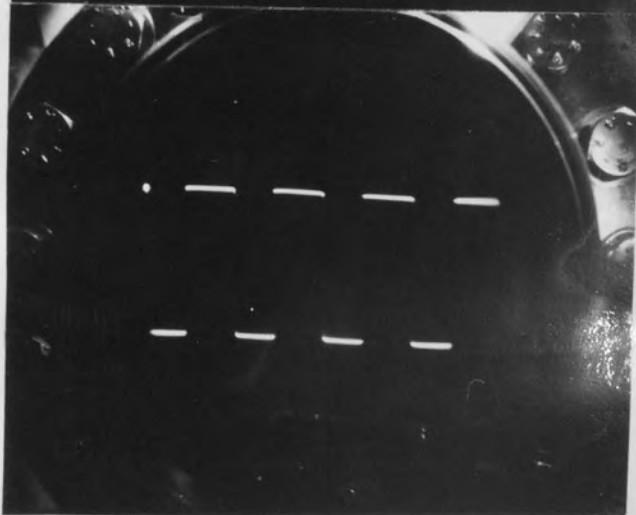
Fig. 4.49 Typical displays (a) Lissajous figure (b) sine wave form
and (c) Square wave form imaged on proto-type C R T.

145.

signal generator.

Lastly, the gun was tested for its focusing stability, which was the main purpose of redesigning the gun. This was carried out by keeping the y deflecting plates at earth potential and applying a slowly varying sweep voltage to the x-plates, so that the focused spot was slowly scanned across the screen. Open shutter recordings were then made for the total scan times ranging from one second to 30 seconds. The typical defocusing encountered is clearly shown in the photograph in Fig. 4.13 (b) for the scan of 20 seconds duration. However, if this is compared with the corresponding scan shown in Fig. 4.13 (a), which was recorded from the original gun design, it is clear that a large improvement has been achieved. Infact, when measured with a travelling microscope, a 0.25 mm focused spot was found to defocus to only about 0.32 mm when the tip voltage was increased by 150 Volts.

The second field emission gun with a 50 mm image point was based upon the lens system whose electron optical properties are given in Fig. 4.42 - 4.45 , with first and second element apertures of 4 mm and 2 mm respectively, and with a lens element separation of 2.2 mm. Here again, a working point of $V_I / V_o = 5$ was considered to be satisfactory, and it can be seen from the computed results in Fig. 4.42 that the cathode must be 5.5 mm from the first element. Accordingly the extracting electrode in this case was positioned at 4.5 mm from the first element L_1 , giving a 1 mm separation between the cathode and 3 mm aperture extracting electrode. To exclude the scattered unfocused rays, and thereby minimise the aberrations in the focused spot, a limiting aperture stop of 1 mm aperture was incorporated at 1.5 mm, (i.e. the principal plane of the lens system) from the second element L_2 , as shown in Fig. 4.50. The gun was then

cathode

Extractor

```
┌──────────────┐        ┌──────────────┐   ↕ 1mm
└──────────────┘        └──────────────┘
        ←——3mm——→
```

4.5mm

Lens L₁

2.2mm

Lens L₂

2mm

1.5mm

aperture stop

←1mm→
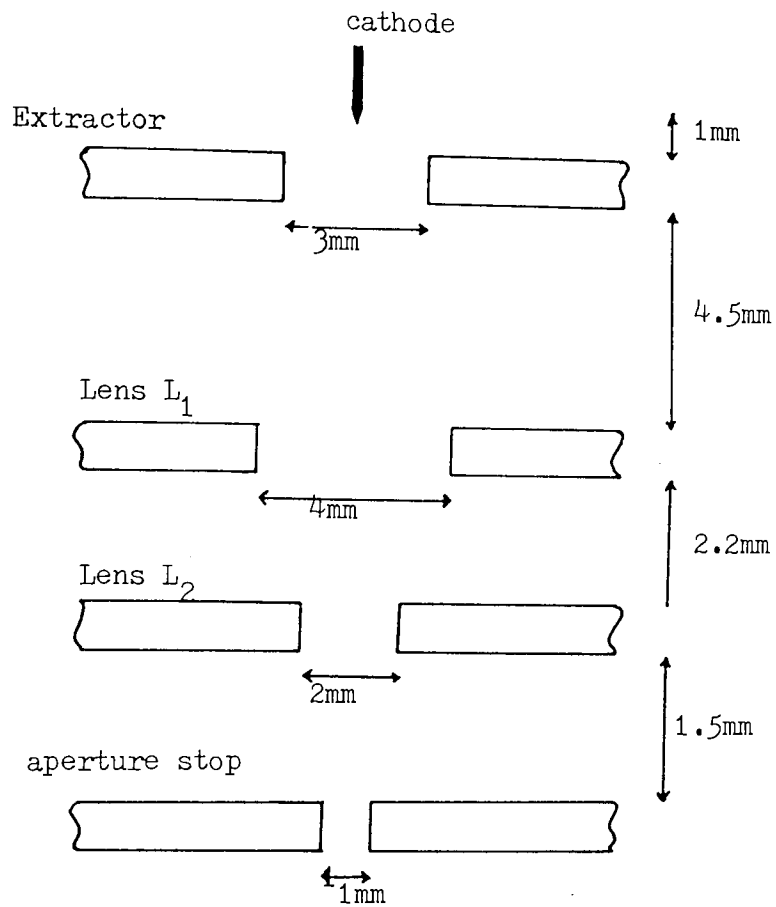
Fig. 4.50   Miniature 50mm focal length gun.

assembled using standard electrodes, the deflecting plates, including
an inter plate shield, as shown in the photograph of Fig. 4.51 . To
evaluate the performance characteristics of this module, it was
mounted in the "short" demountable chamber, (see section 4.2), which
gave a 50 mm image distance between the second element and the
phosphor screen. As with the previous gun, the cathode was pre-aligned
with the extracting electrode, before assembling the chamber and
evacuating it to $\sim 3 \times 10^{-8}$ m bar. The operating voltages were
cathode - 2.2 k V, extractor - 1.8 k V and first element - 1.8 k V
with the remaining electrodes at earth potential (i.e. giving
$V_I / V_o = 5$), where the same precautions were taken when applying
these voltages as described previously. For these operating conditions
the test source gave an emission current ~ 8.4 μ A of which ~ 6.7 μ A
reached the screen, thus making the current efficiency of the gun to
be about 80% . However for   most of the work on this gun, 5 μ A
of total emission current was found to be more than adequate, where
the size of the focused spot, measured with a travelling microscope,
was found to be about 0.075 mm in diameter. It should however be
pointed out here that the size of the focused spot can be further
reduced by using a finer grain phosphor to deposit the screen, as
here the resolution was limited by the size (~ 20 μ m) of phosphor
grain used for this particular screen.

Defocusing defects due to deflection of the beam were examined
in the usual manner; i.e. by causing the focused beam to execute an
ellipse by applying sinusoidal waves simultaneously to the x and y
plates. Thus it can be seen from Fig. 4.52 (a) that the display not
only has even focusing and deflection, but also an adequate brightness.
The performance of the gun in a conventional mode was investigated
in the frequency range of 10 Hz to 10 mHz , and the typical
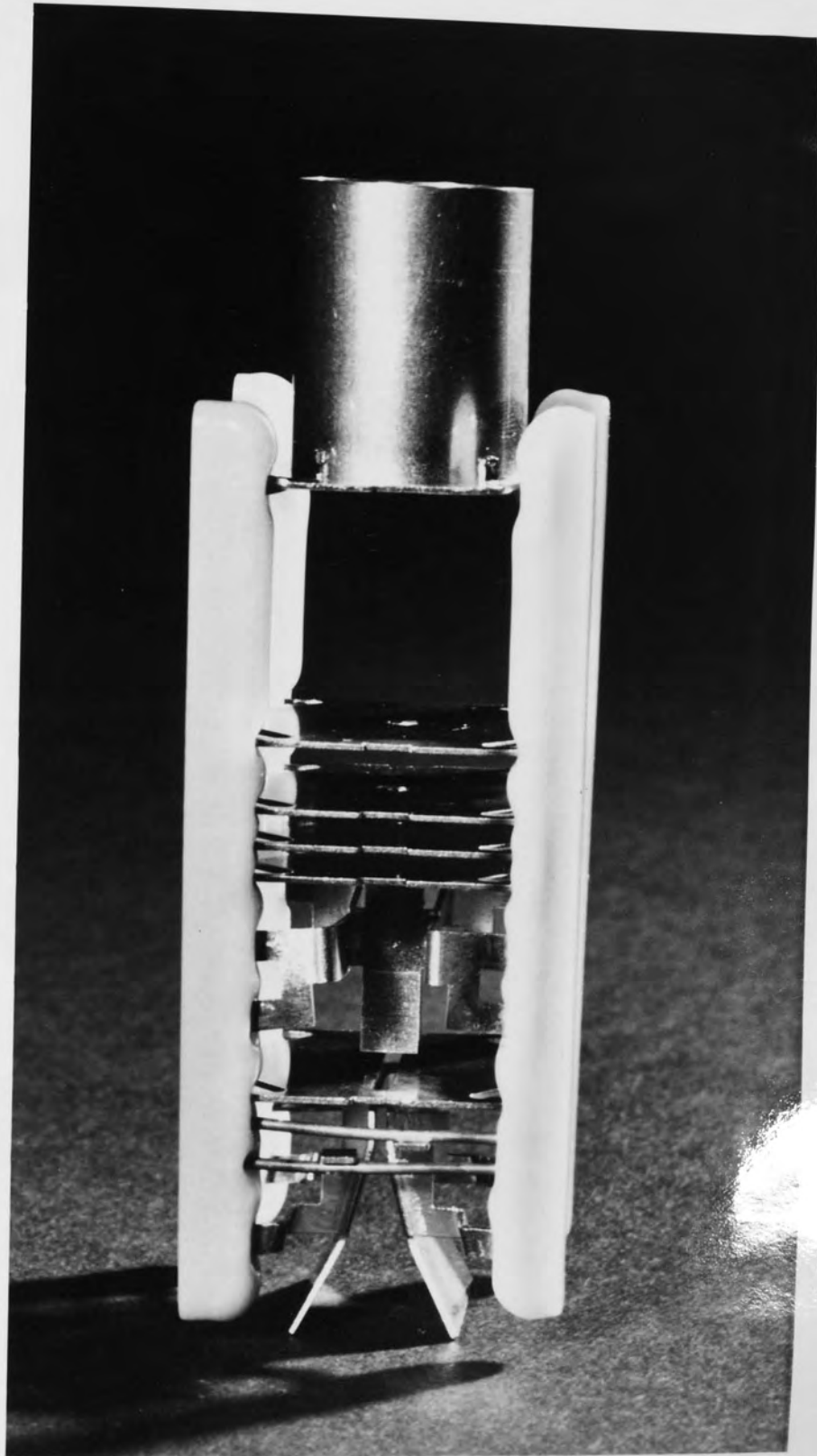
Fig. 4.51   Photograph of assembled 50 mm focal length experimental

module for use in "short" system.
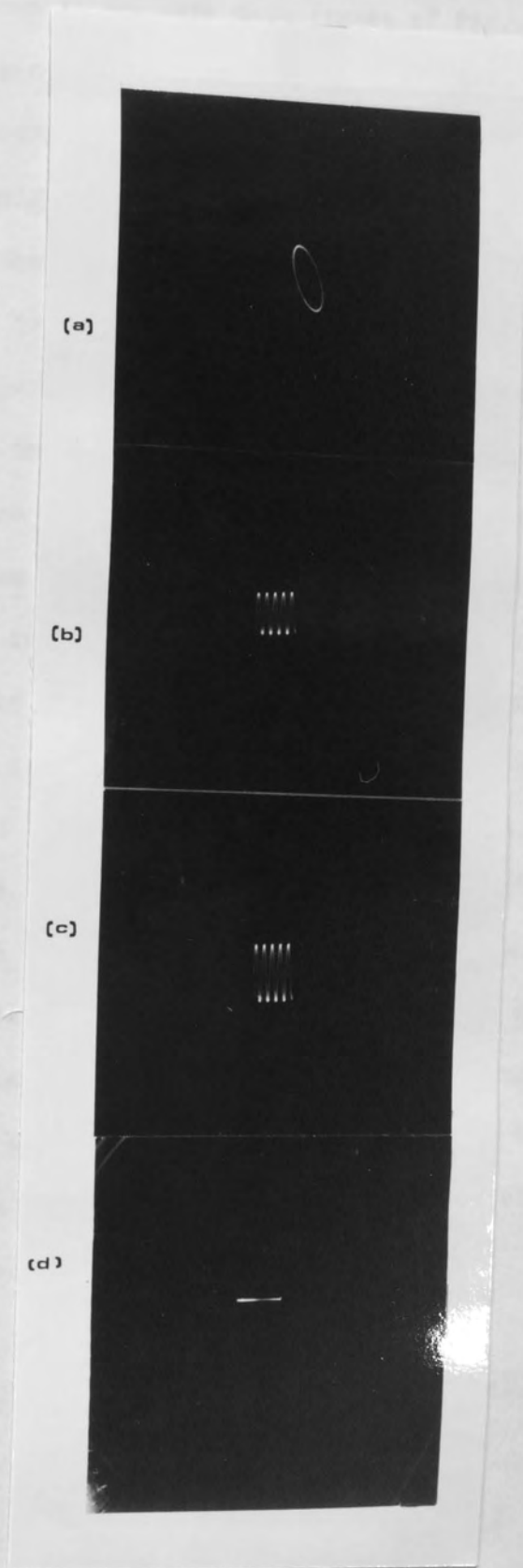
Fig. 4.52 Typical displays (a) ellipes (b) sinusoid-al wave form at
300 HZ and (c) at 300 KH and (d) slow scan

responses obtained are shown in the sine wave traces of Fig. 4.52 (b) and (c) which were taken at 300 H Z and 300 K H Z respectively. These clearly highlight the fineness and sharpness of the images; they also show that the brightness and focus are consistant over the whole image, and the whole frequency range investigated. The small size of the display is due to the fact that these are meant for the 28 mm diameter screen of a "mini" C R T. Lastly, the defocusing effects due to the changes in the tip voltage were investigated using the same technique as previously described (section 4.4). Thus from Fig. 4.52 (d), it will be seen that in this case there is only a relatively minor effect; infact a focused spot only increased in size from 0.075 to 0.086 mm for a change in tip voltage of 150 Volts; i.e. compared to a change from 0.25 mm to 0.32 with the 300 mm focal length lens system. The relatively small change in the present case is just a consequence of the shorter focal length and possibly due to the small magnification coefficient. Whilst the performance data just described points to a very good gun performance, there remained an unacceptable level of low frequency instability in the image, as can be seen from variations in the light intensity in slow scan trace shown in Fig. 4,52 (d), which will be given further consideration in a later section.

4.8   DESIGN AND PERFORMANCE OF TWO "COMMERCIAL" FIELD EMISSION C R T's.

4.8.1   Introduction

Having designed and successfully tested the 300 and 50 mm focal length field emission electrostatic guns under the demountable laboratory conditions, it was now possible to consider how to re-design the conventional thermionic C R T's to accommodate these field

emission guns with carbon fibre as an electron source. Such an innovation would be commercially very attractive since such tubes would have the potential advantages of a small source size for high resolution applications, an instantaneous switch on capability and the virtual elimination of wasted heater power.

4.8.2   DESIGN AND TESTING OF A "COMMERCIAL" 300 mm FOCAL LENGTH FIELD EMISSION GLASSED TUBE.

In designing this glassed field emission tube, a point was made to employ the standard electronic components that were used by the M-O valave company in the manufacturing of their thermionic cathode ray tubes. The field emission gun was based on the design which had already been tested in the laboratory (section 4.6.2), but adopted for use in this tube as shown in Fig. 4.53 (a), where the thermionic cathode assembly was adapted to hold the carbon field emitter as shown in Fig. 4.53 (b). This was achieved by first removing the heater and the thermionic cathode coating from the 2 mm diameter cathode cylinder which is embedded in a ceramic disc. Then by drilling a 0.5 mm diameter hole in this cylinder, a carbon fibre could be inserted into this hole and fixed from behind by filling the tube with silver dag from the end into which the heater was originally inserted; this procedure also ensured good electrical contact between carbon fibre and cathode cylinder. After electrolytically etching the tip of the fibre it was then very carefully positioned into the conventional grid cup so that the ceramic disc containing the cathode cylinder sits on a spacer-ring, such that the carbon fibre tip pratrudes about 2 mm from the grid cup aperture. Another ring is then inserted at the other end (see Fig. 4.53 (b)), and the edges of the grid cup turned over to hold the cathode assembly securely.

cathode

Extractor   1mm

6mm

lens 1st
element

2.2mm

lens 2nd
element

2mm

3mm

4mm

2mm

1mm

(a)

grid cup

cathode holder

cathode

spacer rings

(b)
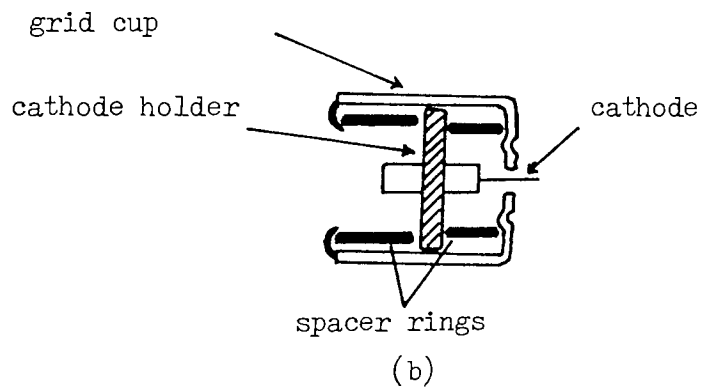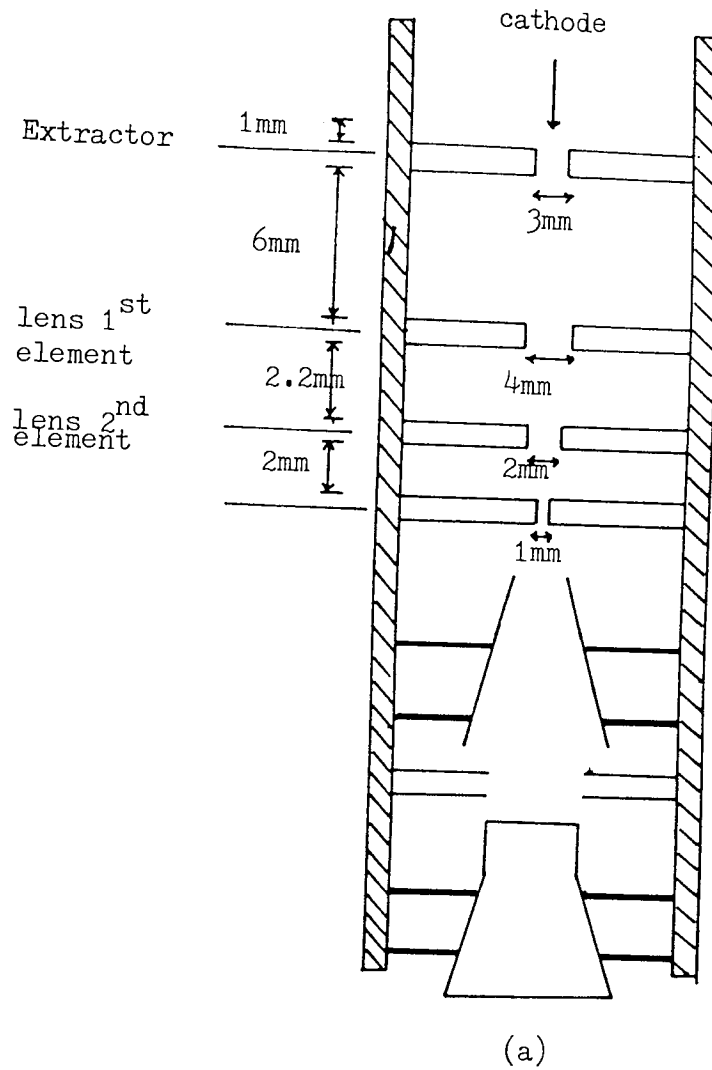
Fig.4.53(a) Gun assembly for use in first glassed tube

(b) adapted thermionic cathode assembly.

Next the phosphor screen in the glass tube was produced in the normal manner by first depositing a thin layer of phosphor by a settling process. Subsequently this was then aluminised by a standard procedure which involved covering the layer of phosphor with a thin film of nitrocellulose lacquer and then evaporating on a thin layer of aluminium. A subsequent vacuum heat treatment removes the lacquer film thus allowing the aluminium film to settle in contact with the phosphor layer. This aluminium layer serves several purposes; firstly, it provides a means of removing the unwanted electrons and so prevents the screen from charging up, at the same time it allows the screen current to be measured. Secondly, it provides a means of applying a post-deflection accelerating voltage to further enhance the brightness of the tube. Thirdly, the aluminium layer acts as a reflecting surface to the direct light from the excited phosphor again to enhance the brightness. Having prepared the screen, the gun is assembled, where the whole cathode assembly, (see Fig. 4.53 (b)) is positioned relative to the extractor such that the cathode tip is about 1 mm from the extractor electrode. To complete the gun, the remaining electrodes and 1400 J type deflector plates are accordingly arranged in the jig, where they are, securely held, and subsiquently the whole module is mounted in the glass rods. Finally to finish off, three getters and a circular spring surrounding the gun are fitted. When therefore the finished gun is inserted into the glass tube the circular spring secures the gun in position. After the gun had been mounted in the glass tube, the standard commercial evacuating, baking and sealing procedure was followed, giving a final pressure in the tube of about 3×10^{-7} m bar. To ensure this vacuum is maintained over the life time of the tube, three getters were induced.

This "commercial" field emission tube was then tested in a

similar manner to the demountable laboratory version. However, to avoid any distortion in the field in the cathode region, the whole cathode assembly, including the grid cup, was kept at the same potential as the cathode. As previously, appropriate voltages were applied to the various electrodes such that $V_I / V_o = 5$ and the total emission current was about 9.3μ A. The resulting focused spot at the phosphor screen was well defined and fairly bright: however, it was very unstable in the sense that it intermittently disappeared and reappeared on a time scale that could vary from a few seconds to a few minutes. When the focused image was visible, the beam current reaching the screen was only $\sim 3 \mu$ A, and heavily fluctuating. Infact, this loss of current was accounted for by monitoring the extractor and lens first element current which were found to be 3.2μ A and 1.3μ A respectively. The remaining 1.8μ A were assumed to be intercepted by the second element and limiting aperture stop. Although the application of a sweep x-voltage and sinusoidal y-voltage to appropriate deflecting plates resulted in a satisfactory deflection of the beam, further tests on this tube were abandoned, since in other respects its overall performance was very poor. Following this investigation it was concluded that the problems arose from the bad alignment of the carbon fibre cathode with the extractor aperture which was clearly a critical factor for the successful operation of a tube: in particular, it appeared that the misalignments were introduced at some later stage after the initial cathode assembly, possibly when the electrodes are mounted in the glass rods to form a gun.

These difficulties in the cathode alignment were overcome by using a combined cathode-extractor assembly, with a built-in cathode manipulator which allows tip alignment even after the gun assembling

process; furthermore, this facility greatly helps to ensure the safety of the etched tip. The cathode-extractor assembly that was designed for this purpose is shown in Fig. 4.54 , where the cathode holder was built from a 4 mm diameter stainless steel rod, one end of which has a removable piece which allows the fibre, after securing with a small drop of silver dag, to be sandwiched between them in a fine groove by a small screw. The rest of the cathode assembly consists of two concentric tubes with a thic ceramic tube (3) on the outside and a thin stainless steel tube (4); the latter having a screw thread that locates with the threaded cathode holder to provide an axial movement of the tip for maintaining the necessary 1 mm cathode-extractor separation. This whole cathode assembly is held securely inside the larger stainless steel tube (5) by means of three screws 120° apart and three grooves, coinciding with screw positions, in the insulating ring, thus allowing the manipulation of the cathode in x-y plane by adjusting the three screws. The stainless steel tube (5) is connected to the extractor electrode (1) by bending over tags on the extractor electrode and spot welding. Thus the manipulation facility described above therefore allows accurate alignment of the cathode in all three, x, y and z directions.

Using this improved cathode-extractor assembly, the field emission C R T was rebuilt as shown in Fig. 4.55 . Its performance characteristics were evaluated in the usual way by applying the required voltages to maintain the condition V_I / V_o = 5 with a total emission current of ~ 9.1 μ A, and under these conditions, the measured screen current was ~ 6.9 μ A, giving an acceptable current efficiency of about 76% . The stability of the screen display was now comparable to the stability obtained in the case of the demountable laboratory tube. To examine that the deflecting properties and the

SIDE VIEW

FRONT VIEW

CATHODE

FINE SLIT
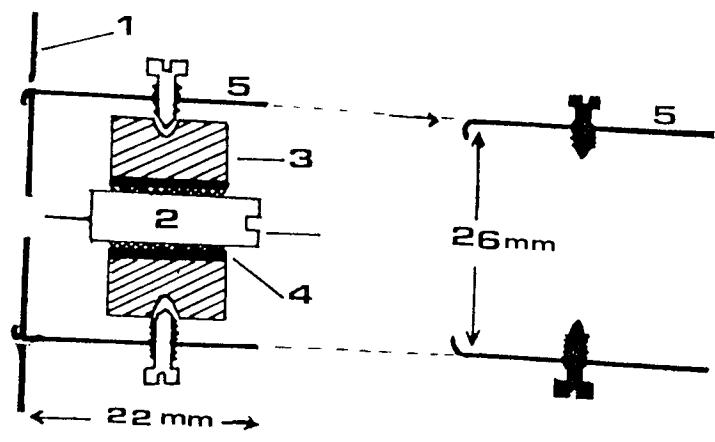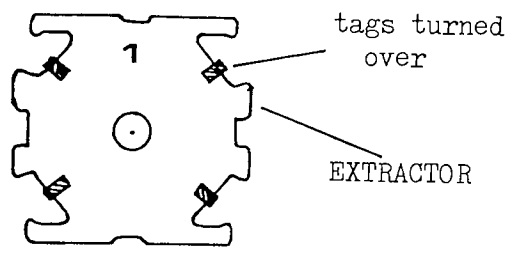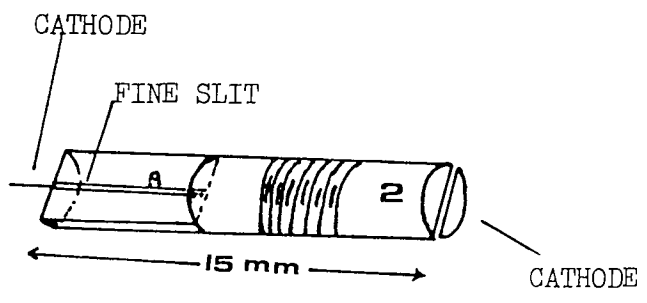
CATHODE

(1) Extractor
(2) Cathode holder
(3) Ceramtec
(4) Inner stainless steel ring
(5) Outer stainless steel ring

Fig. 4.54 Cathode-Extracror assembly for standard tube.

Fig. 4.54 Cathode-Extractor assembly for standard tube.

Fig. 4.55 Photograph of conventional field emission C R T.

defocusing effects associated with beam deflection, the beam was subjected to two mutually perpendicular simple harmonic forces by applying two sinusoidal signals of equal frequencies to the x and y plates. The resulting elliptical displays were photographed and subsequently examined. The deflection properties were found to be satisfactory, with negligible aberrations in the focusing, as can be seen from the typical display shown in Fig. 4.56 (a). For the conventional mode the performance of the tube was evaluated in the frequency range of 10 Hz to 10 mHz and found to be in most respects comparable with conventional thermionic tubes. The typical display obtained at the screen are presented in Fig. 4.56 (b) and (c), where it can be seen that the displays are well-defined, and have even focusing and adequate brightness and furthermore, post deflection beam acceleration was not found to be necessary. The overall performance of the tube was found to be very good and the only defect that the tube contained was the variations in the light intensity which will be dealt with later in this chapter.

4.8.3 THE DESIGN AND TESTING OF A HIGH-RESOLUTION MINIATURE TUBE.

Recent developments of the thermionic cathode ray tube, mainly aimed at higher resolutions, have resulted in the attainment of a spot size of ~ 25 μm diameter, which, although small enough for the majority of applications, does not meet an increasing need for tubes of even higher resolution. It follows that the tubes capable of such high resolution are normally used in conjunction with some form of recording systems rather than by direct visual observations, since an eye would have to be within about 100 mm of the tube face to resolve two adjacent spots 25 μm apart. The typical form of the thermionic electron gun used for this type of high resolution

(a) 160 Hz
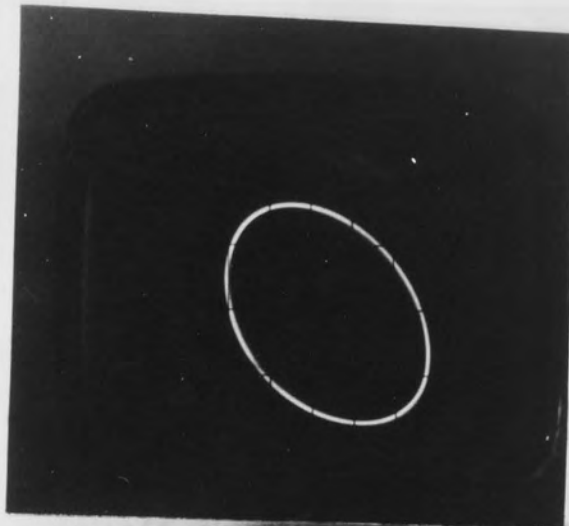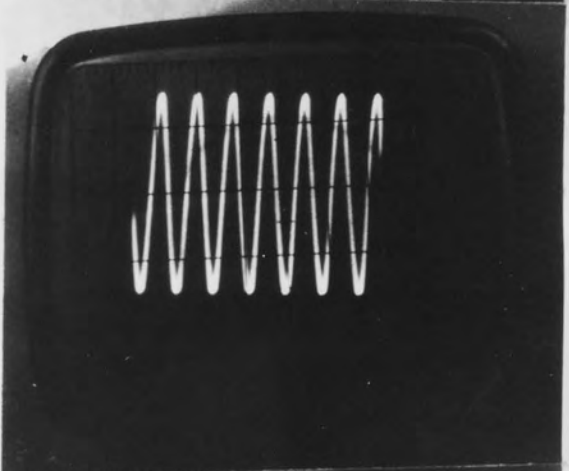
(b) 30 kHz

(c) 30 kHz
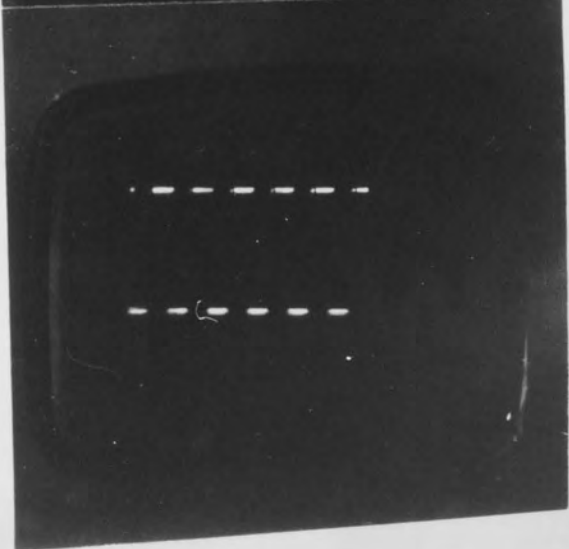
Fig. 4.56 Typical displays formed on conventional C R T, (a) ellipse

(b) sinusoidal and (c) square wave.

work is a triode design consisting of an indirectly heated planar
cathode, a modulator and anode, where the beam is deflected electro-
magnetically. The size of the spot produced on a phosphor screen with
such a gun is given by

$$\text{spot size} = \text{object size} \times v \,/\, u \qquad\qquad (\,4.1\,)$$

where v is image distance from the focusing lens and u is the object
distance. Therefore, small spot sizes can be obtained by having a
small object size or large object distance; however the latter is not
possible in practice since it would lead to excessive divergence of
the beam which will not only reduce the current efficiency but also
give rise to large aberrations. The reduction in crossover size,
and therefore the object size, in the case of the thermionic tube is
achieved by reducing the dimensions of the triode gun until it is
finally limited by the inability to maintain sufficient insulation
between the cathode and modulator.

In contrast it is not difficult to achieve a small object size
when using a field emission electron source, since the electron
emitting area at the tip of the cathode is assumed to have a radius
of $\leqslant 0.1\ \mu m$ which is used directly as an object in an electrostatic
field emission gun; i.e. rather than using a crossover as in a
thermionic gun. It can therefore be seen from equation $(\,4.1\,)$ that
in the case of the miniature gun already tested, which has an image
distance of 50 mm and object distance of 5.5 mm, a spot size of
better than $1.8\ \mu m$ can be easily obtianed; in fact it would only be
limited by the size of the phosphor grains used for depositing the screen.

A description will now be given of how a carbon fibre field
emitting electron source was introduced into a "miniature" 50 mm
focal length electrostatic field emission gun of the type previously

tested using a demountable laboratory system (section 4.6.2).
Firstly, to overcome the difficulties of tip alignment, which are
even more critical in this case, a cathode-extractor assembly was
built, whose design was based on that used for the conventional
300 mm tube, except that it had to be reduced in size for incorporation
into the miniature tube. As shown in Fig. 4.57, the cathode assembly
was further modified to incorporate a heating coil for independently
pre-treating the cathode for the purpose of increasing its emitting
life-time; an important topic that will be discussed in the next
chapter. The complete cathode-extractor assembly, which was mainly
constructed from stainless steel, is shown in the photograph of
Fig. 4.58; the cathode holder was constructed from a 8 BA screw with
a syringe needle embedded in one side (see Fig. 4.57), into which
the carbon fibre is inserted and held in position by a drop of
silver dag. Infact, the dag fills up the needle by capillary action and
hardens to give a very strong joint when heated in vacuum by the
heating coil. Once the carbon fibre is etched, the cathode holder
and the cathode are inserted into the main assembly containing the
heater coil (3). This cathode assembly is then held inside the
stainless steel tube (5) by four screws set at 90° to each other,
which allow the cathode to be manipulated in the x-y plane. To align
the cathode, the four screws are adjusted independently while viewing
the cathode with the aid of travelling microscope positioned at one
of the four clearance holes, intended for viewing the cathode; the
procedure is repeated in turn for each of the screws and their
respective clearance hole, until the cathode is accurately aligned
at the centre of the extractor aperture. Finally, the same
travelling microscope is used to set the required extractor-cathode
separation, which is achieved by turning the cathode holder.

Cathode

5

3

15mm

4

1

2

14mm

10mm

tags

4

Extractor

heater shield

10mm

(1) Extractor
(2) Cathode holder
(3) Inner stainless
    steel ring
(5) Outer stainless
    ring
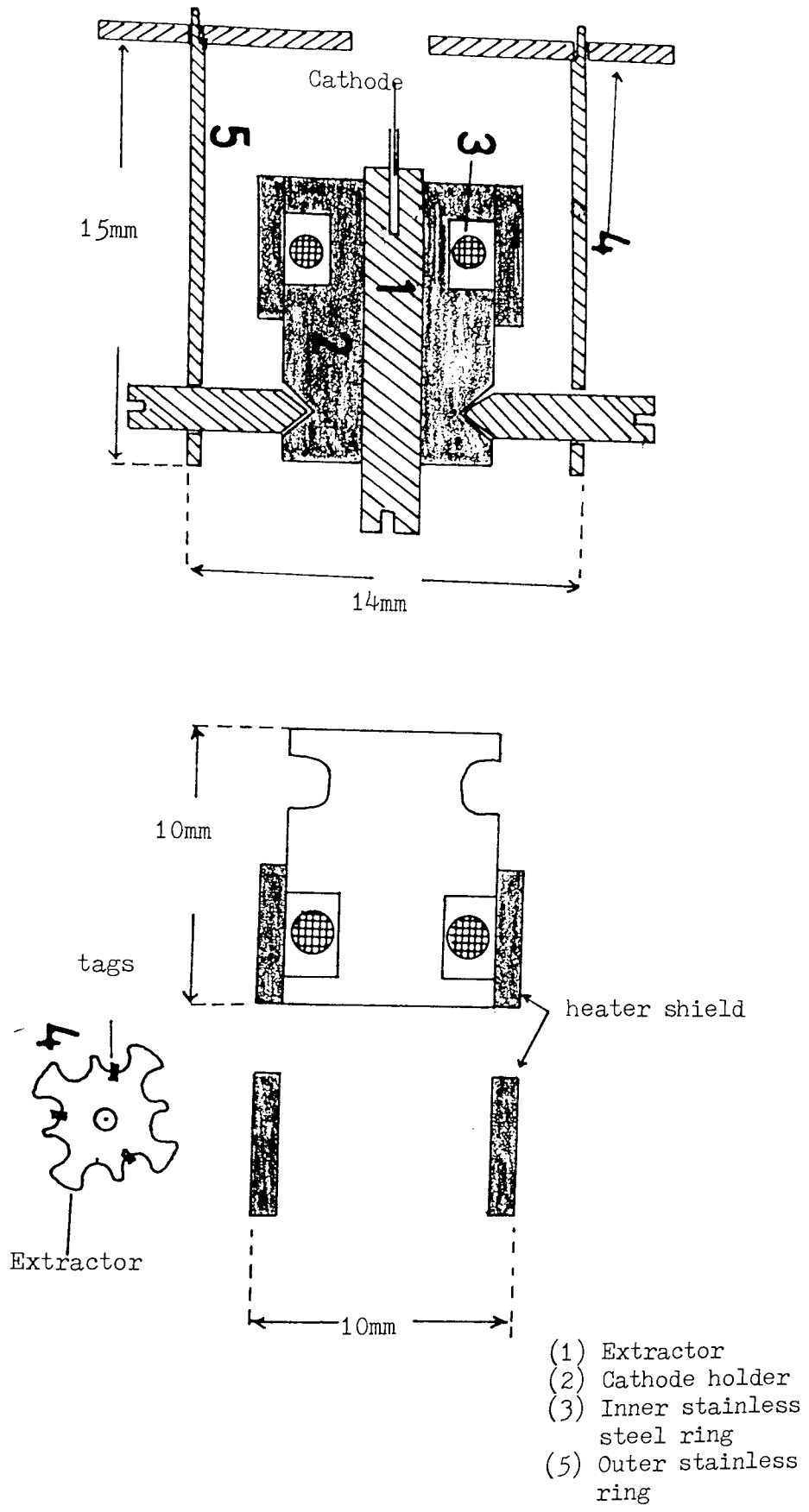
FIG. 4·57   Cathod - extractor assembly for miniature C·R·T
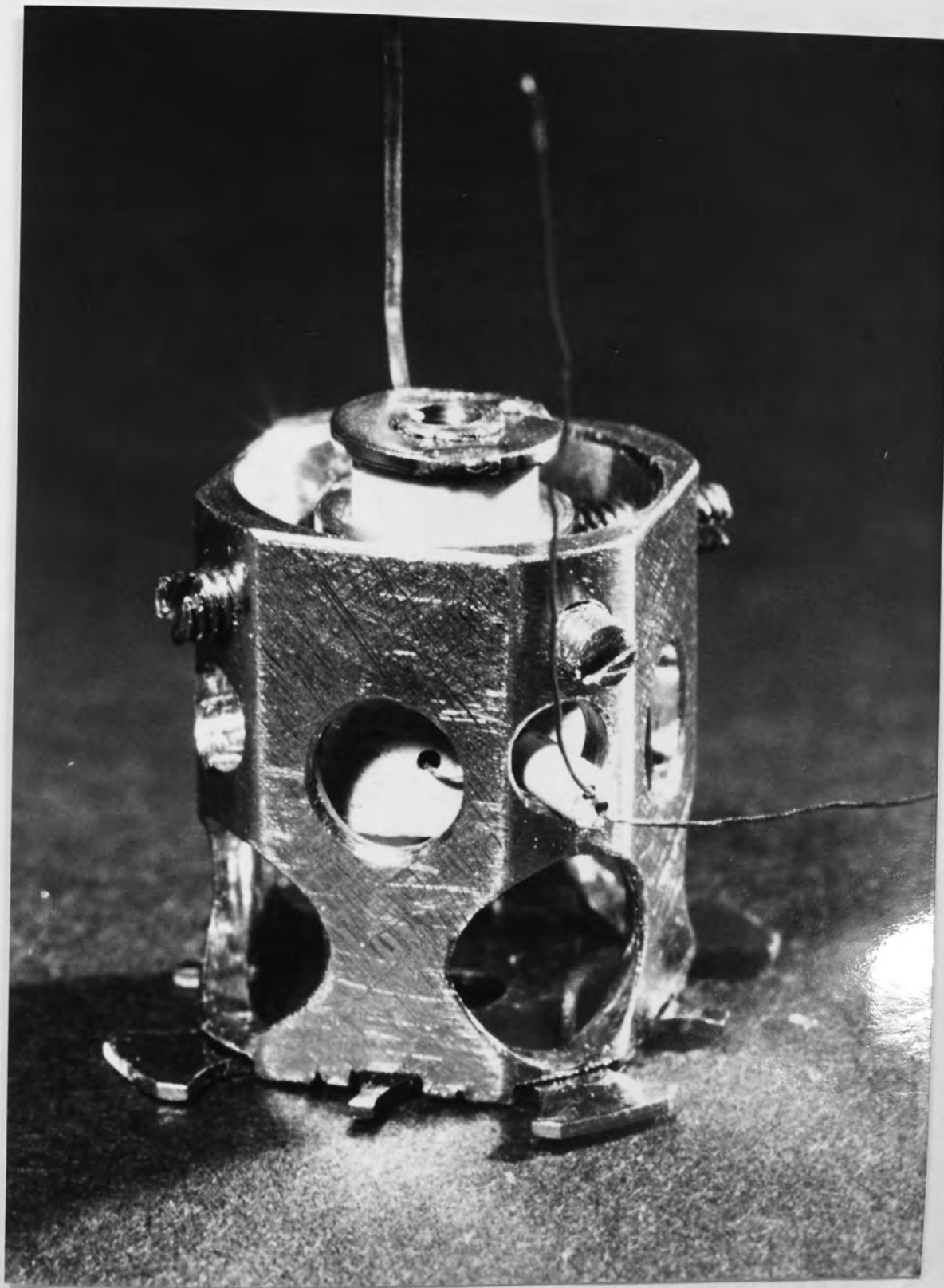
Fig. 4.58 Photograph of cathode-extractor assembly for miniature

C R T.

Following the accurate alignment of the cathode, the complete gun is assembled using the standard electrodes and deflecting plates manufactured by the M-O valve company for use in their miniature tubes. This is shown in Fig. 4.59 , together with three ring getters and collar spring that are used to secure the gun inside the 30 mm diameter glass tube whose inside front face had been previously deposited with fine grain phosphor. This phosphor screen was made in the same way as described previously for the 300 mm focal length tube (see section 4.7.2). However, for this high resolution tube, phosphor particles of size 1 - 2 μm were used compared with 10 - 20 μm used in the conventional tube. Finally, the miniature tube was evacuated for about 18 hours, during which the cathode was heated after 11 hours for five hours to prolong its life-time. On sealing, the pressure inside the tube was about 5×10^{-7} m bar, and to maintain this pressure over the life-time of the tube the three getters were fired using R.F. heating.

The performance of this high resolution tube shown in Fig. 4.60 was evaluated in the usual manner by applying the necessary voltages to the appropriate electrodes, such that $V_I / V_o = 5$. For these conditions the total emission current was 9.2 μ A and it was found that about 7.4 μ A reached the screen, making the gun about 80% efficient. An attempt was then made to measure the size of the focused spot using a travelling microscope; however, this proved unsuccessful at the above currents since the electron and optical scattering effects were too large to allow an accurate assessment of its size. Therefore the emission current was reduced to $\sim 2 \mu$ A when the intensity of the spot had reached the point where it could be just seen with ease, and the size of the measured spot was $\sim 17 \mu$m . It will be recalled however that the resolution of such a tube can be
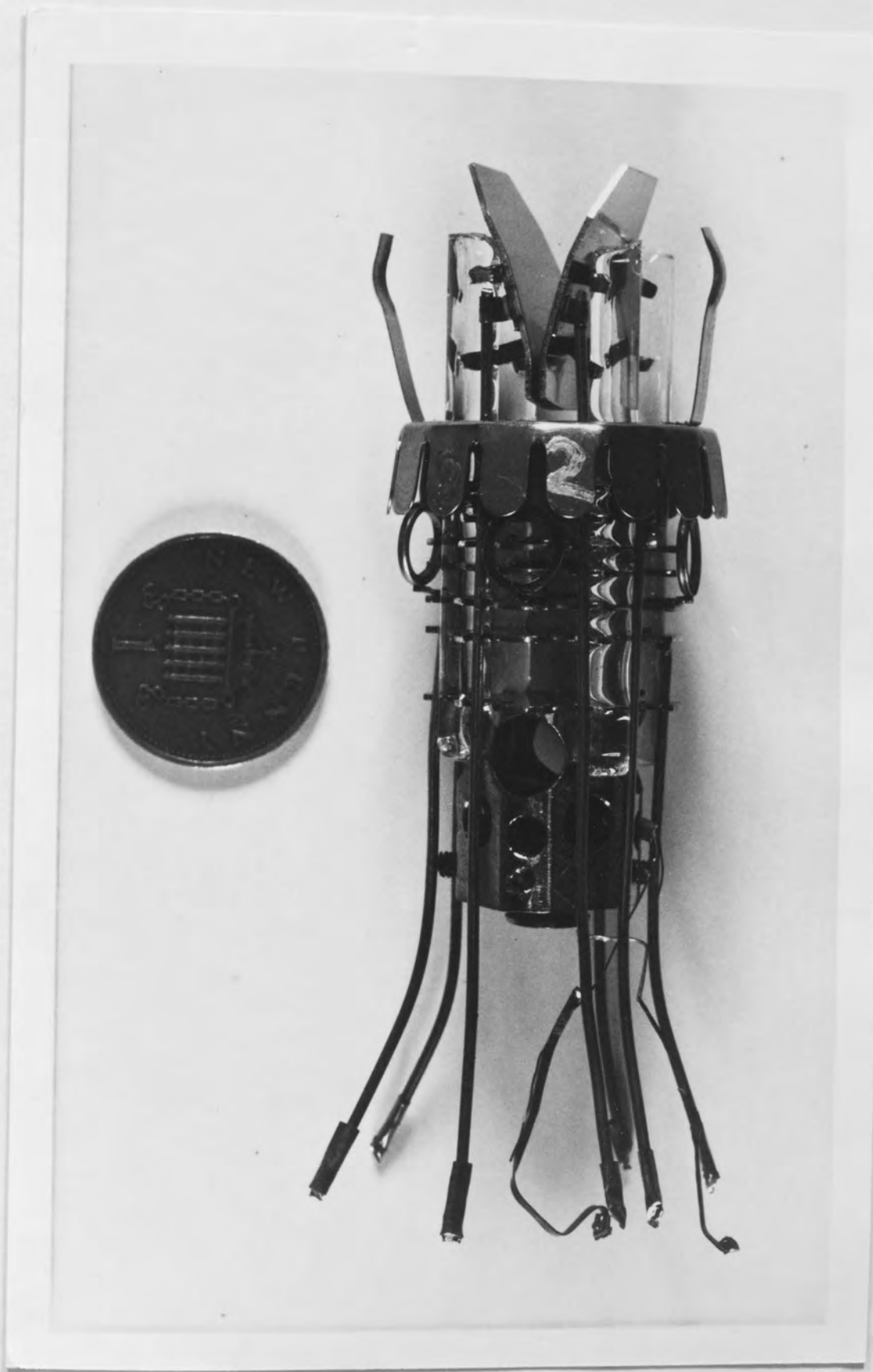
Fig. 4.59   Photograph of assembled gun for miniature C R T.

Fig. 4.60 Miniature field emission C R T.

very much better than this i.e. of the order of 2 μm - although a
limiting case would probably be reached before this, due to chromatic
and spherical aberrations present in this type of electrostatic gun.
It should also be noted that at these small values of the spot size,
the current loading at the screen increases to a level where
saturation takes place, with the possibility that the light output
from the fluorescent screen might become the limiting factor.

Evaluating the performance of this miniature tube in terms of
the elliptical display of Fig. 4.61 (a) showed it to be very satis-
factory with an even brightness and no aberration in the focused
spot due to the beam deflection. Fig. 4.61 (b) and (c) are examples
of its response in the conventional sweep mode to various voltage
waveforms in the grequency range of 10 Hz to 10 mHz , and here
again the displays are very good quality, being very well defined
with even brightness over the whole display even at the reduced
emission currents. However as with all other tubes tested, there
remains the outstanding problem of the variation of the light
intensity over long time periods.

4.9 STABILISATION OF THE FINAL DISPLAY USING USING ELECTRONIC FEED-BACK.

Although the overall electron optical performances of both the
demountable laboratory versions and the sealed commercial field
emission cathode ray tubes were found to be excellent, there remains
however one very undesirable effect, viz the random fluctuations with
time of the light intensity in the final display at the fluorescent
screen. The possible mechanisms which could give rise to this
undesirable effect have already been discussed fully earlier in the
chapter (see section 4.5). Briefly however, the variations in the
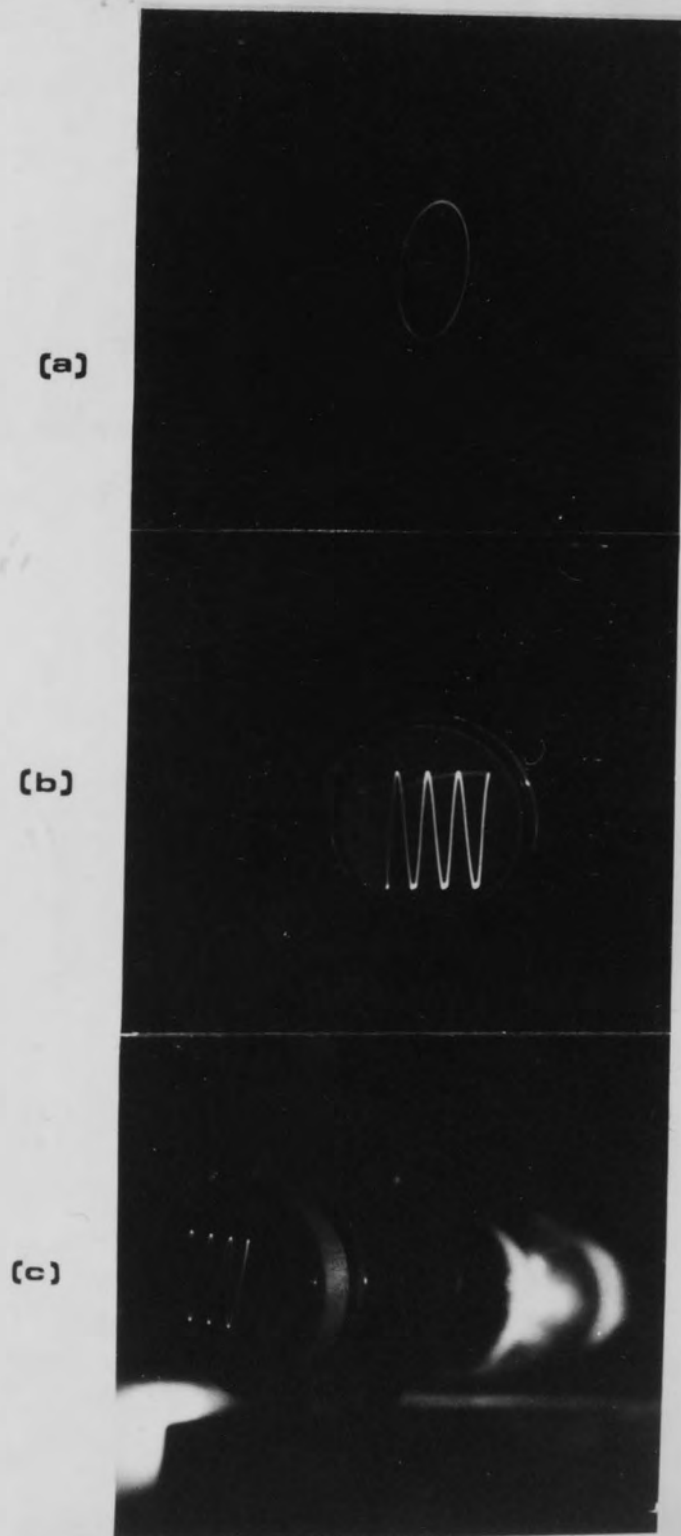
Fig. 4.61 Typical displays formed on miniature C R T, (a) ellipes
(b) and (c) sinusoidal wave form (recorded at 300 kHz).

total emission current and the continuously changing characteristic

emission pattern falling on the extractor aperture have been shown to

be responsible for these fluctuations in the final image. In view

of this strong correlation between the emitted current and the

fluctuations at the phosphor screen it was considered to be worthwhile

to examine various methods for stabilising this total emitted current

with the aim of subsequently minimising the intensity fluctuations

in the final display. Using a high valued resistor ($\sim 10^8 \Omega$)

connected in series with the cathode, a high degree of stabilisation

can be achieved, but this approach results in large fluctuations in

the tip voltage, which, as has already been discussed, can lead to

defocusing effects. These latter effects will only be small for

this redesigned gun, but nevertheless still lead to fluctuations in

the velocities of the emitted electrons, which in turn will cause

unneccessary chromatic aberrations. Therefore, a need existed for

a suitably designed electronic negative feed-back to replace the

100 MΩ resistor and provide a comparable stability in the total

current without the large variations in the tip voltage.

This was achieved very simply by using an electronic valve

connected in series with the cathode such that it acted as a variable

resistor as shown in circuit diagram in Fig. 4.62 (a) with the

cathode of the tube connected to the anode of the valve and the

cathode of the valve connected to the negative high voltage supply

via a self-biasing 2 MΩ resistor, the grid will be kept more

negative from the valve cathode by the whatever voltage is dropped

across this resistor. Thus, a small increase in the emission current

will lead to an increase in the voltage drop across R_1 and hence an

increased negative biasing of the valve and the consequent reduction

in the current flowing in the valve, and hence the emitter.
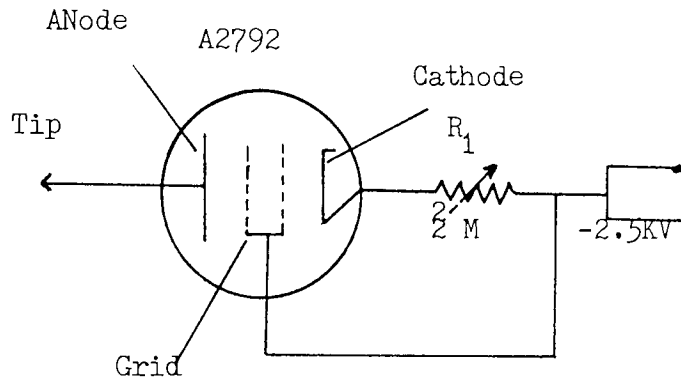
(a)
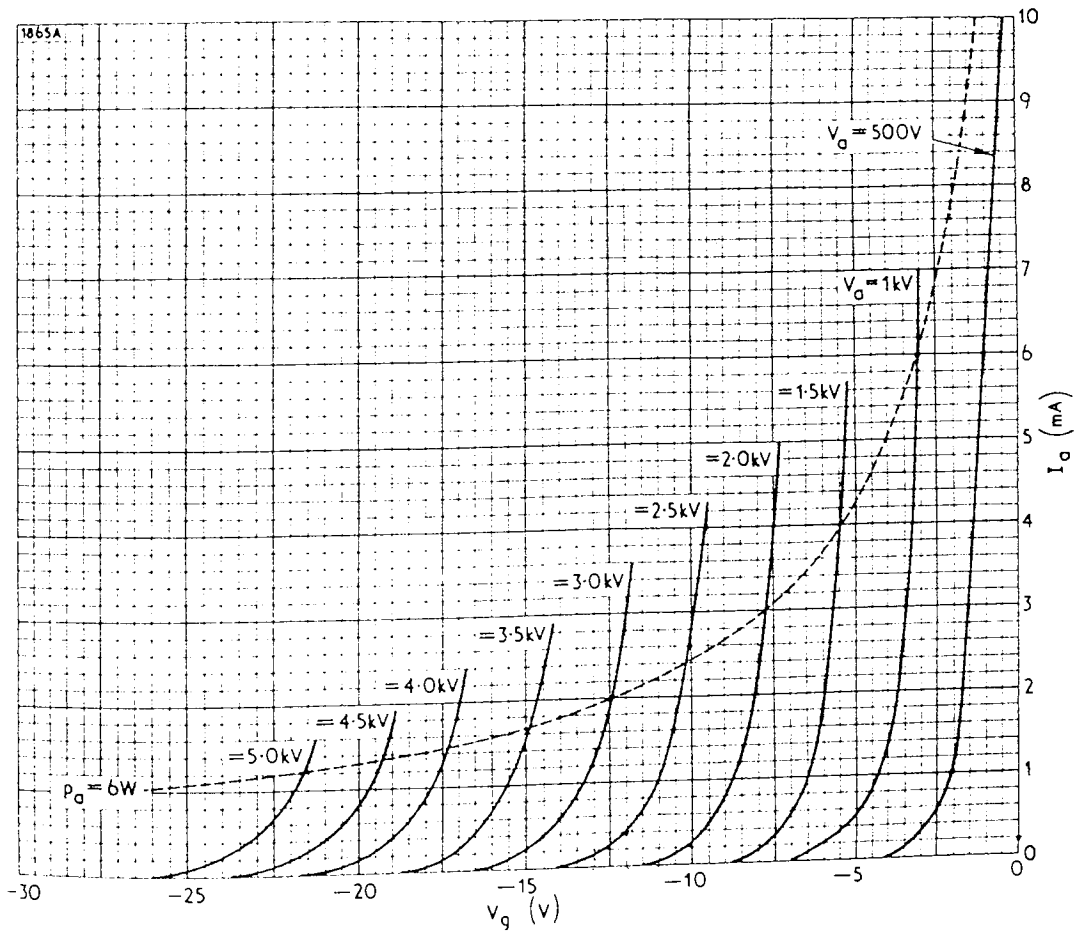
(b)

Fig. 4.62 Valve type feed-back system (a) circuit
diagram and (b) valve characteristics.

Conversely, if the total current tends to decrease, the grid in this case will become less negative, and thus reduce the electron current flowing through the valve, and hence from the emitter. Under typical operating conditions, that is when the emitter is set at - 2.5 k V in order to maintain about 500 Volts between the emitter and the extractor to obtain about 10 μ A emission current, it follows that the valve anode would also be at - 2.5 k V. Therefore from the valve characteristics shown in Fig. 4.62 (b), to keep the 10 μ A total emission constant the voltage drop of 11.8 Volts which is the grid biasing voltage (the voltage difference between cathode and grid) need vary by only ± 1.75 Volts: to satisfy this condition the variable resistor R_1 therefore needs to be set at about 1.18 MΩ . The marked improvement in the stabilisation of the total emission current that can be achieved with this simple circuit is illustrated by the chart recorder traces presented in Fig. 4.63 which compare in (a) the result obtained with the new electronic feed-back system with that in (b) obtained by using a 100 MΩ resistor. A further important advantage of this electronic system in that the tip voltage only varies by about a total of 3.5 Volts as compared to about 150 Volts when using the 100 MΩ resistor. Although this method of stabilising the emission current could readily be used to replace the 100 MΩ resistor without affecting the operation of the gun, it unfortunately leads to very little improvement in the stability in the final display: this is illustrated by Fig. 4.63 (c) where the optically monitored variations of the spot intensity are still very large.

An alternative approach to this problem was therefore examined, which involved sampling and amplifying the screen current and using this to control the cathode-screen voltage (effectively the accelerating voltage), such that if the screen current rose, the
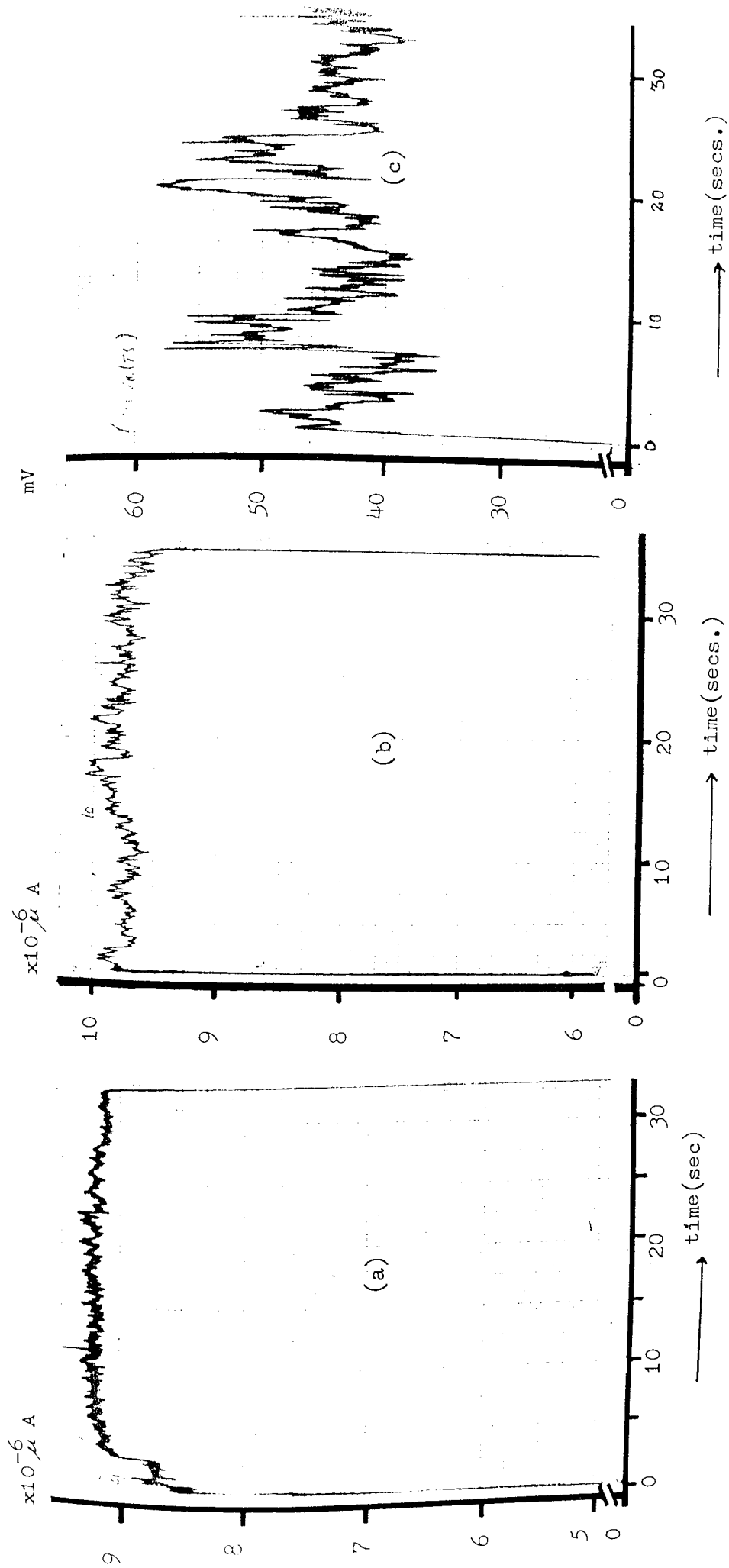
Fig. 4.63 Chart recorder traces of (a) total current stabalised using valve feed-back, (b) total current stabalised using 100M resistor and (c) optically monitored screen signal for (a).

applied accelerating voltage falls, and vice versa of course. For this purpose, the comparator section of the commercial solation power pack, capable of supplying 1 k V either polarity was modified so that the amplified and inverted signal obtained from the screen could be used to control the output voltage, such that its changes were 180° out of phase with those of the screen current. This modified power supply was then used in conjunction with a 5 k V Brandenburg power supply as shown in Fig. 4.64 . However on testing this arrangement, no improvement in the stability of the final image was achieved as can be seen from Fig. 4.65 where the optically monitored signal for (a) with this feed-back system and (b) with the 100 MΩ resistor are compared. This lack of success was due to the fact that the frequency response of the modified power pack was infact too slow to follow the fluctuations of the screen current. Accordingly this particular electronic approach was abandoned, since, to improve its response time, it would have been necessary to redesign the whole of the comparator and voltage stabilising section of the power supply. Instead, it was decided to design a purpose-made unit to overcome the instability at the screen.

This final method of stabilisation that was investigated, and the one that proved most effective, was based on the above principle but in this case the monitored screen current was used to vary the tip-extractor gap voltage, in order to control the emitted current, and to stabilise the current reaching the screen. To vary the gap voltage, one is restricted to only modulating the potential of the cathode, since any change in the extractor voltage will perturb the electric field between the extractor and first element of the lens, resulting in severe defocusing effects, whereas variations in the tip voltage will have little effect on the defocusing properties of the present gun

3 M

50 K

741

screen

solatron power
supply

100k

Brandenburg
power supply

50M

cathode
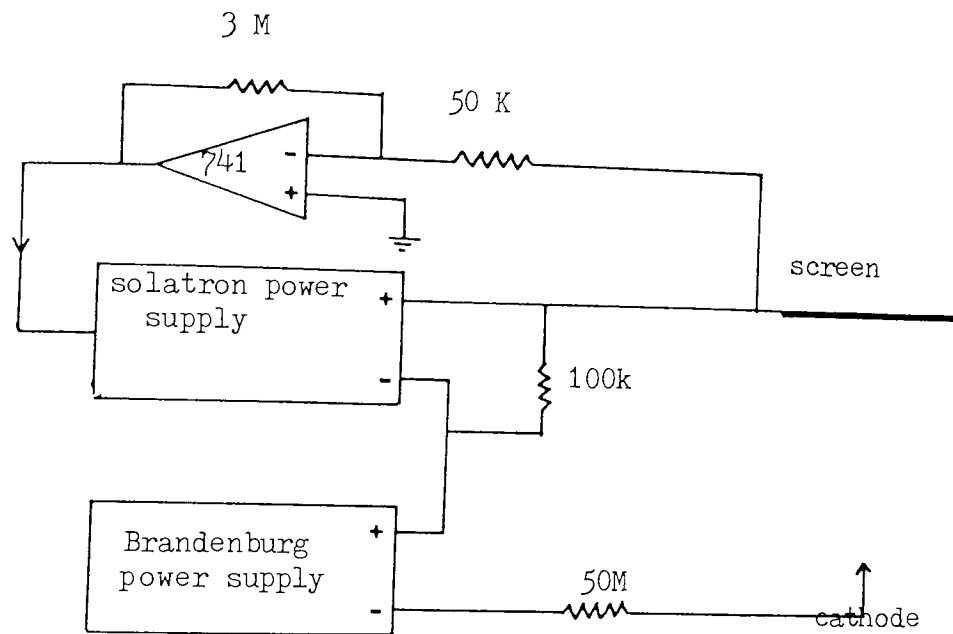
Fig. 4.64   Use of modified power supply in conjnction
with Brandenburg power supply as a feed
-back system.
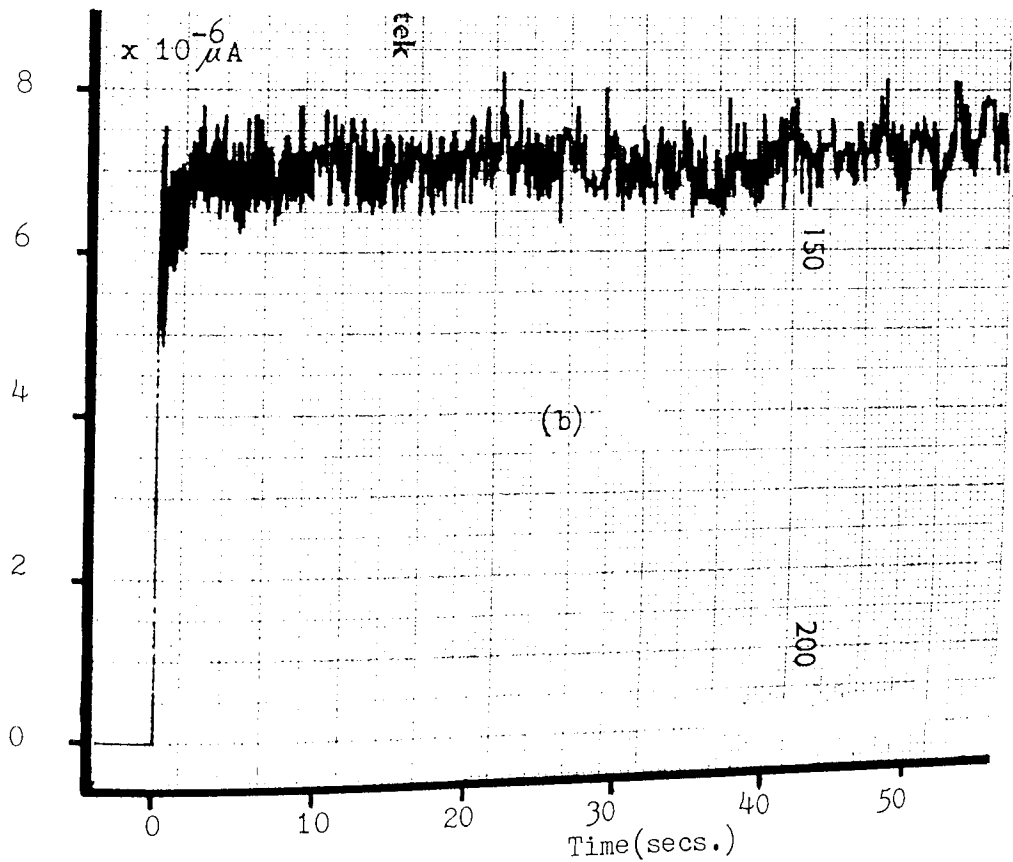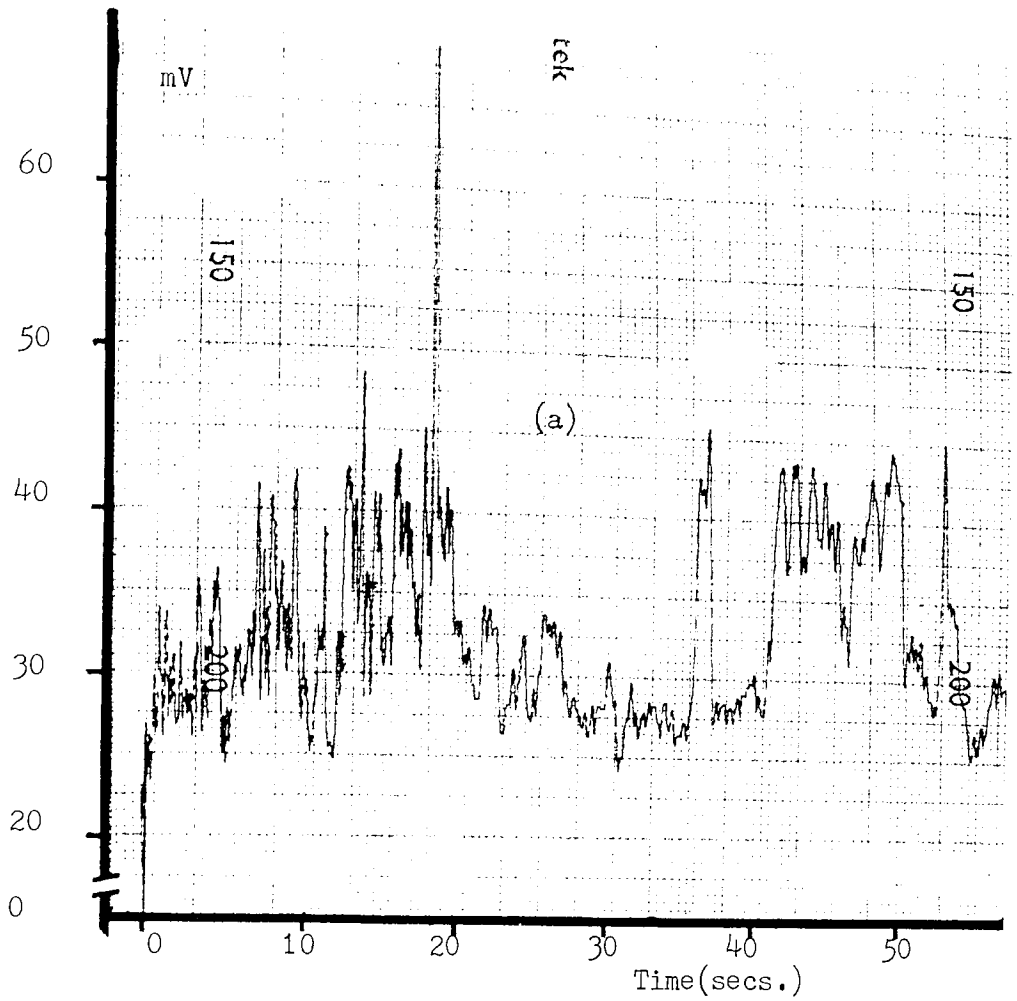
Fig. 4.65 Chart recorder traces of (a) stabilised
optical signal from screen with modified
power supply and (b) total current staba-
lised with 100 MΩ resistor.

system.

Based on these consideration, the feed-back system shown in Fig. 4.66 (a) was developed. For this case, the total current is controlled by using the switching action of a high-voltage transistor (B U 105) (i.e. instead of the valve used earlier), which was driven in the following manner by a signal obtained from the screen. This monitored screen current is first amplified in two stages, and the output of the second stage is used to drive the light emitting diode (L E D) in the opto-isolator, which was used to provide an adequate isolation-up to 4 k V if need be between the high and low voltage sections. Thus when the diode in the opto-isolator lights up, it creates carriers in the base of the opto-isolator transistor T_1 whose number is proportioned to its brightness, which in turn causes a current to flow in transistor T_1 and hence T_2 . The flow of current in T_1 and T_2 will then be proportioned to the current flow in R_1 , and the resulting voltage drop will effectively be the gap voltage between cathode and extractor necessary to obtain electron emission; in this arrangement the extractor voltage is kept at a constant value of - 2 k V by using a separate power supply. Now, if the screen current increases, this will result in an increase in the light intensity emitted from the L E D which will in turn cause the current to flow in transistors T_1 and T_2 , therefore in R_1 , to increase. Consequently, the voltage drop across R_1 will increase and lead to a further increase in the emission current. Infact, this corresponds to a positive feed-back, which is the opposite effect to that required. To convert this to a negative feed-back situation, a standing current, obtained from a constant current source of the same polarity as the screen current, was fed into the circuit after the first amplifying stage, so that the amplified and inverted screen

(a)

(b)

V_C = Control voltage
V_e = Emission voltage
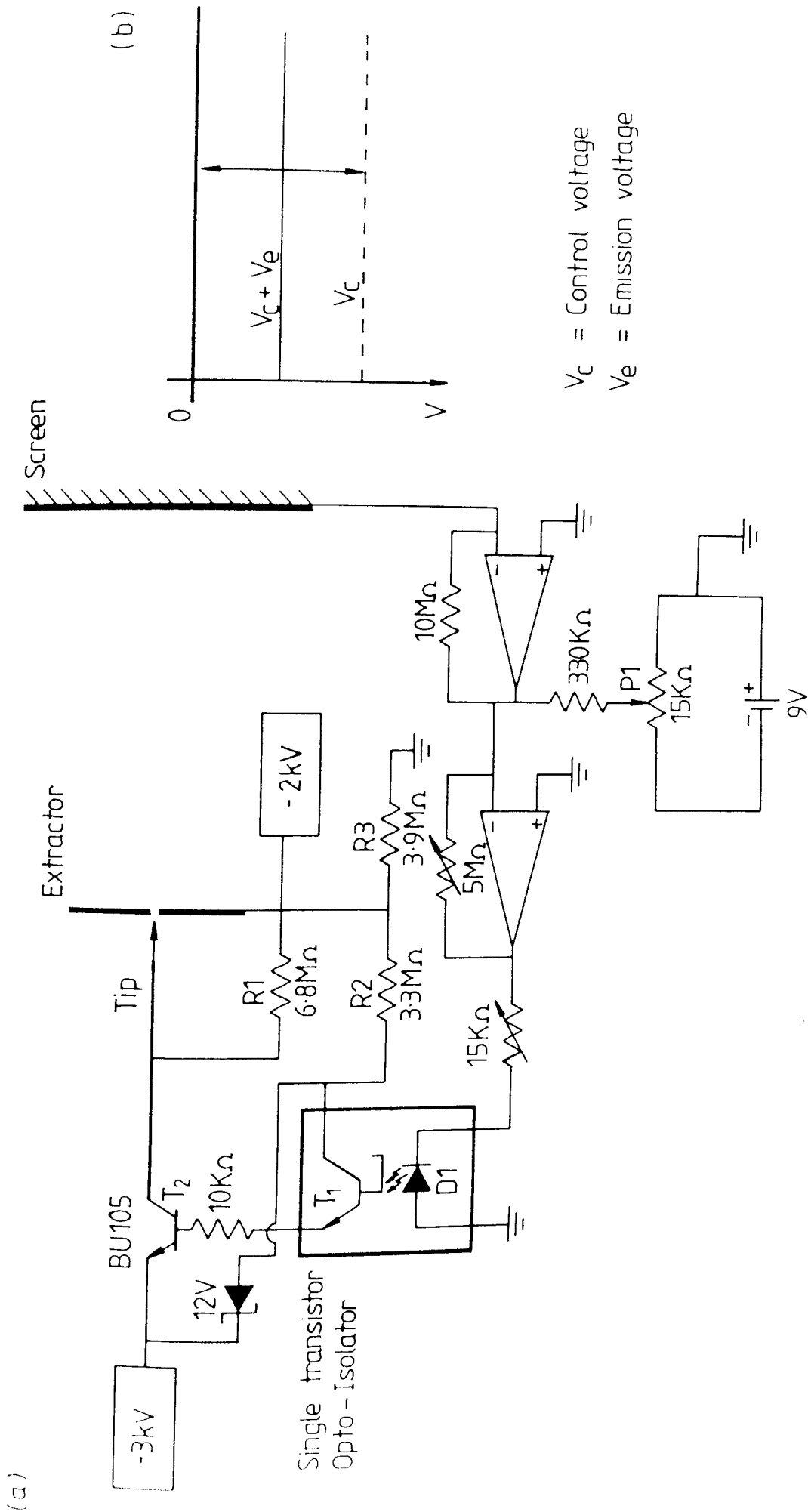
Fig. 4.66 Electronic feed-back (a) circuit diagram and (b) D.C level diagram to show control region.

current will be subtracted from the standing current before the
resultant is amplified and again inverted by the second stage
amplifier and used to drive the L E D. The magnitude of the standing
current can be varied by using the potentiometer P_1 in order to
pre-set the total emission current as required; in this case was
normally about 5 μ A. The method adopted for achieving this is shown
in the D.C level diagram of Fig. 4.66 (b), and the area shown by the
arrows is the control region in which this D.C level will vary in
order to control the total current to stabilise the screen current.
So if now the screen current increases it will be further subtracted
from the standing current whose magnitude is greater than the screen
current, leading to a decrease in the output of the second amplifying
stage. As a result the L E D light output will decrease, and
consequently the current flowing in T_1 and T_2 and therefore R_1
will also decrease and thus reduce the gap voltage. The overall
effect will be to reduce the total emission current and therefore to
bring back the screen current to the pre-set level. Conversely,
when the screen current decreases by a certain amount then the
magnitude subtracted from the standing current will be less (see
Fig. 4.66 (b) which will lead to an increased output from the second
amplifying stage and thus the L E D light output. This will lead
to an increase in total emission current and consequently the screen
current. In this way therefore the screen current is continually
monitored and updated to maintain it at a constant value. The rate
at which this is done is governed by the response time of the circuit
which was measured with a high speed oscilloscope and found to be
~ 1.3 μ S. An important practical precaution taken during the
building of this feed-back system, was to arrange for the high voltage
transistor T_1 and the low voltage amplifier sections to be housed

in separate screened boxes; this was to avoid serious effects of pick up and voltage break-down as a result of the high voltages used and thus damage the low voltage components. Before use with a C R T, the system was tested by simulating the screen current fluctuations with the output of a light sensitive diode that was subjected to controlled levels of illumination.

Having determined that the feed-back system was working satisfactorily, its performance was investigated with the short 50 mm focal length gun, contained in the demountable system (see section 4.3, Fig. 4.4). Referring to Fig. 4.66 (a) emission was obtained by increasing the voltage from the power supply feeding the transistor T_1 to - 3 k V, while keeping the extractor voltage at - 2 k V and the standing current set at a level to give a sufficient gap for about 5 μ A total current. However, when the feed-back was switched on only about 0.5 μ A total current was obtained with a very faint and highly fluctuating display at the screen. Any attempts to increase the emission current by further adjusting the gap voltage by adjusting the standing current only resulted in an increase to ∼ 1 μ A total emission current with no change in stability. This was tracked down to over loading by 40 kHz R.F signal used in the high voltage power supply for stabilising their output; this was fed into the system via high voltage lines from the power supplies. To eliminate this, two R.F filters were connected in series with the two lines feeding the emitter of the transistor T_1 and the extractor electrode. With this modification, it was now possible to adjust the gap voltage by adjusting the standing current to obtain an emission current of about 5 μ A which now fluctuated more than usual about its mean position to maintain constant current collected by the screen. It will be seen from Fig. 4.67 (a) and (b) that this system resulted in a large reduction

191.

Fig. 4.67 Chart recorder traces of optically monitored screen signal
(a) without,(b) with stabilisation with monitored screen
current as feed-back.

in the light intensity fluctuations of the final image, where a comparison is made between the optically monitored chart recorder traces obtained "without" and "with" stabilisation respectively.

However, surprisingly, there still remained an acceptable level of instability as can be seen from the slow scan traces obtained of Fig. 4.68 (a) and (b) respectively "with" and "without" feed-back. This was originally thought to be due to the fact that the magnitude of the variations in the gap voltage swing was insufficient to cope with these large variations at the screen. However, increasing the voltage swing did not result in any further improvement in the stability; this was despite the fact that the feed-back system was checked out to be working as per design specifications. It was then realised that the quantity that was fed into the system, to control the emission current to stabilise the variations at the screen, must be what is stabilised. Therefore the monitoring of the electron beam current impinging on the screen showed it, as can be seen from Fig. 4.69, to be absolutely fluctuation free. Which is understandable since that was the quantity which was fed into the system. Therefore the remaining variations in the light intensity of the final image must be due to variations in the electron energies due to variations in the accelerating field, and should however be possible to eliminate.

The above investigation suggested that if instead of the screen electron currents, the output of the optical detector monitoring light intensity fluctuations in the final image are fed into the feed-back system, it would indeed be possible to stabilise the light intensity at the screen. Therefore, by making a slight adjustment to the amplifying section of the feed-back system, the output of the light detector was fed into the amplifying stage, with the result that the variations in the light intensity were completely eliminated.
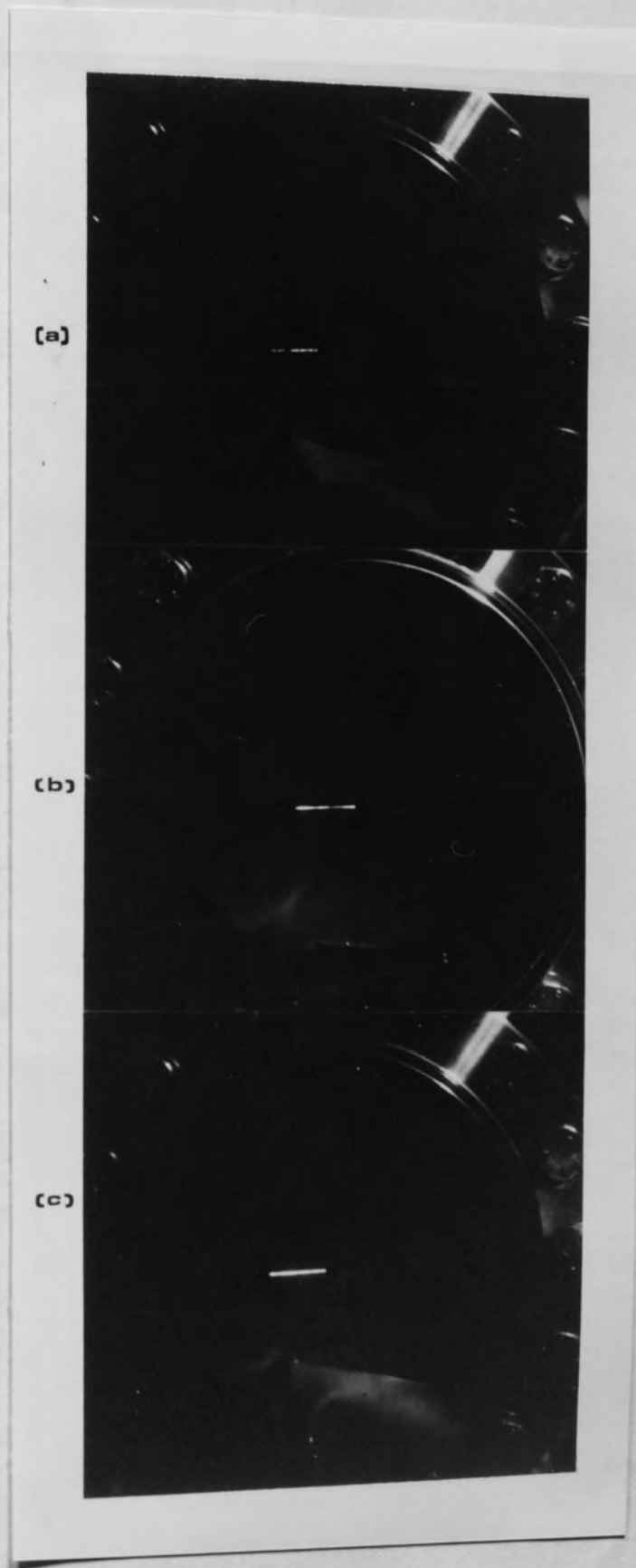
Fig. 4.68   Slow scan traces of (a) without stabilisation (b) with

stabilisation on using screen current as feed-back and

(c) on using optically monitored signal as feed-back.
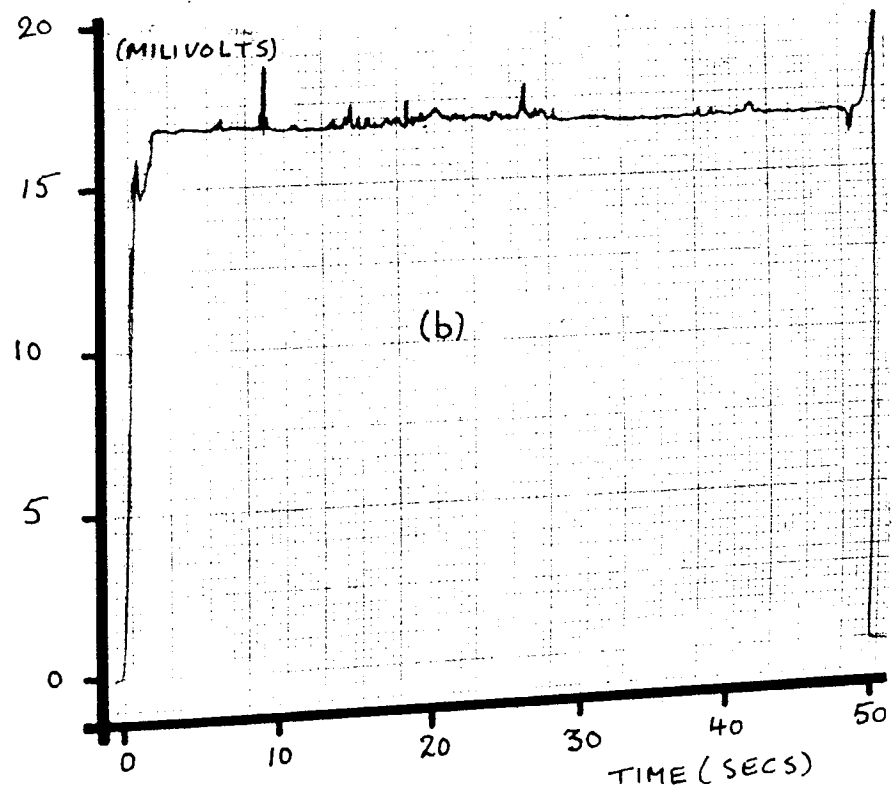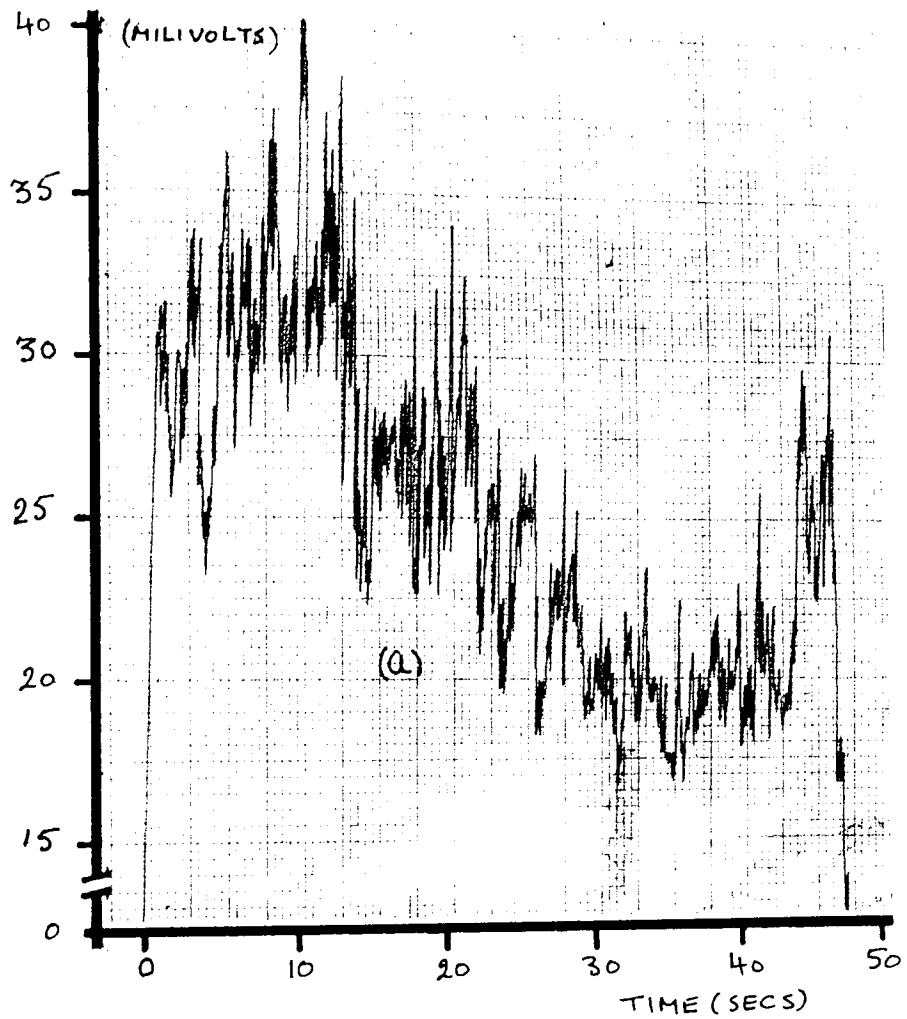
Fig. 4.69   Chart recorder traces of monitored screen current (a)
without (b) with stabilisation on using screen current
as feed-back.

This is illustrated in Fig. 4.70 which shows the chart recorder traces of the light detector output "without" and "with" stabilisation. However, since the maximum variation in the gap voltage required to maintain a stable light intensity of the final display was found to be of the order of $\pm$ 150 Volts, it was again necessary to apply the single-scan technique to check that how serious defocusing effects had been introduced. To provide a clear access to the screen to photograph the scan traces, the light sensitive diode monitoring the display was attached to the screen as can be seen from the photograph of a typical 15 second scan trace, shown in Fig. 4.68 (c), obtained after stabilisation using optical feed-back. The typical stability obtained is obvious when compared with traces obtained without feed-back and with current feed-back respectively shown in Fig. 4.68 (a) and (b). Thus, *here* the best stabilisation, with negligible defocusing, is clearly obtained when using the optical feed-back system. Whilst therefore this method of stabilisation clearly demonstrates that the intensity fluctuations in the final image can be completely eliminated, it is however not very practical since it only allows the tube to be operated in complete darkness. The earlier method of stabilisation, whereby the screen electron current was used to control the emission current, may still however be suitable for many applications if further modifications are made to the system to improve upon the stabilisation already achieved. One possible way may be to use this screen electron current to control the post-accelerating voltage applied after the relevant deflection of the beam. The method employing optical feed-back could perhaps be used successfully by mounting the light sensitive diode inside the tube, and using the signal in the usual manner. To overcome the problem of the light entering the chamber from the outside, the face of the
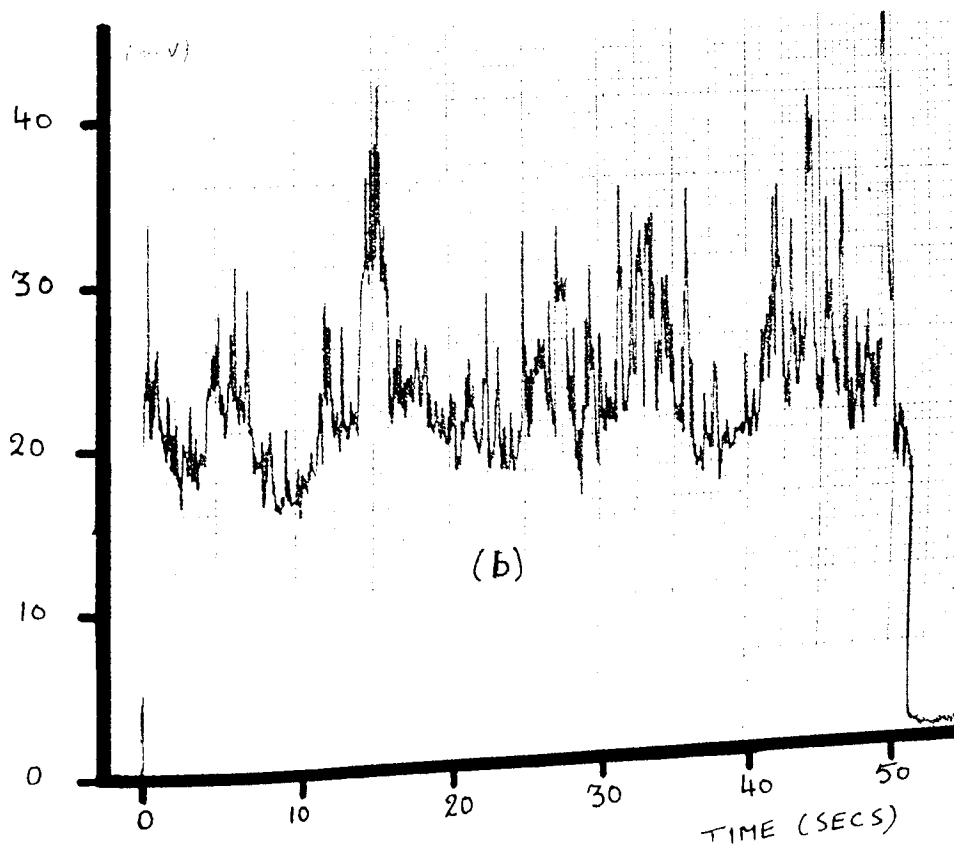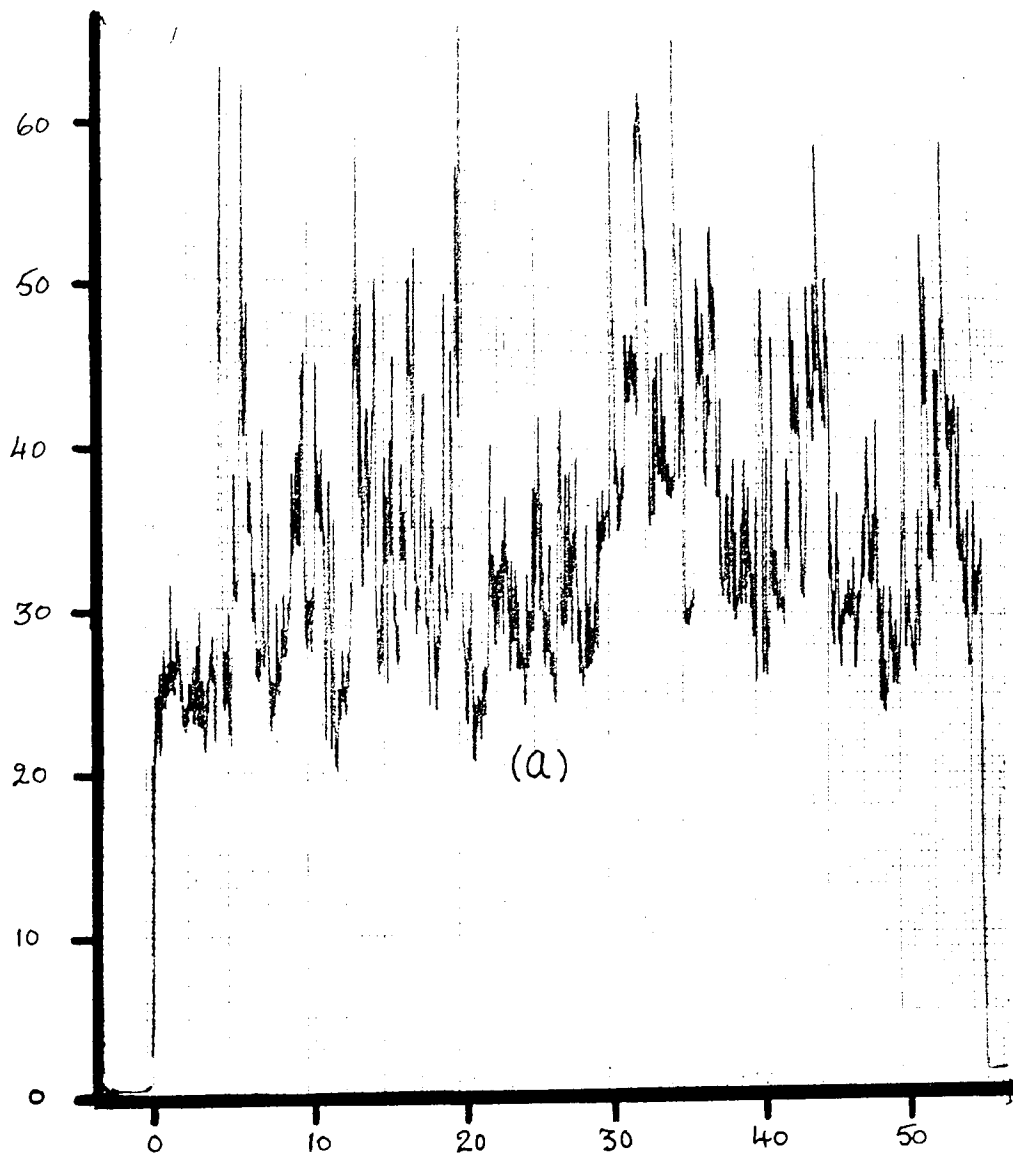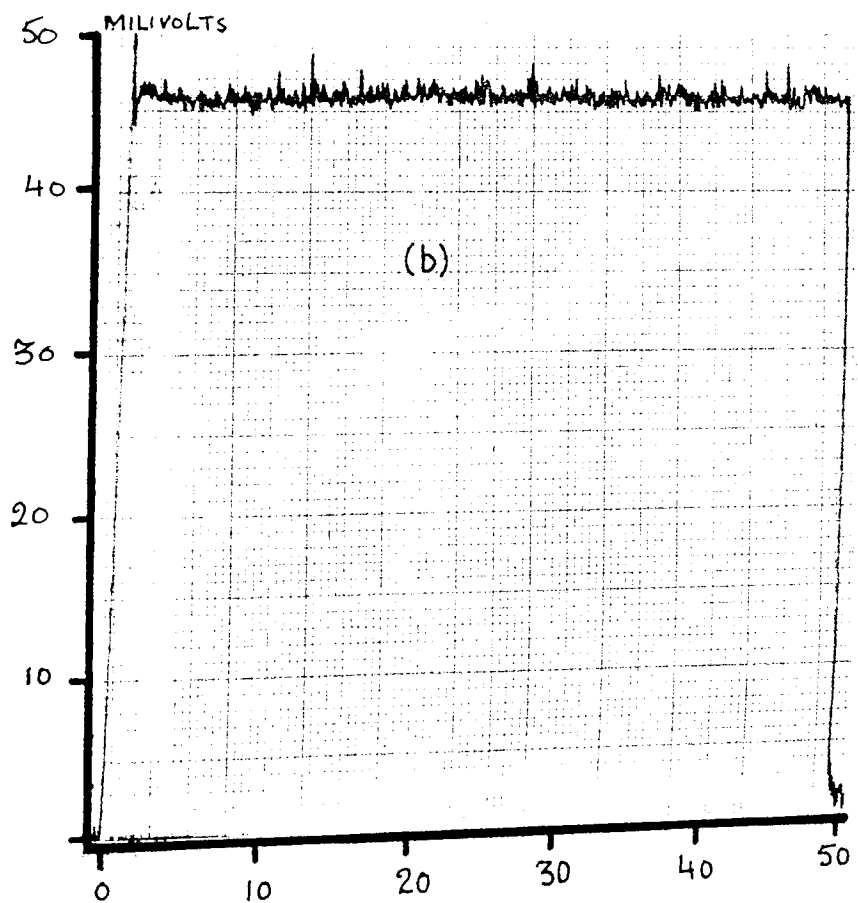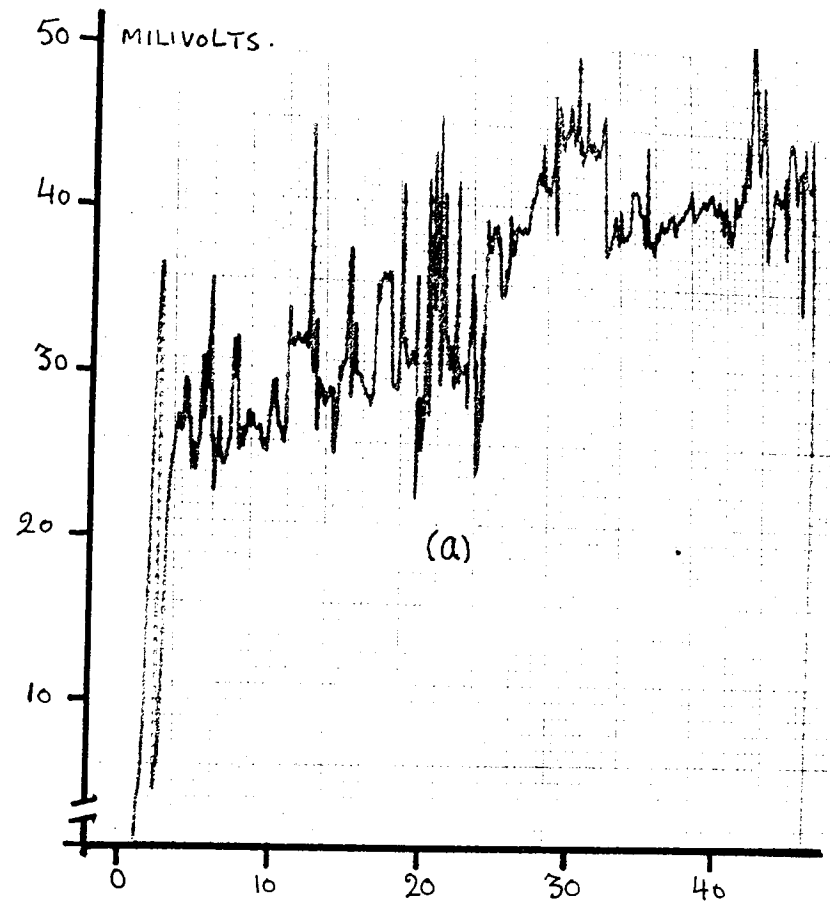
Fig. 4.70 Chart recorder traces of optically monitored screen signal (a) without (b) with stabilisation on using optical signal as feed-back.

tube containing the phosphor screen can be coated with a some kind of semi-reflecting material such that it only allows the light to pass one way, that is from the inside of the tube to the outside. Light proofing the remainder of the tube would be no problem, since the majority of it is already light proof. It is hoped that both of these suggestions are further explored in the future work.

5. EXPERIMENTAL STUDIES OF CARBON FIBRE EMITTER CHARACTERISTICS.

5.1 Introduction.

Although the various feed-back techniques described in the previous chapter were largely satisfactory in stabilising the total emission current and the display at the screen, it is clear from a practical point of view that it would be preferable to avoid using these relatively complicated systems and to stabilise the emission at the source. In this context two phenomena need to be suppressed. Firstly, there is the mechanism that leads to the "explosion" of the emitters when an emission current is first drawn from them, since this results in an increased source size and a more fragmented emission image. Secondly, there is the overall spacial instability of the emission image and more specifically the inherent property of individual sub-emission process to intermittently switch on and off. In this chapter, techniques will be described that have been developed to limit these phenomena.

5.2 INVESTIGATION OF THE EMITTER EXPLOSION PHENOMENON.

The changes in the tip profile that follow emission were first reported by Braun et al (101). They assumed the carbon fibres used in their investigation to be composed of a large number of closely packed fibrils that ran parallel to the carbon fibre axis, and that the emission occured from these fibrils which were believed to protrude above the surface of the etched tip. They further suggested that, during emission, ion bombardment of the emitter surface occurred,

and caused preferential sputtering at the boundaries of these fibrils, where a part or the whole of a fibril sometimes become detached to leave the sort of cavities that have sometimes been observed in the experimental observations. They also pointed out that such a mechanism would result in new fibrils being exposed, and the process could possibly be the regeneration mechanism that is responsible for the relatively good stability of these emitters under poor vacuum conditions (13, 14, 101). It follows that if this mechanism does take place, it would lead to a continuous erosion of the cathode which would therefore have serious implications for its potential life time. Therefore it would be of considerable practical importance to know the period of time over which this erosion can take place before the tip ceases to function properly. This same tip explosive phenomenon was later studied more extensively by Wilson (14), who investigated the effects of such parameters as vacuum pressure, emission current, and the duration for which an emission current was drawn. From these investigations he concluded that most of the erosion of the tip occurred in the first few seconds of switching on the emitter. He further speculated that the phenomenon was associated with the initiation of the electron emission from the carbon fibre. In practical terms, this type of explosive emission can sometimes lead to the complete distruction of the emitter unless it is protected by some sort of feed-back network.

The first of the present experimental investigations into the origin of the explosive phenomenon was to determine if it was connected with the outgasing of the extracting electrode when bombarded with the electrons emitted from the tip. This study used a simple diode arrangement (i.e. tip and extractor), and was performed in the separate subsidiary system shown previously in Fig. 4.2 .

The tip was mounted in the specially constructed auxilliary tip holder shown in Fig. 5.1 (a), in which the carbon fibre is inserted in a fine syringe needle and held securely in place with a drop of silver dag. Having thus mounted a freshly etched "test" tip, its profile was examined in a Scanning Electron Microscope (S.E.M.) prior to mounting it in the system of Fig. 5.1 with tip about 3 mm away from the extracting electrode, in order to minimise the risk of accidental damage to it during assembly. Having evacuated the system to a pressure of $\sim 10^{-8}$ m bar, the extracting electrode was out-gased by electron bombardment using the thermionic filament located ~ 10 mm away from the extracting electrode on the opposite side of the cathode. Typically, ~ 500 Volts is initially applied to the extracting electrode, whilst the heater current is slowly increased until an electron current of ~ 50 m A is measured: under these conditions the extractor is glowing at red heat ($\sim 800^{\circ}$ C). After ~ 20 minutes of this treatment, the tip assembly is carefully removed and the tip re-examined in the S E M . From a comparison of the scanning electron micrographs Fig. 5.2 (a) and (b), taken respectively before and after degasing, it can be seen that the degasing of the extracting electrode had no effect on the tip profile. Having remounted the cathode assembly in the vacuum chamber, it was evacuated to a pressure of $\sim 1 \times 10^{-8}$ m bar and the extractor again degased. Subsequently, the necessary volts were applied to the cathode via a 100 MΩ reisitor, to draw ~ 5 u A emission current for ~ 1 minute. After this, the tip was again examined in the S E M and, as can be seen from Fig. 5.2 (c), the tip had "exploded". It was therefore concluded from this type of experiment that the desorption of gas from the extractor plays no part in initiating this explosive phenomenon.

syring needle

4mm

3·8mm

14·5mm

Screen

Extractor

Tungsten
wire heater
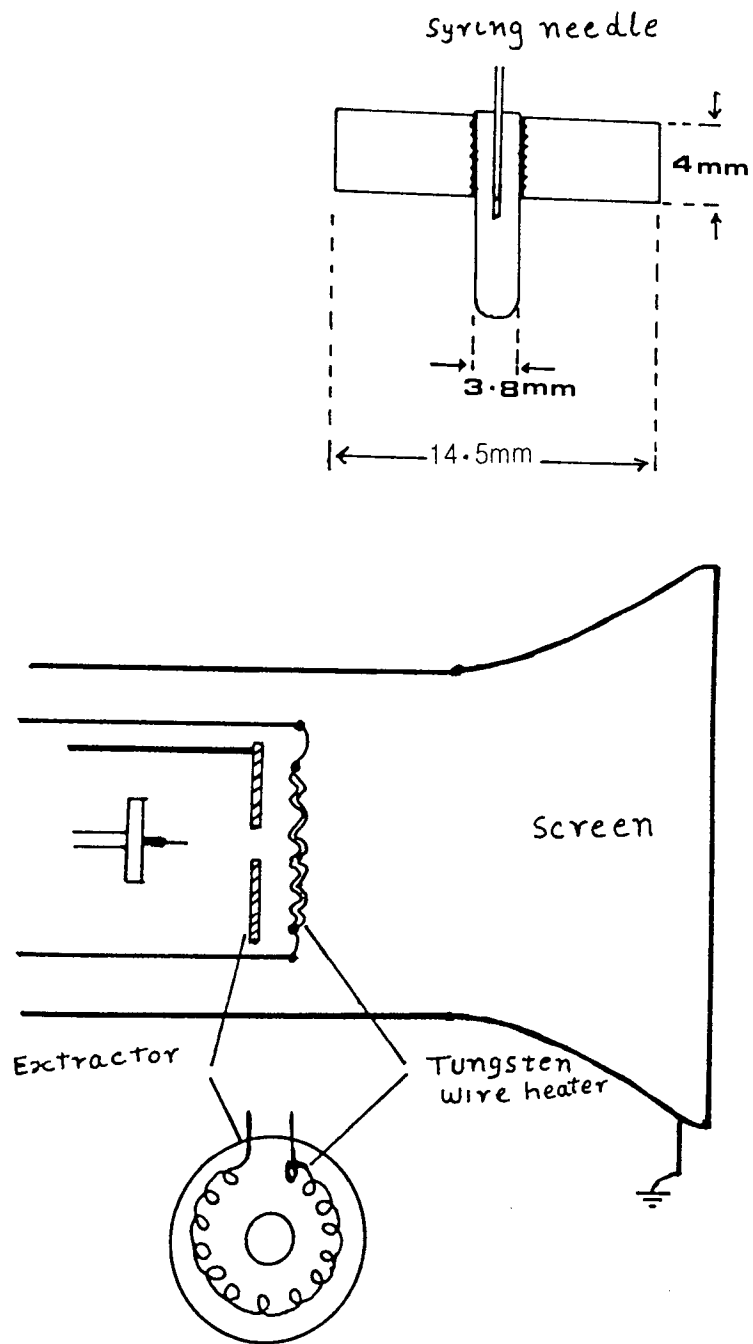
Fig. 5.1   To show (a) the cathode holder which could be fitted in the S E M

in order to examine cathode profile (b) typical arrangement

used for outgasing extracting electrodes.

191.
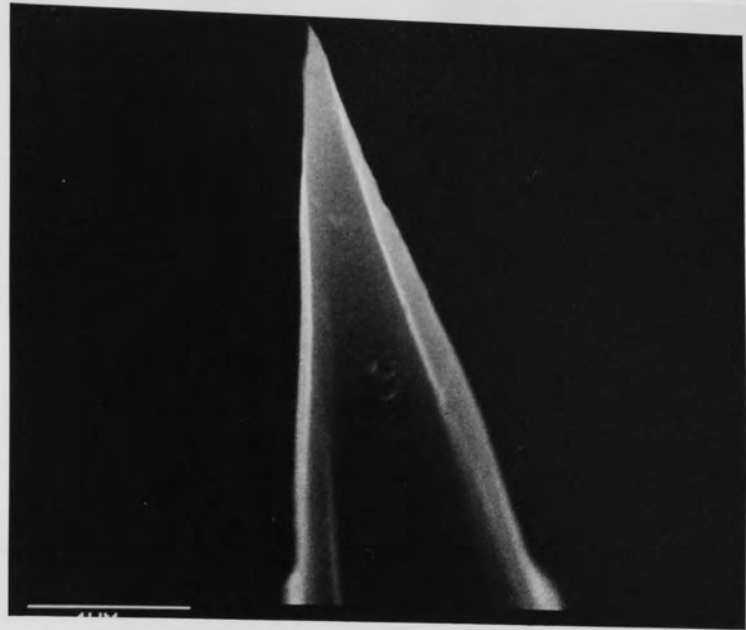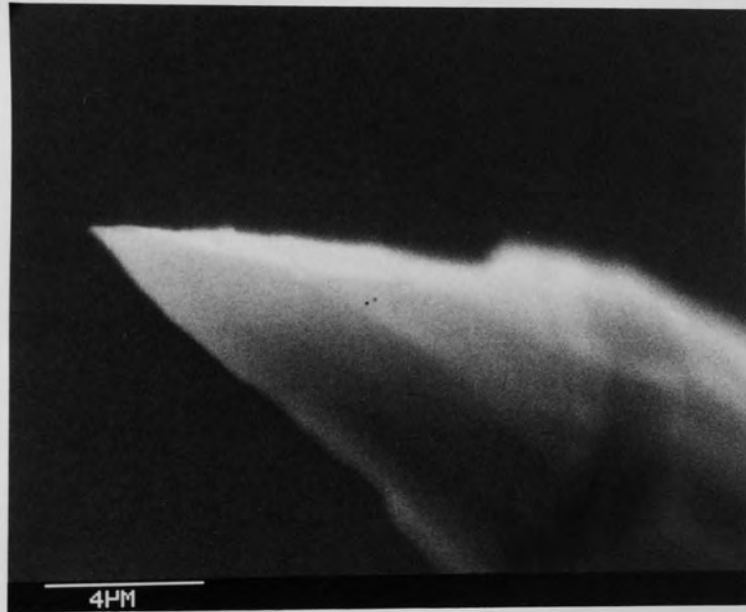
Fig. 5.2 S E M micrograph of (a) freshly etched tip (b) after out-
gasing extractor and (c) after drawing current.

192.

The next series of experiments investigated whether the tip geometry had any influence on the explosive phenomenon. Firstly, a tip having the fairly long profile shown in the micrograph of Fig. 5.3 (a) was prepared and mounted in the vacuum chamber at a pressure of $\sim 3 \times 10^{-8}$ m bar as described above. A slowly increasing voltage was then applied to the tip-extractor until the emission suddenly "switched-on" from an effective zero value to $\sim 3 \times 10^{-6}$ A. The voltage was then further increased to obtain an emission current of $\sim 5 \mu$ A, which was maintained for about 10 mins. Following this sequence, the tip was removed and its profile examined in the S E M and, as shown in the micrograph of Fig. 5.3 (b), the profile has drastically changed. Next, a tip having a shorter profile (see Fig. 5.4 (a)) was investigated in the similar manner. In this case, as the applied voltage was further increased until the tip "switched-on" from a fluctuating current of $\sim 1.3 \times 10^{-10}$ A to $\sim 3.3 \mu$ A, and then further increased until 5μ A was obtained, which was again maintaind for ~ 10 mins. After this, the tip profile was re-examined in the S E M and, as can be seen from Fig. 5.4 (b) the changes that have occurred in its profile are very much more drastic than in the previous case. It can be concluded therefore that the tips of shorter profile are more susceptible to this explosive phenomenon than those of longer profile.

The next possibility to be considered was that the explosive phenomenon resulted from the inevitably "jerky" application of the applied voltage when using a manual control: typically a small movement of the control knob on the power supplies capable of delivering 5 - 30 k V could increase by over 50 Volts which is much greater than the critical voltage range over which the emission initially switches on to a few μ A's. To eliminate such voltage surges, the

(a)
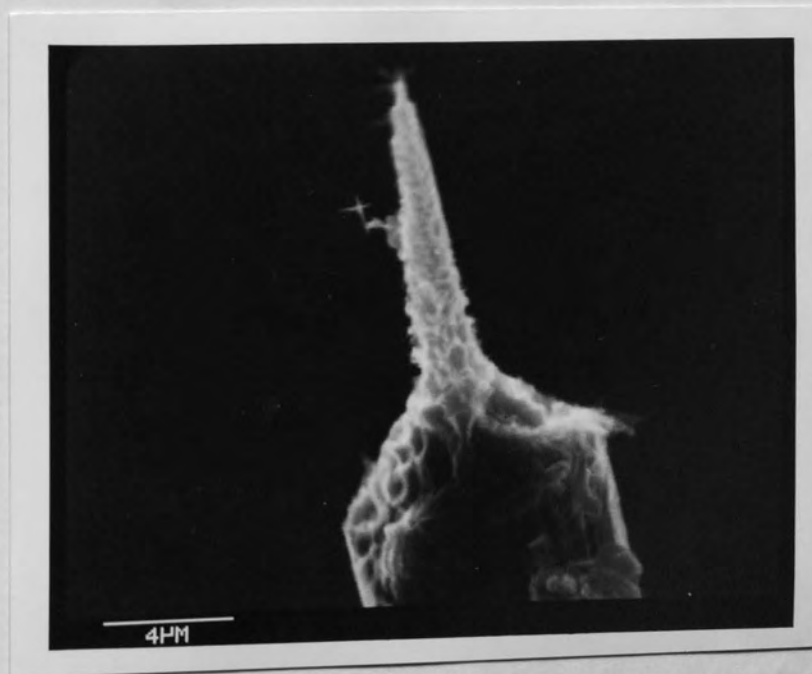
(b)

Fig. 5.3   S E M micrographs of a tip of long profile (a) before and
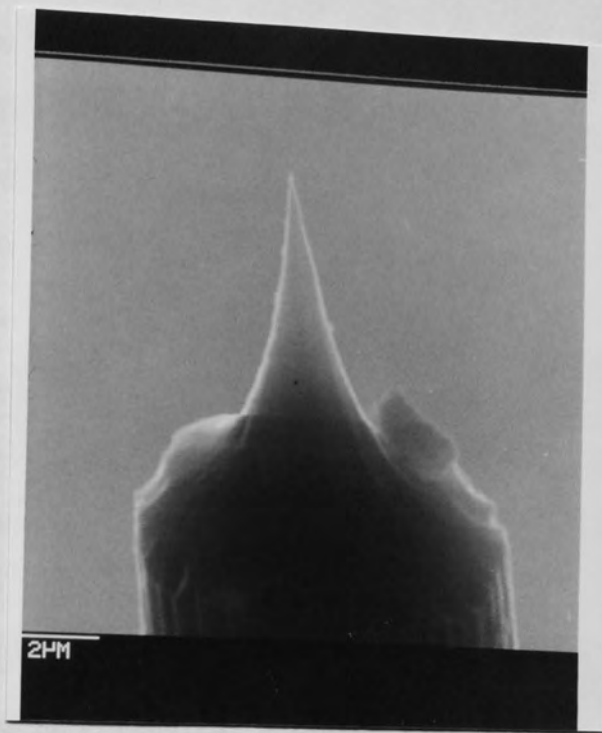
(b) after emission.

(a)
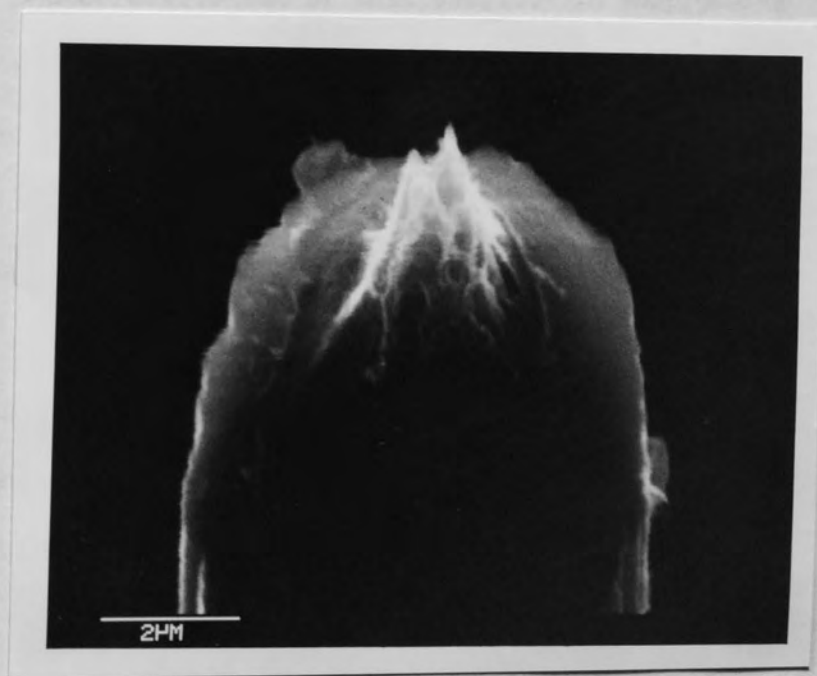
(b)

Fig. 5.4   S E M micrographs of ∧ᵃ tip of short profile (a) before and

(b) after emission.

mechanical drive unit shown in Fig. 5.5 was built and fitted to the potentiometer controlling the output of the E H T unit supplying the tip, such that a very slowly varying ramp voltage (~ 85.7 V/Min) was automatically applied across the tip-extractor diode. This drive unit used a mains operated clock motor with speed of 1 revolution per hour, and this motion was transferred to the potentiometer knob by means of rubber rollers: this system being chosen instead of cogs in order to provide a smooth transfer of the rotational motion. In an emergency, the drive unit could be quickly isolated by adjusting one screw which reduced the pressure of the rubber rollers. Initial tests confirmed that the unit provides a smooth ramp voltage that increased at a rate of ~ 100 Volts in 70 seconds, with a maximum surge level of < 7.5 Volts.

To evaluate the effectiveness of this facility in suppressing the explosive phenomenon, a freshly prepared tip was mounted and examined as described above, where Fig. 5.6 (a) is a micrograph of its initial profile. With a vacuum of $\leqslant 10^{-8}$ m bar, the ramp voltage was now applied using the circuit shown in Fig. 5.7 (a), where the double-pen chart recorder simultaneously monitored the typical voltage and the emitted current. A typical example of the associated voltage and current traces are shown in Fig. 5.7 (b), from which it is seen that whilst the applied voltage rises relatively smoothly, the emission current shows a definite switch-on phenomenon. As soon as the event occurred, the drive unit was isolated and tip voltage reduced to zero. Then, on carefully removing the tip and re-examining it in the S E M its profile was found to have exploded as shown in Fig. 5.6 (b). This type of investigation was performed on several tips and in each case similar results were obtained. However, some tips showed a very much larger switch-on currents the magnitude of
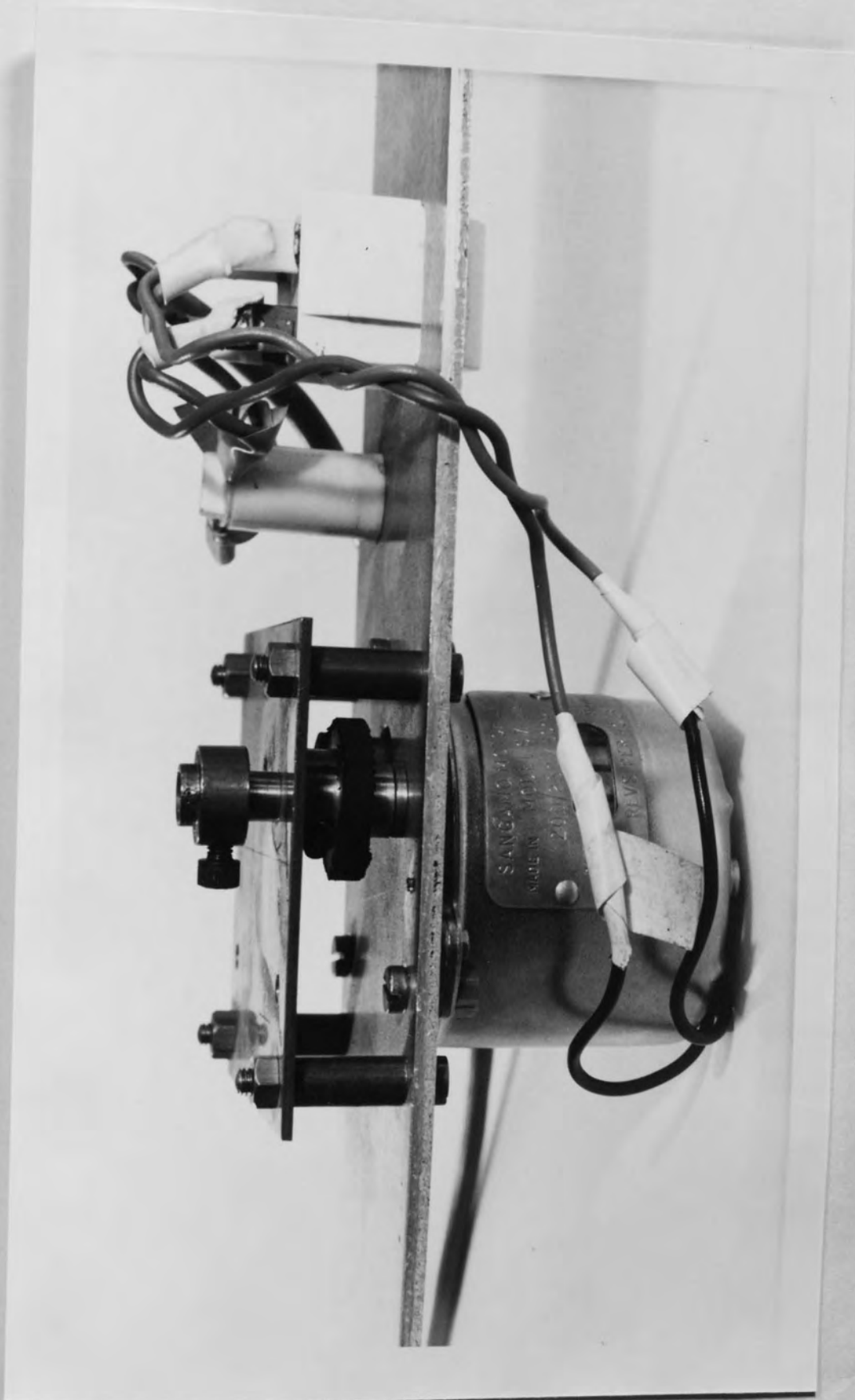
Fig. 5.5 Mechanical voltage drive unit.
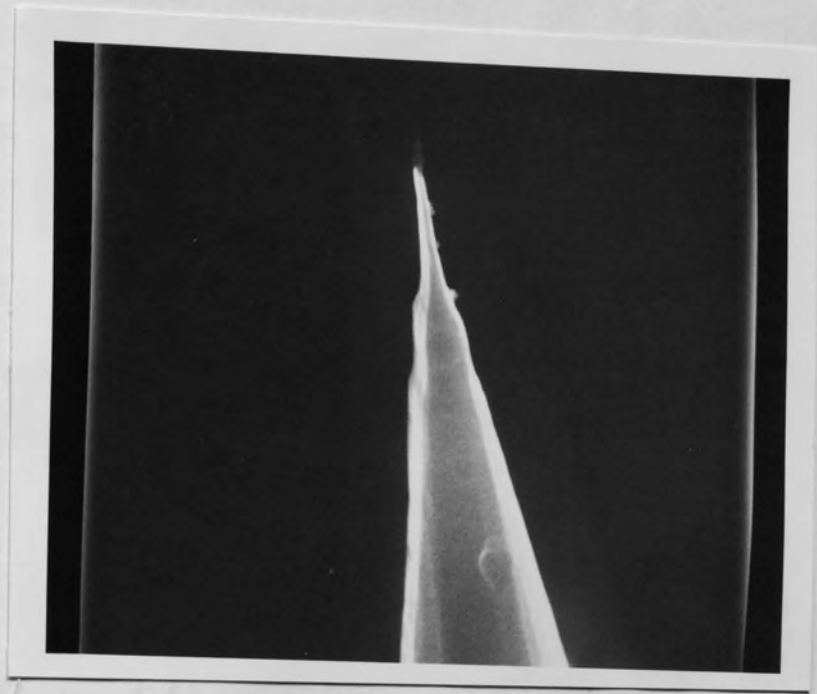
(a)

(b)

Fig. 5.6   S E M micrographs of a tip (a) before and (b) after emission

tested using voltage drive unit.
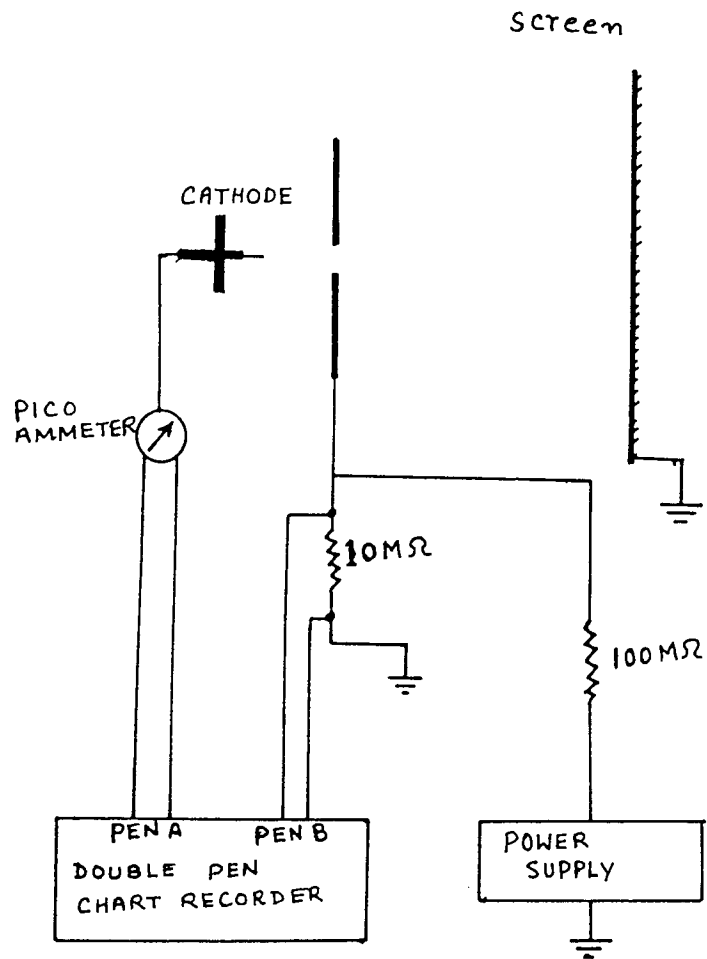
Fig. 5.7 (a)   Typical arrangement used for investigating the origin

of explosive phenomenon.
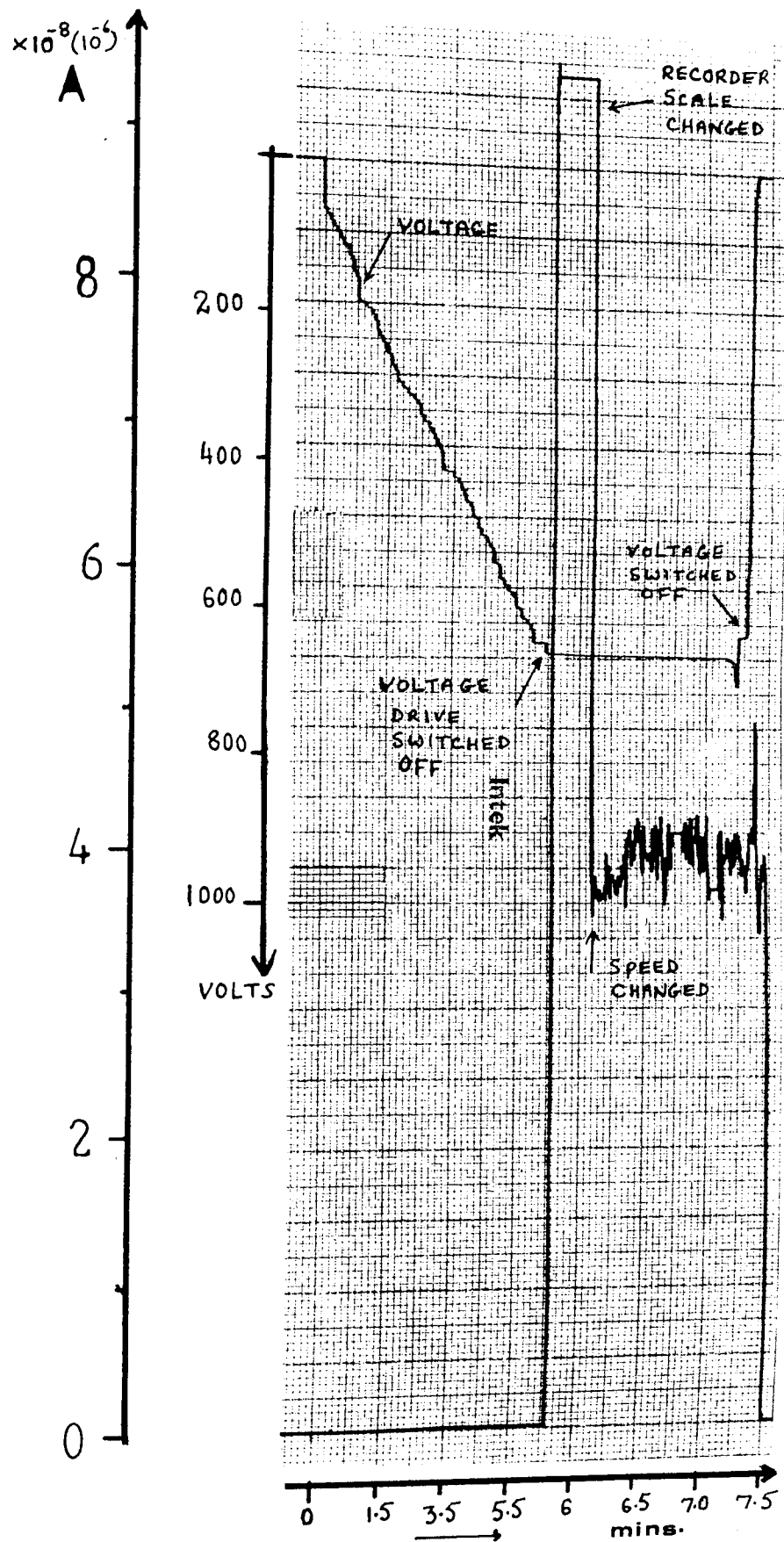
Fig. 5.7 (b)   I-V chart recorder traces obtained using voltage
drive unit for a virgin tip.

200.

which were found to be sensitive to the vacuum pressure and the time the tip remains in vacuum before testing. For example a tip would exhibit a large switch-on if it was tested after only few hours of evacuating the system, in relatively poor vacuum conditions. This fact was further investigated by comparing the behaviour of the known profiles under the vacuum conditions of 9×10^{-7} and 4×10^{-9} mbar, where in latter case the chamber was baked for 24 hours to achieve good vacuum pressure, *in* which the tip was left for one week before testing. In each case the applied voltage was switched off ~ 1 minute after the initial switch-on was detected. The "before" and "after" profiles of both tips can be seen in the micrographs of Fig. 5.8 (a) and (b) and Fig. 5.9 (a) and (b). Thus, although both tips exhibited definate switch-on events, this was however found to be comparatively severe in *the* former case, *of* poor vacuum conditions. This can be seen from the voltage current chart recorder traces shown in Fig. 5.10 and Fig. 5.11 for poor and high vacuum conditions respectively, consequently, here the exploding of tip was also found to be comparatively severe.

Lastly, the effect on the tip profile of drawing a continuous emission current over a long period of time was investigated. Thus

Fig. 5.12 (a), (b) and (c) compare respectively the profiles of a freshly prepared tip, *before* and after it had delivered 10 μ A emission current for 10 minutes and 1 hour at a pressure of $\sim 1 \times 10^{-8}$ m bar. The last two of these micrographs show that, after the initial "explosive" changes in the profile, there is little further deterioration resulting from it running continuously for an hour. However this experiment did reveal the important fact that a given tip can exhibit a second switch-on effect if it is let up to air, say for examination in a S E M between successive voltage applications.

(a)

10PM
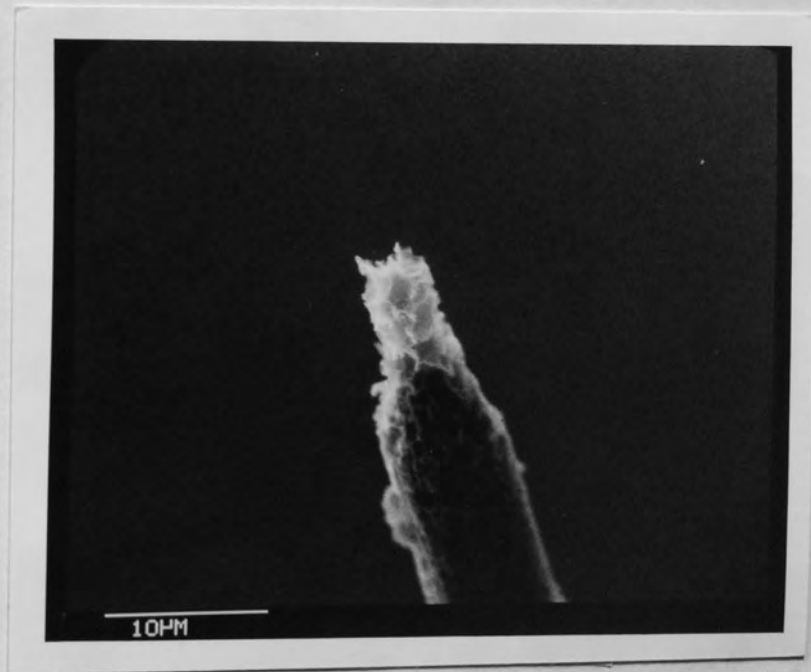
(b)

Fig. 5.8   S E M micrographs of tip (a) before and (b) after emission
tested at a pressure of 9×10^{-7} m bar.

(a)

(b)

Fig. 5.9 S E M micrographs of a tip (a) before and (b) after emission

tested at a pressure of 4×10^{-9} m bar.
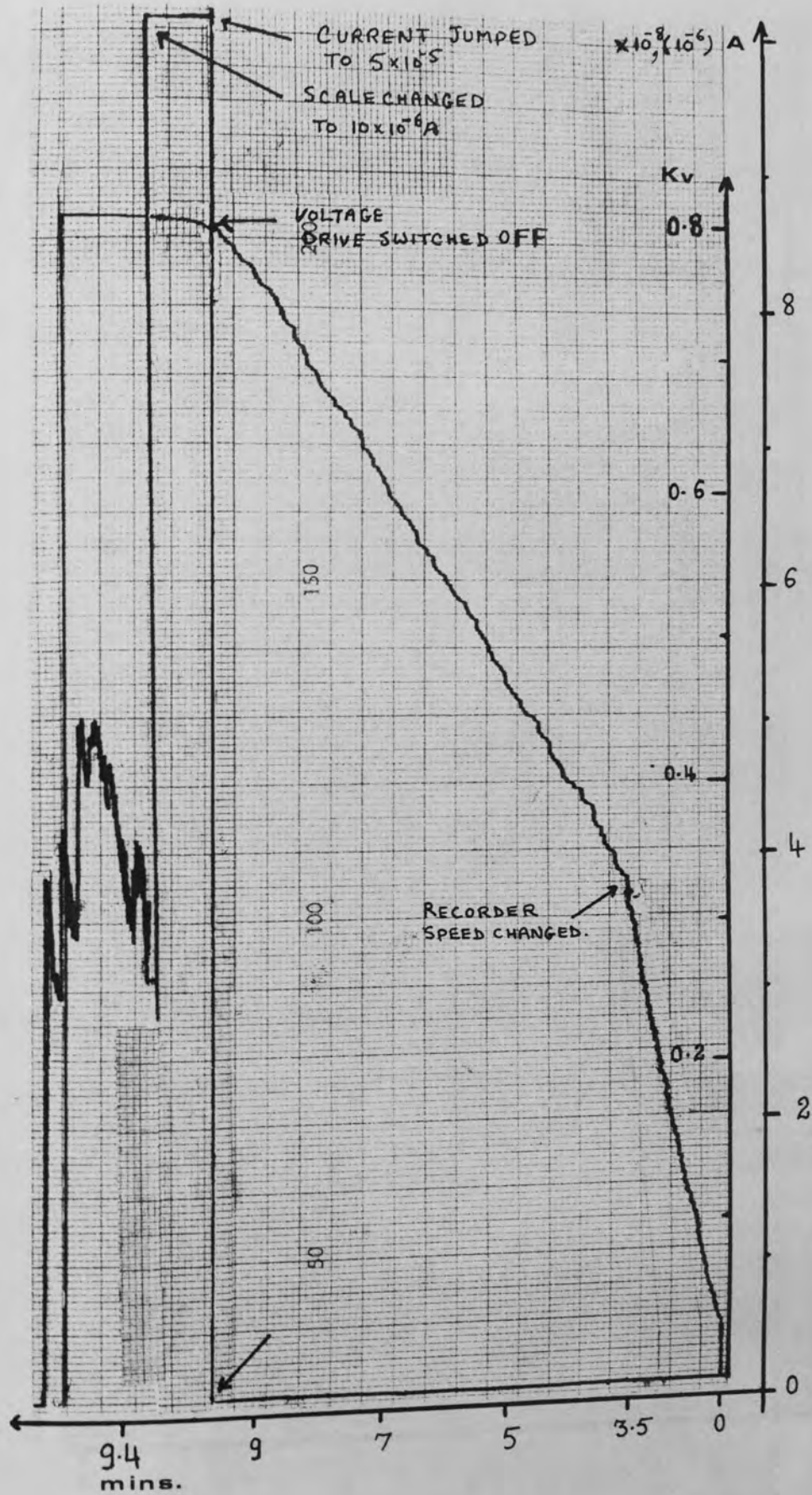
Fig. 5.10   I-V chart recorder traces for tip tested at a pressure

of 9×10^{-7} m bar.

204.
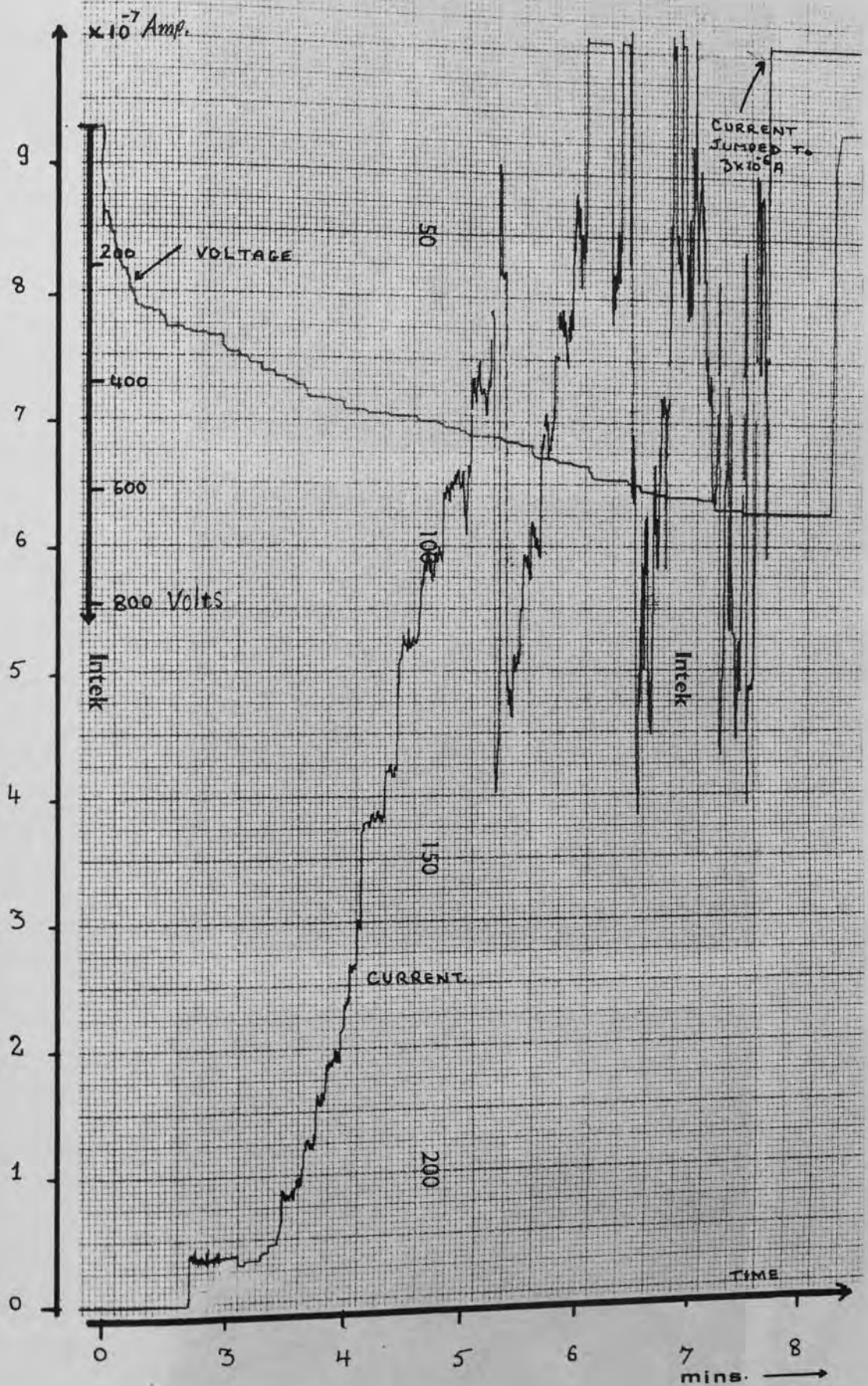
Fig. 5.11 I-V chart recorder traces for tip tested at a pressure of 4×10^{-9} m bar.
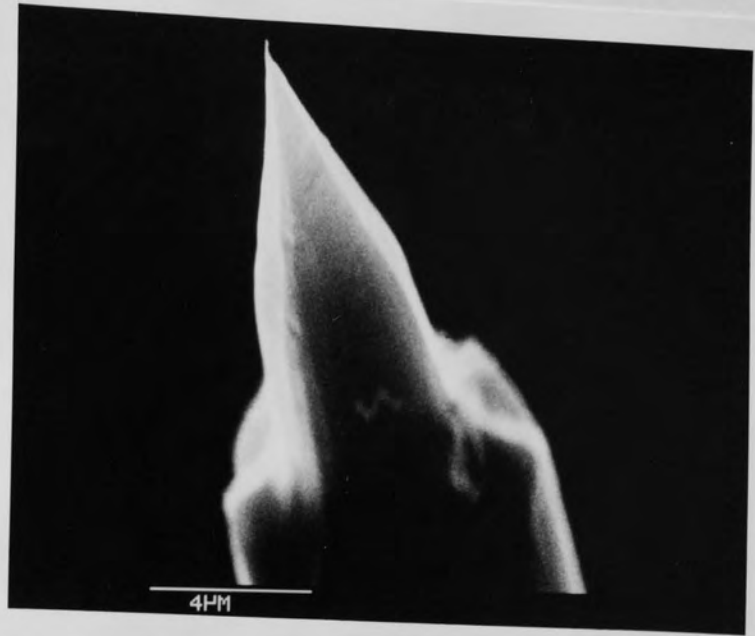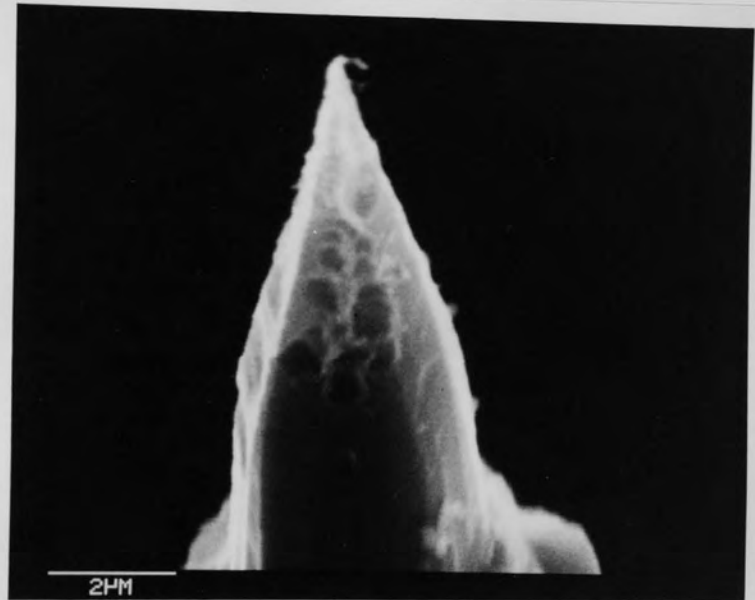
Fig. 5.12   S E M micrographs of $_\wedge^a$ tip profile (a) before emission, (b) after 10 mins and (c) after 1 hour of drawing emission current.

This behaviour is in contrast to the absence of secondary switch-on events when a tip is kept under vacuum and subjected to successive voltage cycling on a similar time scale to, that above (~ 2 hours). It was also noted that the switch-on effect was less marked when the vacuum chamber had been subjected to a prolonged bake-out treatment. These observations therefore suggest that the switch-on effect could be associated with the presence of adsorbed gases. To further explore this possibility, an investigation was undertaken to determine the effects of thermal pre-treatment of the emitters.

5.3 HEAT TREATMENT OF THE CARBON FIBRE CATHODES.

For the in-situ heat treatment of a carbon fibre emitter, it was necessary to develop the special cathode assembly shown in Fig. 5.13. It basically consisted of a ceramic disc with a concentric aluminium rod of 4.5 mm diameter containing a fine central syringe needle for holding the carbon fibre emitters. The whole assembly could be heated to ~ 750°C by a tungsten heating coil embedded in the groove surrounding the ceramic disc, with adequate insulation between it and the emitter. To calibrate the temperature of the device, an initial experiment was performed in which a thermocouple was spot welded to the aluminium rod, containing spring needle for holding the emitter, so that its temperature could be monitored as a function of the heater current.

The effect of pre-heating the cathode was investigated over a range of temperatures, where by using a series of freshly prepared cathodes that were examined for any changes in their profiles before and after emission following the heating of the cathode assembly to a chosen temperature over a 18 hour period. It was found that for a heat-treatment temperature below ~ 100°C had no effect on the
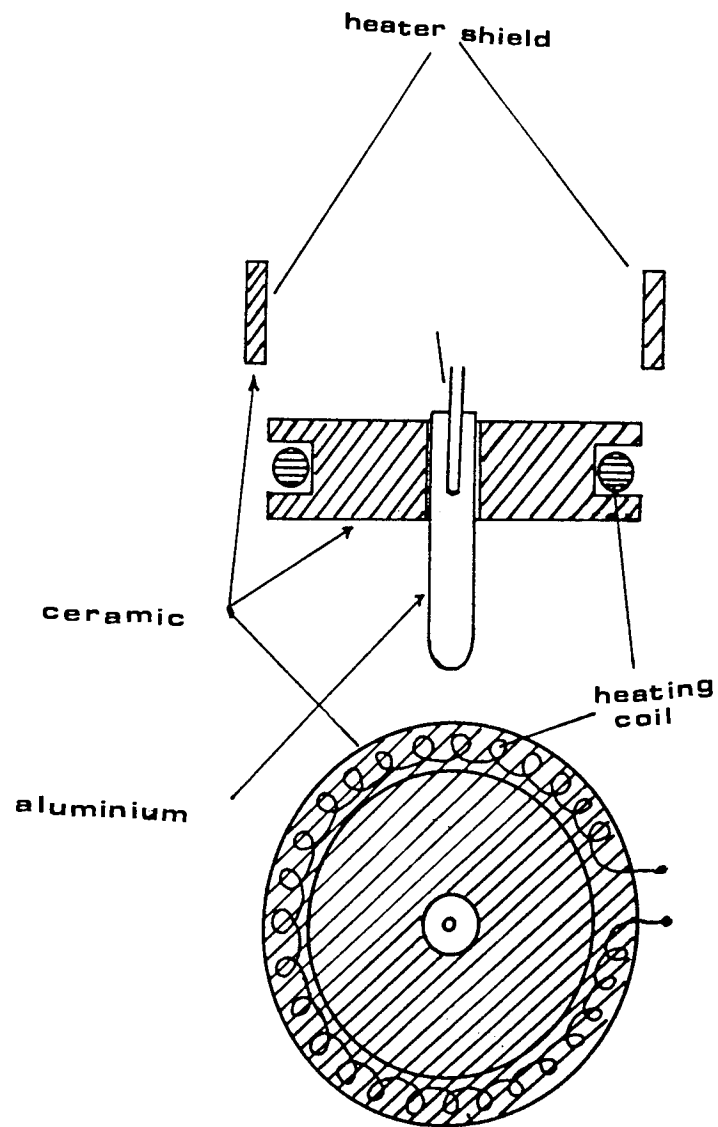
Fig. 5.13 Cathode holder with heating facility.

incidence of the explosive phenomenon. However on heating the cathode to a temperature of $\sim 150^{\circ}$C the starting phenomenon was considerably reduced as can be seen from the current voltage chart recorder traces of Fig. 5.14 where it can be seen that the switch-on current is only $\sim 6.5 \times 10^{-8}$ A compared to $\sim 3.3 \mu$ A for an untreated tip. This improvement can be further appreciated from the S E M micrographs of Fig. 5.15 (a) and (b) obtained before and after emission, where the changes in the emitter profile are clearly greatly reduced. From similar studies of heat treatment temperatures of 250°C, 350°C and 450°C, it was found that above 350°C, the tip no longer exhibited the switch-on phenomenon. This can be seen from the chart recorder traces shown in Fig. 5.16, also from the complement-ary micrographs of Fig. 5.17 (a) and (b) which shows that the explosive phenomenon has been completely eliminated. However, for heat-treatment temperatures of $\gtrsim 350^{\circ}$C, there was a tendency for the tip profiles to broaden. This undesirable effect could be largely overcome by heating the tip to $\sim 250^{\circ}$C over the longer period of 36 hours; furthermore, as can be seen from the chart recorder traces of Fig. 5.18 and the S E M micrographs of Fig. 5.19 (a) and (b) the switch-on and the explosive phenomenon are also eliminated by this longer but low-temperature heat treatment. Thus, not only do the chart recorder traces show that the emission current rises smoothly with the increasing applied voltage, but, in addition the fluctuations in the total current are also considerably reduced.

These experimental findings strongly suggest that the explosive emission phenomenon is connected with the presence of the absorbed gases and possibly surface contamination. This contention is further supported by the fact that the explosive emission phenomenon returns on exposing a heat-treated tip to air: i.e. indicating that the
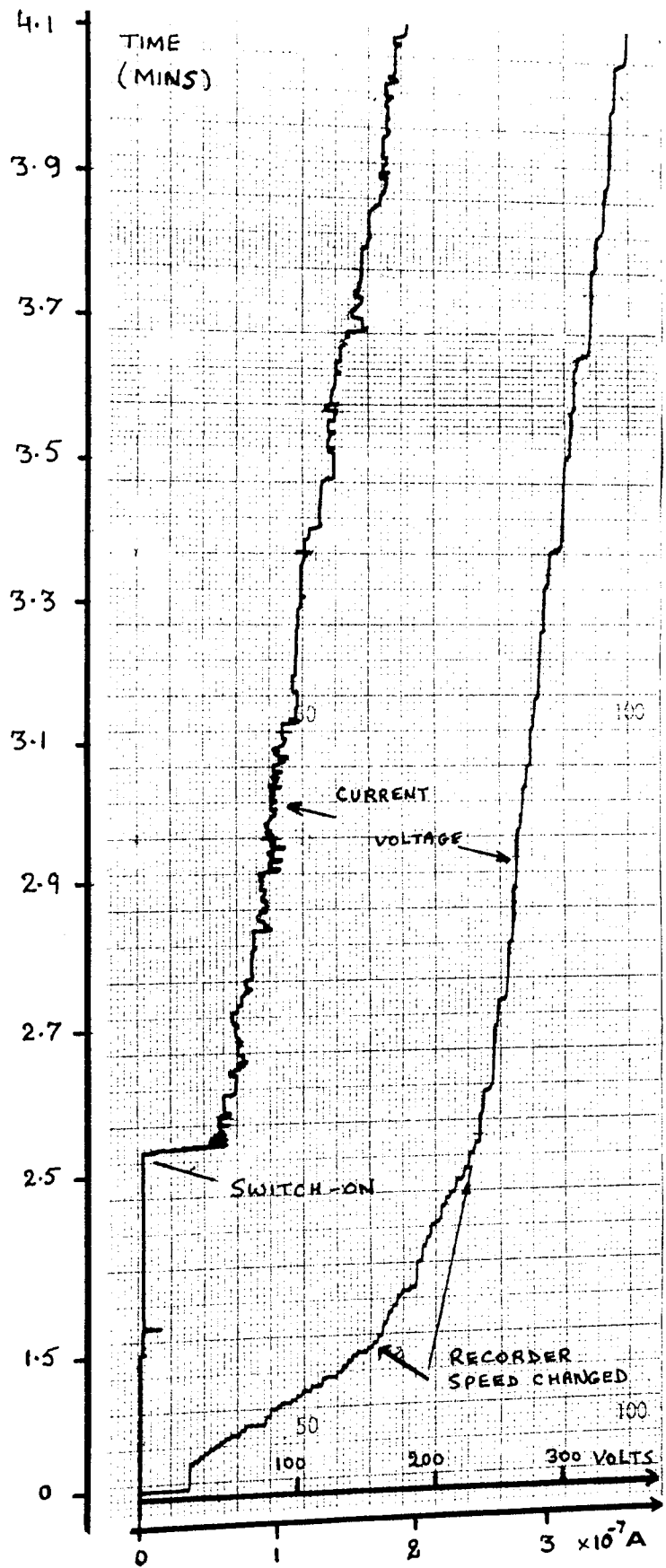
Fig. 5.14   I-V chart recorder traces of tip heat treated to 150°C.

(a)
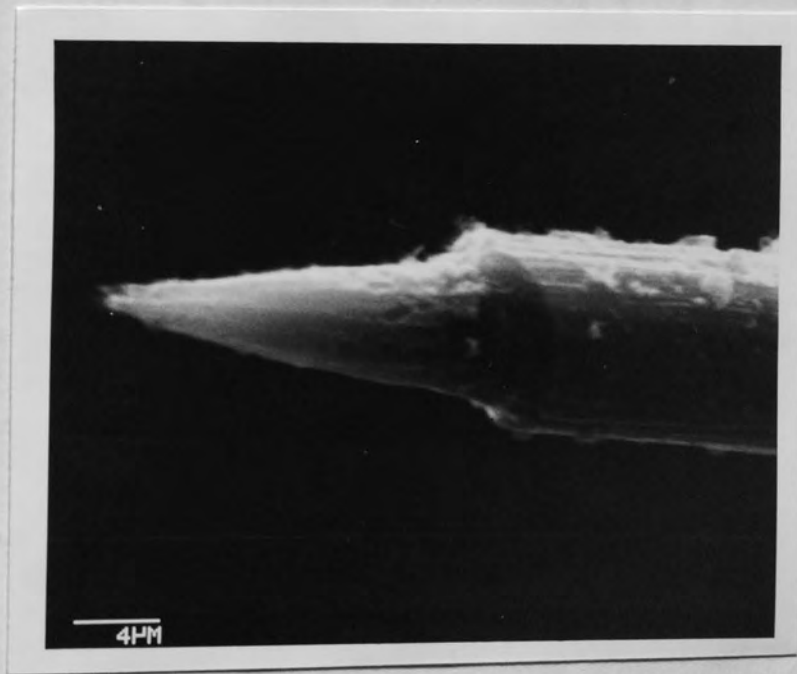
(b)

Fig. 5.15   S E M micrographs of $\overset{a}{\underset{\lambda}{}}$ tip heat treated to 150°C (a) before
and (b) after emission.
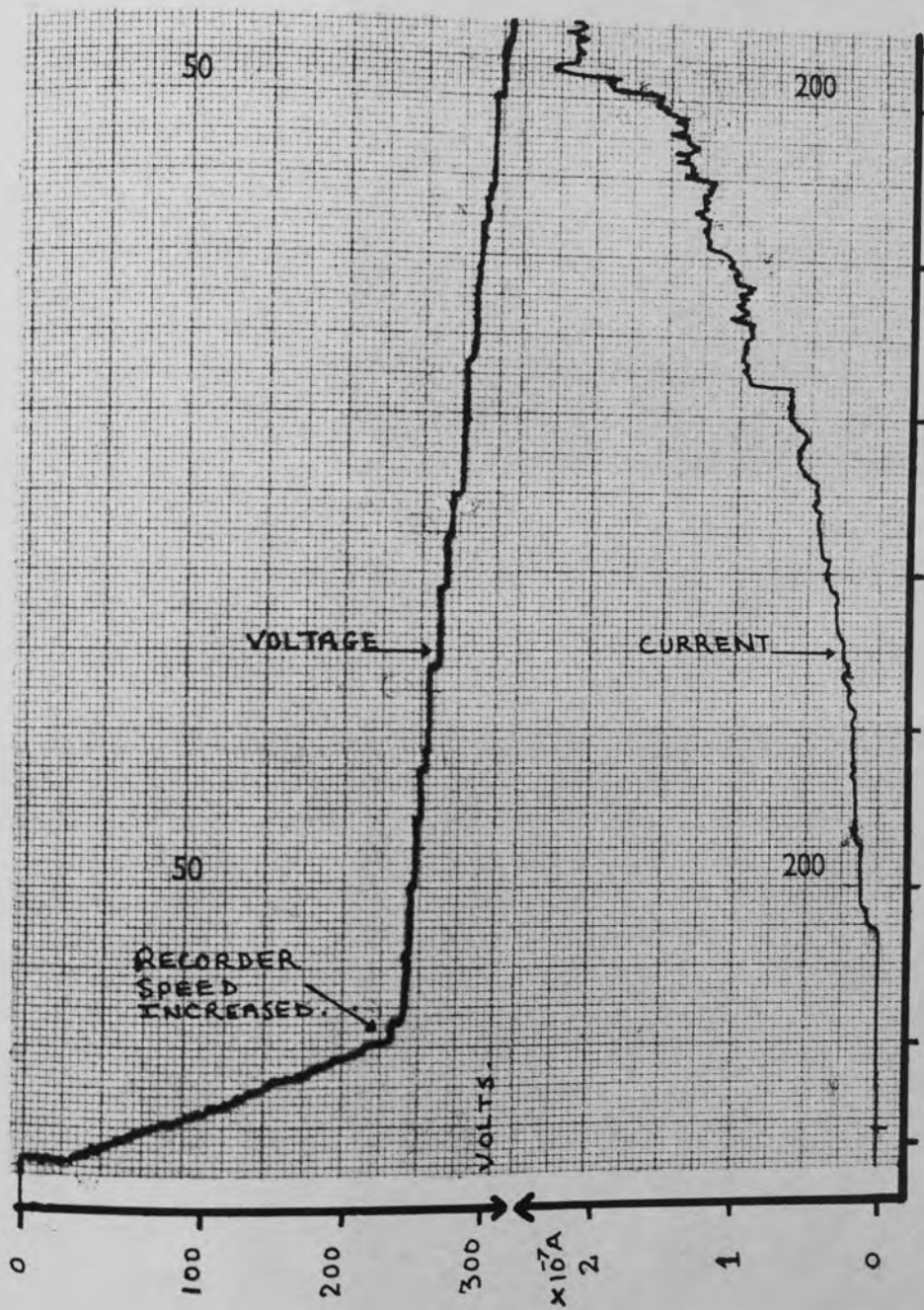
Fig. 5.16 I-V chart recorder traces of tip heat treated at 350°C.
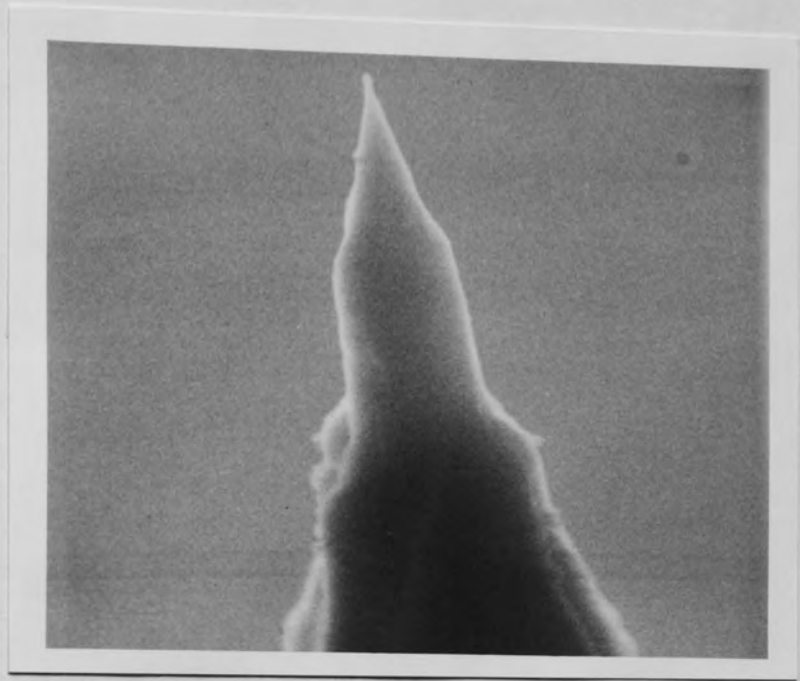
(a)
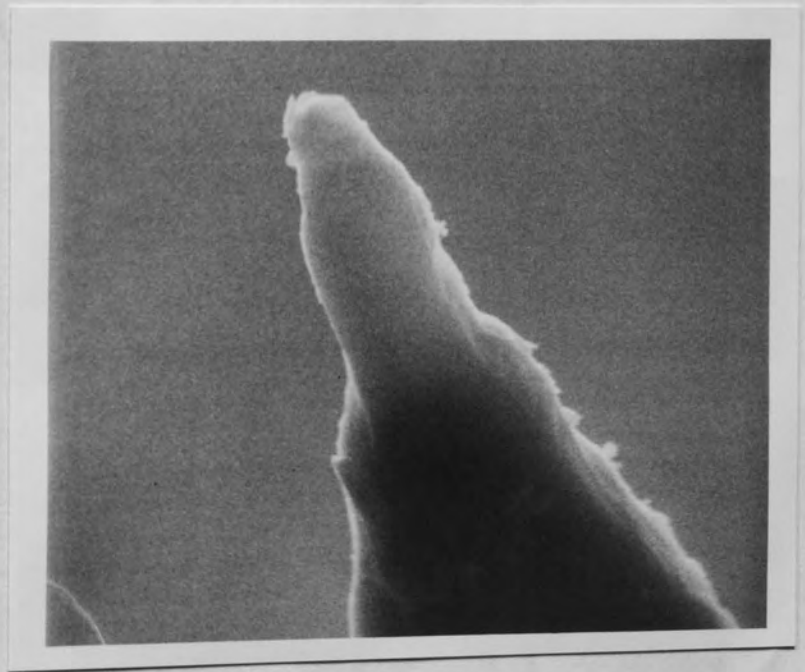
(b)

Fig. 5.17   S E M micrographs of ᵃtip heat treated to 350° C (a) before
and (b) after emission.
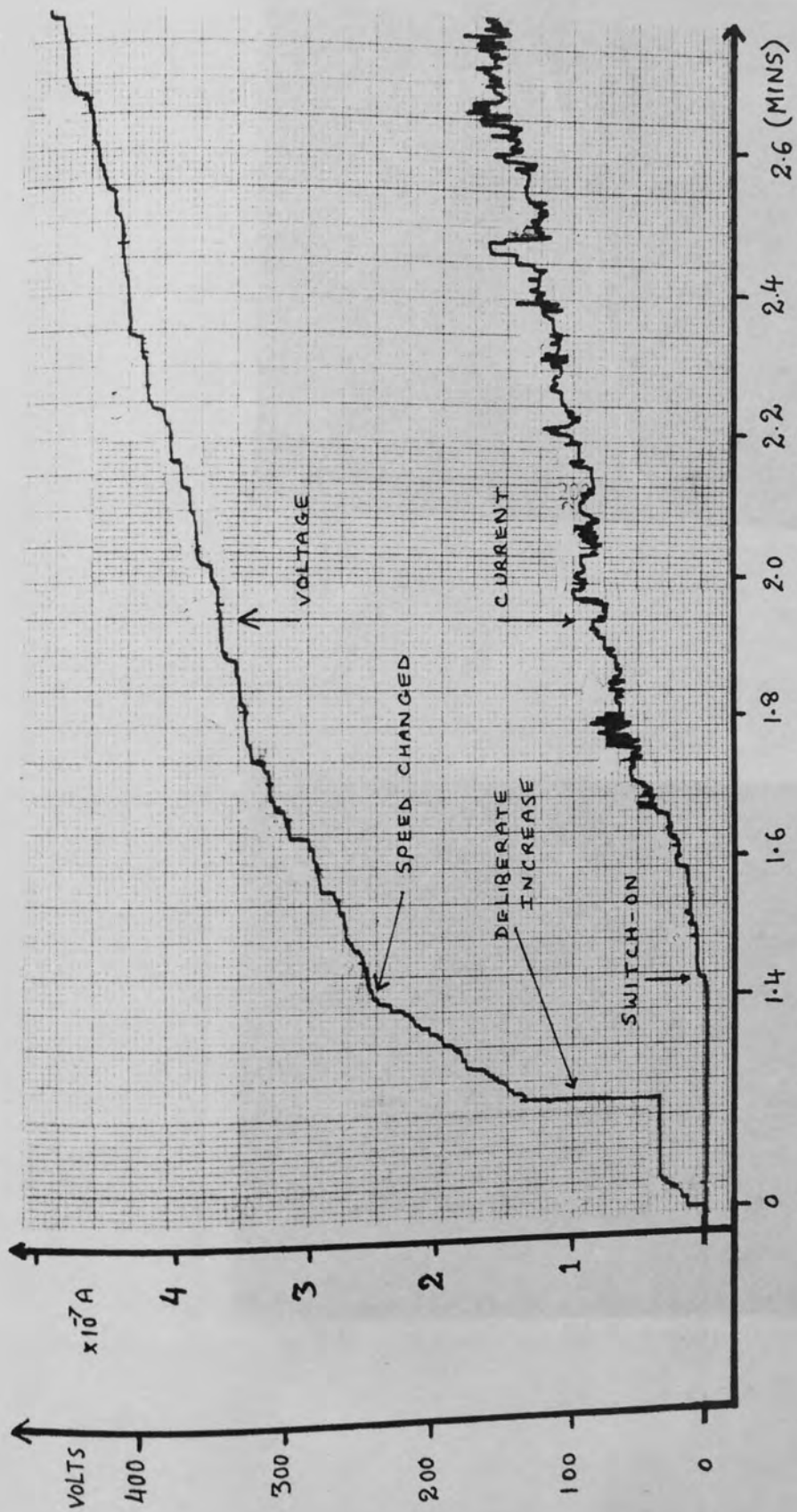
Fig. 5.18 I-V chart recorder traces of tip heat treated to 250°C.

214.

(a)

4μM
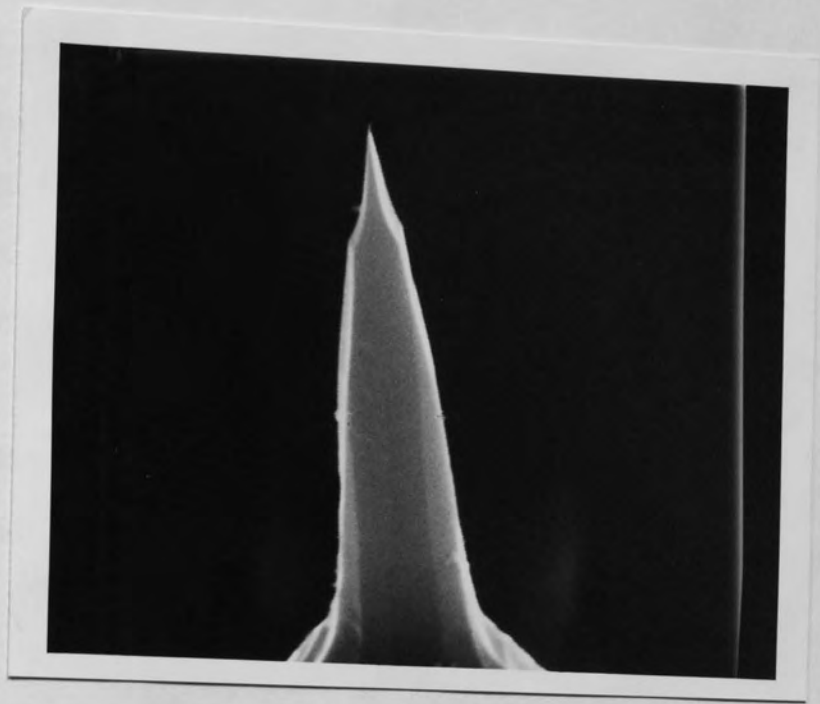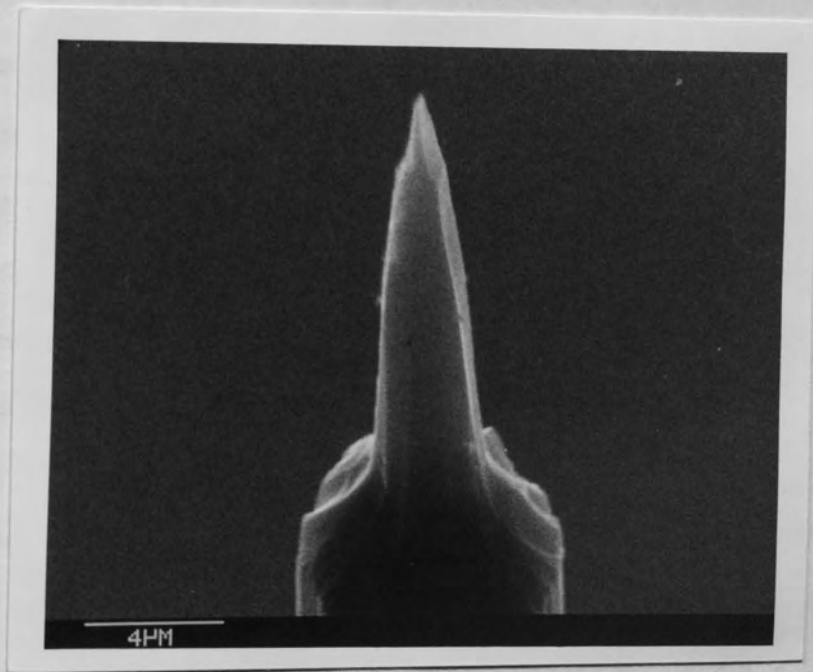
(b)

Fig. 5.19   S E M micrographs of $_\wedge^a$ tip heated to 250°C (a) before and
and (b) after emission.

215.

stabilisation has not been brought about by an irreversible processes such as the changes in the emitter material structure, such as would result from annealing. From the technical point of view, it is important to determine whether there is any long-term relaxation of the beneficial effects of heat-treatment under commercial vacuum conditions ($\sim 10^{-8} - 10^{-7}$ m bar). Accordingly, a programme of life-time testing was undertaken to confirm that the control of the explosion phenomenon does infact lead to substantial improvement in the life-time of an emitter.

5.4 LIFE TIME OF THE HEAT TREATED CARBON FIBRE FIELD EMITTER.

Due to the limited amount of time available, it was not possible to measure the actual life time of all the heat-treated cathodes. However it was possible to make a reasonable assessment by comparing the characteristics of a typical untreated and treated emitter. Therefore, two tips were freshly prepared and their profile images recoreded as shown in Fig. 5.20 (a) and Fig. 5.23 (a). The first tip was then mounted in the vacuum chamber and baked for ~ 16 hours to obtain a pressure of $\sim 1 \times 10^{-8}$ m bar. Then using the diode arrangement of Fig. 5.7 (a) with a 100 MΩ resistor in series with the cathode, its I-V characteristic were recorded, and are presented in Fig. 5.21 (a) in the form of F-N characteristic. The tip was then allowed to emit for 150 hours at an emission current of $\sim 6 \mu$ A with a constant tip-extractor potential difference of 375 Volts. Throughout this time, the tip current was continually monitored on the chart recorder, where Fig. 5.22 (a), (b) and (c) shows a typical example of the emission traces recorded after 40 hours, 80 hours and 120 hours respectively. From these, it can be seen that the emission current varies very erratically; sometimes it rises

(a)

(b)

Fig. 5.20   S E M micrographs of an un-treated tip (a) before emission
and (b) after continuously emitting for 150 hours.
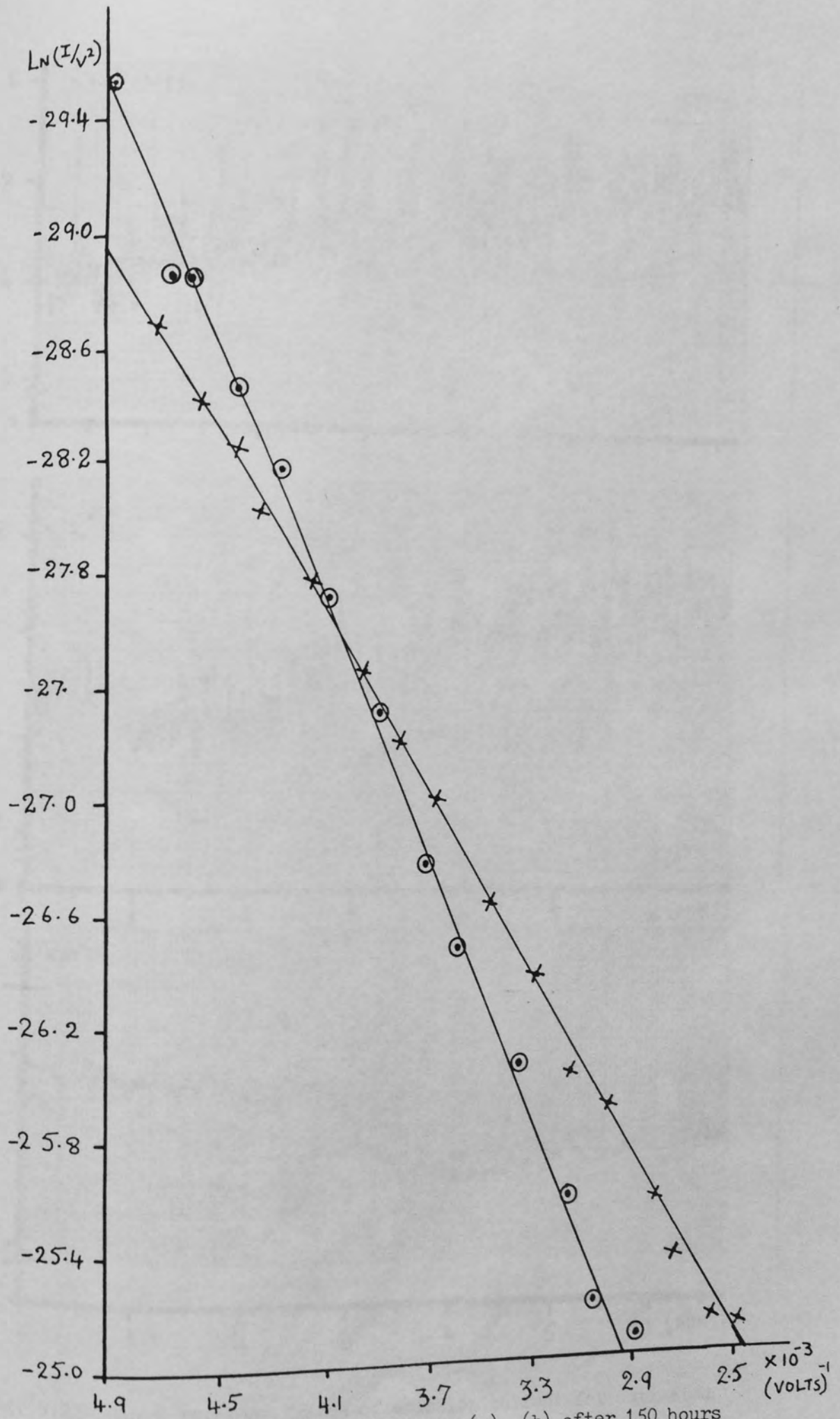
Fig. 5.21   F-N plots (a) at the beginning (x)   (b) after 150 hours
(⊙) of continuous emission.

218.
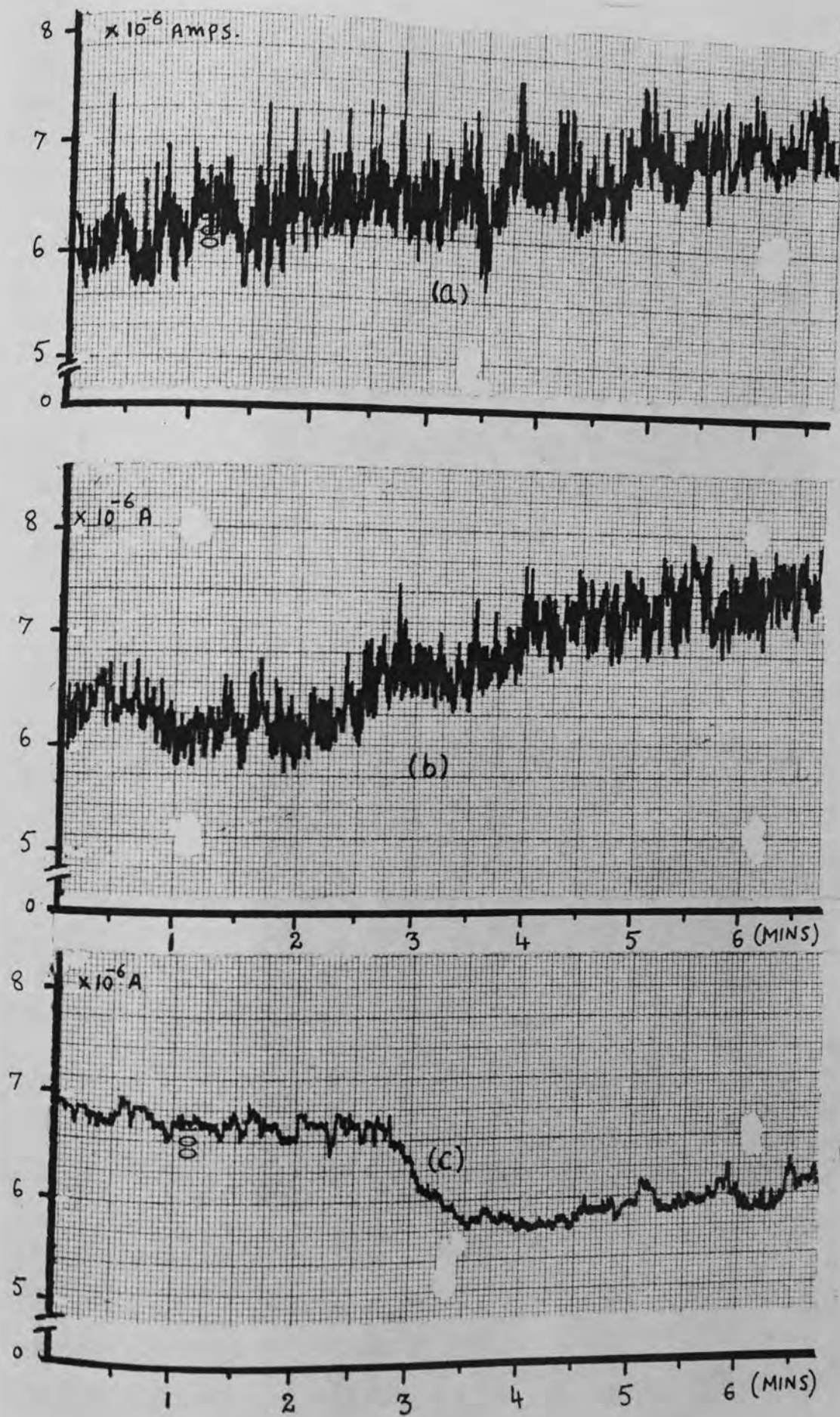
Fig. 5.22 Chart recorder traces of emission current for untreated tip after (a) 40 hours (b) 80 hours (c) 120 hours.
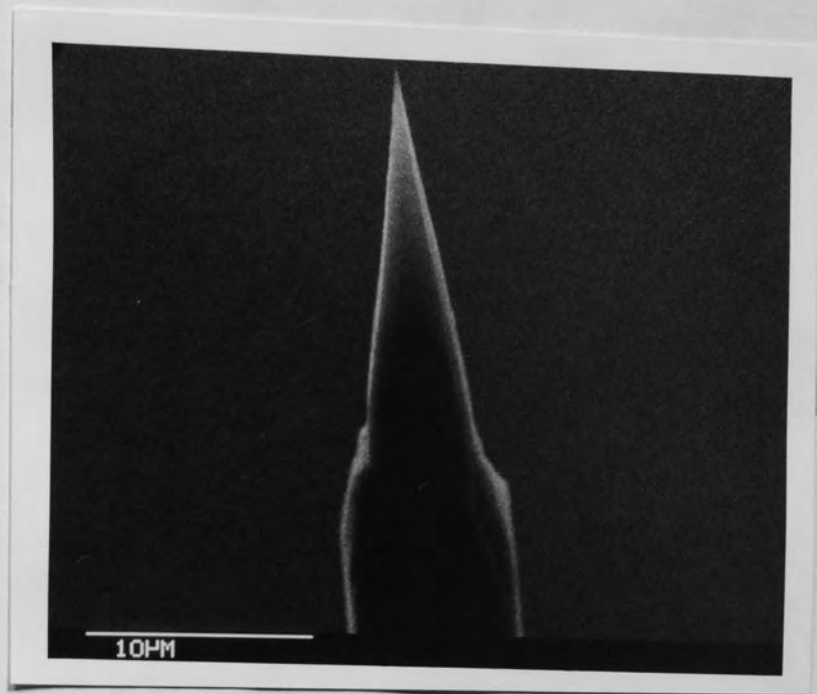
(a)
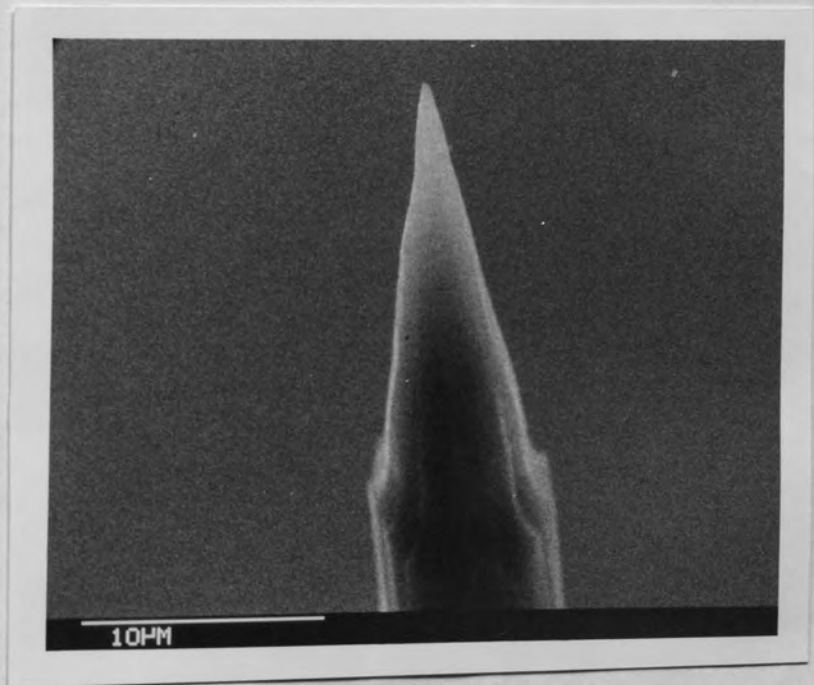
(b)

Fig. 5.23   S E M micrographs of a tip heat treated to 250°C (a) before

emission and (b) after 150 hours of continuous emission.

above the initial reference level sometimes falls to a much lower level; and at other times it remains constant for many hours. Finally, after 150 hours, the I-V characteristic were recorded and are again presented in Fig. 5.21 (b) in the form of an F-N plot. From equasion 2.18 of chapter 2 , the slope of such a plot is given by,

$$m = \frac{2.84 \times 10^9 \times \phi^{3/2}}{(1/K)} \times r = \frac{2.84 \times 10^9 \times \phi^{3/2}}{\beta}$$

where ϕ is work function of the material, r is the radius of the tip, K is a constant, usually taken to have a value of ~ 5 [4], and $\beta = 1/5r$. This gives a β values of $\sim 2.8 \pm 0.3 \times 10^5$ compared to $4.0 \pm 0.3 \times 10^5$ obtained at the beginning of the run, thereby suggesting an increase in the tip radius from $0.50 \pm 0.04 \mu\underline{m}$ to $0.73 \pm 0.06 \mu\underline{m}$.

This indicates a significant change even with experimental errors taken into account.

The second tip was then mounted in the system and evacuated as before to a pressure of $\sim 1 \times 10^{-8}$ m bar. Subsequently, it was heated to a temperature of $\sim 250^\circ$C for ~ 48 hours and its life time characteristic investigated in a similar manner to the first tip. The I-V characteristic taken "before" and "after" a 150 hour run with an emission current of $\sim 6 \mu$A at a tip-extractor potential of 500 V are presented in Fig. 5.24 (a) and (b) as F-N plots. From these it can be seen that the β-value has only changed from $1.3 \pm 0.1 \times 10^6$ to $1.2 \pm 0.1 \times 10^6$, correspondingly approximately to the tip radius changing from $0.15 \pm 0.01 \mu\underline{m}$ to $0.17 \pm 0.02 \mu\underline{m}$, change in the tip radius being within the experimental error and therefore insignificant. As before, the emission current was recorded continuously and sections of it after 40 hours, 80 hours and 120 hours are respectively presented in Fig. 5.25 (a), (b) and (c). A comparison
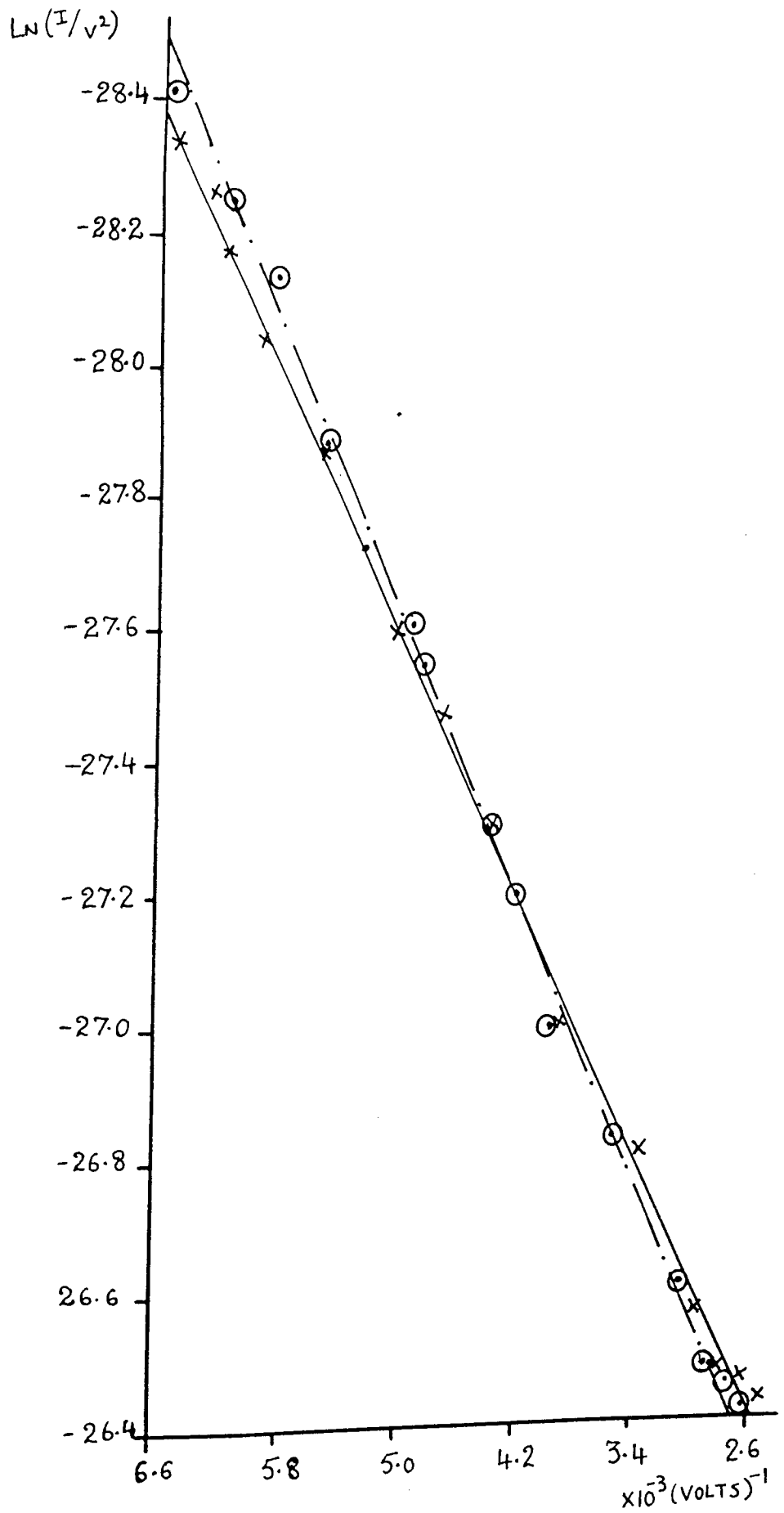
Fig. 5.24 F-N plots for heat treated to 250°C (a) at the beginning

(———) (b) after 150 hours (–·–·) of continuous operation.
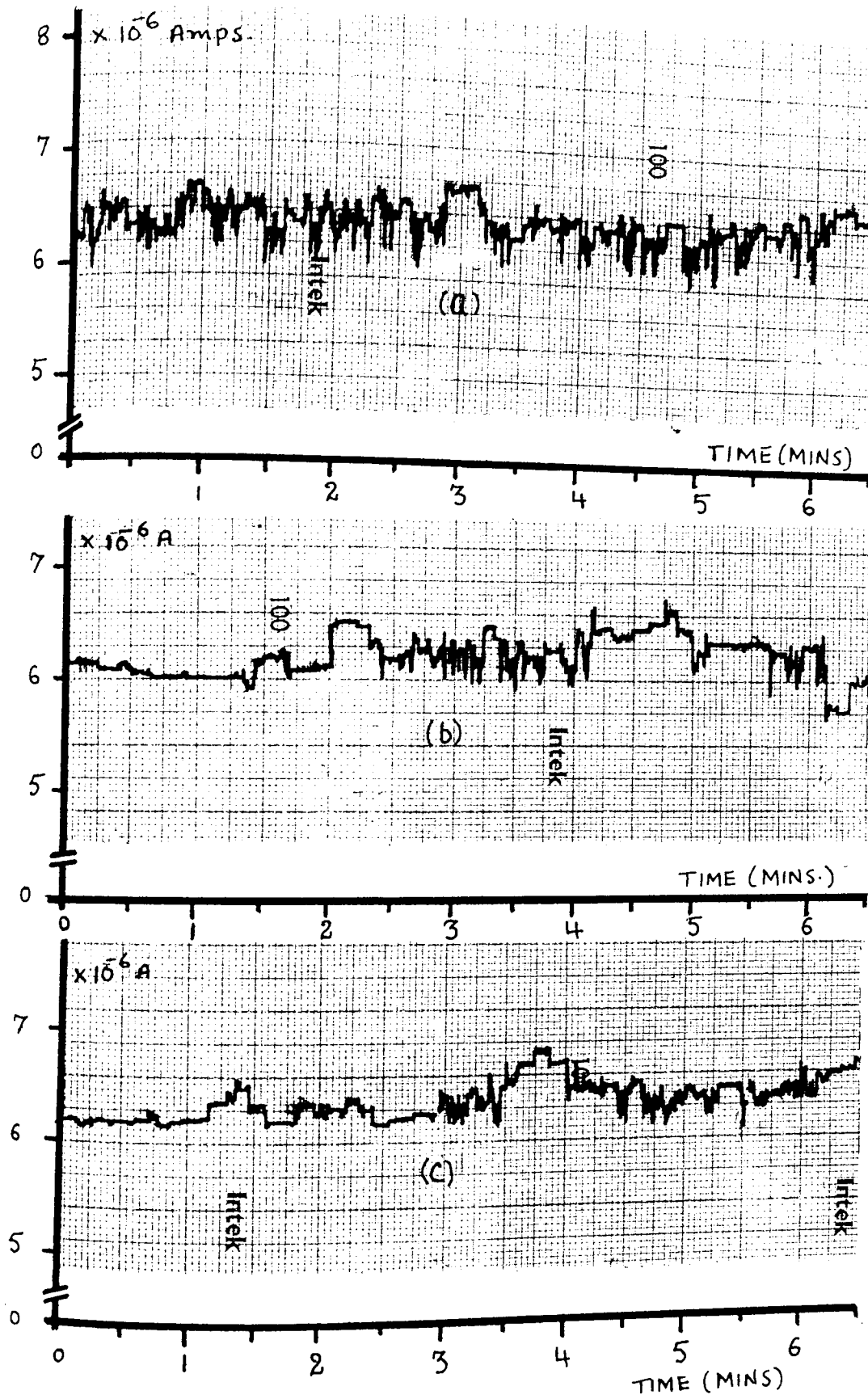
Fig. 5.25   Chart recorder traces of emission current for tip heat
treated to 250°C after (a) 40 hours, (b) 80 hours and
(c) 120 hours.

of these traces show that although the long-term and short-term variations persist, their magnitude is considerably reduced; also the mean D.C level remains constant at ~ 6 u A. Lastly, Fig. 5.23 (b) is a micrograph of this second tips profile after the 150 hour run, which when compared with the "before" profile of Fig. 5.23 (a) shows that little change has occured. From the data of Figs. 5.22 and 5.24 , it is evident that the heat-treated tip not only has vastly improved long-term emission characteristics, but also a significantly lower noise level.

To get better estimate of the ultimate potential of a heat treated tip, it was decided to examine its life time characteristics over a long period of time, in the manner already described. The tip was thus first heat treated in vacuum at pressure of 1×10^{-8} m bar at a temperature of 250° C for 48 hours, and then set emitting at current of ~ 6 μ A, and left to run for a period of 512 hours. The I-V characteristics were taken at the start of the run, after 260 hours and at the end of the run, and these are presented in Fig. 5.26 (a), (b) and (c) respectively, where the corresponding β and r-values are 8.2 ± 0.6 ($\times 10^5$), 7.8 ± 0.5 ($\times 10^5$) and 7.3 ± 0.9 ($\times 10^5$) and 0.25 ± 0.02 um , 0.26 ± 0.02 μ m and 0.27 ± 0.03 u m respectively, it follows that both of these parameters have shown no significant variations over the 512 hr run. To evaluate the long-term stability of the emitter,Fig. 5.27 presents chart recordings of the emission current taken at the intervals of 150 , 350 and 450 hours. These show a progressive improvement in the stabilisation, and particularly a reduction in the high frequency noise. It is also seen that the very low frequency noise is considerably smaller than that encountered with untreated tips. At the end of the run,the tip was removed and its profile examined as previously. Fig. 5.28 shows that the apex of
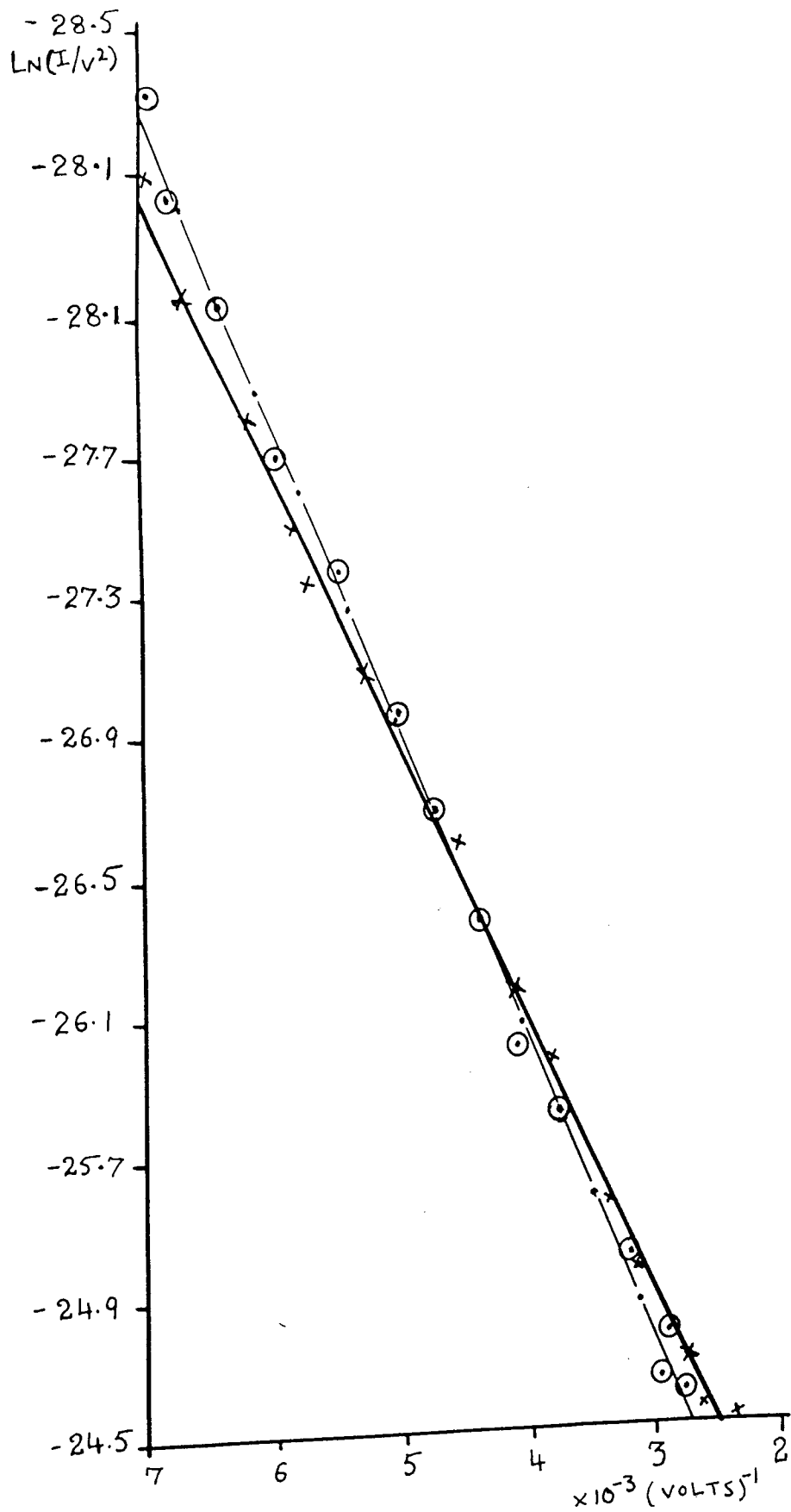
Fig. 5.26   F-N plots for heat treated tip (a) at the beginning, and (b) after 500 hours of continuous operation (—·—·—).
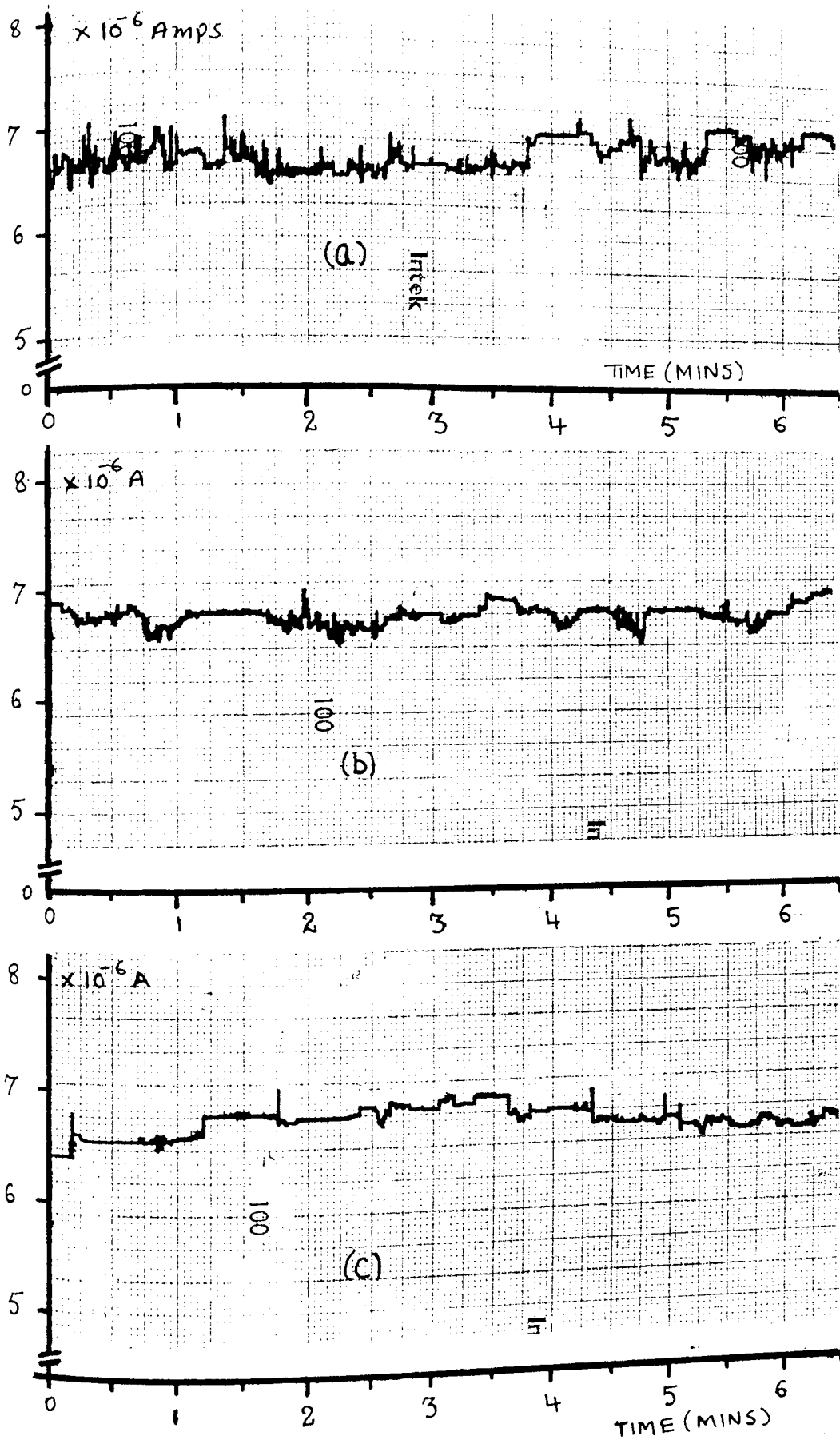
Fig. 5.27   Chart recorder traces of emission current for tip heat
treated tip after (a) 150 hours (b) 350 hours and
(c) 450 hours.
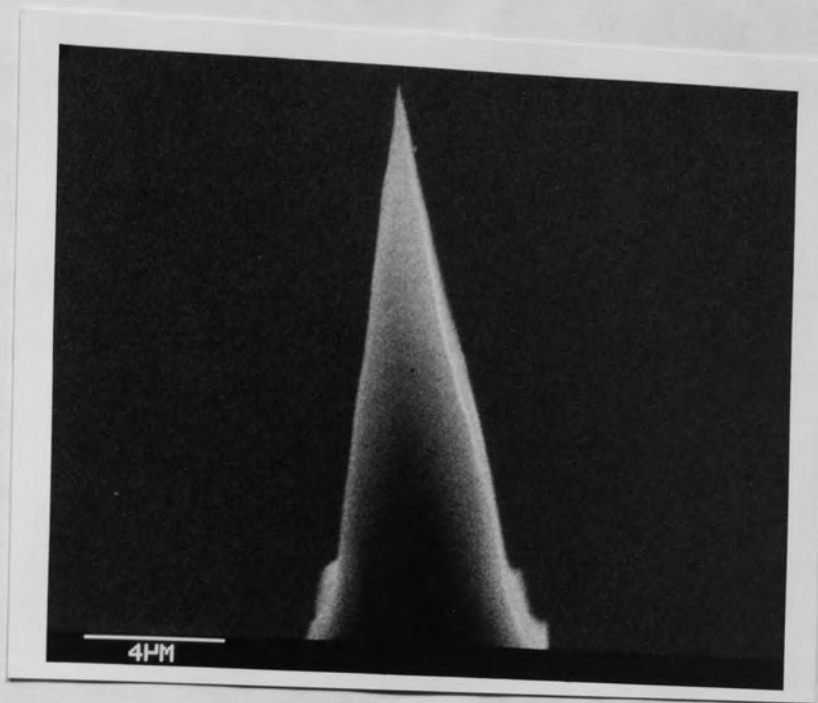
(a)
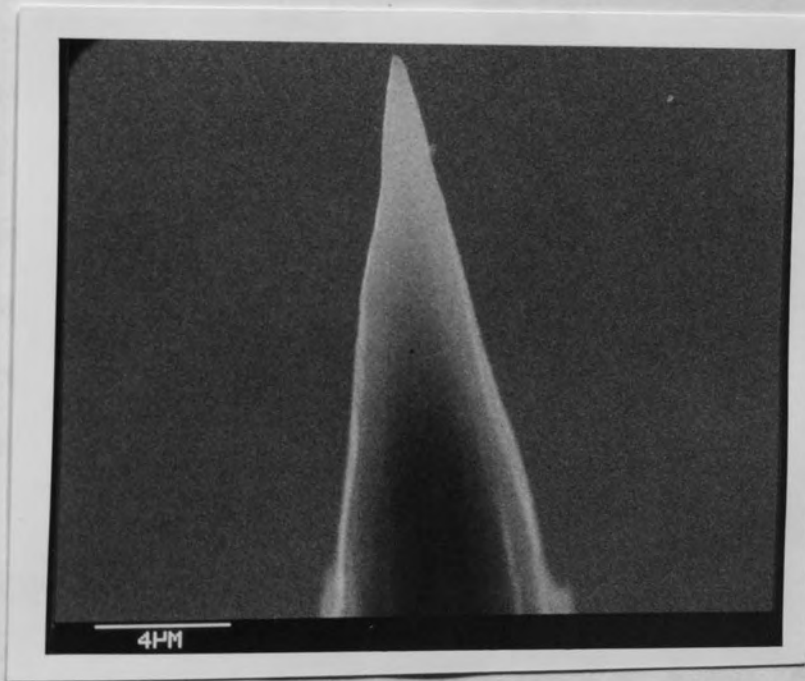
(b)

Fig. 5.28   S E M micrographs of tip heat treated to 250°C (a) before
and (b) after 500 hours of continuous operation.

the tip is somewhat broader than that of the freshly prepared tip, presumably the result of an extended heat treatment: however, the erosion of the tip due to field emission appears to be negligible. Overall, the data presented in Fig. 5.26 and Fig. 5.27 indicates that the life time performance of the heat-treated cathode is excellent, and it suggests that the life time performance could easily be extended to several thousand hours.

5.5 ENERGY SPECTRA OF ELECTRONS FIELD EMITTED FROM HEAT-TREATED CATHODES.

The investigations reported before showed that the heat treatment of a carbon fibre cathode results in an improvement of its "commercial" emission characteristics. However, it is also of considerable interest to know whether this treatment influences the fundamental physical mechanism by which the electrons are emitted from carbon fibre tips. An obvious technique that would provide a sensitive test for such changes is electron spectroscopy since the character of the spectrum will be determined partly by the form and nature of the electronic states from which the electrons are emitted, partly by the statistical distribution of electrons among these states, and partly by the form of the surface potential barrier which is affected by the surface conditions such as the presence of adsorbed gas and general contamination. Accordingly, it was decided to measure the energy spectrum of electrons emitted from heat-treated tips, and compare this with the spectrum obtained from an untreated tip.

Historically, several groups have measured the electron energy distribution of carbon fibre field emitters. The first measurement was made by Braun et al (101) who using a Van Oostrom type of retarding potential analyser, reported a narrow half-width of

0.21 ± 0.01 e V and concluded that it was comparable to the "metallic" type of emission characteristics obtained from tungsten emitters. Later, Heinrich et al (106) measured the energy distribution of electrons that had previously been accelerated to 30 k V, and under the relatively poor vacuum conditions $\sim 10^{-6}$ m bar. They found the half width of the spectrum at low currents of $\leqslant 10^{-9}$ A to be ~ 0.215 e V, which grew to ~ 1 e V at $\sim 10 \mu$ A. They explained this effect in terms of instabilities in the surface structure and the presence of more than one emission sites on the emitter surface. More recently, measurements were made by Latham and Wilson (21) under ultra high vacuum condition ($\leqslant 10^{-10}$ torr), employing an advanced high resolution $\leqslant 30$ m e V 180° deflection field emission spectrometer, due to Braun et al, with the capability of relating the emission spectrum to the Fermi level of the substrate cathode: i.e. providing valuable information about the origin of the field emitted electrons. These latter authors (21) reported the existance of both single and double peaked spectra, although the former type were more common. Generally, they observed that the energy spectra were shifted towards the low energies from the cathode Fermi level, where typically the shift increased from ~ 0.30 e V to 0.60 e V with increasing emission current from $\sim 1 \times 10^{-10}$ A to $\sim 1 \times 10^{-7}$ A, the behaviour was reversible and reproducible. The half width of the single peaked spectra similarly increased from 0.24 e V to 0.50 e V over the same current range. They also reported that the double peaked spectra were very current-sensitive, in that the detailed structure of a given spectra could change dramatically over a current range of 3×10^{-8} to 5×10^{-8} A. It was suggested that the general features of the spectra were uncharacteristic of a simple metallic type of emission process; instead they explained their

results in terms of a hot-electron model (75) that was initially used to explain emission mechanism in broad area high voltage electrodes (19, 70). This mechanism involves a microregime consisting of a metallic substrate that is overlayed by a thin layer of an insulating material and has already been discussed in chapter 2 section 5.

The electron energy spectra of a heat treated carbon fibre tip was measured with the same U H V high resolution 180° deflection analyser developed by Braun et al (101), and used previously by Latham and Wilson (21). A freshly etched tip was therefore mounted in the spectrometer, and roughly pumped to $\sim 10^{-7}$ m bar; subsequently, both the tip and the system were subjected to an 18 hour bake at $\sim 250^{\circ}$ C , so that after cooling a normal operating pressure of $\lesssim 10^{-10}$ m bar was obtained. Referring to Fig. 5.29 the tip was mounted in the system ~ 2 cm away from the ring anode 'B' which was mounted about 10 cm away from the screen anode 'A' having a central 0.5 mm diameter aperture. Here, this screen anode served a dual purpose: firstly, it provided a means of imaging the electron emission pattern, and secondly, its fine probe aperture allowed a small portion of the image to be selected for spectral examination. In order to measure the total emission current, the cathode was earthed via a pico-ammeter. To obtain emission, the ring anode B was firstly set at a constant potential of 600 Volts, and then an increasing voltage was applied to the screen anode until an emission current of $\sim 8 \times 10^{-8}$ A was obtained. At this stage a number of micro mechanical adjustments were made to the specimen in the x-y plane, together with adjustments to the input lens voltages of the spectrometer, in order to maximise the output signal from the electron multiplier detecting circuit. Once this output signal has been

to
spectrometer

screen
anode

A ▨▨▨▨▨   ▨▨▨▨▨

phosphor
Coating

ring   B ▨ ⋯⋯⋯ ▨ 6oovolts
anode
            calhode

            ▨▨▨ HOLDER
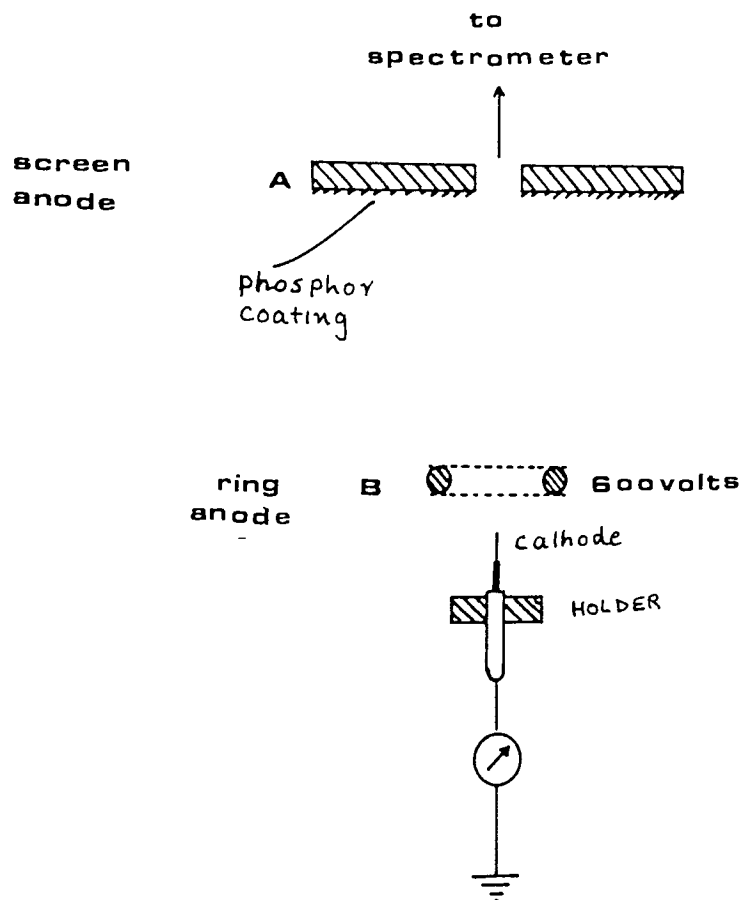
Fig. 5.29   Diagram of a typical electrode arrangement used for

measurement of electron energy spectra.

231.

optomised, the system was ready to measure the energy spectra of the field emitted electrons. For convenience, the spectra could be "frozen" on a storage oscilloscope, so that the previously callibrated position of the substrate Fermi level of a metallic emitter could be superimposed on the spectrum before recording it on film.

Referring to Fig. 5.30 the typical electron energy spectra obtained from a heat treated tip were found to be of two types, namely single and double peaked. In these traces, the x-axis represents the electron energy in e V and ranges from high to low energy from left to right, whilst the y-axis represent the electron current per unit energy. The Fermi level of the substrate cathode is shown as a superimposed small line in the opposite direction on the x-axis. At low emission currents, typically $\leq 8 \times 10^{-8}$ A, the single-peaked type of spectra shown in Fig. 5.30 were commonly observed; however on increasing the current, these would suddenly switch into a multi-peaked spectra such as shown in Fig. 5.30 . The position of the single peaked spectra, which in accordance with Young [37] is measured from a point 78% up on high energy slope of the spectra, is shifted by 0.84 e V relative to the Fermi level of the metallic substrate, furthermore, the spectrum has a broader half width of ~ 0.30 e V compared to 0.24 e V for a clean tungsten emitter at the same temperature. Lastly, the high energy slope width (defined as the energy difference between 10% and 90% peak height points) is found to be of the order ~ 0.19 e V compared to a steeper slope of width 0.14 e V for tungsten. These observations therefore confirm earlier findings [16, 21], and point to a non-metallic type of emission processes.

The spectral characteristics were then examined in more detail over a larger range of emission currents, starting with the lowest
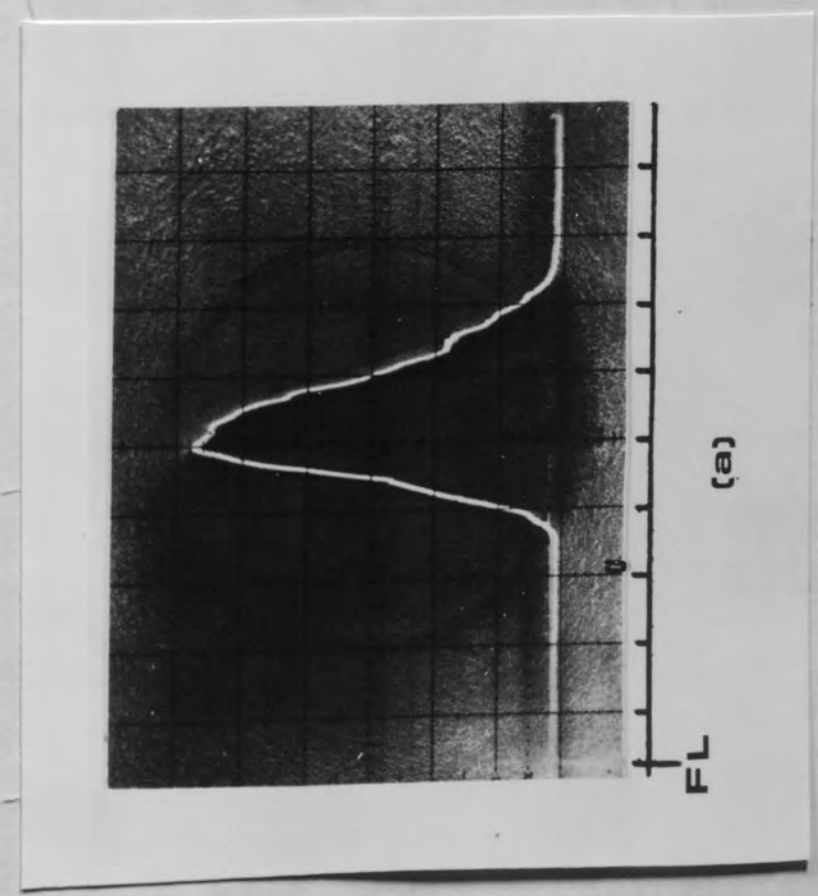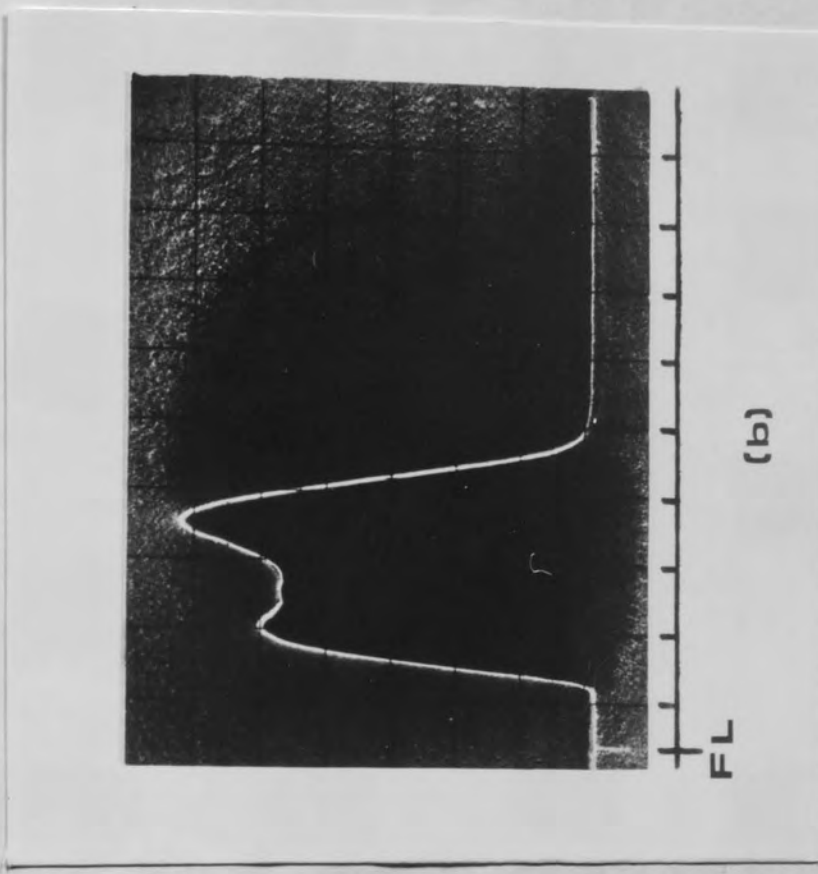
Fig. 5.30   Two types of electron energy distributions (a) single peaked (0.2 m V / Division) and (b) multi-peaked (0.2 e V / Div) obtained from carbon fibre, heat treated to 250°C.

value that gave a detectable signal through the anode probe hole.
Thus referring to Fig. 5.31 , a series of spectra are presented for
the current range 4.0×10^{-8} A to 6×10^{-7} A, which corresponds
to a applied voltage range of 1.5 K V to 5 K V . It can be seen
that up to a current level of 1×10^{-7} A (i.e. frames a - d), the
spectra are dominated by a single peak, although a low energy shoulder
can be clearly seen in frames b - d . For an emission currents in
the range of 4×10^{-8} to 1×10^{-7} , the corresponding energy shift of the single
peaked spectra was found to decrease from 0.73 e V to 0.63 e V
and the corresponding half width, in the same current range, increased
from 0.38 e V to 0.63 e V. On further increasing the emission
current, the double peaked spectra of frames e, f, g and h were obtained,
where the high energy peak remains dominant, but with the low-energy
peak becoming progressively more clearly defined. Tests were also
made with both types of spectra to see if micro-movements of the
cathode led to any changes in the spectral character: infact, these
were found to be negligible, except when the tip was moved through a
distance $\geqslant$ 30 μm . It was also determined at this stage that the
spectra was reproducible, without any significant difference in
shape, when the current was cycled within the above range. However,
during this investigation, as the applied field was increased beyond
5 k V a sudden current surge was observed at the power supply,
presumably this caused the tip to "explode", since subsequently the
spectra suddenly changed to a much broader multipeaked distribution
such as shown in Fig. 5.31 (i). In this emission regime, every
small increase in the voltage was found to irreversibly change the
detailed shape of the multi-peaked spectrum: This behaviour persisted
to the lowest currents where the spectrum remained multipeaked.
Furthermore it was found that the detailed shape of these spectra

Fig. 5.31   Set of energy spectra for tip heat

treated to 250°C obtained for different

applied field emission currents.

(0.4 e V / Div)

(a) (b) (c)
(d) (e) (f)
(g) (h) (i)
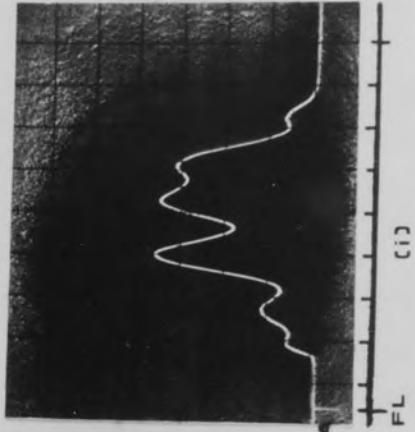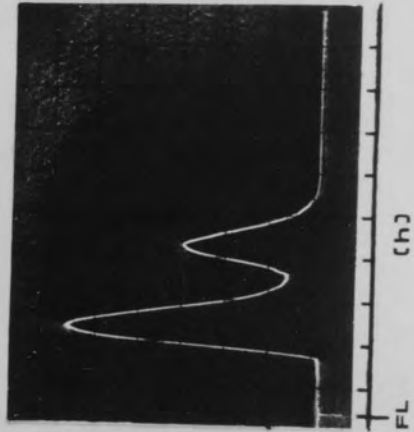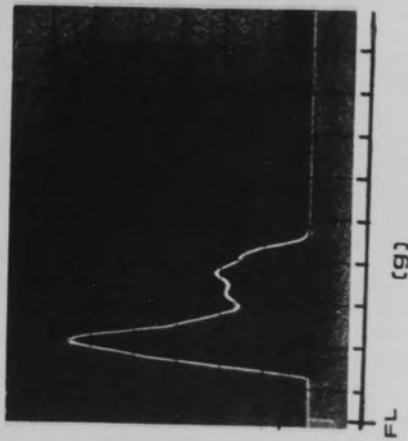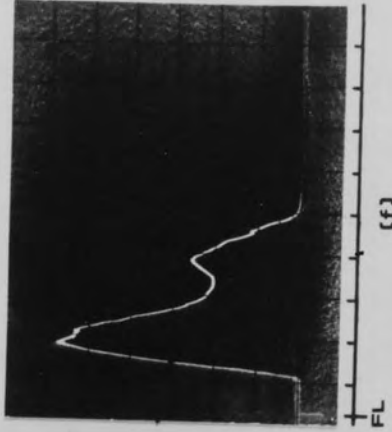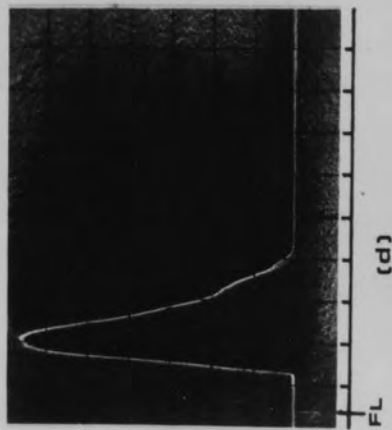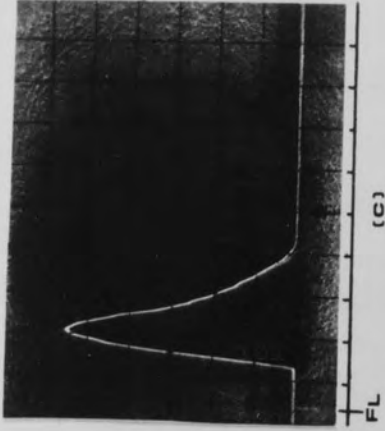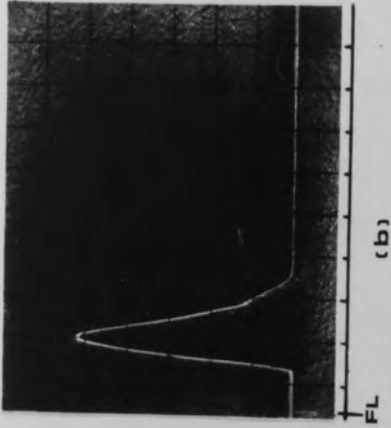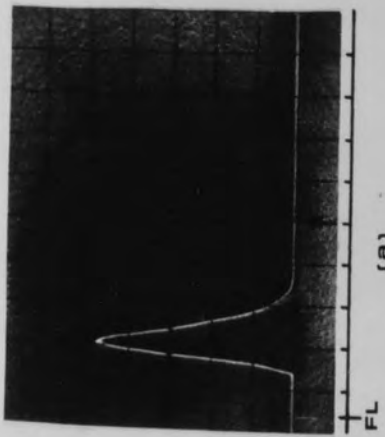
square wave pulses in the frequency range of 15 Hz - 5 mHz
(obtained from an Advance 40405 type pulse generator) to ~ 700 Volts.
The circuit diagram of the amplifier is shown in Fig. 5.32 (a) and
it operates in the following manner. The signal from the pulse
generator is fed into the 6N137 type high-speed opto-isolator,which gives
a good response at the higher frequencies (see Fig. 5.32(b)).This
electrically isolates the input from the high voltage, whilst
optically transmitting it with ~ 70% efficiency. The output from
the opto-isolator is then fed into the base of the high voltage
transistors connected in the form of a Darlington pair to increase its
sensitivity, and are used as an electronic switch. Thus when the
transistors are conducting due to a pulse step reaching the base of
the Darlington pair,the current then flows through it and thus the
33 kΩ high wattage resistor. As a result,about 699 Volts from
700 Volts, the supply voltage, are dropped across 33 kΩ resistor.
However, when the voltage pulse step is zero at the base,then the
transistors remain in non-conductive state in which case there is no
current flow and therefore there is no voltage drop across the
resistor. In this way an amplified pulsed voltage appears across
the 33 kΩ resistor and is used to feed the tip.

The experimental investigation into the pulsed mode operation
was carried out in the simple field emission microscope with the set-
up shown in Fig. 5.33 . Here, the cathode is placed ~ 20 mm away
from a ring anode which is placed nearly in contact with the screen,
where the diameter of the ring anode is fractionally smaller than the
internal diameter of the glass tube containing the screen. The first
stage in obtaining pulsed field emission from a freshly prepared
and then pre-heated tip, was to apply a constant d - c voltage of
~ 400 Volts to the ring anode; where this value was carefully chosen
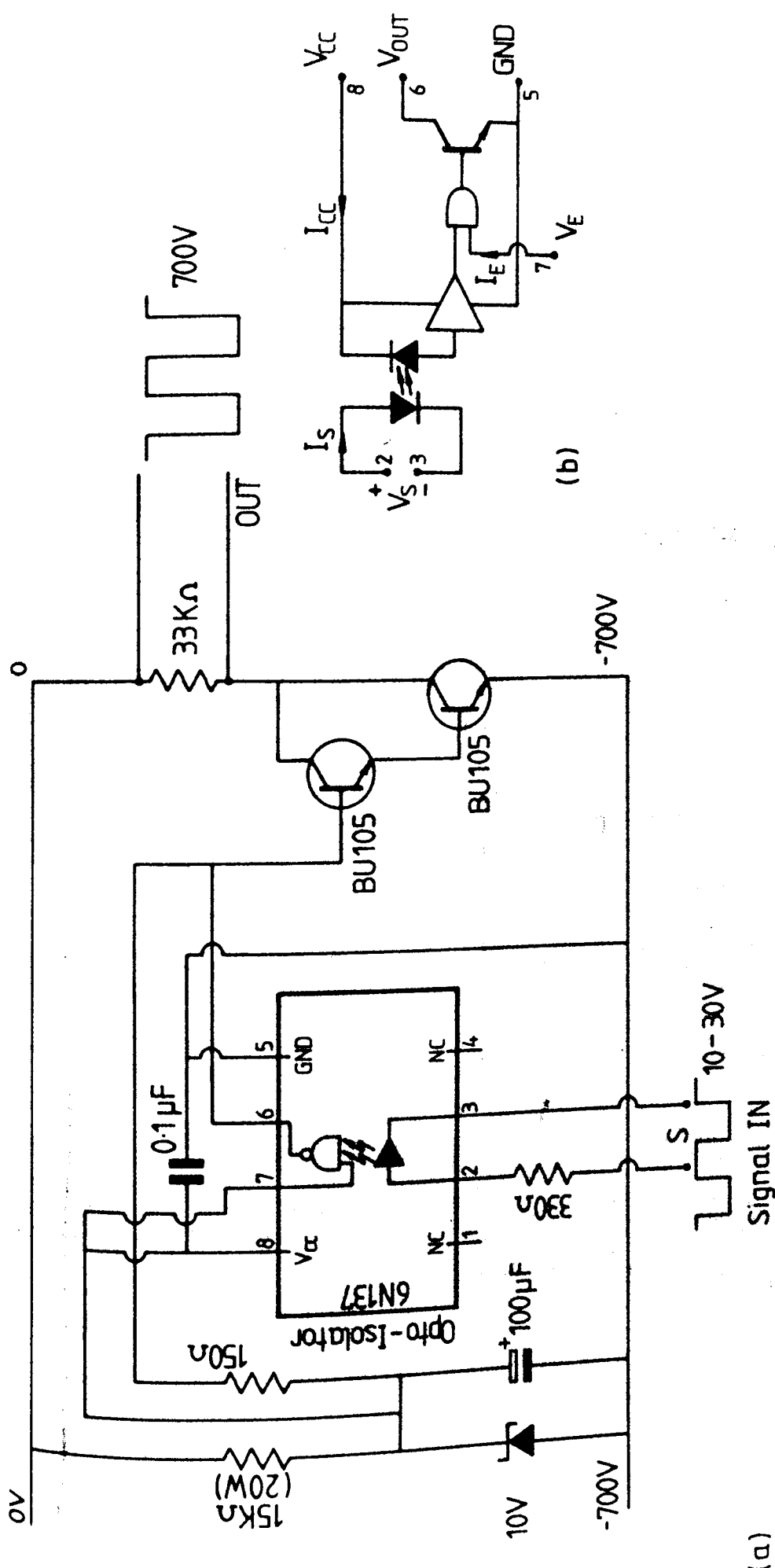
Fig. 5.32: Circuit diagram of (a) pulse voltage amplifier and (b) opto-isolator.
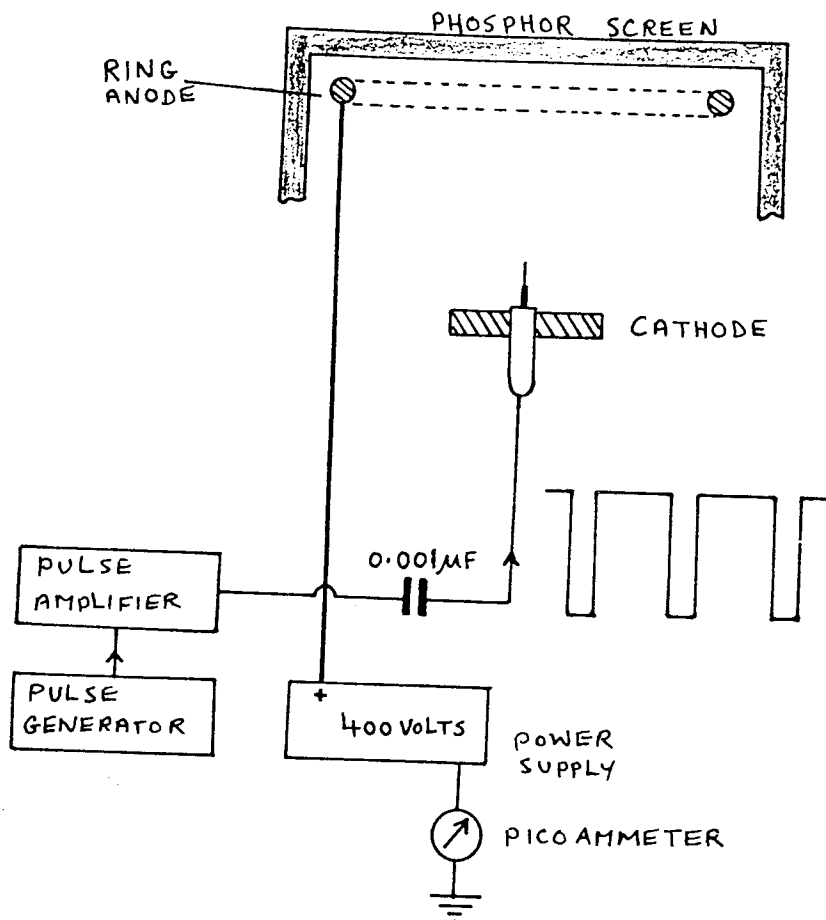
Fig. 5.33 Typical set-up used for pulsed field emission from carbon fibre cathodes.

such that it was below the critical voltage for initiating d - c
emission. Next, the capacitatively-coupled to the tip, pulse
amplifier is used to superimpose a gradually increasing pulsed field
upon this standing d - c field, until an emission image of adequate
brightness is obtained on the screen. It was usually found that
negative going pulses of height 450 Volts were adequate.

Having thus obtained emission, the first experiment was to
investigate whether the frequency of a pulse train having 1 : 1
mark-space ratio (M S r) had any influence on the emission behaviour.
This was done by slowly increasing the frequency from 15 Hz whilst
continually observing the emission pattern both visually and with
the aid of the optical monitor and chart recorder (see section 4.6).
It was found that in the frequency range of $\sim$ 800 kHz to 2 mHz ,
the flicker noise in the emission image was somewhat reduced; also,
there was some indication that the frequency of the flickering tended
to be reduced a little. These effects can be seen from the chart
recorder traces presented in Fig. 5.34 (a) and (b) which compare
respectively the D.C mode with pulsed mode taken at $\sim$ 950 kHz .
Varying the applied pulse height resulted in variation in brightness
otherwise it had no effect on the emission pattern. Next the effect
of changing the mark-space ratio (m s r) was investigated. Thus,
starting at 15 Hz , the m s r was scanned between the limits 20 : 1
and 1 : 20 in 5 - 10 kHz steps upto 5 mHz . Remarkably, it was
found possible with this technique to stabilise the emission image,
i.e. eliminating flickering, over vertually the whole frequency
range by an appropriate choice of the m s r. For frequencies above
$\gtrsim$ 1 kHz , stabilisation required a m s r of $\sim$ 1 : 5 : however,
between 150 Hz and 1 kHz , a smaller m s r of $\sim$ 1 : 8 was required,
whilst from 20 Hz to $\sim$ 150 Hz it was necessary to reduce the m s r
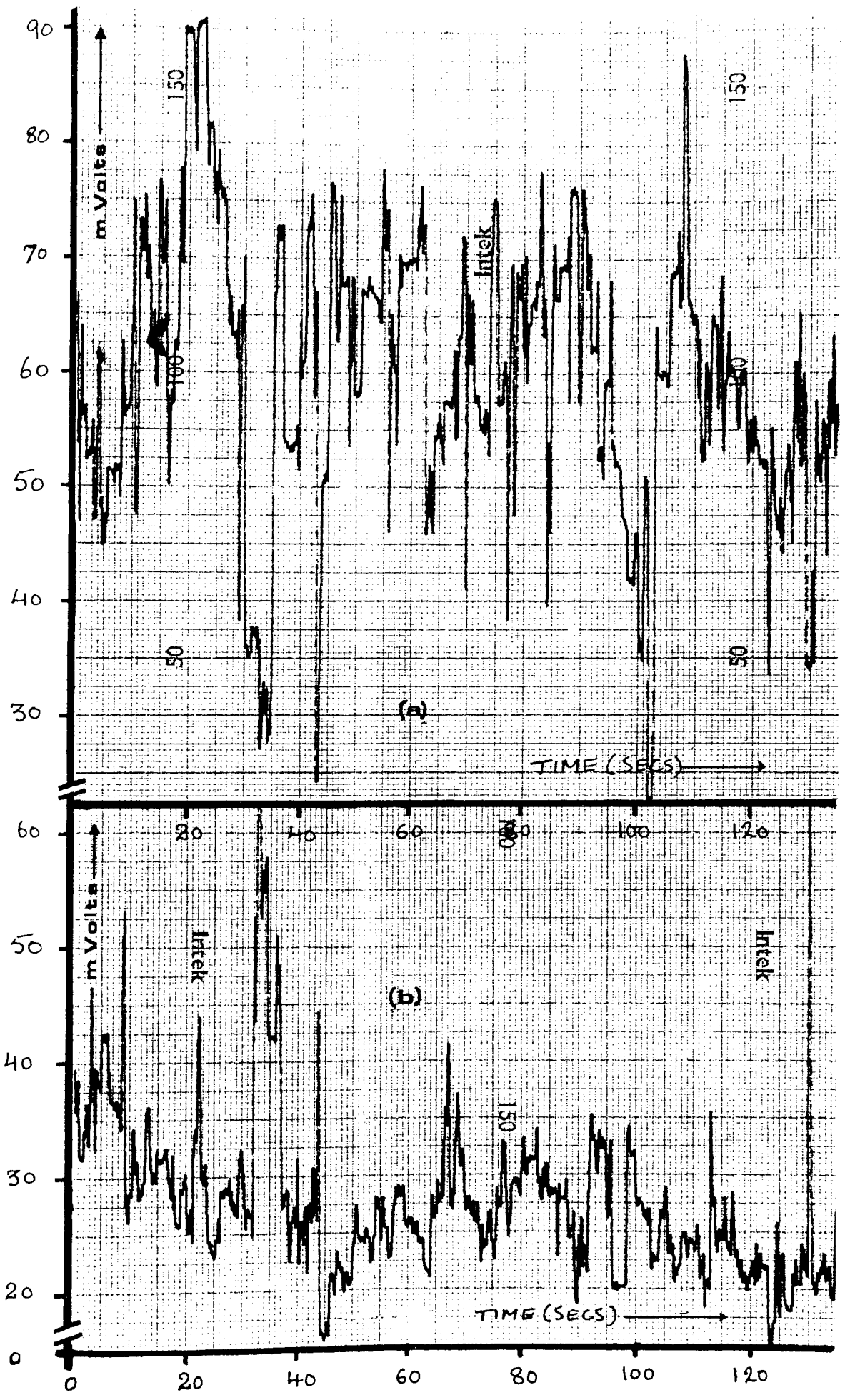
Fig. 5.34 Chart recorder traces of optically monitored signal from
the screen in (a) D.C mode and (b) pulsed mode for
frequency of 950 kHz and M S r of 1 : 1.

to ~ 1 : 15 . During the course of these experiments it was found that, in order to achieve good stabilisation, it was necessary that emission from a virgin tip should first be initiated   in a pulsed mode, and that the contribution due to the constant D.C field should be zero. Furthermore, if after achieving these pulsed field stabilisation conditions, the standing D.C voltage, and hence the emission current, was increased above its initial value, the emission pattern would again become unstable, but this time with an increased frequency of flickering, including the emission spots that were previously stable under constant D.C field conditions. Finally, the degree of stabilisation achieved in the pulsed mode operation was not affected by the changes in the amplitude of the applied pulse.

To quantify the degree of stabilisation by this technique, optically monitored chart recorder traces are presented in Fig. 5.35 (a) and (b) taken, for the same tip to anode voltage difference, "before" and "after" stabilisation was established. From these recordings, it can be seen that in the latter case in comparison the noise level in the emission pattern is considerably reduced. It should also be appreciated that the stabilisation achieved due to the pulsed emission is in fact more impressive than shown by Fig. 5.35 (a) and (b) since, in the stabilised mode, the optical detector tends to pick up noise from the applied pulsed voltage, despite elaborate screening precautions. Typically, it was observed that about 75% to 90% of the sub-emission centres forming the d - c image would become "frozen", i.e. stay switched on, throughout the time that the applied pulse voltage remained switched on. Even for the one or two sub-emission centres that remained unstable, the frequency of flickering was drastically reduced.

To demonstrate this latter property, the emission pattern
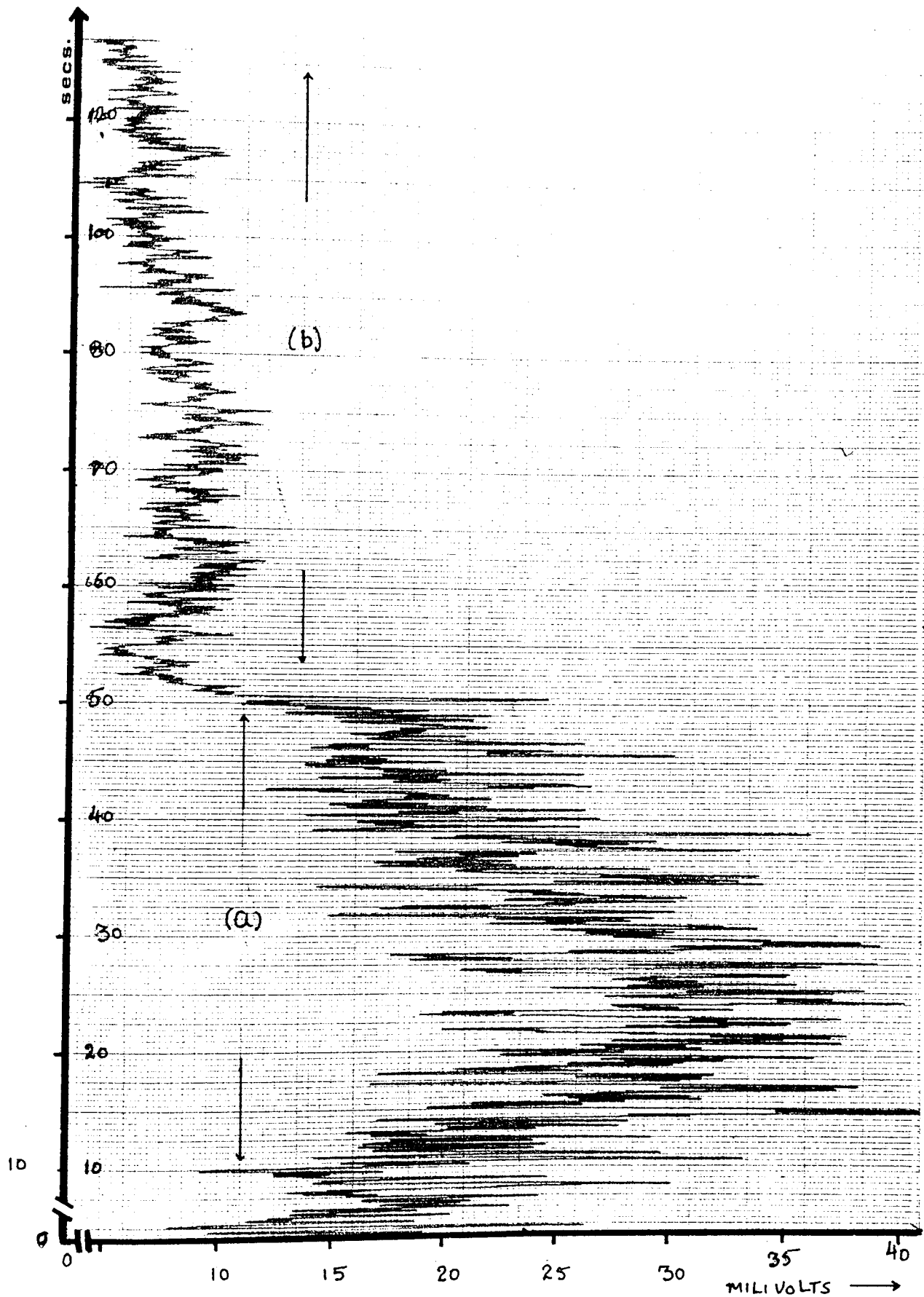
Fig. 5.35 Chart recorder traces of optically monitored signal from

the screen at frequency of 40 kHz   and m s r of 1 : 5

(a) in D.C mode and (b) in pulsed mode.
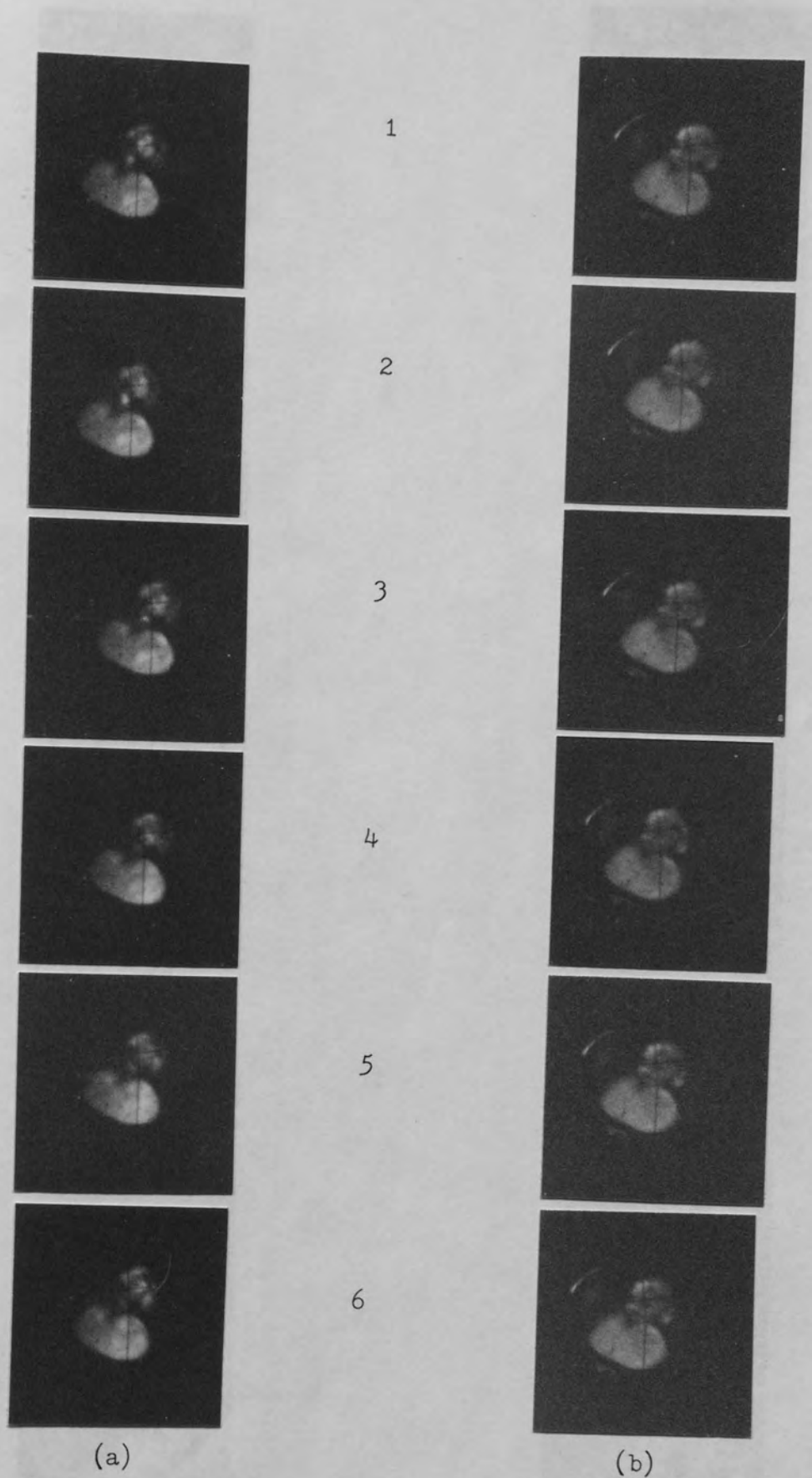
Fig. 5.36 A selection of cinematographically recorded frames (a) D.C
mode and (b) in pulsed mode at frequency of 45 kHz msr of
1:5 to demonstrate freezing of the emission spots in
later case.

7

8

9

10

11

12

13

(a)   (b)
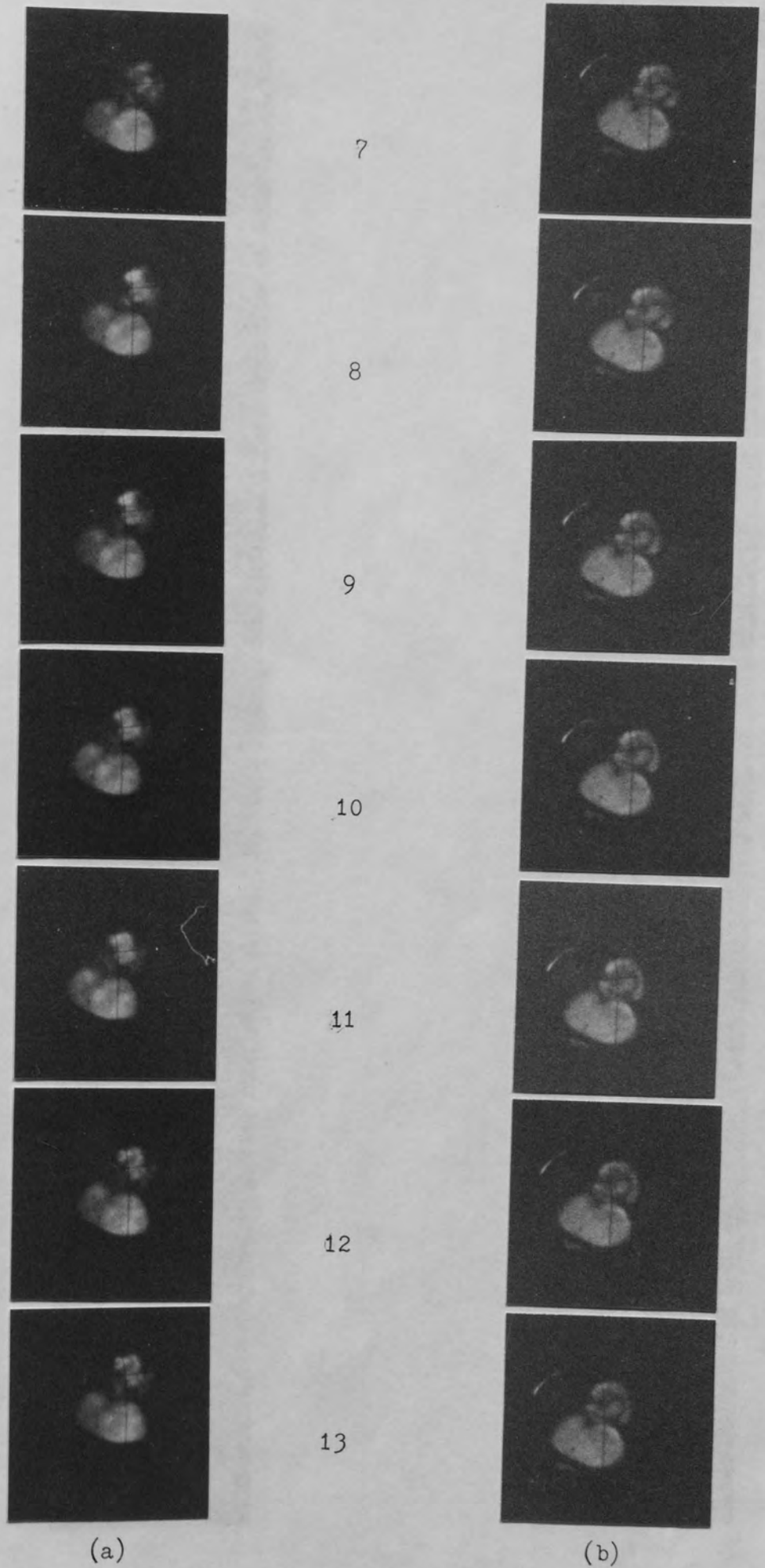
Fig. 5.36   Frames 7 to 13

245.

14

15

16

17

18

19

20

(a)   (b)
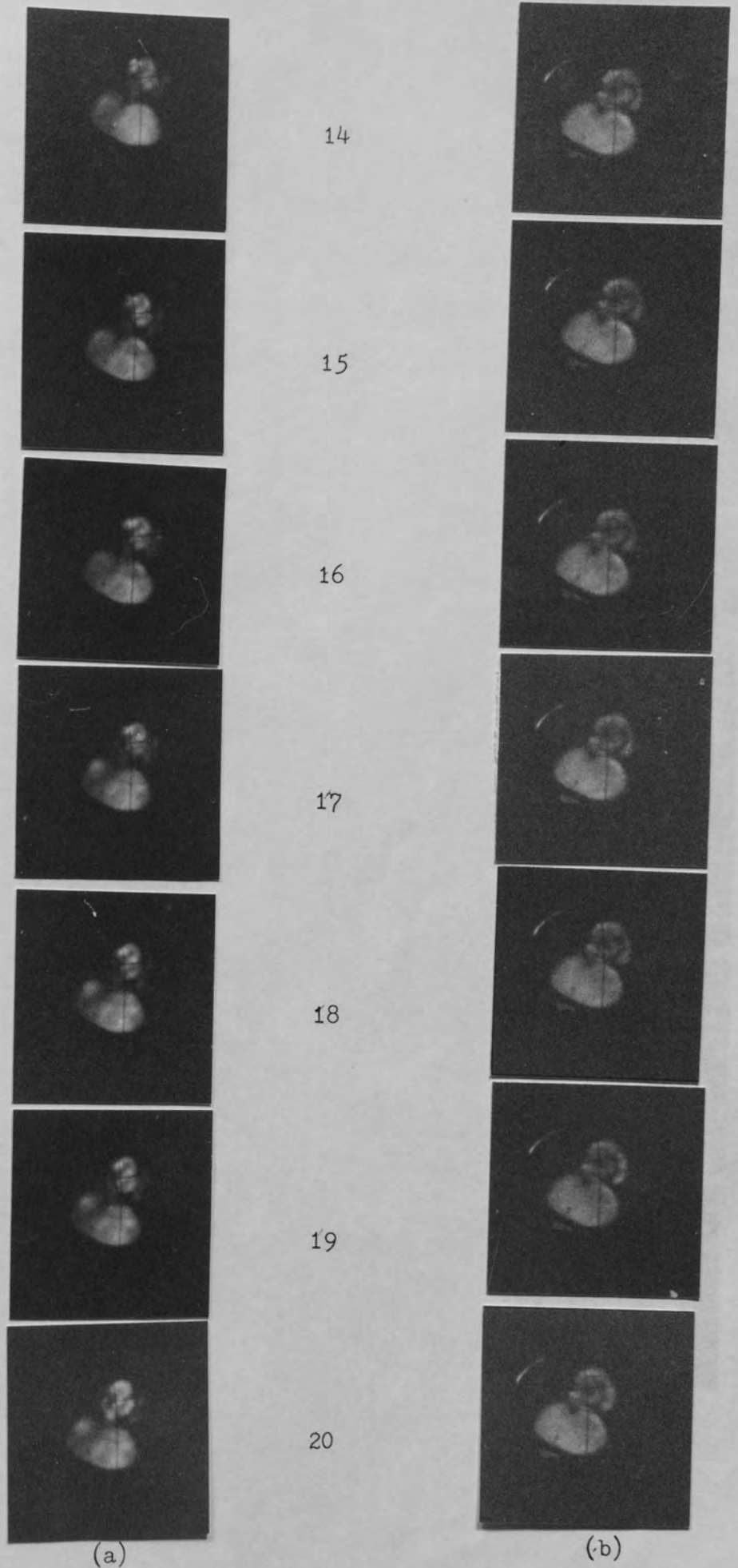
Fig. 5.36   Frames 14   to   20.
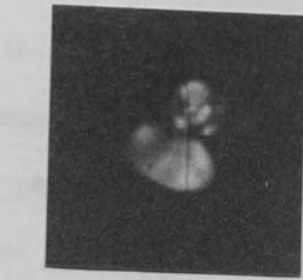
21
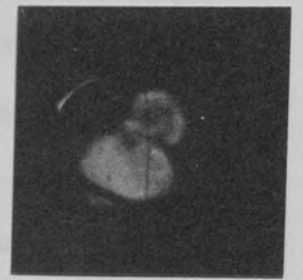
22

23

24

25
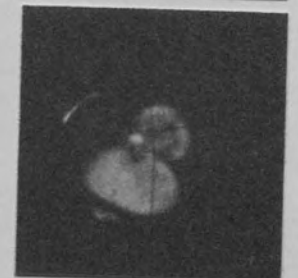
26

(a)   (b)

Fig. 5.36   Frames 21   to   26.

obtained at the phosphor screen with both the pulsed and D.C emission modes were recorded using a cine-camera operating at a speed of ~ 24 frames per second, and with the aid of an image intensifier placed between the camera and the screen. Each mode was filmed over a 5 minute sequence, and Fig. 5.36 presents respectively two series of selected frames; presented here side by side for easy analysis, from (a) the d.c mode and (b) the pulsed mode. In both cases the general character of the emission pattern is very similar; however, whilst the detailed character of the d - c image is seen to change from frame to frame, the pulsed field image is absolutely frozen, i.e. with no detectable changes in the detailed structure from frame to frame. This method of stabilisation was found to be applicable to all tips studied, provided the emitters were initially switched on by a pulsed voltage.

CHAPTER 6

DISCUSSION

The results reported in the last two chapters will now be discussed on two levels. Firstly, considerations will be given to the physical implications of the experimental findings and will be considered with particular reference to the possible physical mechanisms involved in the various phenomenon encountered during the course of the study. Secondly, a quantitative assessment will be given of the practical potential of the field emission source that has been developed for the high definition C R T's.

Previous studies by Baker et al (13, 100), Lea (98) and Wilson (14) had shown that carbon fibre field emission sources have very satisfactory electron optical and life time performances in the pressure range of 10^{-6} m bar to 10^{-8} m bar, such as is typically found in conventional sealed-off vacuum tubes. In particular they were shown to have definite advantages over tungsten micropoint emitters, which when operated at pressures of $\lesssim 10^{-8}$ m bar become very unstable with a drastically reduced life time of a few minutes. Furthermore, compared with carbon fibre tips, the emission current distribution from tungsten emitter is highly non-uniform due to the strong influence of the adsorbed contaminants on the emission properties of tungsten tips. The practical potentialities of carbon fibre cathodes has been further high-lighted by the present studies of chapter 4 and 5, where it has been demonstrated that this type of source can be used to replace the conventional thermionic cathodes in the production of, sealed, glass cathode ray tubes. In particular, the high current density ($\sim 10^{10}$ A m^{-2}) point source, with an electron optical source size of about 3 nm , makes such a substitu-

tion particularly advantageous in the case of the high-resolution miniature micro-focus C R T.

Apart from the desirable properties of a carbon fibre source, the present work has also shown that they exhibit two undesirable properties. The first of these is associated with the initial application of an increasing voltage to a virgin carbon fibre cathode, where, at some critical voltage, the emission current suddenly "switches-on" from an effective zero-value and increases uncontrollably at constant applied voltage, invariably resulting in the destruction of the tip. Baker et al [100] in their later work showed that this explosion phenomenon could be considerably reduced by employing a 100 $m \Omega$ feed-back resistor in series with the emitter; these workers also showed that this technique has the further advantageous effect of considerably reducing the noise in the total emission current. However, it has been shown in chapter four, that the simple application of this technique to field emission C R T, employing electrostatic lens, leads to serious problems at the screen. This is because the stabilisation of the total current is achieved at the expense of variations in the voltage drop across the 100 $m \Omega$ resistor (typically of a few hundred volts), and hence the stability of the tip voltage. As a result, this gives rise to fluctuations in the beam energy and, finally, to unacceptable level of defocusing effects. To circumvent this disadvantage, two alternative approaches have been developed to compensate for the inherent fluctuations in the emission current. Firstly (as described in chapter 4), the existing lens system (Wilson [14]) was replaced by one that was specifically designed to reduce its sensitivity to beam energy fluctuations. Secondly, the 100 $m \Omega$ was replaced by a valve-type of electronic variable resistor in which the variation in the tip voltage is

basically the variation in the valve biasing voltage (to keep the current flowing through it constant), which is the order of few volts compared to few hundreds of volts, therefore having a minimal effect on the focusing properties of the lens system.

However, even with a stabilised emission current, there remains the serious "spacial" instability which arises from the characteristically complex field emission pattern of carbon fibre emitters. This is composed of a large number of independent emission spots which are continually switching on and off and randomly varying in intensity, so that when the emission is trimmed by the aperture of the extracting electrode, the transmitted beam current will fluctate and give rise to a "flickering" of the final image at the phosphor screen. To overcome this problem, an extended feed-back system was developed, similar to that used by Cleaver (111), whereby the screen current was sampled and then used to control the voltage applied to the tip, and thus the current reaching the screen. Although the screen current was effectively stabilised by this technique, it was found that the flickering of the final image persisted, although at a somewhat reduced level. The explanation for this somewhat surprising finding is thought to be due to the fact that the variation in the tip voltage necessary for controlling the emission current causes variations in the electron energies, and therefore the light output at the screen, where the voltage fluctuation at the tip can be as much as ~ 43% of the total tip-extractor gap voltage. Subsequently, the flickering of the final image was successfully overcome by another feed-back technique in which the light output of the screen was converted into voltage signal and used to control the emitted current from the tip. However, although the system was very successful in stabilising the "flickering" effect, it could

only be used in complete darkness, and hence was of limited practical application. In common with the first system, it also introduces spherical aberrations resulting from variations in the tip voltage, and these effects would therefore ultimately limit the resolution of the microfocus tube.

A more profitable approach was based upon a consideration of ways in which it might be possible to stabilise the emission at the source. To do this, it was first necessary to examine the physical process by which the electrons are emitted from carbon fibres, and in particular, to explain the origin of the complex field emission images of these sources. The experimental evidence suggests that the electrons are emitted from many discrete emission sites on the surface of the emitter, and early experimentation by Lea (98) attributed them to individual fibrils or micro-spikes of the order of ~ 5 n m in diameter that protrude on the conical emitter surface as a result of electrolytical preferential etching of carbon fibre which is composed of such fibrils. This interpretation was supported by other workers (101, 106) who measured the energy distribution of the electrons field emitted from a carbon fibre field emitter and inter-preted their results in terms of a "metallic" emission originating from such surgace asperities. More recently however, Latham and Wilson (21, 16) showed that there were several features of the characteristic emission from carbon fibres that could not be explained in terms of a simple metallic type of emission processes. These included (a) the shift of the energy distribution towards lower energies with respect to the Fermi level of the metal substrate, (b) the photo-sensitivity of the emission and (c) the observation of an associated electroluminescence phenomenon. Furthermore, it was pointed out that the latter is not observed during field electron

emission from metallic or semiconducting tip. To explain their observations, these authers proposed an alternative hot-electron emission mechanism, involving a micro-regime consisting of a metallic substrate that is overlayed by a thin layer of an insulating material; i.e. as originally proposed for explaining the origin of pre-breakdown electron emission from broad-area high voltage electrodes (80, 70). This model was based on the property of carbon fibres reported in chapter 3 that they are composed of, in addition to graphatic layers, numerous pockets of amorphous carbon which are aligned along the fibre axis and constitutes an average of 12% on the total cross-sectional area (92). According to this model, electrons tunnel from the metal substrate into the insulating regime, and because of the high penetrating field are "heated" by the several e V necessary for them to escape over the insulator-vacuum surface potential barrier: as discussed in chapter 2 and 3. The observed electroluminescence is then a consequence of scattering processes involving electron-hole pair production.

In its simple form, this model suffered from several limitations when applied to the specific case of carbon fibre emitters. The first of these concerned the initial tunnelling of electrons from the Fermi level of the metal into the bottom of the conduction band of the insulator, since for this to occur the barrier width must be $\leqslant$ 5 n m, which would require an extreme bending of the bands. Secondly the model is vague about exactly how a sufficient number of hot electrons are able to cross the 0.1 - 1 μ m bulk of the insulator, without losing most or all of their energy through electron-phonon scattering processes. To overcome the first limitation, Latham and Wilson (16, 21) proposed that the conical surface geometry of the virgin tip provides the necessary field enhancement and resulting

band bending to initiate the tunnelling of electrons from the metal into the insulator. These will then be heated and, due to electron-phonon scattering, will create an avalanche of further charge carriers through the production of electron-hole pairs by impact ionization. Then, as discussed by Athwal and Latham (75), these charges separate and migrate to their respective interfaces; i.e. the electrons towards the insulator-vacuum interface, and holes towards the metal-insulator interface, where they help to sustain the high field for electron tunnelling from the metal. This charge separation also provides the necessary high field for the insulating material to undergo an Ovshinsky type switching processes (74) from a low conductivity to an energetically more stable high conductivity state (Fig. 2.18), where the conductivity of the insulating material is locally changed by a factor of 10^8 (73) in $\lesssim 0.1$ n S. It is significant that this type of switching is consistent with the behaviour of the carbon fibres where, during the initial voltage application to the virgin cathode, the current suddenly switches on at some critical voltage and the current instantaneously increases from about 10^{-11} A to 10^{-5} A; infact, it is during this "switch-on" that the emitter profile is drastically deformed. It was further proposed that, during this transition in carbon fibre field emitters, a permanent electroforming of many emission sites takes place such as known to occur in metal-insulator-metal switching devices (73), where the typical electroforming times are $\gtrsim 10$ m S. Such sites then would remain permanently in high conductivity state and emit stable currents. The flickering in the emission image then can be invisaged as being due to the remaining emission sites not being permanently formed, such that they reversibly switch between low and high conductivity states, and thereby give rise to a fluctuating

emission current. This is the most likely explanation of the flickering effect, since in the case of the metal-insulator-metal switching devices, Dearnally et al (73) pointed out that, although the critical electroforming voltage does not depend on the insulator thickness, the degree of electroforming in each case does however depend on this insulator thickness. Therefore, this type of switching and electroforming in carbon fibre emitters can be justified since the size of the pockets of the insulating material associated with the emission sites are known to vary considerably (92), so that during the starting procedure, some of the emission sites will be permanently formed and the remainder will reversably switch between the two states. Dearnally et al (73) have further reported that the electrical characteristics of such metal-insulator-metal switching devices can be permanently formed at room temperature in vacuum by application of a voltage pulse of a few seconds duration and of a magnitude that is greater than a certain critical voltage V_c.

During the course of the experimental investigation described in chapter 5, it was shown that by heat treating a virgin cathode in vacuum to a temperature in excess of 250° C over a period of about 24 to 48 hours it was possible to suppress the initial explosive switching phenomenon. This study also indicated that the switch-on effect with untreated tips decreases somewhat with improving vacuum. Of particular significance, was the observation that the switching phenomenon would return to the treated tips that had previously been tested and shown to give a stable emission current if they are re-exposed to the atmospheric pressure for a two-hour period. This therefore suggests that this switching phenomenon is most likely to be due to some form of process associated with adsorbed gas.

One possible explanation of the explosive phenomenon can be given in terms of explosive emission that has been demonstrated to occur with metallic (112) and semiconducting (113) micropoint tips. Here, the application of a high electric over-voltage and the resulting high emission current density causes thermal vaporization of the end form and

the generation of a localised micro-plasma which shields the tip from applied field. The micro-plasma then undergoes a spontaneous expansion with an associated charge separation, and as a result of this, and the accumulation of positive charge at the emitter surface, there is a further increase in the field acting on the emitter. This then leads to a sudden increase in both electron emission current density and hence the rate of vaporization of the emitter material. The experimental investigations of chapter 5 have however shown it to be sensitive to the quality of the vacuum in the test chamber and the heat treatment of the cathode. It is therefore difficult to see how the vaporization, which causes the micro-plasma and therefore the switching phenomenon, could be sensitive to the above conditions. Based on the findings of the experimental investigations of chapter 5, the explosive and switching phenomena are therefore proposed to be associated with adsorbed gases and the surface contamination of the emitter. According to this interpretation, it is the desorption of gases under the influence of high electric field and resulting high emission current density, rather than the vaporization of the substrate emitter material, that produces the localised micro-plasma which consequently causes the switching and the explosive phenomena in the manner already discussed. If however these gases are desorbed by pre heat-treatment of the cathode, it follows that no gases are desorbed during the initial

application of the field and the field emission current, and hence no possibility of a plasma generation. Accordingly, one would expect to observe a gradually increasing current with applied field without exhibiting a switching or explosive phenomena. The individual emission sites should therefore start smoothly emitting at fields determined by their particular characteristics e.g. such as insulator thickness. It follows therefore that the integrated total emission current should similarly exhibit a smoothly rising behaviour as the applied field is slowly increased; i.e. as is indeed found experimentally. With the untreated tip on the other hand it is believed that the presence of the initial micro-plasma has the effect of switching on a large number of emission sites all at once, and hence giving rise to a large current step that is typically observed in practice.

Since heat treated tips are heated in vacuum to a relatively low temperatures (< 300°C), it is highly unlikely that any significant structural changes will take place in the cathode material; particularly since the final curing temperature of   carbon fibre during production is > 2500°C. Some corroboration of this assumption was obtained from the measurement of the energy distribution of electrons field emitted from heat-treated carbon fibre tips. Thus, it could be reasoned that structural changes would effect the electronic properties of the tip, and hence their emission properties. Infact, it was found that the general characteristic of the measured energy spectra was almost identical to those obtained by Latham and Wilson (21) for "exploded" tips; i.e. strongly suggesting that the electrons are being emitted by the same mechanism in both cases, (section 3.4). Thus, referring to Fig. 2.18, the observed shift in the energy distribution with respect to the Fermi level of the metallic substrate is due to the combined effect of an initial energy loss in thermo-

lising the electrons into the bottom of the insulator conduction band, an ohmic loss in the low-field region and losses due to electron phonon scattering in the high field region near the insulator-vacuum interface. These losses may be expected to increase with increasing field and result in an increase in the shift of the distribution; i.e. as was found experimentally by Latham and Wilson (21). In the present measurements however, the heat treated tips were found to differ from untreated tips in that the shift in their energy distribution was found to decrease with increasing field and emission current. It is however possible to explain this effect in terms of surface states. Thus, during the heat treatment of the cathode, the density of these surface states could well be reduced, so that as the emission current increases with increasing applied field the surface states are quickly filled and hence exert only a minimised controlling influence over the emitted current density. In particular, their screening effect will be much reduced. Equally, the volume density of trapped states could well be reduced by the heat treatment, so that they now become filled at relatively low current densities. One consequence of this latter process would be to lower the effective resistance of the conducting channels; i.e. as suggested by the reduction in spectral shift with increasing emission current (see Fig. 5.33).

Again in common with earlier findings (21), the general shape of the energy distribution was found to be more symmetrical compared to that obtained from micropoint metallic cathodes which are characterised by having a much steeper high energy slope. The less steep slope obtained from carbon fibre emitters is consistent with the quasi-thermionic hot electron model discussed previously. It was also found that as the applied field was increased additional

peaks begin to appear and grow on the spectra, presumably due to electrons being emitted from previously dormant sites. In sharp contrast to this reversible behaviour, it was noted that if a heat treated emitter was to explode during operation, as evidenced by a current surge, it was invariably found that the spectrum changed irreversibly to a multi-peaked form and remained like this even at low emission currents. It is therefore believed that the tip explosion results in the exposure of many new sites and that the individual peaks are associated with these independent microscopic sites that are distributed over an extended emitting area. This conclusion is further supported by the fact that the detailed structure of such spectra are sensitive to small displacements of the emitter: i.e. different samples of the total emission current are collected by the anode probe hole of the analyser. In contrast, the less structured spectra obtained before the tip had exploded did not respond to a comparable emitter displacement, presumably because the emission is more localised, and hence the composition of the analysed sample electrons remains effectively constant. The mechanism that offers a plausible explanation for the distribution of spectra peaks is due to Athwal (107) where he proposes that the effect could arise from the electrons that have crossed the insulator in more than one conduction band minima, differing in energy by tenth of e V (114). Since it would be reasonable to expect there to be several minima with such an amorphous material. This is confirmed experimentally, where for example the main peak of Fig. 5.33 is displaced from the Fermi level by ~ 0.3 e V and remains constant with the applied field.

Consideration will now be given to the effects observed when carbon fibre emitters are operated in a pulsed field mode. Firstly

the observation that a pulsed voltage having a mark to space ratio of 1 : 1 tends to stabilise the total emission current in the frequency range of ~ 800 kHz to about 3 mHz is thought most likely to result from a reduction in ion bombardment of the emitter, as discussed by Swann and Smith (110) rather than being due to resistive heating effects, since no changes are observed in the field emitted pattern with this pulsed mode of operation. The second observation that the stability of the emission is sensitive to the mark to space ratio of applied pulse train is of considerable physical and practical significance. It must also be pointed out that the pulsed stabilisation is not simply a spurious optical effect, since the time durations between switching on and off of the individual emission are $\gtrsim 0.5$ sec (see cine film technique of section 5.6) whereas the time duration between the individual applied pulses are very much less than 0.02 m sec. Therefore the sites which remain unstabilised can be detected with greatest of ease. Thus it will be recalled that for frequencies greater than 1 kHz stable emission can be obtained for a fixed mark to space ratio (m s r) of 1 : 5, whilst for lower frequencies the ratio changes to $\sim 1 : 10$. In general, these observations would appear to suggest that the temporal variations of the applied field influences some sort of relaxation process involved in the emission mechanism. One possible explanation for this phenomenon is to be found in the model of Athwal and Latham (75) and Athwal (107) discussed earlier which requires there to be a critical current density in the conduction channels, of $\sim 10^8$ A m^{-2}, to maintain the "on" state. Now for the type of amorphous material that is believed to exist in carbon fibres, it is reasonable to assume that the existance of a high density of trapping levels, and that these will begin to fill as the emission current

starts to flow. However, if the rate at which the traps are filled is slower than the rate of rise of the current density, it can be imagined that there would be a time delay for the onset of instability: i.e. when the net current density in the conducting channels falls below its critical limit for stability. It follows therefore that using pulse field operation, with an appropriate "off" time for charge relaxation to occur (i.e. the emptying of the traps), it would be possible to avoid entering the range of unstable current densities. According to this interpretation, the experimentally observed variation of the mark to space ratio with frequency possibly reflects the existance of some mean density of filled traps that is acceptable on space charge consideration.

The above interpretation is clearly a speculative one, and it has to be recognised that the effect could equally well be associated with some other form of charge relaxation effects. Evidently, there is an urgent need for further fundamental information about the precise nature of the emission mechanism before further progress can be made in understanding such time-dependent effects.

Consideration will now be given to the technological implications of the findings of the present experimental work. The use of a field emission electron source in cathode ray tubes as an alternative to conventional thermionic cathodes was inspired by the potential advantages offered by the source, particularly resulting from its small source size (~ 3 n m) and the large emission current density ($\sim 10^{10}$ A m^{-2}) that can be obtained under continuous operation. Further obvious advantages are its instantaneous switch-on and the avoidance of a heater-power supply. The performance of a carbon fibre tip as field emission electron source in a proto-type cathode ray tube has already been investigated by Wilson (14), where it was

reported to have a satisfactory electron optical performance in that it produced a well focused spot of 0.2 mm in diameter which was suitable for forming a display of adequate intensity for a 10 μ A total emission current; however in this system the focused spot seriously suffered both from fluctuations in its intensity and defocusing effects. Therefore for such an emitter to be commercially viable for use in cathode ray tubes it must satisfy two important requirements, firstly the current in the finely focused beam of a few microramps stable to a few percent. Secondly, the source should be readily incorporated into current C R T manufacturing techniques; this requires that the emitter functions according to the above specifications in relatively poor vacuum conditions of about 10^{-7} m bar with life times that are compatable with the existing thermionic source in conventional cathode ray tubes.

In the course of the present work, the first priority was to improve the electron optical performance of the carbon fibre field emitter, in particular to eliminate the defocusing effects and the intensity variations of the final image. As already has been discussed, these objectives were successfully tackled by redesigning the electro-static gun system, introducing an electronic feed back system (although this requires some further modifications), and the use of pulsed field emission techniques. Furthermore, by using a pre-heat treatment of the emitter, it was possible to both prevent the tip from exploding and increasing the operational life time of the emitters to many hundreds of hours at 10 μ A of total emission current without any deteriation of the tip profile. This meant that the long term fall-off of the emitter current at constant applied voltage, as it is experienced with the exploded tips, could now be minimum. This is an important requirement in the case of the commercial sealed off cathode ray tubes,

since such a drifting current would require a regular adjustment of the applied voltage to keep the emission current constant.

Overall, the performance of a carbon fibre field emission cathode in the proto-type cathode ray tube with the above modifications was found to be very good. Thus a 300 mm focal length gun produced a finely focused spot of 0.25 mm diameter which was able to give a high quality raster of adequate brightness from 10 μ A total emission current. In the case of the 50 mm focal length gun, a 0.075 mm diameter focused spot could be obtained with only 5 μ A total emission current which was sufficient for adequate brightness of the raster display. In both cases, the raster pattern was evenly illuminated and well focused. To maximise the electron efficiency of the gun, the tip has to be placed very close to the extracting electrode aperture and has to be precisely aligned at the centre of its axial aperture. This is a consequence of its large emission conic angle (~ 60°) and its small dimension (~ 7 μm), since otherwise, a large portion of the emitted current would be stopped from reaching the phosphor screen by the intermediate electrodes. In fact, this beam conic angle could be reduced to as small as 10° if the electric field near the tip of the fibre was modified by reducing the distance of the tip from the flat geometry of the tip holder.

The performance of the carbon fibre field emitter was further assessed in real systems, where two commercial, 300 mm and 50 mm focal length, thermionic tubes were redesigned to accommodate field emission electrostatic guns for use with carbon fibre field emitters. Here the main problem which had to be overcome was the initial tip alignment where frequently during the gun assembly procedures, the carbon fibre would become mis-aligned. This problem was overcome with a tip-extractor assembly which allowed the tip alignment and the

tip extractor separation to be adjusted after the gun has been assembled. One other problem, which seriously limited the performance of these tubes, was that during the initial switch-on, the tip explodes and results in not only an increased emission area, but also the emission conic angle and therefore an increase in the beam current intercepted by the intermediate electrodes. At times this effect resulted in the tip emitting to the side. In all cases, the image at the screen would become very faint and highly unstable. To eliminate this problem, a tip heating facility was incorporated in the tip-extractor assembly, so that the tip could be heat-treated during the evacuation of the tube before sealing. As a result of taking these two precautions, the electron optical performances of the two tubes were found to be very good. In the case of the standard 300 mm focal length tube a 0.25 mm diameter sharply focused spot was obtained from 10 μ A total emission current and gave an evenly focused raster display of more than adequate intensity, and was comparable to that obtained from the conventional thermionic emitter. In the case of the miniature, 50 mm focal length, C R T, the image obtained was also of high quality, being produced by a very finely focused spot of 17 μm in diameter, that was suitable for giving a raster pattern of more than adequate intensity from only a 5 μ A total emission current. Such a high resolution in this miniature tube was a consequence of the small emission area, and the nearly monochromatic electron beam that was obtained from a simple two element electrostatic lens system. To achieve similar results in the case of a thermionic high resolution tube (115), it is firstly necessary to have a small object size, which in this case is the cross-over; the spot size is then given by the object size multiplied by the image distance (V) divided by object distance (U). Alternatively, a small image size

can be achieved by having large object distance. In practice, the reduction of the "cross-over" size is achieved by reducing the dimention of the triode gun, until it is finally limited by the voltage break down. Therefore in practice there is often a compromise between "cross-over" size and the object distance necessary to obtain a spot size of 25 μ m diameter. Therefore, thermionic high resolution tubes are often very long and usually require a very complex electron gun system; also to focus and deflect the beam, a very high quality focusing and deflecting coils are required. The resolution of the field emission high resolution tube could be further improved, where the theoretical limit is of the focused spot size is the order of 1 μ m, if attention is paid to eliminating all the instabilities. For example, the high voltage power supplies used to focus the beam and the beam deflecting voltages should be ripple free, the latter of which being particularly important since the stationary spot of 17 μ m in diameter found to increase in size when the sweep voltage and the signal to the respective deflecting plates are applied.

Therefore in summary, it has been shown that the carbon fibre field emission tip offers many practical advantages as a field emission electron source for use in cathode ray tubes, especially for high resolution tubes where space charge limitation becomes important. Such tubes can also be small with no wasted heat dissipation, where the final images are of adequate intensity and clarity. Therefore use of carbon fibre in field emission cathode ray tube offers many advantages over the thermionic electron source, especially since it has now been shown that the final image can be satisfactorily stabilised using the feed-back techniques developed in the course of the present work.

CHAPTER 7

CONCLUSION.

The central conclusion of the investigation reported in this thesis is that it should be practically feasible to use a carbon fibre field emission gun as a suitable electron source in "commercial" sealed-off cathode ray tubes. Indeed, it has also been shown that there are several important operational advantages of using such a source; e.g. its small electron source size (~ 3 nm) , high current density (10^{10} Am $^{-2}$), non-requirement of heater power and instantaneous switch-on.

As a first step towards experimentally demonstrating the suitability of such a source, two electrostatic field emission guns with 300mm and 50mm focal length were designed and subsequently tested using a demountable ultra high vacuum electron optical bench incorporating a high precision cathode manipulator. The two guns had satisfactory electron optical performances, producing well focused spots of 0.25mm and 0.07mm diameter respectively: they were also found to exhibit negligible defocusing effects as a result of variations in the tip volrage. Furthermore, with respective total emission currents of ~ 10 μ A and 5 μ A , sufficient current reached the focused spot for forming a raster of more then adequate intensity. Subsequently, these two field emission guns were successfully substituted for the conventional thermionic sources in both a standard and a high resolution miniature cathode ray tube. The overall performances of the emitter and the gun in these real systems were found to be satisfactory, producing well focused spots of 0.25mm and 17 μm diameter respectively. In the latter case, it would have been possible to reduce the spot size even further; i.e. approaching a theoretical limit of ~ 1.8 μm .

There remained however an inherent temporal instability in the
intensity of the focused spot produced by a carbon fibre field emission
source. Accordingly a thorough investigation was conducted into the
origin of this undesirable effect which resulted in a unacceptable
level of temporal instability or "flickering" in the final C R T screen
display. These latter instabilities were found to be due to the comb-
ined effects of a) variations in the total emission current, and
b) characteristic spatial fluctuation in the current distribution in
the emission image which, when the beam is *trimmed* by an aperture, results in a
fluctuation in the transmitted current. However, these effects were
successfully overcome by using two types of electronic feed back systems.
Firstly, stabilisation of the total emission current was improved to
better than 1 %, by replacing the conventional 100 MΩ current limiting
resistor in series with the tip by a valve type feed-back circuit.
This approach had the added advantage that the system was designed to
keep the tip voltage constant, and hence left the focusing properties
of the gun unaffected. It must be emphasised however that the stabil-
ization *of the* total current, whilst essential, is not in itself a sufficient
precaution for the complete stabilization of the final image intenity.
Thus remaining instability was successfully eliminated by using an
electronic feed-back system which used a signal derived from the screen
to control the tip-extractor gap voltage, and hence the emitted current,

such that the beam current reaching the screen remained constant. If
the actual electron current reaching the screen is sampled, this quantity
can be stabilised to better then 0.5%. Surprisingly however, this
approach leaves the intensity fluctuations almost unaffected: presumably
because the current is being stabilised at the expence of the beam
energy. The second and more successful approach was to control the
feed-back circuit by a signal derived from an optical sensor that was
directly monitoring the screen intensity: with this system it was

possible to stabilise completely the intensity of the focused spot. The typical voltage variations to maintain this degree of stabilisation were ~ ± 200 volts, which was well within the acceptable levels for avoiding serious defocusing effects.

The second part of the investigation concentrated on an examination of the properties of the emitter itself, since it was hoped that the instabilities refered to above could be cured "directly" at the source, rather than directly using electronic compensating systems. From an extensive study of the initial tip explosion phenomenon, it was established that this resulted from the presence of surface contamination and adsorbed gases. Accordingly, a pre-heating treatment was developed in which the tip was maintained at a temperature of 250°C in situ under U H V condition for a period of ~ 36 hours which minimised both the switch-on and explosive phenomena, and to some extent, the noise level in the total emission current. Furthermore, a heat treated tip shows a marked improvement in life-time over an untreated tip, such that, even after hundreds of hours running at a current of ~ 6 μ A, the tip profile remains intact.

The energy spectra of electrons field emitted measeured from a heat- treated tip was found to be identical with that obtained from untreated tip, where a single-peaked spectrum was obtained for currents $\leq 8 \times 10^{-8}$ A and a double peaked spectrum for higher current. For emission currents in the range of 4×10^{-8} to 1×10^{-7}A, the half-width of a single peaked spectra was found to increase from ~0.38 e V to ~ 0.63 e V, however, the spectral shift from the Fermi level decreased from 0.73 e V to 0.63 e V, for the same current range. This could possibly be due to a reduction in the density of unoccupied surface states following their saturation at higher currents.

In a final attempt to stabilise the emission "at source" an investigation was carried out into operating the emitters in a pulsed

field mode. The main findings of this study were as follows :

(i)   A significant improvement in the image stability could be achieved on the application of a pulsed voltage train having a mark-to-space ratio (m s r) of 1 : 1 in the frequency range of 800 kHz to 5 mHz . Thus the physical origin of this improvement is thought to be due to a reduction in the ion bombardment of the emitter.

(ii)   By using a m s r of > 1 : 5 for lower frequencies < 1 kHz , and a m s r of 1 : 5 for frequencies ≳ 1 kHz , it is possible to "freeze" over 90% of the sub-emission centres, as demonstrated using a cine recording technique, provided no d.c. component is present in the applied pulsed voltage.

(iii)   In all cases, the superimposition of a d.c. voltage on the applied pulsed voltage caused all the emission sites, even the previously stable sites, to become unstable with an increased frequency of fluctuation.

Although the various approaches described in this thesis have greatly improved the prospects of using a carbon fibre electron source in a commercial C R T, there remain certain residual limitation that would have to be eliminated before such a source could realistically be considered as an alternative to the conventional thermionic source. Accordingly, a future study could profitably concentrate on the following aspects.

(i)   In the case of the miniature tube, where a spot size of 17 μm diameter was obtained there remains a possibility of improving the resolution by reducing the spot size closer to the theoretical limit of ~ 1.8 μm . One suggested approach would be to use computer technique , to refine further the properties of the present gun, particularly by minimising the aberrations in the focused spot. This could be done by further reducing the magnification factor, as indicated by the graph of magnification M voltage ratio (V_1 / V_0) shown in

Fig. 4.46. Another approach would be to consider some alternative field emission gun designs.

(ii) In order to use electronic feed-back more effectively, some further modifications are required in its design. It was seen that in order to satisfactorily control the intensity fluctuations, the optically monitored signal from the screen had to be fed into the system, which limited the use of the tube to dark conditions only. To overcome this, it is suggested that the monitored screen electron current is fed into the system as before, but that instead of using the output to control the tip-extractor gap voltage, it should instead be used to control the post-accelerating voltage which could be applied to the cage which is already incorporated, near the phosphor screen. By using this, it is hoped that when the screen electron current and therefore the light intensity is low than the post-accelerating voltage and therefore the beam energy will be increased; thus having an effect of increasing the light intensity at the screen, and vice versa of course.

(iii) Finally, the possibility should be considered of incorporating the pulsed emission mode of the carbon fibre emitters into a commercial sealed-off tube: i.e. to check its performance under more practical conditions. Also, attempts should be made to obtain a better understanding of how a pulsed field influences the emission process, and why it is not apparently pratical to superimpose a pulsed field onto a passive d.c. field.

REFERENCES.

1.   R. W. Wood, Phys. Rev., 5 , 1 - 10 ,   (1897).

2.   E. W. Muller, Z. Physik, 13 , 136 - 142 ,   (1951).

3.   W. P. Dyke and W. W. Dolan, Advances in Electronics and
     Electron Phys., 8 , 89 - 185 ,   (1956).

4.   R. Gomer, "Field emission and Field ionization",
            (Oxford University Press: Oxford)   (1961)

5.   R. H. Fowler and L. Nordheim, Proc. Roy. Soc. London., A119 ,
     173 - 181 ,   (1928).

6.   R. Stratton, Proc. Roy. Soc. London., B68 , 746 - 757 ,
                                                             (1955).

7.   A. Modinos, "Field Emission from Surface States in Semi-
     conductors". Surface Sci. 42 , 205 - 207 ,   (1974).

8.   J. W. Gadzuk, Phys. Rev. 81 , 2110 - 29 ,   (1970).

9.   C. Kleint, Surface Sci., 25 , 394 - 410 ,   (1971).

10. W. P. Dyke, I R E Trans. Mil. Electron. MIL - 4 , 38 - 45 ,
                                                             (1960).

11. A. V. Crewe, M. Isaacson and D. Johnson, Rev. Sci. Instrum.,
     40 , 241 - 246 ,   (1969).

12. L. W. Swanson and L. C. Crouser, J. Appl. Phys., 40 ,
     4741 - 4749 ,   (1969).

13. F. S. Baker, A. R. Osborn and J. Williams, Nature, 239 ,
     96 - 97 ,   (1972).

14. D. A. Wilson, Ph.D Thesis, Aston University In Birmingham,
                                                             (1981).

15. R. V. Latham and D. A. Wilson, J. Phys. E: Instrum., 15 ,
     1 - 10 ,   (1982).

16. R. V. Latham and D. A. Wilson, J. Phys. D: Appl. Phys., 14 ,
     2139 - 2145 ,   (1981).

17. L. Malter, Phys. Rev. 50 , 48 - 57 ,   (1936).

18. R. V. Latham, "High voltage vacuum insulation - a physical
     basis", Academic Press.   (1981)

19. N. K. Allen and R. V. Latham, J. Phys. D: Appl. Phys., 11 ,
     L55 - L57 ,   (1978).

20. R. V. Latham, Vacuum, 32 , No. 3 , 137 - 140 ,   (1982).

21. R. V. Latham and D. A. Wilson, J. Phys. D: Appl. Phys.,
     16 , 455 - 463 ,   (1983).

22. W. Schottky, Z. Physik., 14 . 63 - 106 , (1923).

23. A.P.French & Taylor R.Taylor "Introduction to quantum Quantuam mechanics"'Thomas & sons Ltd. (1979).

24. R. H. Good and E. W. Muller, Handbuch Der Physik, 21 , 176 - 231 , Springer-Verlag, Berlin, (1956).

25. L. Nordheim, Proc. Roy. Soc. London., A121 , 626 - 639 , (1928).

26. A. Van Oostrom, J. Appl. Phys., 33 , 2917 - 2922 , (1962).

27. R. Haefer, Z. Physik (Zeitschrift Fur Physik) 116 , 604 - 622 , (1940).

28. W. P. Dyke, J. K. Trolan, W. W. Dolan and G. Barns, J. Appl. Phys., 24 , 570 - 576 , (1953).

29. W. P. Dyke, J. K. Trolan, E. E. Martin and G. Barbrous, Phys. Rev., 24 , 1043 - 1057 , (1953).

30. I. Tamm, Physik. Z. Sowj., 1 , P.733 , (reference to Tamm is made in - D. Frankl, Electrical Properties of Semiconductor Surfaces, P.192 , Pergamon Press, (1967)). (1932).

31. W. Shockley, Phys. Rev., 56 , 317 - 323 , (1939).

32. J. Bardeen, Phys. Rev., 10 , 717 - 727, (1947).

33. N. K. Allen, Ph.D. Thesis, Aston University In Birmingham U.K. (1979).

34. J. E. Henderson and R. E. Badgley, Phys. Rev. 38 , 590 - 598 , (1931).

35. R. K. Dalstrom, K. V. MacKenzie and J. E. Henderson, Phys. Rev., 48 , 484 - 489 (1935).

36. R. D. Young and E. W. Muller, Phys. Rev., 113 , 115 - 121 , (1959).

37. R. D. Young, Phys. Rev., 113 , 110 - 114 , (1959).

38. J. W. Gadzuk and E. W. Plummer, Rev. Mod. Phys., 45 , 487 - 548 , (1973).

39. L. W. Swanson and L. C. Crouser, Phys. Rev. Lett., 16 , 389 - 391 , (1966).

40. L. W. Swanson and L. C. Crouser, Phys. Rev., 163 , 622 - 641 , (1967).

41. E. W. Plummer and A. E. Bell, J. Vac. Tech., 9 , 583 - 590 , (1972).

42. J. P. Jones and E. W. Roberts, Surf. Sci., 64 , 355 - 381 , (1977).

43. N. Kar and P. Soven, Solid State Commun., 19 , 1041 - 1043 , (1976).

44. L. W. Swanson and L. C. Crouser, Phys. Rev. Letts., 19 , 1179 - 1181 , (1967).

45. N. J. Dionne and T. N. Rhodin, Phys. Rev., B14 , 322 - 340 , (1976).

46. N. Rihon, Phys. Stat. Solidi., A49 , 697 - 703 , (1978).

47. A. E. Bell and L. W. Swanson, Phys. Rev., B19 , 3353 - 3364 , (1979).

48. C. Lea and R. Gomer, Phys. Rev. Letts., 25 , 804 - 806 , (1970).

49. W. Gadzuk and E. W. Plummer, Phys. Rev. Letts., 26 , 92 - 95 , (1971).

50. J. J. Czyzewski, Surf. Sci., 39 , 1 - 20 , (1973).

51. R. Stratton, Phys. Rev., 125 , 67 - 82 , (1962).

52. R. Stratton, Phys. Rev., 135 , 794 - 805 , (1964).

53. J. R. Arthur Jr, Surf. Sci., 2 , 389 - 395 , (1964).

54. O. H. Hughes and P. M. White, Phys. Stat. Solidi. 33 , 309 - 316 , (1969).

55. B. F. Lewis and T. E. Fischer, Surf. Sci., 41 , 371 - 376 , (1974).

56. P. Handler,J.Chem. Solids., 14 , 1 - 8 , (1960).

57. W. B. Shephard and W. T. Peria, Surf. Sci., 38 , 461 - 498 , (1973).

58. I. Brodie, J. Appl. Phys., 35 , 2324 - 2332 , (1964).

59. D. W. Williams and W. T. Williams, J. Phys. D: Appl. Phys., 5 , 280 - 290 , (1972).

60. D. W. Williams and W. T. Williams, J. Phys. D: Appl. Phys., 6 , 734 - 743 , (1973).

61. N. K. Allen, C. S. Athwal and R. V. Latham, Vacuum 32 , 325 - 332 , (1982).

62. R. P. Little and W. T. Whitney, J. Appl. Phys., 34 , 2430 - 2432 , (1963).

63. G. P. Beukema, Physica., 104c , 35 - 45 , (1981).

64. G. A. Farrall and M. Owen, J. Appl. Phys., 43 , 938 - 943 , (1972).

65.   G. A. Farrall, M. Owen and F. G. Hudda, J. Appl. Phys, 46, 610 - 617,   (1975.).

66.   B. M. Cox,   J. Phys. D : Appl. Phys., 8, 2065 - 2073,   (1975).

67.   B. M. Cox and W. T. Williams,   J. Phys. D : Appl. Phys., 10, L5 - L9,   (1977).

68.   R. E. Hurley and P. J. Dooley, J. Phys. D : Appl. Phys, 10, L195 - 201,   (1977).

69.   R. E. Hurley,   J. Phys. D : Appl. Phys, 12, 2229 - 2245,   (1979).

70.   N. K. Allen, B. M. Cox and R. V. Latham,   J. Phys. D : Appl. Phys. , 12 , 969 - 978,   (1979).

71.   R. E. Hurley , J. Phys. D : Appl. Phys ., 13, 1121 -128,   (1980).

72.   G. Dearnaley, Phys. Lett. , 25A , 760 - 761,   (1967).

73.   G. Dearnaley, A. M. Stoneham and D.V. Morgan, Rep. Prog. Phys, 33, 1129 - 1191,   (1970).

74.   K. W. Boer and S. R. Ovshinky, J. Appl. Phys. 41, 2675 - 2681,   (1970).

75.   C. S. Athwal and R. V. Latham,   Proc. IX - DEIV, Physica, 104C, (189 - 195) ,   (1981).

76.   R. E. Hurley,   J. Phys. D : Appl. Phys . , 12, 2247 - 52   (1979).

77.   B. Juttner, W. Rohrbech, H. Wolf ,   Proc. IX - DEIV, 65 - 69,   (1972).

78.   B. Juttner, H. Wolf and B. Altrichter, Phys. Stat. Sol, 27 , 403 - 412,   (1975).

79.   G. Dearnaley ,   Thin solid films, 3, 161 174,   (1969).

80.   N. K. Allen and R. V. Latham,   Proc. 8th Int, Symp. Disch. and Elect. Just in vacuum Alburquerque, E Proc. VIII - DEIV B3 , 1 - 13,   (1978).

81.   D. Adler, H. K. Henisch and S. N. Mott,   Rev. Mod. Phys., 50, 209 - 220,   (1978).

82.   R. E. Peterson and D. Adler, J. Appl. Phys. 47, 256 - 263,   (1976).

83.   T. A. Edison. U. S. Pat. 223898,   (1880).

84.   R. Bacon, A. A. Polozzi and S. E. Slosarik, Society of the plastics industry 21st Technical and Management Conference , Section 8E , Feb .,   (1966).

85.   A. E. Standage and Prescott, Nature, 211, P. 169,   (1966).

86.   W. Watt, L. N. Phillips, and W. Johnson, The Engineer, 221,
      815 - 816,   (1966).

87.   W. N. Raynolds, ELSEVIER   (1968).

88.   D. J. Johnson and C. N. Tyson, Brit. J. Appl. Phys. (J. Phys.
      D) , 2 , 787 - 795,   (1969).

89.   W. Ruland, Chemistry and Physics of Carbon, 4 , 1 - 84 ,
                                                        (1969).

90.   A. Fourdeaux, R. Perret and W. Ruland, Int. conference on
      carbon fibres their composites and applications, The plastic
      Institute, London, Paper 9,   (1971) .

91.   R. Perret and J. Ruland, J. Appl. Cryst., 2, 209 - 218,
                                                        (1969).

92.   F. R. Barnet and M. K. Norr, Composites , 7 , 93 - 99,
                                                        (1976).

93.   B. J. Wicks and R. A. Coyle,   J. Mat. Soci., 11, 376 - 383,
                                                        (1976).

94.   P. W. Manders, Nature, 271, 142 - 143 ,   (1978).

95.   M. Barber, P. Swift, E. L. Evans and J. M. Thomas, Nature 227,
      1131 - 1132,   (1970).

96.   F. Hopfgarten , " Fibre Sci. and Techn. ,   12, 283 - 294 ,
                                                        (1979).

97.   F. Hopfgarten, Fibre Sci. and Tech., 11, 67 - 79,   (1978).

98.   C. Lea, J. Phys. D : Appl. Phys. , 6, 1105 - 1114, (1973).

99.   T. H. English , C. Lea and M. T. Lilburne,   Scanning Electron
      Microscopy, Systems and Applications , Newcastle (London :
      Inst. of Phys.) 12 - 14 ,   (1973).

100. F. S. Baker, A. R. Osborn and J. Williams, J. Phys. D : Appl.
      Phys ., 7, 2105 - 2115,   (1974).

101. E. Braun, J. F. Smith and D. E. Sykes , Vacuum , 25, 425 -
      426,   (1975).

102. W. Rohrbeck , B. Juttner and P. Siemroth , VII International
      Symp. Discharges and electric insulation in vacuum , U S S R ,
      193,   (1976).

103. A. J. Sangster, Solid state and Electron Devices , 1 , 151 -
      157 ,   (1977).

104. A. Knon , J. Moss and A. J. Sangster, IEE Colliquim on electron
      Emission , Feb. Digest 1977/5   (1977).

105. M. Faubel , W. M. Holber and J. P. Toennies , Rev. Sci Inst. , 49, 449 - 451, (1978).

106. H. Heinrich , M. Essig and J. Geiger, Appl. Phys., 12 , 197 - 202, (1977).

107. C. S. Athwal , PHD Thesis 1981, Aston University in Birmingham.

108. A. V. Crewe, J. Wall and L. M. Welter, J. Appl. Phys. 39, 5861 - 5868, (1968).

109. E. Munro, Phd. Dissertation, Cambridge University ,(1972).

110. D. J. Swann and K. C. A. Smith, IIT, Research Institute Chicargo , 41 - 48 (1973).

111. J. R. A. Cleaver, Int. J. Electronics, 38, 513 - 529 (1975).

112. V. M. Zhukov and G. N. Fursei, Sov. Phys. Tech. Phys., 21 , 1112 - 1117 , (1976).

113. V. M. Zhukov and G. N. Fursei, E. I. Givargizov, I. D. Ventova and N. V. Egorov, Sov. Phys. Tech. Phys. 21, 1110, 1112, (1976).

114. F. H. Pollak, C. W. Higginbottom and M. Cardona, J. Phys. Soc. Japan , 21 , 20 - 26 (1966), Kyoro Proc. Int. Conf. Phys. of Semiconductors, (1966).

115. L. S. Allard , " High resolution cathode - Ray tubes " Medical and Biological Illustrations, Vol XIV, 3, 184 - 190, (1964).

ACKNOWLEDGEMENTS